Polytechnic University of Marche
Ph.D. School in Engineering Sciences
Curriculum in Civil, Environmental, Building Engineering and Architecture

---

Robustness of industrial precast buildings due to damage accumulation

Ph.D. Dissertation of:

Marina Poiani

Advisor:
Prof. Stefano Lenci

Co-Advisor:
Prof. Francesco Clementi

Curriculum supervisor:
Prof. Stefano Lenci

XXXI cycle

Polytechnic University of Marche
Department of Civil, Environmental, Building Engineering and Architecture
Via Brecce Bianche 12 - 60131 - Ancona, Italy

Acknowledgements

I wish to thank Professor Stefano Lenci and Professor Francesco Clementi for their support and for giving me the opportunity to attend this PhD course.

I'm grateful to Melissa Recanatini, Michela Bisceglia and Valentina Gazzani: this work is for them.

Abstract

Robustness of industrial buildings, defined as the capacity of the structure to withstand exceptional actions like seismic events avoiding a global collapse, is one of the main topics of research due to the serious human and economic loss that the lack of such feature could cause. Most of the existing industrial buildings are made with precast elements realised with low-code without specific detailed standards for precast structures in which the technical achievement of them relies on the individual producers with their design solutions.

Existing Italian precast structures for large-scale industrial buildings can be divided into two main categories depending on the evolution of prefabrication techniques. The first category was developed from the early thirties up to the mid-sixties, with RC industrial structures cast in place with a widespread use of precast vault to cover a large span, while the second one started to be produced at the beginning of the fifties and is still in use as regards the typical precast frame structure with all its main elements made in factory and assembled in place.

In the first type of industrial buildings, only the roof is precast and usually made in reinforced hollow brick light-weight vault and the robustness is defined considering several limit states of chord-rotation and shear capacity of columns and main beams combined with specific vulnerabilities of the precast vault, considering that every seismic sequence is usually a combination of a mainshock and several aftershocks which lead to the damage accumulation on the structure.

In the second case the robustness of precast frame structures is usually based on the connections of structural and non-structural elements (cladding panels) and on the activation of the domino effect passing from local to global collapse.

In this work several finite element models to best represent the linear and nonlinear structural behaviour of both types of precast structures considered are analysed.

Keywords: industrial buildings, precast vault, cladding panels, fragility analysis, mainshock-aftershock sequence.

Sommario

La robustezza degli edifici industriali, definita come la capacità della struttura di resistere ad azioni eccezionali come eventi sismici evitando un collasso globale, è uno dei principali argomenti di ricerca a causa della grave perdita umana ed economica che causa la mancanza di tale caratteristica. La maggior parte degli edifici industriali esistenti sono stati realizzati con normative senza specifici standard per strutture prefabbricate in cui la progettazione degli elementi costruttivi si basava sulle singole soluzioni progettuali dei produttori.
Le strutture industriali prefabbricate italiane esistenti a grandi luci possono essere suddivise in due categorie principali a seconda dell'evoluzione delle tecniche di prefabbricazione. La prima categoria si sviluppa dai primi anni trenta fino alla metà degli anni sessanta con strutture industriali in c.a. gettate in opera con un uso diffuso di volte leggere prefabbricate per coprire ampie luci, mentre la seconda è prodotta a partire dagli anni cinquanta tutt'ora in uso riguardante la tipica struttura a telaio prefabbricato con tutti gli elementi realizzati in stabilimento ed assemblati sul posto.
Nelle prime tipologie di edifici industriali, la robustezza è definita considerando diversi stati limite di deformabilità e resistenza di pilastri e travi combinati con la vulnerabilità specifica del sistema voltato prefabbricato, sapendo che la struttura è soggetta ad una combinazione di eventi sismici ravvicinati nel tempo che portano all'accumulo del danno.
Nel secondo caso la robustezza della struttura del telaio prefabbricato è solitamente basata sulle connessioni di elementi strutturali e non (pannelli di tamponamento) e nell'attivazione dell'effetto domino passando dal collasso di tipo locale a quello globale.
In questo lavoro sono analizzati diversi modelli ad elementi finiti per rappresentare al meglio il comportamento strutturale lineare e non lineare di entrambi i tipi di strutture prefabbricate considerate.

Parole chiave: edifici industriali, volta prefabbricata, pannelli di tamponamento, analisi di fragilità, sequenza sismica.

Contents

List of Figures

List of Tables

1 Chapter - Introduction

Robustness of industrial buildings, defined as the capacity of the structure to withstand accidental actions like seismic events avoiding a global collapse, is one of the main topics of research due to the serious human and economic loss operativity that the lack of such feature could cause. Most of the existing industrial buildings are made with precast elements realised with low-code without specific detailed standards for precast structures in which the technical achievement of them relies on the manuals of the time of the individual producers with theirs design solutions. Existing Italian precast structures for large-scale industrial buildings can be divided into two main categories depending on the evolution of prefabrication techniques. The first category was developed from the early thirties up to the mid-sixties, with industrial structures cast in place with a widespread use of reinforced hollow brick light-weight vault to cover a large span, while the second one started to be produced at the beginning of the fifties and is still in use as regards the typical precast frame structure with all its main elements made in factory and subsequently assembled in place.

In the first type of industrial buildings, only the roof is precast and usually made in in reinforced hollow brick light-weight vault and the robustness is defined considering several limit states of chord-rotation and shear capacity of columns and main beams combined with specific vulnerabilities of precast vault (technologies to build structural elements are the same as those of reinforced concrete structures cast in place). From the architectural point of view in the scientific literature, several studies are carried out for the enhancement and restoration of this construction system.

In the second case, the main peculiarities of precast frame buildings are connections of all precast structural and non-structural elements whose compose the structure: tiles or roofing panels-beams, beams-columns, columns-foundations, columns-horizontal cladding panels, beam-vertical cladding panels. Robustness of precast frame structures is usually based on the non-effective connections of structural and non-structural elements and in the subsequent activation of the domino effect passing from local to global collapse.

The vulnerability of non-structural elements like cladding panel became the object of research mainly after the 2012 Emilia Romagna earthquake, which underlined the importance of evaluating and analysing not only the unions of the primary elements already available of research extensively studied (column-beam connection) but also the interaction of the structure with the secondary elements

(connection of cladding panels with structure became object of design with the Italian code NTC2018).
Several finite element models to best represent the linear and nonlinear structural behaviour of both types of precast structures considered are analysed.

1.1 Research purposes and thesis outline

Some concepts of robustness are presented in the scientific literature; the main explanations are reported below.
According to Model Code 2010 [1], *"Robustness is a specific aspect of structural safety that refers to the ability of a system subject to accidental or exceptional loadings (such as fire, explosions, impact or consequences of human errors) to sustain local damage to some structural components without experiencing a disproportionate degree of overall distress or collapse".*
Asprone et al. [2] define it with a meaning more stronger than the word vulnerability. Robustness is declared as *"the measure of the capability of a structure to withstand an exceptional event of extreme intensities, or multiple events are unexpectedly occurring together, beyond the accepted design event and based on all the contribution to its structural capacity."*
For the new design, Italian code NTC2018 [3] in chapter 2.1 defines this word as one of the main requirements necessary for a building as "*ability to avoid disproportionate damage compared to the extent of possible exceptional triggering causes such as explosions and shock*." In chapter 2.5 the same code lists some design strategies to satisfy this requirement in addition to mention this term in all code.
This thesis dissertation is organised in six chapters where robustness of industrial building is investigated in different ways especially in chapters four and five.
Chapter two describes the state of art of precast structures starting from a national seismic code evolution, very useful because during the various historical phases precast structures have a uniformity of solutions connected to main law, a summary documents of existing precast frame structural types from the sixties up to today and technical documents and manuals to design and for structural reinforcement of precast structures written by CNR, ASSOBETON, ETAG and JRC. A specific paragraph is also dedicated to the observation of damage to precast structures deriving from the earthquakes of Friuli in 1976, Emilia Romagna in 2012 and Central Italy in 2016: the vulnerabilities of the precast structures are underlined, in particular for last earthquake an inspection in the earthquake zones is carried out a few months after the seismic events.

Chapter three lists typical vulnerabilities of two main precast structures analysed in this work: RC industrial structures cast in place with precast reinforced hollow brick light-weight vault and precast frame structures. In both typologies, a careful description is made including the references of the international scientific literature which have investigated the main connections using experimental tests.
Through a fragility analysis carried out with different probabilistic methods, in *Chapter four* the structural robustness of RC industrial structure cast in place with precast reinforced hollow brick light-weight vault is evaluated by nonlinear analyses. After a short list of the scientific literature concerning the fragility curves realized for precast frame structures, a description of the characteristics of the vault is made including a brief history of the birth of this system, the structural scheme and the operational construction phases of the vault. A case study of the sixties with all the peculiarity of the period is considered and the influence of numerical modelling through three different representations of the vault system with a different application of the loads according to the finite elements used is evaluated. Fragility curves are realised by IDA curves considering as damage limits threshold values that correspond to the local limit conditions regarding bending or shear that first occurrence in few elements determined through pushover analyses. A comparison of fragility curves of X-Y directions of all three models is carried out.
Regarding the model with the major probability of collapse, in *Chapter five* seismic sequence effects on the damage of this structure considering the same ground motions for mainshock and aftershock are taken into account. A D-IDA with a mainshock with fixed several percentages of near collapse PGA previous evaluated in X-Y direction and scaled aftershocks are realised and compared with IDA. Fragility curves created with D-IDA curves considering only damage limit threshold value of Near Collapse are likened with a case that consider a single seismic event (only mainshock). Also, ductility damage indices are calculated with a maximum of displacements obtained by every nonlinear dynamic analysis of IDA and D-IDA.
Chapter six changes topic and it takes into account precast frame structures through linear analyses. After Emilia Romagna earthquakes, whereas the international scientific research has focused on cladding panels, on their types of connection through experimental tests and on the drafting of guidelines with their interaction with the bare frame, the first period of these structures is investigated through the creation of numerical models that follow recent studies.
After evaluating the formulas deriving from the scientific literature to determinate the first period of the structure, the connection types described in the JRC design guidelines specific for the cladding panels are summarised and studied alongside the experimental tests of single connections performed to several universities

thanks to the European project SAFECLADDING. These connections of vertical and horizontal cladding panels are implemented in a preliminary case study of small dimensions useful to understand the influence of each single type of coupling on the bare frame varying the choice of finite elements (beam, shell and wall) to represent the individual panels.
Always with the same setting but only with vertical cladding panels, the main case dating back to the seventies is chosen by varying the stiffness of roof, the height, the length and the asymmetry of the loads: the corresponding first periods with the various types of cladding panel modelling are put in comparison.

2 Chapter - State of The Art – Technical literature

This chapter focuses on an analysis of state of the art to summarise the laws and all the technical documents realized to design, verify and identify the problems of precast structures. Furthermore, the research of some papers concerning the existing typologies of these structures and the surveys of the damages recorded during the previous earthquakes are listed.

2.1 Main features of the precast industrial building

In Italy, precast structures are mainly used in the industrial field, where buildings require wide space and a square or rectangular plan. Precast industrial buildings can be classified according to different variables: the structural typology, the number of stories and the roof type.
The main structural typologies can be divided into three groups: precast arch or vault structures, frame structures, and wall panel structures.
Depending on the number of stories, precast frame structures can be grouped into multi-storey framed structures and single-storey structures with isostatic columns, according to the capability of the connections in transferring bending moments. Respect to the roof type, roof elements supported by beams with variable section, continuous plane roof, discontinuous plane roof and shed roof can be found.
In Italy the most common precast buildings are frame structures (in the nineties, precast frame structures account for approximately 85% of the entire existing assets of industrial facilities): they consist of socket footing foundations in which precast columns are placed and fixed in-situ by cement mortar; the columns support pre-stressed precast beams that can have different shapes.
The main aspect of precast structures regards the connections between structural elements that they are made in-situ and realise to reflect the structural behaviour assumed in the design phase.
Typical connections can be divided into floor or roof elements connection, roof element-to-beam connection, beam-to-column connection, column-to-foundation connection and cladding panels-to-structural element connection.

2.2 National Seismic Code Evolution

The evolution of the Italian Seismic Code is very useful for the industrial building because during the various historical phases these type of structures show well recognizable solutions with a certain constancy and uniformity.
The Italian code concerning prefabricated structures can be divided into three major periods: the first initial period considered is 1939-1987 which already introduce a few rules regarding reinforced concrete structures.
The law of 1962 *"Provvedimenti per l'edilizia, con particolari prescrizioni per le zone sismiche"* [4] is not dedicated to precast structure but it is the first code that introduces some important changes in the design of structures like the definition of acceleration for the various Italian seismic areas, the introduction of the vertical component of earthquake that until previous law was unknown (very interesting for massive structures such as industrial building) and the concept of infinitely rigid roofs, which shows completely different structural behaviours compared to a deformable deck where large structures start to vibrate asynchronously. This law also introduces the accidental eccentricity of the masses.
The problems of prefabrication begin to be discussed with *"Circolare del Ministero dei Lavori Pubblici n.1422 del 6 Febbraio 1965"* , which prohibits the use of horizontal connections without mechanical devices if the ratio between the maximum value of shear force and expected axial compression force is greater than 0.35 (hypothetic friction coefficient of the connection).
From then on, with the subsequent law of 1971 "*Norme per la disciplina delle opere di conglomerato cementizio armato, normale e precompresso ed a struttura metallica"*[5] , law of 1974 "*Provvedimenti per le costruzioni con particolari prescrizioni per le zone sismiche*" [6] and law of 1975 *"Norme tecniche per le costruzioni in zone sismiche*" [7], procedures for the prefabrication of prefabricated units in series and the first rules for structure with a load-bearing panels are described. Also, with these laws, the minimum values of fi10mm for longitudinal bars, fi5mm for stirrups and of 1.2mm for concrete cover for a column of precast buildings are fixed with the awareness that the precast elements are made in an industrial plan with precise tolerances. After these laws, columns of 8-10 meters very slender with a little ductility are built.
Decreto Ministeriale of 1987 *"Norme tecniche per la progettazione, esecuzione e collaudo delle costruzioni prefabbricate"* [8] is the first law written entirely for precast buildings used up to DM1996 [9] which prohibits, in seismic zone, supports in which the transmission of forces is entrusted only to friction; it also defines the minimum depth of the support of panel floors and beams and it fixs that the

structure must be verified under the action of horizontal forces equal to 2% of the building mass. Starting from this decree, many structures designed in the seismic area have already connectors between main elements and connections are not based on friction: the biggest problem is that not all of Italian territory up to the OPCM3274/2003 [10] was considered seismic (Figure 2.1).

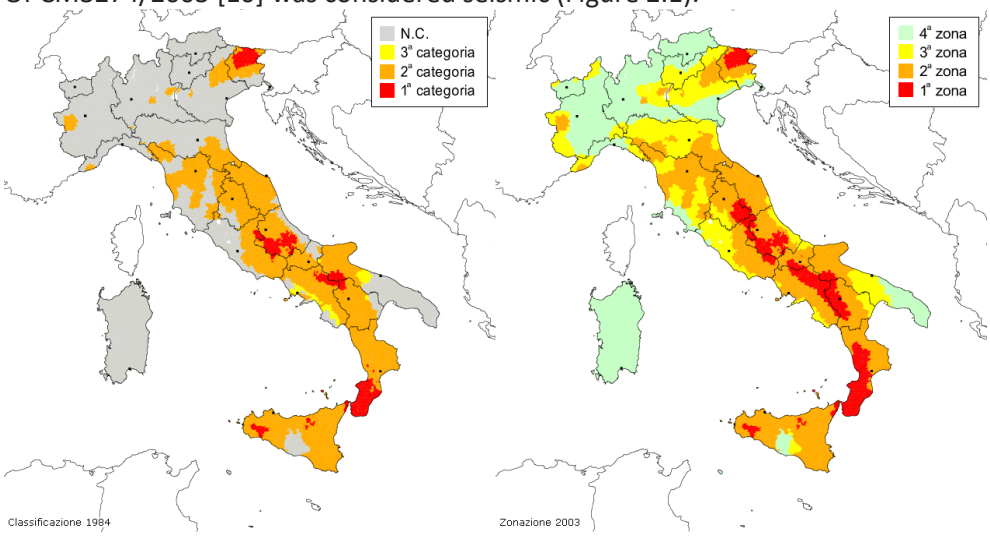

Figure 2.1 Seismic zone classification in Italy (a) in 1984 and (b) in 2003 (INGV2018).

DM1987 [8] also defines the difference between union and joint: the union is a connection between structural parts while the joint allows movement. In the case of precast buildings, the use of a union, if it is located in the seismic area, have to transmit the stresses.

With Circ. M. LL.PP. n.31104/1989 *"Istruzioni in merito alle norme tecniche per la progettazione, esecuzione e collaudo delle costruzioni prefabbricate"* [11] are dictated the methods of production of manufactured products in series.

The second major period considered is 1996-2003 and it starts with DM 9/01/1996 *"Norme tecniche per il calcolo, l'esecuzione ed il collaudo delle strutture in cemento armato, normale e precompresso e per le strutture metalliche"* [12], DM 16/01/1996 "Norme tecniche per le costruzioni in zone sismiche" [9] and its relative Circ. M. LL.PP. n.65/AA.GG. del 1997 "*Istruzioni per l'applicazione delle "Norme tecniche per le costruzioni in zone sismiche di cui al D.M. 16/01/1996*" [13] that fix constructive indications for generic structures (local and global ductility) in normal and pre-compressed reinforced concrete (many scientific articles consider this date as another watershed for low-code prefabrication). Furthermore, in these codes, the response coefficient linked to the vibration period is considered, which allows

the transition to the equivalent static method. Moreover, the design of a structure passes from the verification regarding resistance (ultimate limit state) to that in terms of displacement (exercise limit state).
The third period considered is 2003-2018 and it begins with the OPCM 3274/2003 *"Primi elementi in materia di criteri generali per la classificazione sismica del territorio nazionale e di normative tecniche per le costruzioni in zona sismica"* [10], mandatory only in the case of infrastructure and strategic buildings. This code has a specific chapter (5.7) that takes into account the structural typologies of precast buildings (Multi-storey framed structures and single-storey structures with isostatic columns) and that regards the static and dynamic behaviour of the connections according to the considered structural typology. Indeed, in the case of frame structures, this code distinguishes three possible conditions:
1. connections locate well outside critical regions not affecting the energy dissipation capacity of the structure;
2. connections locate within critical regions but adequately over-designed concerning the rest of the structure, so that in the seismic design situation they remain elastic while inelastic response occurs in other critical regions;
3. connections locate within critical regions properly designed regarding strength, ductility and quantity of energy to dissipate.
For one-storey structures with isostatic columns, the beam-column connections may be fixed or free to slide horizontally. The connections must transfer the seismic design horizontal forces, without taking into account the friction strength. Another important characteristic of this code is that the entire national territory is considered seismic.
The DM2008 *"Norme Tecniche per le Costruzioni"* [14] with the ministerial circular of 2009 includes both OPCM 3431/2005 and EUROCODE 8 [15] taking up the previous concepts described by these codes.
Currently, DM2018 [3] highlights important changes compared to the DM2008 regarding the design of precast structures.
The definition of single-storey structures with isostatic columns become *"pilastri incastrati alla base con orizzontamenti ad essi incernierati"* that it underlines only the transmission of shear force between beam-column connections.
But the major difference compared to DM2008 is that, even for precast structures, a verification regarding ductility is required in terms of global and local capacities. Each connection must have Rigidity, Resistance, Ductility and Dissipation and have to be qualified products guaranteeing certain performances (The types of connections remain those defined in OPCM3274/2003 and DM2008).

Another important change is in terms of design of non-structural elements like infill masonry and cladding panels that, if with DM2008 they are not considered except in terms of mass to a lesser extent, with DM2018 they have to be defined in terms of mass, stiffness and resistance: there are the assumptions that cladding panels interfere with the ductility of the whole structure and that they lead to damage to structural elements. Precast structures defined of strategic importance are designed regarding the limit state of operations (SLO).
In Tables 2.1 - 2.3 the evolution of the Italian legislative code is summarised.

FIRST PERIOD 1939-1987				
Code	**Acronym**	**Title**	**Precast structures requirements**	**Main features**
Decreto Legge 16/11/1939 n. 2229	D.L. n.2229/1939	"Norme per l'esecuzione delle opere in conglomerato cementizio semplice od armato"	No	Chapter III Design standards - art. 18 Description of strength and steel
Legge 25/11/1962 n. 1684	L. n.1684/1962	"Provvedimenti per l'edilizia, con particolari prescrizioni per le zone sismiche"	No	List of municipalities in seismic areas (Ancona) art. 7 identification of 1st and 2nd category buildings art. 12 stability calculations - design of structures with a horizontal force equal to 0.10% of building mass 1 ° cat. (h max = 21 mt 6 floors) and 0.07% building mass 2nd cat. (h max = 26mt 7 floors)
Legge 5/11/ 1964 n.1224	L. n.1224/1964	"Integrazioni della legge 25 novembre 1962, n.1684, concernente provvedimenti per l'edilizia con particolari prescrizioni per le zone sismiche"	No	previous law integration
Circolare del Ministero dei Lavori Pubblici n.1422 del 6/02/1965	Circ. M. LL.PP. n.1422/1965	"Istruzioni per il rilascio dell'idoneità tecnica dei sistemi costruttivi e strutture portanti prevista negli art. 1-2 della legge 5 Novembre 1964 n.1224 con particolare riferimento alle strutture prefabbricate"	Yes	*"Nei giunti orizzontali il rapporto tra l'azione tagliante massima T e l'azione assiale di compressione N concomitante deve essere T/N < 0,35. Se le precedenti condizioni non sono verificate, l'azione tagliante deve essere per intero assorbita da armature metalliche localizzate o diffuse."* PROHIBITION ATTRITIVE CONNECTIONS IF T/N>0.35
Legge 5/11/1971 n.1086	L. n.1086/1971	"Norme per la disciplina delle opere di conglomerato cementizio armato, normale e precompresso ed a struttura metallica"	Yes	art. 9 procedures for the construction of mass-produced buildings (material characteristics, construction methods, all the artefacts marked to understand the origin of elements)
Legge 2/02/1974 n.64	L. n.64/1974	"Provvedimenti per le costruzioni con particolari prescrizioni per le zone sismiche"	Yes	art. 7 buildings with prefabricated vertical bearing panels art. 9 seismic actions - the introduction of two horizontal orthogonal force systems
Decreto Ministeriale 03/03/1975	D.M. 3/3/1975	"Norme tecniche per le costruzioni in zone sismiche"	Yes	C.7 Buildings with a load-bearing structure The concept of "vibration period of a structure" Static analysis, linear dynamics (defined with more precision)

Table 2.1 First period national seismic code evolution (1939-1987).

SECOND PERIOD 1987-2003				
Code	**Acronym**	**Title**	**Precast structures requirements**	**Main features**
Decreto Ministeriale 3/12/1987	D.M. 3/12/1987	"Norme tecniche per la progettazione, esecuzione e collaudo delle costruzioni prefabbricate"	Yes	2.4 Definition of UNIONS and JOINTS
				2.4.1 In the seismic zone, supports are not allowed in which the transmission of horizontal forces is entrusted only to FRICTION.
				2.4.1 ROOF Depth of support not less than 3 cm if the continuity of the union is foreseen, 5 cm if definitive
				2.4.1 BEAM The minimum depth of the final support must be not less than 8cm + l / 300 (l = net beam light)
				2.7 The structure must be verified under the action of conventional horizontal forces of calculation equal to at least 1.5% of the concurrent vertical loads (permanent and overload) combined most unfavourably during TRANSITORY PHASES and at 2.0% during the FINAL PHASE.
				2.11.1.2 Additional sizing of forks
Circolare del Ministero dei Lavori Pubblici n.31104 del 16/03/1989	Circ. M. LL.PP. n.31104/1989	"Istruzioni in merito alle norme tecniche per la progettazione, esecuzione e collaudo delle costruzioni prefabbricate"	Yes	1.1 The precast panels are not included in the code, as they are not essential for the stability of the building
				1.4 Products produced in series (declared series, controlled, mass production)
Decreto Ministeriale 09/01/1996	D.M. 9/01/1996	"Norme tecniche per il calcolo, l'esecuzione ed il collaudo delle strutture in cemento armato, normale e precompresso e per le strutture metalliche"	Yes	PART I Normal and pre-stressed reinforced concrete PART II Steel PART III Prefabricated products manufactured in series
Decreto Ministeriale 16/01/1996	D.M. 16/01/1996	"Norme tecniche per le costruzioni in zone sismiche"	No	Non-specific standards for precast structures
				Seismic zone III - 4% total mass
				Seismic zone II - 7% total mass
				Seismic zone I - 10% total mass
Circolare del Ministero dei Lavori Pubblici n.65/AA.GG. del 10/04/1997	Circ. M. LL.PP. n.65/AA.GG. DEL 1997	"Istruzioni per l'applicazione delle "Norme tecniche per le costruzioni in zone sismiche" di cui al D.M. 16/01/1996"	No	ANNEX 1 Constructional indications for reinforced concrete structures (geometric definitions and limits longitudinal and transverse reinforcements BEAMS, COLUMNS, NODES, WALLS)

Table 2.2 Second period national seismic code evolution (1987-2003).

THIRD PERIOD 2003-2018				
Code	**Acronym**	**Title**	**Precast structures requirements**	**Main features**
Ordinanza del Presidente del Consiglio dei Ministri 20/03/2003 n.3274	O.P.C.M. n.3274/2003	"Primi elementi in materia di criteri generali per la classificazione sismica del territorio nazionale e di normative tecniche per le costruzioni in zona sismica"	Yes, obligatory only for strategic buildings	5 Buildings with reinforced concrete structure (definitions DUCTILITY CLASSES: high (CDA) and low ductility (CDB)) 5.7 Buildings with precast structure (structural types and structural factors - MULTIPLE FRAME STRUCTURES (continuity constraints - 3 types of CONNECTION) and ONE-STORY STRUCTURES AT ISOSTATIC COLUMNS (fixed or sliding constraints)
Ordinanza del Presidente del Consiglio dei Ministri 2/10/2003 n. 3316	O.P.C.M. n.3316/2003	Modifiche ed integrazioni all'ordinanza del Presidente del Consiglio dei Ministri n. 3274 - 20 marzo 2003	Yes	Changes in OPCM 3274/2003
Decreto del Presidente del Consiglio dei Ministri 21/10/2003	D.P.C.M. n.3685/2003	Disposizioni attuative dell'art. 2, commi 2, 3 e 4, dell'ordinanza del Presidente del Consiglio dei Ministri n. 3274 - 20 marzo 2003	Yes	List of categories of buildings considered of strategic importance concerning OPCM 3274/2003
CEN (Comitato Europeo di Normazione)	EUROCODE 8 2003	Design of structures for earthquake resistance - Part 1: General rules, seismic actions and rules for buildings (EN 1998-1)	Yes, but not obligatory in Italy	IMPORTANCE OF CONNECTIONS: it requires ignoring the resistance due to friction in evaluating the resistance of the BEAM-COLUMNS, BEAM-ROOF ELEMENTS 5 Structural systems considered (frame structures, wall structures, mixed frame-walls, wall panels, cellular systems)
Ordinanza del Presidente del Consiglio dei Ministri del 3/05/2005 n.3431	O.P.C.M. n.3431/2005	Ulteriori modifiche ed integrazioni all'OPCM n. 3274 del 20 marzo 2003 recante		Changes in OPCM 3274/2003
D.M. 14/09/2005	D.M. 14/09/2005	"Norme Tecniche per le Costruzioni"	Yes	5.1.10 Complementary rules for prefabricated structures 5.7.9 Buildings with the prefabricated structure
D.M. 14/01/2008	NTC2008	"Norme Tecniche per le Costruzioni"	Si	11.8 Precast components in C.A. and C.A.P.
Circolare 02/02/ 2009 n. 617	Circolare 2009 n. 617	Istruzioni applicazione NTC 2008	Si	C.7.4.5 Resumes OPCM 3431/2005 for the structural types Resumes EUROCODE 8 for CONNECTIONS
D.M. 17/01/2018	NTC2018	"Norme Tecniche per le Costruzioni"	Si	Design of non-structural elements Subdivision between ductile and fragile cladding panel/infill it distinguishes between a non-structural element cast in place and assembles on site with the definition of the responsibilities of designers and installers

Table 2.3 Third period national seismic code evolution (2003-2018).

2.3 Summary documents of existing structural types

During the last twenty years, several authors tried to list all the types of precast elements made in the Italian historical buildings. One of the most important projects is realised by Reluis together with Assobeton lasting about three years (2005-2008) for the cataloguing of the most widespread precast structures from the sixties up to today. The classification adopted strongly depends on the ten companies managed by ASSOBETON who provided the details and the existing types are catalogued based on roof adopted. At the end of the work, research group produces three documents related to a file of connections [16], a catalogue of existing typologies [17] and a register of RC precast buildings. [18]: the first one is released in 2007 and the remaining two in 2008. These papers are very useful for the terminology to be used for this type of structures.
Another important project [19] is realised by Eucentre (European Center for Training and Research in Seismic Engineering) after 2012 Emilia-Romagna earthquakes. This work aims to classify the majority of the industrial RC precast structures in Italy built in the last five decades, based on criteria like a year of construction and corresponding design code, static scheme, geometry, types of connections, materials and non-structural elements. For the research three different databases are used: the first one is based on a survey carried out between June and November 2012 in the province of Piacenza, the second database is collected between 2003 and 2008 by the Seismologic Service of Tuscany region (currently Seismic Division) while the third database is the Reluis-Assobeton project described above.

Code	Year	Main features
THREE-YEAR PROJECT 2005/08-DPC/RELUIS	**(in collaboration with ASSOBETON)**	
Strutture prefabbricate: SCHEDARIO DEI COLLEGAMENTI	2007	union between elements (floor-slab, slab-beam, beam-column, column-foundation, wall-structure panels) - May 2007
Strutture prefabbricate: CATALOGO DELLE TIPOLOGIE ESISTENTI	2008	Seismic classification (normative) and existing types defined by a roof: double slope, flat, shed, multi-floor (February 2008)
Strutture prefabbricate: SCHEDARIO DI EDIFICI PREFABBRICATI IN C.A.	2008	Connection database of 10 companies (February 2008)
EUCENTRE – PAVIA		
Single-storey precast buildings: probabilistic distribution of structural systems and subsystems from the sixties	2014	Classification of the majority of the industrial RC precast structures in Italy built in the last five decades, based on year of construction and design code, static scheme, geometry, types of connections, materials and non-structural elements.

Table 2.4 Summary documents of existing structural types of industrial buildings.

2.4 Technical documents to design and for structural reinforcement of precast structures

Respect the non-compulsory literature, before the nineties there is no precise technical documentation on precast structures. Technical manuals of the sixties-seventies are available mainly concerning precast floors, but the most important documents are the CNR 10025/84 [20] and CNR 10025/98 [21]. They provide a summary of state of the art in the technical and applicative field, indicating typologies, executive procedures, methods of analysis, verification and test for the correct design of the elements and for their good execution and conservation over time. In the CNR previously described, the contents of the standards are almost the same, the provision and the relevant laws vary in some topics. The CNR 10018/87 and CNR 10018/99 concern the types of elastomeric bearings of connection of structural elements that they can be simple, armed, disk, etc. Also, in this case, the contents of these two CNR do not vary.
After DM2008, the most important documents that regard the design of precast structure are "Linee Guida ASSOBETON per la progettazione sismica di strutture prefabbricate" published by ASSOBETON (Associazione Nazionale Industrie Manufatti Cementizi) [22], several ETAGs (European Technical Approval Guidelines) about the typologies of connections and three important technical documents realised by Joint Research Centre of Ispra that are design guidelines for connections [23], design guidelines for wall panel connections [24] and design guidelines for precast structures with cladding panels [25]. In Table 2.5 all technical documents described above are summarised.

Code	Year	Main features
MANUALS		
AGENDA CILA	1962	Description of slabs prefabricated beams, floors laid, precompressed floors, light decks, special roofs in reinforced hollow bricks
MANUALE FIB 1998	1998	Planning and design of prefabricated structures
CERIB	1998	Study of the rotational behaviour of the connections
CNR Consiglio Nazionale delle Ricerche		
CNR 10025/84: Istruzioni per il progetto, l'esecuzione ed il controllo delle strutture prefabbricate in conglomerato cementizio e per le strutture costruite con sistemi industrializzati	1984	PART I General Problems of the precast system
		PART II Structures with one-dimensional elements (glass-abutment check, plug-cut resistance (3.2.4.1) contact tension problems, simple supports)
		PART III Structures with two-dimensional elements (septa-large panels, load-bearing and non-load-bearing panels)
CNR 10025/98: Istruzioni per il progetto, l'esecuzione ed il controllo delle strutture prefabbricate in conglomerato cementizio e per le strutture costruite con sistemi industrializzati	1998	PART I General rules (general design criteria, union and joints, production controls, execution problems)
		PART II Structures with one-dimensional elements (beams: support constraints, tolerances, fire resistance, slender beams instability)
		PART III Slabs and roofing (structural types, stress analysis, verification of resistance, fire resistance)
		PART IV Structures with load-bearing walls (general rules, chaining, construction regulations)
		PART V Special and complementary elements (foundation - prefabricated foundation stones - and infill panels)
		PART VI and VII Inserts (Assembly and lifting phases)
CNR 10018/87: Apparecchi di appoggio per le costruzioni	1987	Classifications, executive procedures, calculation methods and test methods for the correct drafting of support equipment designs, for their good execution, installation and maintenance (elastomeric support - NEOPRENE)
CNR 10018/99: Apparecchi di appoggio per le costruzioni	1999	
ASSOBETON: Associazione Nazionale Industrie Manufatti Cementizi		
Linee guida ASSOBETON per la progettazione sismica di strutture prefabbricate	2009	Design of precast structures under seismic action
EOTA: European Organisation for Technical Assessment		
ETAG 030: Dowels for structural joints	2013	https://www.eota.eu/en-GB/content/etags-used-as-ead/26/
JOINT RESEARCH CENTER (JRC) OF ISPRA		
Design Guidelines for Connections of Precast Structures under Seismic Actions	2012	Seismic Behaviour and capacity design of connections
Design Guidelines for Wall Panel Connections	2016	Seismic Behaviour and capacity design of cladding panel connections
Design Guidelines for Connections of Precast Structures with Cladding Panel	2016	Seismic Behaviour and capacity design of cladding panel connections

Table 2.5 Technical documents for the design of precast structures.

Technical documents for risk assessment and structural reinforcement of precast structures are realised after 2012 Emilia-Romagna earthquakes. With the name of *"Gruppo di Lavoro Agibilità Sismica dei Capannoni Industriali", Reluis, Assobeton and Protezione Civile* create a series of specific guidelines to industrial structures related of photos of the damages recorded after seismic events with the reported vulnerabilities and details, advantages and disadvantages of consolidation

interventions proposed [26] [27]. In addition to these guidelines, an AeDES schedule relating to precast large-scale structures is realised [28] (Table 2.6).

Code	Year	Main features
Gruppo di Lavoro Agibilità Sismica dei Capannoni Industriali PROTEZIONE CIVILE - RELUIS - ASSOBETON		
Linee di indirizzo per interventi locali e globali su edifici industriali monopiano non progettati con criteri antisismici	2013	Projects of the interventions to be carried out for the safety of one-storey industrial buildings
Linee guida per riparazione e rafforzamento di elementi strutturali, tamponature e partizioni	2013	Photos of the structural interventions realised on industrial buildings (description) - not only for precast structures
PROTEZIONE CIVILE		
SCHEDA AeDES: Manuale per la compilazione della scheda di valutazione di danno ed agibilità post-sisma per edifici a struttura prefabbricata o di grande luce	2014	Manual for the compilation of the post-earthquake damage and usability assessment form for buildings with a prefabricated or large-dimension structure

Table 2.6 Technical documents for structural reinforcement of precast structures.

2.5 Damage observation of precast structures during Italian Seismic Events

2.5.1 Friuli Seismic Events (1976)

At 21:00:12 on 6 May 1976 a seismic event of magnitude 6.5 struck Friuli region with further shocks on 11 and 15 September of the same year. These seismic sequences are the first case of damage to precast buildings in the national historical context. A few days after the first seismic event, a famous phrase of the archbishop of Udine about reconstruction is recalled highlighting the damage of industrial buildings «First the factories, then the houses and then the churches».
For the prefabrication, this period is characterized by the vaults roofs with tie rods produced by the company RDB in the industrial field to cover space of at least 20 meters made with precast reinforced hollow brick joists. After this event, it was possible to observe how the seismic behaviour of these structures strongly depended on the presence or absence of an already existing damage underline the concept of “damage accumulation” never considered until that time.

Figure 2.2 Historical photos concerning the damages suffered by the industrial company during the 1976 Friuli earthquakes https://www.snaidero.it/gallery-40°-anniversario-terremoto-friuli .

2.5.2 Emilia Romagna Seismic Events (2012)

A series of strong earthquakes struck the Emilia region, in Northern Italy, on May in 2012. Two main earthquakes can be identified in the seismic sequence, with mainshocks featuring similar energies: the first event with moment magnitude, Mw = 6.1, struck on May 20th, while the second, with Mw = 6.0, on May 29th. The May 20th earthquake caused the collapse of several RC precast buildings in the industrial areas of S. Agostino, Bondeno, Finale Emilia, S. Felice Sul Panaro, while on May 29th the earthquake was particularly severe for industrial buildings in Mirandola, Cavezzo and Medolla. In the industrial areas close to the epicentres (less than 5 km), according to some estimates, more than 60% of RC precast buildings with frame structures collapsed or were severely damaged.

This seismic event involved a huge economic loss due to the direct economic damage amounts and indirect losses, as the industrial production interruption [29]. The large economic loss compared to the intensity of the event was basically due to the mixture of two factors: the high percentage of industrial precast buildings in the struck area and the vulnerability caused by no mandatory seismic design rules in the area until 2003, where an updated seismic hazard map for Italy classified the Emilia region as a low-to-moderate seismicity area.

The most common precast industrial buildings in the area of interest are single-storey statically-determined frame structures with pocket foundations: the seismic behaviour of these structures is characterized by great flexibility and large displacements.

In particular, these structures are typically built as an assembly of monolithic elements (roof elements, main and secondary beams, columns) in statically determinate configurations. The most common failure causes identified are: the absence of mechanical connectors between precast monolithic elements, the interaction of structural elements with cladding panels, the insufficient column bending capacity, the rotation of pocket foundations, the inadequacy of connections of external precast cladding walls to bearing elements (columns and beams) and the overturning of racks in buildings used as warehouses or in automated storage facilities [30] [31].

Liberatore et al. highlight the high percentage (50%) of severe damage suffered by cladding elements and infill panels. In cladding panels, the damage is related mainly to the failure of fastening elements and the consequent out-of-plane overturning. The occurrence of severe damage to columns amounts to almost 50% as well (considering together the damage at the base, at the top and the short-column mechanism). Damage to shed beam is due to their unseating in almost 30% of the

buildings surveyed; the vertical component of ground motion, together with the lack of connection between column and beam, play a significant role in the activation of this kind of collapse [32].

Figure 2.3 Damage of a) vertical and b), c) horizontal cladding panels and d) infill masonry observed during 2012 Emilia Romagna seismic event.

2.5.3 Central Italy Seismic Events (2016)

Between August 2016 and January 2017, nine events of magnitude greater than or equal to 5.0 struck the central part of Italy. The first two events, which took place on August 24th, had Mw 6.0 and 5.4, the third and the fourth (Mw 5.4 and 5.9) occurred on October 26th, the fifth (Mw 6.5) on October 30th, and the other four on 18th January 2017 (Mw 5.1, 5.5, 5.4, and 5.0). The earthquake of October 30th (Mw 6.5) was the strongest that occurred in Italy after the 1980 Irpinia earthquake (Mw 6.9). The hypocentres of all events were at a shallow depth (8-10 km). The main events of the seismic sequence took place in a territory that was affected by relevant earthquakes in the past. The progressive damage of the Amatrice civic clock tower, symbol of the destruction of 2016 central Italy seismic sequence, is investigated by Poiani et al. [33] with an advanced numerical model.
Another study that analyses the effects of central Italy seismic events is proposed by Gazzani et al. [34] regarding Pomposa Abbey belfry.
The first event of August 24th caused severe damage to the municipalities of Amatrice, Arquata del Tronto and Accumoli, with 299 fatalities and several hundreds of people injured.
The October events produced significant damage to the municipalities of Norcia and Castelsantagelo sul Nera, without additional fatalities.
Norcia, which was an important municipality in the affected area, was not significantly damaged by the August events. This circumstance could be attributed to its seismic history of the last centuries and, particularly, to its 1860 building code, as well as repair and strengthening interventions made after the 1979 Norcia and, to a lesser extent, 1997 Umbria-Marche earthquakes. However, during the October events, almost all churches in Norcia suffered extremely severe damage and the industrial area exhibited significant damage related to the precast structures [35].
In this section, the structural and non-structural damages, that occurred in precast structures during Central Italy seismic sequence, are presented by photographic documentation carried out on 3 April 2017.

The absence of mechanical devices among structural elements:

The use of friction creates a highly vulnerable mechanism against seismic actions and structures strongly sensitive to loss of support of the roof elements from the main beams or of the main beams from columns. There is also full collapses in the case of deformable roofs, not allowing to transfer the seismic forces to the other elements (The absence of a rigid roofs increases the vulnerability of these buildings). The interaction of portal frames with irregular masonry infill walls is often an important contributory cause (Figure 2.2a).

a b c d

Figure 2.4 Absence of mechanical devices among structural elements: Partial a) e b) and complete c) e d) collapses of roof elements.

Non-effective mechanical devices between beam-column and beam-beam:

One of the most common beam-to-column connections providing mechanical devices in resisting horizontal actions is the dowel system and many cases of damage involve this connection. It generally consists of one or more steel dowels, embedded in the column and inserted in a beam hole, filled with mortar. The connection behaviour is quite complex because it is influenced by the performance of different materials, by the established contacts between elements and by the behaviour of the jointed structural elements themselves (rotational capacity of beam and column).

a

b

c

Figure 2.5 Non-effective mechanical devices between beam-column and beam-beam: a) the spalling of concrete cover occurs before the yielding of the dowel; b) e c) high displacements in the beam-beam connection that led to the breaking of the roof slab.

Deficiencies regarding resistance and ductility in vertical resistant systems and foundation systems due to design realised with obsolete code:

Columns are generally precast elements connected at the bottom to a socket foundation and at the top by horizontally sliding or fixed support to the beams and they can be assumed to act as cantilevers fixed at the base.

In presence of strong earthquakes, precast columns display loss of verticality due to a rotation in the foundation element caused by a possible inadequate column-to-foundation connection or plastic hinge development at the column base evidenced by extensive cracks at the base with the expulsion of a part of the concrete cover in the critical zone of the column (Figure 2.4c).

a b c

Figure 2.6 Column rotation due to the formation of a flexural plastic hinge.

Inadequacy of the connection between cladding panels and structures:

Several failures of external cladding panels are observed. Usually, two different layouts of RC cladding panels walls are adopted, consisting of horizontal or vertical panels.

The main reasons of the collapse of cladding panels can be attributed to the lack of seismic design in cladding panel-to-structural element connection devices, the hammering of roof elements, columns or other precast panels and the additional lateral forces in the connection devices caused by the panel-to-structure interaction, not considered during the design process.

Horizontal cladding panels are particularly vulnerable, because of the lack of appropriate fastening devices to anchor the panels: usually, each level of cladding panels is supported by the lower level. Each panel has two connectors in its upper part, attached to specific steel profiles fixed only in the concrete cover of columns but, since columns exhibit large horizontal displacements in the plane of panels and panels are very stiff in plane, high relative displacement demands are produced in the connectors (especially in the upper cladding panels).

The behaviour of vertical cladding panels is better than horizontal ones when clamped at the base on RC foundation beams and/or on concrete pavements; they also provid a significant additional stiffness and strength to the external columns of the building. Some collapses of vertical panels are observed when they are not properly restrained on the foundations (Figure 2.5a).

In Figure 2.5c the collapse of a vertical panel-to-beam connection is shown: in this case, a particular connection device is used, a steel profile is embedded in the beam and some hammerhead elements are welded to the profile and inserted into the anchor channel of the vertical precast panels. Under the seismic action, the screw-to-profile welding fails and causes the collapse of the panels.

a

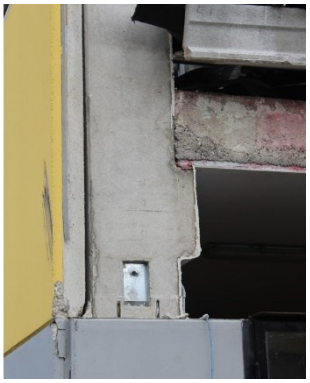

b

c

Figure 2.7 Inadequacy of the connection between cladding panels-structures: a) Collapse of precast cladding panels not properly restrained at the base; b) e c) Damage of fastening devices for the panel-column connections when their deformation capacity is exceeded.

3 Chapter - Vulnerabilities of industrial precast structures

The seismic behaviour and the vulnerabilities of industrial structures are taken into account in this chapter. In the first part vulnerabilities of reinforced concrete structures cast in place with precast reinforced hollow brick light-weight vaults (in particular SAP vault) are evaluated.
Only scientific literature from the architectural point of view is reported despite the huge diffusion of this constructive system.
In the second part, typical vulnerabilities of precast structures are identified in the frame structures, with the awareness that the most diffuse construction concerning the precast buildings consists of this typology. Scientific literature and the associated European projects concerning these aspects are summarised.
At the end of the chapter, vulnerabilities valid for both types of structures analysed are listed. A brief description of research related to economic loss for contents and business interruption due to the occurrence of seismic vulnerabilities is also reported.

3.1 Specific vulnerabilities of reinforced concrete industrial structures cast in place with precast reinforced hollow brick light-weight vaults (SAP vault)

The columns and main beams that compose reinforced concrete industrial structure cast in place are the same of normal RC building designed during low-code before the seventies. The presence of slender columns with poor reinforced longitudinal bars and stirrups and main beams designed stronger than the column can only bring a worse situation with very high load and huge dimensions of structures.
The vulnerability of this type of structure depends on the poor design of main elements that characterise structural design but also from vaulted system SAP.
SAP vault is composed of reinforced hollow brick joints with longitudinal concrete ribs (quantity depending on the span) with eliminated thrust thanks to the chains.
The static scheme and the specific vulnerabilities of this particular vault are analysed in detail in the following paragraphs.

3.1.1 Static scheme of SAP vault

Vaulted structures are mainly widespread at the beginning of the thirties to cover span starting from 20 meters for their ease of assembly and the low cost of raw materials (brick).

The static schemes of vault structures depend on the span/rise ratio:

- Vault with three hinges on fixed springer;
- Two-hinged vault (span/rise≤10);
- Vault to a hinge;
- Continuous vault without hinge (span/rise≤6).

The continuous vault without a hinge and the one or two hinged vault patterns are obtained starting from an arch with three hinges (one in keystone and two in the springers) for subsequent sealing with concrete cast in place respectively of all, two or one hinges. Sap vaults are continuous vaults with longitudinal ribs usually positioned in the vault so as not to exceed the length of three meters to SAP joists composed by reinforced hollow brick.

Usually, the study of the stability of the elastic equilibrium of the vault is conducted in the hypotheses:

- initial shaping of the vault made according to the funicular of its weight q passing through the springer and the key to guarantee the absence of the bending characteristic;
- the axial force and the thrust H are constant;
- not very low vault.

As emphasized by Capozzi's research [36], the main problem of vaults in curvilinear direction is the horizontal thrust that arises from the springers. This thrust, sometimes very high, cannot be absorbed by the slender column: the most widely adopted solution, also for RDB system, consists of vaults with thrust eliminated by some chains placed at the springers at a distance of about 1.50mt.

The chains are made up of large diameter steel bars connected to the vault by small diameter rods (ϕ10 ÷ 12), to reduce the bending of own weight and any loads and equipped with one or more tensioners. The turnbuckles, besides serving to lightly pull the chain before the disarming of the vault, have the function of allowing the junction of the chain sections, stretch that with rounds of ϕ20 ÷ 28 can be long at most on 10-15 m, depending on the diameter.

3.1.2 Specific vulnerabilities of SAP vault

SAP vault has a series of vulnerability due to:

- lack of a continuous slab in the extrados of SAP vault so for this structure deformable floor is considered (there are some pieces of concrete slabs only for two meters near springers to cover eventual negative bending);
- oxidation of the reinforcement bars inside the hollow bricks due to the very small cement mortar covers (This vulnerability is visible only once it happens).
- Industrial live load usually hangs on the vault that they bring additional mass to the roof in case of a seismic event and that they change the line of thrust of the vault.

Particular attention has to be guaranteed for the state of conservation of the chains and of turnbuckles in all conditions and in any work environment to avoid the rupture of chains and the consequent fragile collapse of the vault.

3.2 Typical vulnerabilities of precast frame structures

As defined by chapter 7.4.5 of NTC2018 industrial frame structures are classified as "Precast structure with columns fixed at the base and hinged with horizontal structures at the top". This sentence underlines how the connections between structural elements play a fundamental role in the vulnerability of this structures.
Typical vulnerabilities of precast frame structures can be summarised as:

- Lack of good connection between different structural elements such as roof elements, roof element-beam, beam-column, column-foundation and cladding panels-structural element;
- Loss of lateral stability of high main beams. This kind of failure highlights the importance of evaluating overturning actions on tapered beams in design criteria.

All the topics listed above are examined in detail.

3.2.1 Lack of good connection between different structural elements

The lack of good connection between different structural elements can be defined as the crucial problem of precast frame structures because, as shown in chapter 2.2, in Italy the first formal indications of the design of this element start only from

DM1987 (Every company was free to design the construction detail without the request for certain performance characteristics).
The scientific literature tries to investigate the seismic behaviour of the most recurring connections even with the activation of European projects. In the Table 3.1 the European funds allocated for the projects concerning the connections in the precast structures are listed: the issues addressed concern the beam-column and the cladding panels-structure connections.

EUROPEAN PROJECTS			
Code	**Topic**	**European funds**	**Link**
GROWTH	"Precast structures EC8: Seismic behaviour of precast concrete structures concerning Eurocode 8."	FP5 project (1998/2002)	http://cordis.europa.eu/programme/rcn/642_en.html
PRECAST IB	"Seismic Behaviour of Precast Reinforced Concrete Industrial Building"	FP6 project - MOBILITY (2006/2007)	http://cordis.europa.eu/project/rcn/99014_en.html
SAFECAST	"Performance of innovative mechanical connections in precast buildings structures under seismic conditions."	FP7 project (2009/2012)	http://cordis.europa.eu/project/rcn/90245_it.html
SAFECLADDING	"Improved Fastening Systems of Cladding Panels for Precast Buildings in Seismic Zones"	FP7 project (2012/2015)	http://www.safecladding.eu/ http://cordis.europa.eu/project/rcn/104571_en.html
STREST	"Harmonized approach to stress tests for critical infrastructures against the natural hazard."	FP7 project (2013/2016)	http://www.strest-eu.org/opencms/opencms/ http://cordis.europa.eu/project/rcn/110339_en.html

Table 3.1 European projects concerning precast structures.

All types of connections are analysed in detail, except the cladding panels-structure interaction, which will be dealt in detail in chapter six, as one of the main topics of precast structure treated in this research.

3.2.1.1 Beam-Column connection

The beam-column connection is of particular importance because it combines two "primary" elements in the resistance to the seismic action of buildings. The main function of this connection is a union that it has to resist horizontal forces, preventing relative translation between the elements and, therefore, the loss of support of the beam. In Italian contest, this union is mainly schematised in two ways: only a friction union with a neoprene bearing interposed between the two main elements and a union characterised by neoprene support by one or two steel pin-dowels; these are drowned in the column and solidarised in operation on the beam.

An innovative enhanced structural frame system, based on the adaptation of hinged beam-column joints into rigid through the activation of special mechanical connection devices is proposed by Dal Lago et al. [37]. While keeping all the benefits of the dry prefabrication, the resulting moment-resisting frame is provided with enhanced redundancy and stiffness. A design comparison among three precast frames with similar geometries and different static schemes shows how the joint adaptation can be exploited to optimize the structure by modifying the distribution of bending moment.
With the aim of allowing the structure to dissipate an appropriate amount of energy, Belleri et al. [38] propose several devices to apply at the beam-to-column connection of hinged portal-frames in order to increase the connection degree of fixity, to limit the damage at the column base and to reduce residual drifts during a seismic events.

Friction type connection
Before DM1987 in Italy, many precast industrial buildings built between the 1950s and 1970s have beam-column connections with strength coming from neoprene–concrete friction. Technical bibliography like CNR10018/87, CNR10018/99 and UNI-EN 1337:3 provides many and different formulas to evaluate this coefficient. Several numerical studies and experimental tests are realized to evaluate the neoprene–concrete friction coefficient.
Concern this topic, Magliulo et al. [39] carry out three types of experimental tests: tests on neoprene hardness, tilting and pulling tests; in the last case, the specimen is also axially loaded. Tilting tests provide a value of the mean friction coefficient equal to about 0.5. Pulling tests underline a friction strength dependence on axial load and, in particular, a decrease in the friction coefficient as the axial load increases.
By experimental results, authors propose a relationship for compressive stress–neoprene–concrete friction coefficient:

$$\mu = 0.49 \quad if\ \sigma_v \leq 0.14\ N/mm^2 \tag{3.1}$$

$$\mu = c + \frac{\beta}{\sigma_v} \quad if\ 0.14 < \sigma_v \leq 5\ N/mm^2 \tag{3.2}$$

where σ_v is the compressive stress in N/mm^2, β = 0.055, c = 0.1 and $\sigma_v = 5\ N/mm^2$ is neoprene maximum compressive strength according to CNR 10018. Considering that tilting tests are less realistic than pulling tests, the only formula (3.2) should be practically applied, limited to the range $1.5 < \sigma_v \leq 5\ N/mm^2$. The friction coefficient determined by experimental tests with compressive stress between $\sigma_v = 1.7 N/mm^2$ and $\sigma_v = 5.3 N/mm^2$ varies in the range 0.09–0.13;

furthermore, it lightly decreases as the normal stress increases, confirming the data found in bibliography. The low values of the friction coefficient provided by the tests and the results of numerical analyses reported in other papers underline the low resistance to the seismic actions of the precast industrial buildings whose beam–column connections are not pinned; they, even for earthquakes of medium intensity, can collapse for loss of support.
Ercolino et al. [40] use this formula to evaluate the seismic assessment of a real precast RC industrial building with friction connections with a detailed nonlinear structural model made with OpenSees code and nonlinear dynamic analyses are performed with the recorded accelerations time-histories of the two seismic events of Emilia Romagna. By comparing the numerical results with the real response of the structure, the adopted model is validated and the main damage typologies are also justified.

Dowels connection
The dowel system is one of the most common beam-column connections in some areas recently considered as seismic. It is a mechanical device that allows the transmission of horizontal actions and it generally consists of one or more steel dowels embedded in the column and inserted in a beam hole, filled with mortar. The dowel connection can be defined as a semi-rigid transverse union. Significant experimental and numerical researches on the seismic behaviour of new precast structures with dry pinned connections are conducted in the framework of two European projects: the "Growth" FP5 project, "Precast structures EC8: Seismic behaviour of precast concrete structures with respect to Eurocode 8 (Co-Normative Research)" and the FP7 project, "SAFECAST: Performance of innovative mechanical connections in p.c. structures under seismic conditions".
In scientific literature, the pins are assumed to be a pile in a Winkler material loaded by a horizontal force H located at a certain distance from the concrete surface. Two main cases of dowel interaction are presented.
The simplest one is a one-sided pin dowel (Figure 3.1a). The bar is embedded at one end and it is loaded by shear force acting along the joint face. The second case, double-sided pin dowel, is a dowel pin embedded in elements on each side of joint and plastic hinges will ultimately be formed on each side (Figure 3.1b).

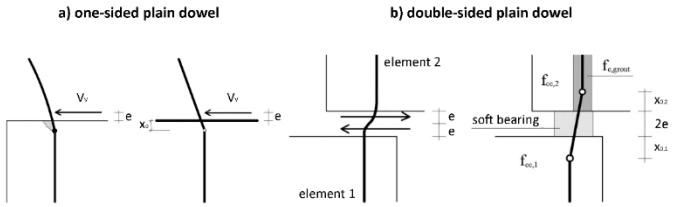

Figure 3.1 Shear transfer by dowel action: a) one-sided pin dowel; b) double-sided pin dowel.

The failure of these connections is assumed to take place when such a mechanism is formed.

Various failure modes are possible depending on the strength, dimension and position of the dowel pin: steel shear failure, concrete crushing failure or steel flexural failure (combined steel/ concrete failure). A weak bar in a strong concrete element might fail in shear of the bar itself. A strong steel bar in a weak element or placed with a small concrete cover will more naturally result in spalling of the element itself. However, when the bar is placed in well-confined concrete, the dowel pin normally fails in bending by the formation of a plastic hinge in the steel bar. The same occurs when the spalling effects are controlled by properly designed spalling reinforcement.

Clementi et al. [41] summarise all the formulas to calculate the shear strength of the connection.

First of all, they are reported formulas of the shear strength of the one sided-dowel connections.

The CNR 10025/84 provides a formula to evaluate the monotonic shear strength of the dowel connection. According to this code, the connection shear strength is equal to:

$$V_{Rd} = c\, d_b^2 \sqrt{f_{yd} f_{cd}} \tag{3.3}$$

where d_b is the dowel diameter, f_{cd} is the concrete design compressive strength, f_{yd} is the dowel design yielding strength and c is equal to 1.2 (without confinement) or equal to 1.6 (with confinement). The confinement effect refers to the presence of compressive stresses, perpendicular to the shear direction. This formula is valid if the eccentricity (e) of the shear force is less than half of the dowel diameter (d_b). The CNR formulation does not consider the influence of the concrete cover on the connection shear strength, because it supposes that the connection failure always occurs for steel flexural failure.

According to Vintzeleou and Tassios [42], there are two possible dowel connection failure: the steel flexural failure based on the same model of CNR, and the concrete

spalling based on the equilibrium of system forces in cracked reinforced concrete. The two mechanisms depend on the concrete cover size in the direction of the load (frontal cover) and the perpendicular direction (lateral cover) concerning the dowel diameter. The steel flexural failure occurs when the concrete covers are greater than 6–8 times the dowel diameter. If the shear force eccentricity is negligible, the connection shear strength is equal to:

$$V_{Rd} = 1.3\, d_b^2 \sqrt{f_{ys} f_{cc}} \tag{3.4}$$

where f_{ys} is the yield stress of the steel and f_{cc} is the concrete compressive strength, 1.3 is the coefficient that considers the influences of distance to free edges. If the concrete cover is lower than 6–8 times the dowel diameter, the strength of the connection is related to the concrete failure rather than to the dowel crisis (concrete spalling). Depending on the ratio between the concrete cover in the load direction (frontal cover C_F) and in the perpendicular direction (lateral cover C_L), a bottom spalling (the failure of the frontal cover) or a side spalling occurs. For low values of C_L/C_F, a side spalling occurs, and the connection shear strength is equal to:

$$V_{Rd} = 2\, d_b\, b_{ct}\, f_{ct} \tag{3.5}$$

where b_{ct} is the net width of the concrete section, evaluated as the section width (normal to the load) minus the diameter of the dowels, and f_{ct} is the concrete tensile strength. For high values of C_L/C_F, on the other hand, a bottom spalling occurs, and the connection shear strength is equal to:

$$V_{Rd} = 5\, d_b\, c\, f_{ct}\, \frac{c}{0.66\, c + d_b} \tag{3.6}$$

where c is the frontal concrete cover. The concentrated reaction splits the element, but the spalling can be controlled by reinforcement designed to establish an equilibrium system in cracked reinforced concrete. Different formulas are proposed for cyclic loads and eccentric force by Vintzeleou and Tassios. In the existing RC precast buildings, there is at least a thin neoprene film. So that there is a low eccentricity for the shear force and the only equation valid for cycling load is used:

$$V_{Rd} = 0.65 {d_b}^2 \sqrt{f_{yd} f_{cd}} \tag{3.7}$$

which is the Eq. (3.4) reduced by a factor 0.5.

For the Fib n. 43 [43], when the dowel pin is not very weak respect to the surrounding concrete, the steel bar fails when a plastic hinge appears in the cross-section with the maximum bending moment. This corresponds to the steel flexural failure mode which is associated to a significant dowel settlement bar that crushed under the high compressive stresses. With reference to a one-sided pin dowel,

without end anchor and loaded by shear along the joint face with no eccentricity, the monotonic shear capacity is equal to:

$$V_{Rd} = \alpha_0 {d_b}^2 \sqrt{f_{yd} f_{cd}} \tag{3.8}$$

where $\alpha_0 = \sqrt{\beta_c / 3}$ is taken equal to 1.0 like recommended by the Fib n. 43. In the previous, β_c is a factor that considers the tri-axial local state of stress of concrete. The shear capacity of one-sided dowel pin is evaluated with $\alpha_0 = 1.16$.
For the Model Code 2010 [1] the resistance of the dowel pin is calculated with

$$V_{Rd} = k_2 \, A_s \sqrt{f_{ys} f_{cc}} \leq \frac{A_s \cdot f_{ys}}{\sqrt{3}} \tag{3.9}$$

where $k_2 = 1.6$ and A_s is the dowel area.
According to Soroushian et al. [44], the shear strength for the dowel bars if the force is applied against the concrete core is:

$$V_{Rd} = 0.5 f_b (0.37 \gamma d_b - c') \frac{0.45}{\gamma} \, f_{ys} d_b^2 \, (1 - \frac{T^2}{T_y^2}) \tag{3.10}$$

where γ = $\sqrt[4]{E_s / K_f \cdot d_b}$ k_f is the concrete foundation modulus (271.7 MPa/m), $f_b = 37.6 \left(\sqrt{f_{cc}} / \sqrt[3]{d_b} \right)$ is the concrete bearing strength, $c' = 0.05 \, {f_{ys} \cdot d_b} / {f_{cc}} \cdot \sin \alpha$ is the length of the crushed concrete zone and it takes into account the inclination α of the bar, T is the dowel bar axial force, T_y is the dowel yield axial force. When the force is applied against the concrete cover the same authors provide an equation to calculate the strength of connection:

$$V_{Rd} = 0.83 \, \psi b_{ct} f_{ct} \tag{3.11}$$

where $\psi = \pi \left(2 \cdot \sqrt[4]{\frac{K_f \cdot d_b}{4 \cdot E_s I_b}} \right)$ is the distance from the crack face to the inflexion point.
When the dowel pin is embedded on the two sides of the joint (Figure 3.1b), a point of deflection develops at the joint interface. For a certain shear force, a plastic hinge is formed in the dowel pin at the weaker side, while the dowel still has an elastic behaviour at the stronger side. Hence, the load can be increased further until a plastic hinge is also formed on the other side. However, the stiffness of the shear connection is reduced by the formation of the first plastic hinge. The ultimate capacity of the connection is determined by the formation of the second hinge. The new formulation is reported in the SAFECAST Project [23], for the spalling of concrete edges. It is assumed that the shear strength is

$$V_{Rd} = \frac{1.4 \, k \, d_b^{\alpha} \, h^{\beta} \sqrt{f_{ck,cube} \, c^3 \, \psi_{re}}}{\gamma_c} \tag{3.12}$$

where $f_{ck,cube}$ is the characteristic compressive cubic strength of concrete, c edge distance of the dowel axis, $h = 8d_b$ length of the dowel, b width of the column, n number of dowels, $\alpha = 0.1\left(h/c\right)^{0.5}$, $\beta = 0.1\left(d_b/c\right)^{0.2}$ and $k = b/(3c) \leq n$.

Based on the results of experiments performed in SAFECAST project context, modified formulas (3.4) are proposed by Psycharis and Mouzakis [45], which take into account the cyclic behaviour of the realistic beam-to-column dowel connections:

$$V_{Rd,sr} = 1.1\ d_b^2 \sqrt{f_{yd} f_{cd}} \tag{3.13}$$

$$V_{Rd,lr} = 0.9\ d_b^2 \sqrt{f_{yd} f_{cd}} \tag{3.14}$$

where $V_{Rd,sr}$ is the ultimate resistance of the connection if small rotations between beam and column are expected, $V_{Rd,lr}$ is the ultimate resistance of the connection if large rotations between beam and column are expected.

Several experimental tests and FE numerical model using concrete smeared crack approach are done to validate failure mechanisms and the formulas described above.

Inside European FP7 project SAFECAST, D. Kremmyda et al. [46] say that the shear resistance of precast pinned beam-to-column connection is affected by the presence of confinement reinforcement at the connected elements and close to the loading interface, especially in the cases of cyclic loading.

Magliulo et al. [47] confirm the expected behaviour of this kind of connection under horizontal load, showing a brittle splitting failure in the concrete lateral cover of the column. They show many case studies that they are implemented by varying the diameter of the dowels as well as the lateral and frontal concrete covers of the column that underline the sensitivity of the model to the parameter's variation regarding strength and failure mechanism. It is confirmed that, if the lateral and the frontal covers are lower than 6–7 times the dowel diameter, the failure involves the concrete splitting, also in the case of a force acting against the concrete core. Furthermore, if the lateral cover is equal or lower than the frontal cover, the side-splitting occurs; otherwise, only in the case of a force acting against the concrete cover, the failure also involves the bottom splitting. The results of the parametric study are finally compared with the CNR 10025/ 84 and the Vintzeleou and Tassios relationships and the failure mechanism that involves the steel dowel and the surrounding compressed concrete are very similar and generally they are the closest to the results of the numerical analyses.

In their experimental tests, Zoubek et al. [48] [49] validate that the failure mechanism is initiated by flexural yielding of the dowel and crushing of the

surrounding concrete, the strength of the connection depends on the depth of the plastic hinge in the dowel, neoprene bearing pad can increase the strength of the connection, especially when large relative displacements between the beam and the column are developed. In the end, experimental and analytical results demonstrate a 15– 20% drop in the resistance of the connection due to the damage induced by large rotations between the beam and the column.

3.2.1.2 Roof elements and roof element-beam connections

In general, one of the main damage to precast structures with the deformable floor is related to the failure of connections between beams and roof elements which led to the loss of support of the structural elements.
For the deformable roof, tiles are usually bound to the beams using simple support without the mechanical device, bolted metal brackets in the case of a tile provided with ribs or bottom, beaten nails for flat or pseudo-flat tiles and longitudinal or connecting metal bars. The dynamic behaviour of all precast structures with this type of connection is not simple to determinate: Ferrara et al. [50] analyse with a sample structure different arrangements of the roof deck through a modal analysis to evaluete the transfer and diaphragm forces referred to the interconnected roof elements.
To resolve the problem of loss of support of roof elements, the use of ductile connections between precast beams and roof elements suitable for both new structures and as a retrofit measure of existing ones is investigated [51]. These connections can transfer the horizontal inertial loads and to accommodate deformations arising from seismic displacement compatibility.

3.2.1.3 Column-Foundation connection

The pocket foundation is the traditional column-to-foundation connection, a monolithic connection [52] where the column is inserted into a special pocket arising from the base footing. The temporary bearing is ensured by the crane and provisional props are fixed after the verticality regulation is made with wedges. The joint is finally filled in-situ with concrete pouring.
The efficiency of the pocket foundation is investigated by Saisi [53] who shows extensive experimental tests.
Dal Lago et al. [54] study different types of mechanical connections which are characterised by dry or semi-dry assemblage, temporary self-support of the column (to reduce the crane holding time) and mechanical regulation of verticality. These

mechanical connection devices, even if correctly designed for what concerns resistance, may affect the behaviour of the whole joint improving the ductility capacity of the columns and their energy dissipation properties: this experimental campaign is performed at Politecnico di Milano as part of the Safecast project.
Other alternatives are constituted by the use of precast piles or foundations superficial ribbons, respectively in the case of poor load-bearing capacity or problems of structural verification of the plinth.
If mat foundation is more convenient than isolated footings, the following column-to-foundation connections are typically used: bolted base plates embedded in the foundation, foundation pockets in which the columns are placed and grouted, grouted sleeves and mechanical splices.
Belleri et al. [55] analyse the behaviour and performance of grouted corrugated steel sleeve connections in mat foundation under cyclic loading. The experimental program shows that grouted steel sleeves are suitable as column-to-foundation connections in seismic regions (The high ductility of these connections is related to the confining effect of the corrugated steel sleeves on the grout).

3.2.2 Loss of lateral stability of high main beams

During the Emilia-Romagna earthquake, numerous cases of loss of the beam-column support concern the double-slope tapered beams: in the early prefabrication periods, typical pre-stressed beams of the Italian built were around 18 meters and 1.20 meters of mounts while in the last phases they arrived up to cover a light of 28 meters with mounts of 2.20 meters.
These structures have a huge mass concentrated in the apex of the mount and therefore at the point of maximum displacement, but usually, in the realization of the numerical model, these beams are erroneously schematised with a constant section beam with consequent lowering of the periods concerning reality, greater force but even less displacement.
To avoid overturning of the main double-tapered beams during the fixing, in several cases RC forks are placed at the column's top. In the constructive practice, the forks can be armed, weakly armed or armed only with completion elements. Subsequently to seismic events, it is observed how these elements react very well to the first damage preventing at least in an initial phase the rocking of the boomerang beam.
Cornali et al. [56] consider concrete fork at the top of the column modelling it in different ways, realising different types of finite element models to evaluate the influence of modelling assumptions in the expected loss.

3.3 Typical vulnerabilities of an industrial building

The typical vulnerabilities of each industrial building independent of the type of structure considered are listed and explained in detail in the following paragraph:

- Infill masonry usually displaced for industrial aims on the irregular manner within the structures;
- Shear crisis of short column;
- Damage for the loss of stability of the items stocked in warehouses.

3.3.1 Infill masonry usually displaced for industrial aims on the irregular manner within the structures

Irregularities are weak points in a building which may cause failure of one element or total collapse of the building during an earthquake.
The irregular arrangement of the infill masonry can lead to a change in the dynamic behaviour of the structure, creating a strong eccentricity of the stiffness of the structure and different stress of the structural elements involved. They also increase the dispersion of the participating masses of the main vibrating modes.

3.3.2 Shear crisis of short columns

Short columns may be formed because of different geometrical situations like band windows, mid-storey beams for crane supports or semi-infilled frames: sometimes, they are slender columns that have heavy cracks due to the shear stress concentration in points not calculate to resist of this action.

3.3.3 Damage for the loss of stability of the items stocked in industrial buildings

Storage shelves, given the huge mass carried, can cause damage to the structure and/or losing the contents they brought as observed during the Emilia Romagna earthquake. Removal of any connection is recommended between the racks and precast structure unless the connection is verified and the structure is safe under the transmitted forces.
A distinction have to be made between indoor or self-supporting shelves as reported to *"Linee di indirizzo per interventi locali e globali su edifici industriali mono piano non progettati con criteri antisismici"* [26].

Indoor shelving is affected by the weight of stored goods and by the seismic action. The height varies from a few meters in case of shelving in warehouses open to the public, up to 18m-20m in the case of intensive warehouses. It is useful to note that more attention must be paid if the heights are less than 10 m because, above them, the pallets are moved only automatically (without any manual operator).
Self-supporting shelving are shelving directly attached to the cladding panel of the structures, affected by the climatic loads as well as by the weight of the stored goods and by the seismic action. The heights range from 10 m to 35 m and the movement of goods takes place automatically. It is underlined how the connections between racks and precast structure have to be flexible and permit displacements.

3.4 Effects of occurrence of vulnerabilities of industrial buildings: an economic loss for contents and business interruption

The value of contents and business interruption (in terms of revenue per day) is directly connected to structural vulnerabilities. Rodrigues et al. [57] compute the economic loss for 300 buildings in the province of Arezzo using a probabilistic event-based risk approach presented regarding annual average losses and losses at given annual rates of exceedance. They observe that risk reduction should be applied as a priority in the facilities that are compromising the current level of acceptable risk, and their results show that business interruption has a significant contribution for economic losses, whose repercussions go beyond the regional level.
Another approach for the probabilistic estimation of economic losses induced by the structural vulnerability is realised by Demartino et al. [58]. The economic losses are evaluated considering seismic hazard, structural response, damage resulting from the structural vulnerability and only structural-vulnerability-induced economic losses, structural repair and content losses induced by structural collapse. The uncertainties are accounted with Monte Carlo simulations. The estimation results are expressed regarding economic losses for each occurrence that stakeholders can use to make risk management decisions.
With a specific case study, Cornali et al. [56] compare fragility assessment with economic loss: they realise appropriate fragility curves under selected engineering demand parameters defined and provided within the Performance Based Earthquake Engineering methodology for the assessment of the expected losses under a scenario-based earthquake.

4 Chapter - Fragility curves of RC industrial structures cast in place with precast reinforced hollow brick light-weight vaults (SAP vault)

Seismic fragility is a measure of the likelihood of a building suffering damage for a given severity of ground shaking, represented by fragility curves, which describe the probability of reaching or exceeding a certain damage limit state for a given intensity of ground motion.

In this chapter the assessment of the robustness of the one of the first structures that started the precast process is analysed: this industrial building, in addition of specific vulnerability of the vaulted system, has problems with main elements designed in the thirties-sixties with low-code only with qualitative prescriptions.

This topic will be treated as follows: after a first analysis of the fragility curves realized in the scientific literature for the precast frame structure and a brief description about precast reinforced hollow brick light-weight vaults, the case study analysed is described with the creation of three numerical models all suitable to represent the vault. Definition of intensity measure and damage measure bring to the following realization of IDA curves with several ground motions according to the site.

Fragility curves are obtained with the main statistical methods suitable for the analysis of IDA curves and with alternative statistical methods for the treatment of other data deriving from other types of nonlinear dynamic analyses.

The comparison of fragility curves with different types of statistical methods is carried out between different numerical models and between X-Y directions, taking into account the behaviour of the vault and main structural elements.

Also, capacity curves are obtained from nonlinear static analysis and incremental dynamic analysis, relating them in terms of base shears and displacements for each direction considered.

4.1 Seismic fragility analysis for precast frame structures

Several studies are performed to evaluate the probability of reaching or exceeding a certain damage limit state for precast structures. Regarding fragility analysis, all typical vulnerabilities of precast frame structures are analysed concerning beam-column and cladding panels-structure connections.
Main researches are listed below.
Bolognini et al. [59] show a simplified pushover-based method for the definition of vulnerability curves with the analysis of four structural typologies defined as representative of the majority of the current Italian production and used to generate a random population of buildings. The structural behaviour of this population is evaluated through simplified pushover analysis and the generation of fragility curves is based on displacement capacity limits of the structures and the displacement demand, taking into account in the model the strength capacity of the connections calculated for pre-code buildings as the sum of the shear capacity of the RC elements on the top of the columns and the friction resistance of the connections identifing them as one of the weak points in terms of local resistance capacity and global seismic response.
After the earthquake of Emilia Romagna, systematic seismic risk studies are performed with incremental dynamic analysis (IDA) on some Italian precast industrial buildings respect the typical vulnerabilities of these structures.
To realise fragility curve, Casotto et al. [60] perform nonlinear dynamic analysis using two main categories of single-storey bare frame to represent the most common geometrical configurations of the Italian precast industrial building stock based on Bellotti's studies [19]. The first typology consists of a series of one-storey basic portal frames. Each portal is comprised of two or more columns fixed at the base and a saddle roof beam, usually simply supported by the columns or with shear resistant connections. The second common typology is one-storey frames linked by perpendicular straight beams, which carry the main roof beams or directly support the large span slab elements.
Based on these two typologies, hundreds of structures are produced through a Monte Carlo simulation to represent the common precast structure in Italy. The geometric properties of the structures generated are randomly sampled from probabilistic distributions obtained from 650 field surveys, while the material property distributions are found in the literature. As typical vulnerabilities, they consider the weak beam-column connections, which is the main cause of the total

collapse of the building due to loss of support of the beams (failure due to shear is not considered).
In Turkey, similar studies are performed by Palanci et al. [61] where damage limits of the building (Slight, Moderate, Extensive, Collapse) are determined by taking the critical value (minimum) of column damage limits.
With a specific case study of a precast frame structure with pin-dowel connections between beam-column designed with low-code, Mezzapelle et al. [62] propose a comparison with fragility curves realised with three different models varying the beam-column connection. In model one the connections are cylindrical hinges, in model two the connections are spherical hinges while model three has the same bending joints of model 2 but it has also horizontally deformable connections: main conclusions show that the fragility curves associated with Model three are major probability of collapse than those of Model one and Model two for all three damage states considered (thresholds damage state are considered for a determined number of elements that reach chord rotation or shear strength).
Compared to the two categories previously analysed by Casotto et al., with the same methodology Beilic et al. [63] add fragility curves of a new category of industrial buildings designed with NTC2008 Italian code. In this study two modelling approaches for the beam-column connections are implemented in the numerical analysis: in the first approach, the connection is conceived as a hinge (pinned connection) while the second approach is developed to reproduce more realistically the behaviour of beam-column joints subjected to seismic excitation.
Also, Ercolino et al. [64] calculate the vulnerability concerning the collapse limit state of a parametric study of 40 industrial single-story RC precast buildings designed according to Italian NTC2008 seismic code. They carry out a comparison between the Italian code and the Eurocodes and multi stripe analyses are performed at ten intensity levels.
In all described studies, the effects of non-structural components are not taken into account for the estimation of the fragility functions.
Conversely, Babič et al. [65] investigate the seismic performance of existing single-storey industrial precast buildings, typical for Italy, conducting fragility analyses for twelve building classes which take into account different structural configurations, different design approaches and the effect of non-structural components such as vertical panels, horizontal panels and masonry infills. The vulnerability of load-bearing structures and cladding panels are analysed considering that the effect of the panels on the overall performance of a structure is often underestimated in the design. A lumped plasticity model is developed for each building using Open Sees software. The fragility functions are calculated for four damage states, which are

defined by the physical damage depending on how many non-structural components are dislocated until structural collapse.
These studies observe that the impact of non-structural components on the collapse fragility functions is reflected in the shift of the fragility functions to the left and in an increase in the slope of the functions (the largest decrease is observed when there are masonry infills and structural configuration with low-code design).
Very interesting study but realised only for RC structure is Brunesi's research [66] that uses a fragility analysis in order to assess the probability of exceedance of different damage states given that a column loss event occurs for two building classes representative of European buildings designed for gravity loads and earthquake resistance in accordance with Eurocodes 2 and 8.

4.2 Main features of precast reinforced hollow brick light-weight vaults

4.2.1 History of the precast vault roof system

Reinforced hollow brick light-weight vaults have been widespread in all of Italy from the beginning of the Thirties of the last century to realise very large roofing structures mainly for industrial buildings.
In Italy, the methods used to construct vaults cast on place involved the use of light hollow brick blocks shaped to accommodate the reinforcement bars, supported by arch frames on which the concrete is poured.
In 1925 the S.A.P. (Senza Armatura Provvisoria) system of Erredibi have already been patented. It was based on a parallelepiped-shaped brick with holes near the edges and in the centre of the lower area, which were the slots for small-diameter metal support bars. Using this type of reinforced hollow brick, joists were quickly built. The assembly of curved beams of this type required a temporary scaffolding of simple load supports corresponding to the longitudinal ribbing joints. Moreover, there were then placed chains and lengths of added section reinforcements longer than the springers, whose length was calculated based on the pressure curve for more adverse load conditions.
The final laying was carried out beginning from the longitudinal ribbing joints and the springers, after the bricks were thoroughly soaked, and there then followed the positioning of the ribbing along the generating lines, filled with plastic sealing, rather than cement mortar, a rib every 10 m so as to create an expansion joint for the structure.

The SAP vault was cited in the Bollettino Ufficiale del Ministero LL.PP. n° 27 of 21-9-1937 –XV, as being able to be used in state buildings or those subsidised by the state.
In the same years, the R.D.B. Company was testing barrel vaults constructed with SAP curved beams of various sizes covering spans of more than 40m with 20cm thick hollow bricks in the experimental area of the Pontenure plan (Piacenza).

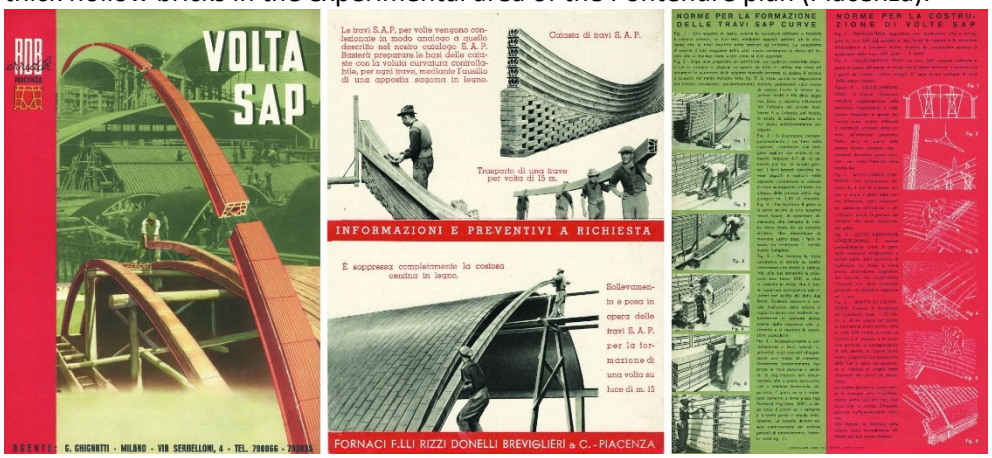

Figure 4.1 Construction phases of the SAP curved joists.

Several industrial structures were built with SAP20 system like “Saponificio Ambrogio Silva” in Seregno or “Azienda Tabacchi Italiani” in Piacenza.
The SAP system of the R.D.B. quickly spread and it was adopted in some particularly interesting projects, even from an architectural point of view, designed by Giuseppe Pagano, Piero Bottoni and Gaetano Minnucci. A brief description of this work is reported in Paolini et al. [67].
Evolution of the SAP system was the BISAP vault, a double precast hollow brick panel containing all the fast-fitting current reinforcement, CELERSAP vault, made up of very light joists in c.a. with curvilinear profile and ST’AR vault, a constructive system based on the properties of the special brick St'ar to hook upwards and lean down on the previous analogous elements placed in place so that the single arcs just complete can stand on their own.
Figure 4.2 shows images of structure systems of precast reinforced hollow brick light-weight vaults obtained from Italian user’s manual.

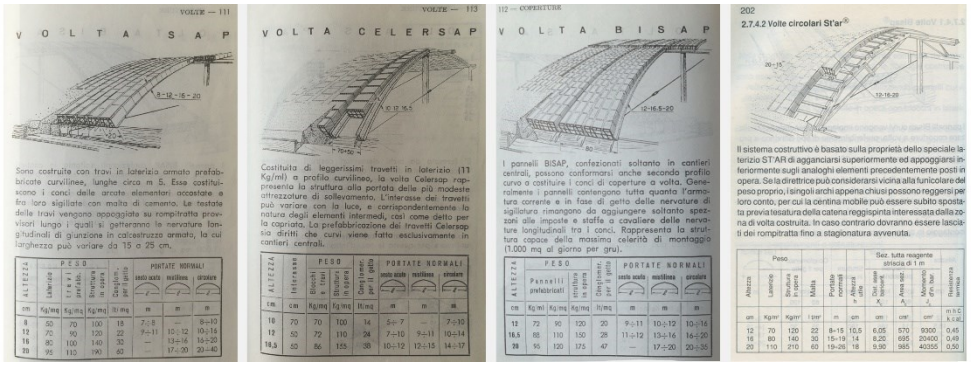

Figure 4.2 Images obtained from Italian user's manuals of reinforced hollow brick light-weight vault.

4.2.2 Structural scheme of SAP vault

In the sector of vaulted structures with eliminated thrust, the barrel vaults represent the most typical and widespread form in structural applications. Geometrically they are roofs generated by the translation of an arc of a circle; as already mentioned in the previous paragraph, they are characterised by constant cross-section made with hollow brick light-weight elements incorporating almost all the flexing reinforcement steel bars required. Using these precast joists, it was convenient for the companies to set up research on the best use of the span/rise ratio to identify a series of radii of curvature: in this case, the choice of the radius was of fundamental importance. The geometrical characteristics of the vault, the preferential rays with the corresponding rises and the structural scheme that leads to perfect interlocking reactions for a uniformly distributed load retrieved from RDB manual are shown in Figure 4.3.

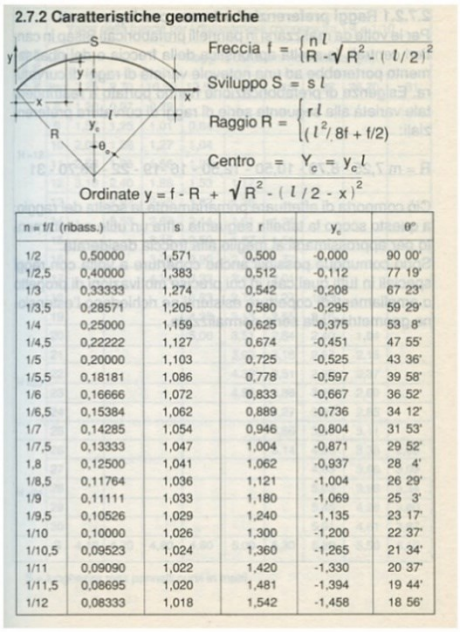

2.7.2 Caratteristiche geometriche

Freccia $f = \begin{cases} n\,l \\ R - \sqrt{R^2 - (l/2)^2} \end{cases}$

Sviluppo $S = s\,l$

Raggio $R = \begin{cases} r\,l \\ (l^2/8f + f/2) \end{cases}$

Centro $= Y_c = y_c\,l$

Ordinate $y = f - R + \sqrt{R^2 - (l/2 - x)^2}$

n = f/l (ribass.)		s	r	y_c	θ°
1/2	0,50000	1,571	0,500	-0,000	90 00'
1/2,5	0,40000	1,383	0,512	-0,112	77 19'
1/3	0,33333	1,274	0,542	-0,208	67 23'
1/3,5	0,28571	1,205	0,580	-0,295	59 29'
1/4	0,25000	1,159	0,625	-0,375	53 8'
1/4,5	0,22222	1,127	0,674	-0,451	47 55'
1/5	0,20000	1,103	0,725	-0,525	43 36'
1/5,5	0,18181	1,086	0,778	-0,597	39 58'
1/6	0,16666	1,072	0,833	-0,667	36 52'
1/6,5	0,15384	1,062	0,889	-0,736	34 12'
1/7	0,14285	1,054	0,946	-0,804	31 53'
1/7,5	0,13333	1,047	1,004	-0,871	29 52'
1,8	0,12500	1,041	1,062	-0,937	28 4'
1/8,5	0,11764	1,036	1,121	-1,004	26 29'
1/9	0,11111	1,033	1,180	-1,069	25 3'
1/9,5	0,10526	1,029	1,240	-1,135	23 17'
1/10	0,10000	1,026	1,300	-1,200	22 37'
1/10,5	0,09523	1,024	1,360	-1,265	21 34'
1/11	0,09090	1,022	1,420	-1,330	20 37'
1/11,5	0,08695	1,020	1,481	-1,394	19 44'
1/12	0,08333	1,018	1,542	-1,458	18 56'

Altezza struttura	Luce	Valori della freccia per i ribassamenti compresi fra 1/4 e 1/10 — Raggi di curvatura normalizzati (m)								
	(m)	7,25	8,70	10,50	12,50	16	19	22	26,70	31
H=12	8	1,20	0,97	0,79						
	9	1,57	1,25	1,01	0,84					
	10	2,00	1,58	1,27	1,04					
	11	2,53	1,96	1,56	1,27					
	12	3,18	2,40	1,88	1,53	1,17				
	13		2,92	2,25	1,82	1,38				
	14		3,53	2,67	2,14	1,61	1,34			
H=16	15			3,15	2,50	1,87	1,54			
	16			3,70	2,90	2,14	1,77			
	17			4,34	3,33	2,44	2,01			
	18				3,83	2,77	2,27	1,93		
H=20	19				4,38	3,13	2,55	2,16		
	20				5,00	3,51	2,84	2,40	1,94	
	21					3,93	3,16	2,67	2,15	
	22					4,38	3,51	2,95	2,37	
	23					4,88	3,88	3,25	2,60	
	24						4,27	3,56	2,85	
	25						4,69	3,90	3,11	
H=24	26						5,14	4,25	3,38	2,86
	27							4,63	3,66	3,09
	28							5,03	3,96	3,34
	29							5,45	4,28	3,60
	30							5,91	4,61	3,87
	S	4,10	4,70	4,80	4,80	5,00	5,30	5,30	5,50	6,10

S = lunghezza max pannelli curvi in metri

2.7.3 Reazioni d'incastro perfetto per carico uniformemente distribuito.

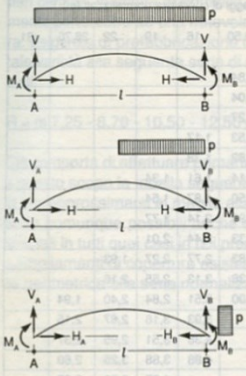

$M_A = M_B = (m_a + m_b)\,p l^2$

$H = 2\,h\,pl$

$V = 0{,}5\,pl$

$M_A = m_a\,pl^2$

$M_b = m_b\,pl^2$

$H = h\,pl$

$V_A = v_a\,pl$

$V_B = v_b\,pl$

$M_A = \overline{m_a}\,pl^2$

$M_B = \overline{m_b}\,pl^2$

$H_A = \overline{h_a}\,pl$

$H_B = \overline{h_b}\,pl$

$V = \overline{v}pl$

Incrementi per allungamento elastico del tirante e per variazione termica uniforme

Tirante elastico (mod. elastico E_t sez. unitaria A_t)

$\gamma = \dfrac{W_v}{l\,E_t A_t}\,\mu = c\,\gamma \qquad \eta = d\,\gamma \qquad \xi = \dfrac{1}{1+\eta}$

$Z = \xi H \qquad \Delta\overline{M} = -\mu\,\xi\,H\,l \qquad \Delta\overline{H} = -\eta\,\xi H$

Variazione termica + Δ°t = aumento

ε = coeff. dilatazione termica volta

$M = c\,W_v\,\varepsilon\,\Delta°t \qquad H = d\,\dfrac{W_v}{l}\,\varepsilon\,\Delta°t$

PARAMETRI MECCANO-ELASTICI E COEFF. PER IL CALCOLO DELL'ARCO CIRCOLARE INCASTRATO

n	c	d	h	100 m_a	100 m_b	100 v	100 v_a	100 $\overline{m}_a$	100 $\overline{m}_b$	100 $\overline{h}_a$	100 $\overline{h}_b$	100 v
1/2	8,5579	26,8856	0,14002	2,27711	-0,38743	10,610	39,390	2,3285	-4,8415	10,995	-39,005	5,3300
1/2,5	12,5273	48,553	0,16891	2,03439	-0,29345	10,172	39,828	1,0312	-3,0820	-8,732	-31,268	3,5768
1/3	16,6507	76,7897	0,18940	1,89724	-0,67247	9,930	40,070	0,8840	-2,1087	7,243	-26,090	2,5629
1/3,5	20,8150	111,359	0,22829	1,81206	-0,90446	9,783	40,217	0,6266	-1,5343	6,189	-22,383	1,9208
1/4	24,9689	152,061	0,25847	1,75558	-1,05656	9,688	40,312	0,4677	-1,1667	5,403	-19,587	1,4905
1/4,5	29,0925	198,751	0,28885	1,71620	-1,16157	9,622	40,378	0,3629	-0,9176	4,796	-17,427	1,1887
1/5	33,1803	251,329	0,31940	1,68774	-1,23701	9,575	40,425	0,2898	-0,7406	4,310	-15,690	0,9696
1/5,5	37,2323	309,722	0,35006	1,66649	-1,29303	9,540	40,460	0,2369	-0,6104	3,914	-14,267	0,8056
1/6	41,2494	373,863	0,38080	1,65005	-1,33592	9,514	40,486	0,1977	-0,5117	3,587	-13,080	0,6795
1/6,5	45,2410	443,770	0,41164	1,63747	-1,36907	9,493	40,507	0,1671	-0,4355	3,306	-12,078	0,5808
1/7	49,2127	519,444	0,44258	1,62787	-1,39498	9,477	40,523	0,1427	-0,3756	3,069	-11,217	0,5021
1/7,5	53,1462	600,641	0,47345	1,61907	-1,41696	9,464	40,536	0,1243	-0,3264	2,864	-10,469	0,4362
1/8	57,0640	687,543	0,50438	1,61206	-1,43475	9,453	40,547	0,1090	-0,2864	2,684	-9,816	0,3859
1/8,5	60,9787	780,277	0,53545	1,60701	-1,44874	9,444	40,556	0,0958	-0,2540	2,526	-9,239	0,3423
1/9	64,8588	878,413	0,56640	1,60171	-1,46153	9,437	40,563	0,0858	-0,2259	2,384	-8,727	0,3056
1/9,5	68,7352	982,314	0,59744	1,59766	-1,47190	0,430	40,570	0,0768	-0,2026	2,259	-8,267	0,2745
1/10	72,5954	1091,78	0,62847	1,59488	-1,48100	9,425	40,575	0,0695	-0,1828	2,144	-7,856	0,2480
1/10,5	76,4806	1207,43	0,65976	1,59244	-1,48727	9,420	40,580	0,0625	-0,1657	2,041	-7,483	0,2253
1/11	80,2902	1327,66	0,69058	1,59014	-1,49557	9,416	40,584	0,0571	-0,1509	1,947	-7,144	0,2052
1/11,5	84,2025	1455,37	0,72221	1,58789	-1,49826	9,413	40,587	0,0518	-0,1391	1,862	-6,834	0,1871
1/12	88,0016	1586,92	0,75312	1,58565	-1,50461	9,410	40,590	0,0471	-0,1275	1,783	-6,550	0,1726

Figure 4.3 Italian user's manual for the design of the SAP vault.

4.2.2.1 Horizontal tie bars

In thrust roofs like the vault system, the horizontal component of the springer reaction was normally countered by special metal tie rods equipped with a pulling device generally consisting of a double-acting tensioner at an intermediate point. The length of the chains was in general equal to the distance between main beams less 10 cm.
The peripheral anchorage from the inner one had to be evaluated separately. The peripheral anchorage was formed by turning the chain over into the peripheral beam around a crossbar, which acted as a key and which had a section approximately equal to that of the chain.
Several studies about hook anchorage of smooth rebar are done by Fabbrocino et al. [68].
The shaping schemes of peripheral anchorage reported from Italian user manual are shown in Figure 4.4.

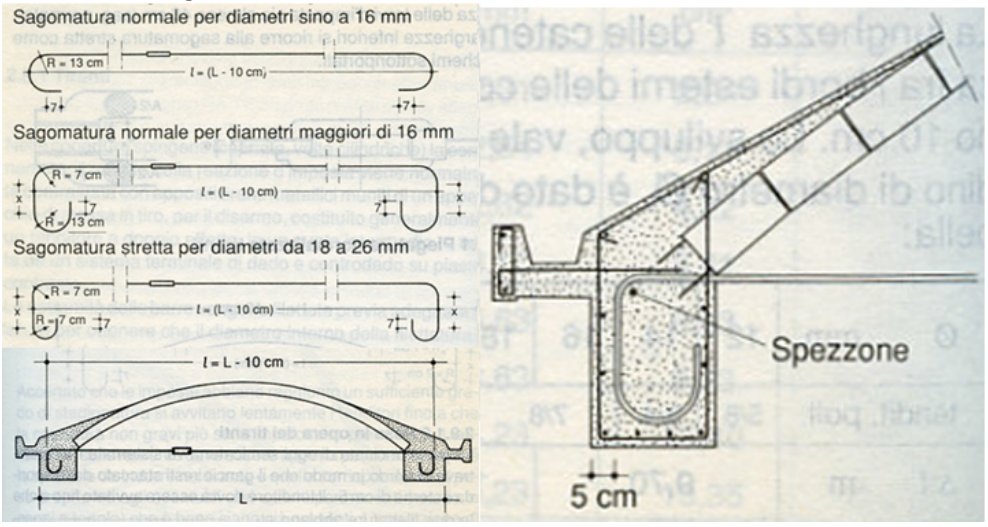

Figure 4.4 Shaping schemes of peripheral anchorage.

To anchor the chains in structures on which it was once set on both sides, it was also possible to have the continuous chain of continuous passage, without any anchorage, since, if the vaults were of the same size, the thrust of the one was equal to that of the other and therefore there was no need to transmit any force between the chains and the springer of the structure. This disposition in exercise was correct if the vaults were all equally loaded (Figure 4.5).

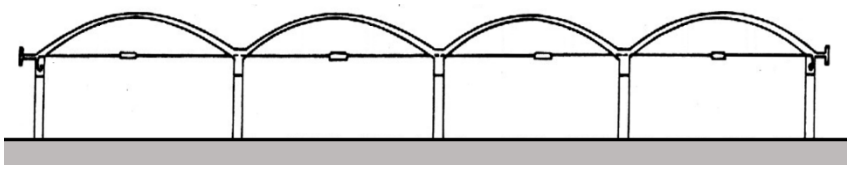

Figure 4.5 Continuous chains between subsequent vaults.

4.2.3 Operative phases of creation of SAP vault

The main supporting points of the scaffolding had to be made in correspondence with the longitudinal curves of the segments in which the arch was subdivided. For structures with precast curvilinear panels, the temporary scaffolding implied that it was realized in such a way that the panels rested both at the ends and at the centreline (assembling with cross-sections). There was the possibility of installation without intermediate cross-sections with panels that only rested at the ends on the ribs and intermediate lines. Several types of temporary scaffoldings are illustrated in Figure 4.6 obtained from RDB Italian manual.

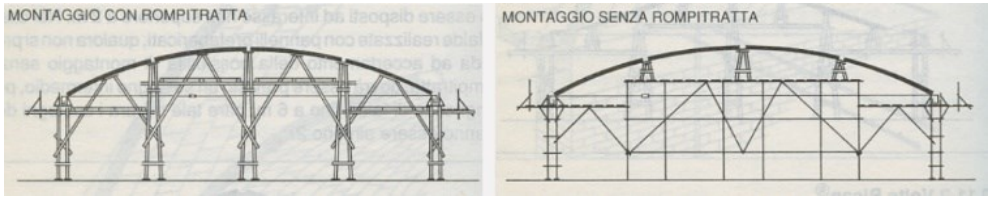

Figure 4.6 Assembly with and without a cross section of the vaulted system.

Once the placement of longitudinal curves of the segments composed by precast reinforced hollow bricks was completed, concrete casting operations had to take place in a single time starting from the springer beams together with the areas of the vault affected by the conglomerate abutment, subsequently the longitudinal joining ribs and the transversal current ribs in the transverse direction.
Assumed that the concrete of main beams (springer) reached sufficient mechanical properties, the tensioners were slowly screwed up until the vault no longer weighs on the temporary scaffolding. The lifting of the vault had to be barely perceptible since the tension to be induced in the tie rod was that corresponding to the own weight and any other possible permanent loads. This operation had to be carried out gradually with two or three successive phases.

4.3 Case study

A typical example of Italian reinforced hollow brick light-weight vaults structure is considered. From the analysis of the technical documents of this case study, necessary information for a proper definition of the numerical models as regards the main structural elements, containing details on light-weight vault, vault-beam, beam-column and column-foundation are extrapolated. All the characteristics of the structure taken into account are shown below.
The considered structure is a part of RC one-storey structure made in 1962 with 40x59.7 m rectangular shaped composed by three spans and a height under the beam of 6.00 m, consisting of columns, beams and precast vault roof.
For columns and beams, the concrete Class is C20/25 with elastic modulus equal to 26083 MPa and the steel Class is AQ50. External and internal columns have dimensions, respectively, 30x70cm and 40x70cm for the first 4mt of height starting from the concrete slab and dimensions of 30x50 and 40x50cm from 4mt to 6mt. External and inner beams are of 5.00 meters length with a rectangular section of 50x85cm. The roof is a SAP20 vault patented by RDB composed by reinforced hollow brick with three longitudinal ribbing joints of 28x20cm. The line of the barycentric axis of the vault is parabolic with a rise, at the centre line equal to 1/7 of the span (2.80mt). The vault is fixed in the main beams and the horizontal thrusts are absorbed by the fi30 diameter chains placed at a distance of 1.66mt in the springer. Near the connection beam-joists and for a length of about 2 meters, above the roof, an armed slab of maximum thickness up to about 20cm is added. The weight of the SAP20 vault is 1.72 kN/mq as reported by technical documents.
The columns and beams are cast-in-place while the roof is precast.
The foundations consist of plinths with piles and 20cm of concrete slab with an electro-welded net (industrial floor).
Some drawings concerning the project are reported in Figures 4.7- 4.9.

Type of precast structure	One-storey RC structure CAST IN PLACE with PRECAST ROOF
Year of construction:	1962
Plan dimensions:	40x59.7
Height under main beam:	6.00m
Dimension of columns:	40x70cm, 30x70cm
Dimension of main beam:	50x85cm
Type of roof:	Precast SAP20
Concrete Class:	C20/25
Steel Class:	AQ50

Table 4.1 Main features of the case study.

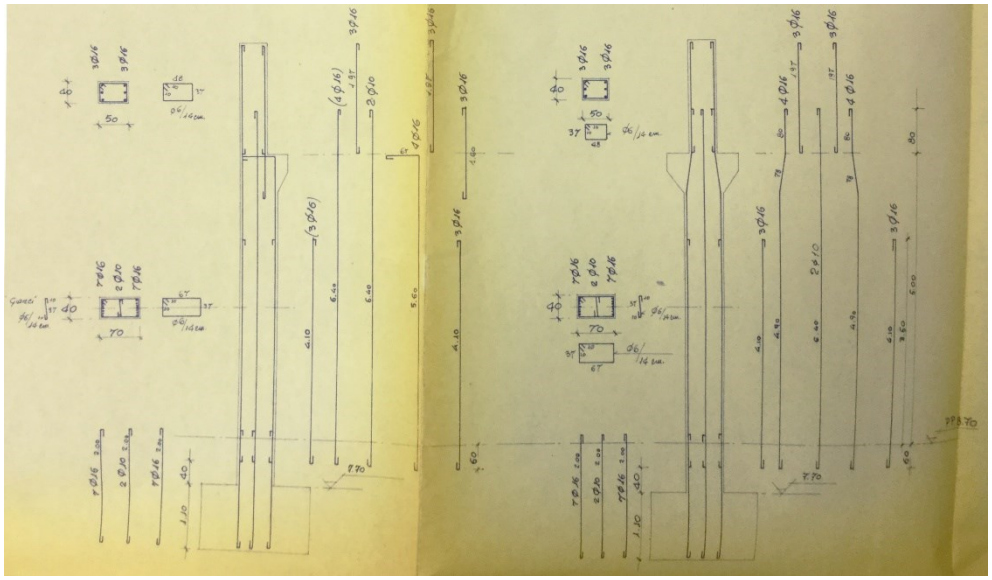

Figure 4.7 Longitudinal rebars and stirrups of columns of the case study.

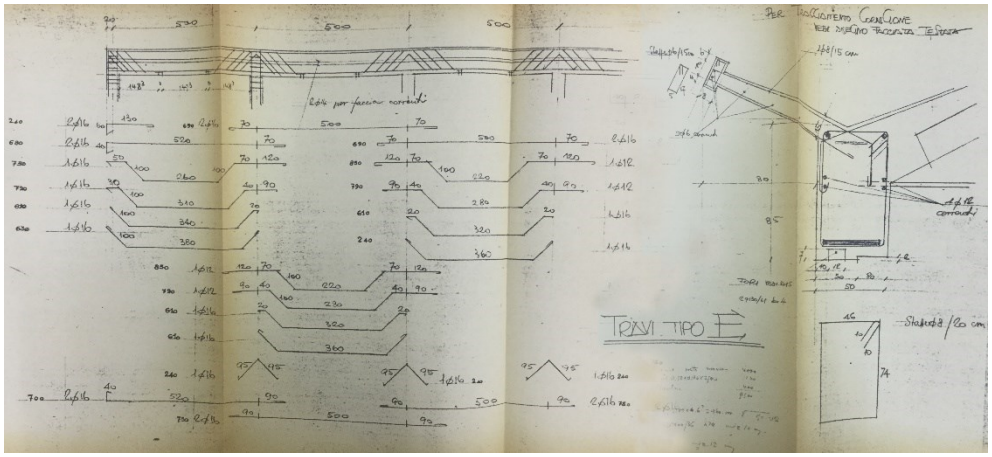

Figure 4.8 Longitudinal rebars and stirrups of beams of the case study.

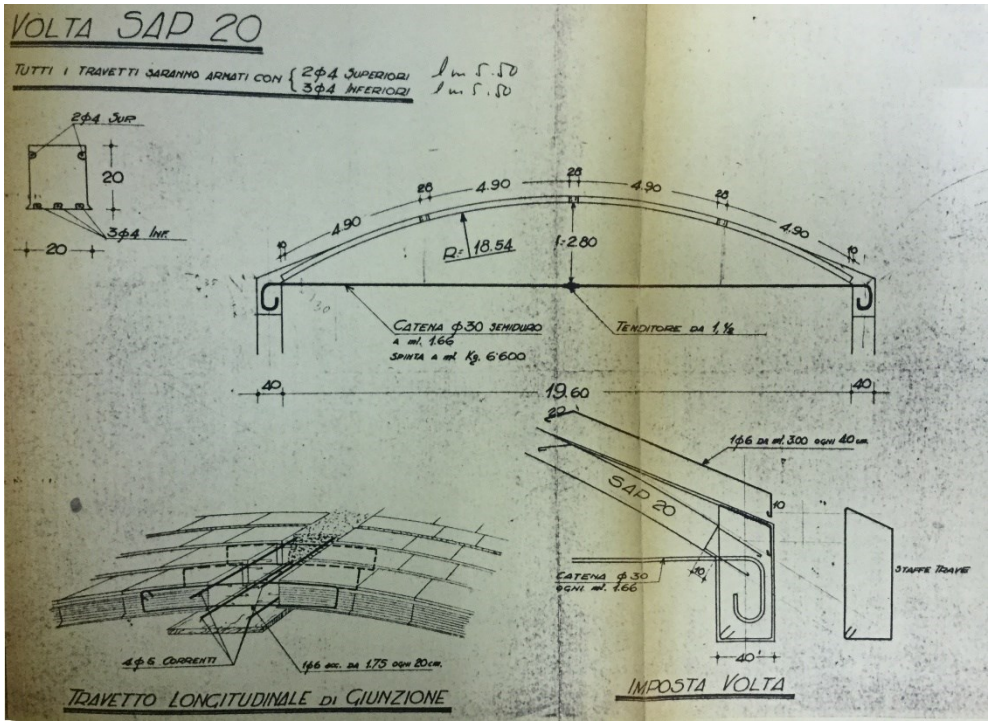

Figure 4.9 Design of SAP 20 vault of the case study.

4.3.1 Numerical Models

Using a commercial calculation code, three different models are realised to take into account the use of several method and elements to represent precast vault. The main features of all three models are reported below.
The main structural elements, used for the spatial discretization of beams and columns, are modelled as "beam" and they are made to act both in the elastic-linear and plastic field. The structure is fixed at the base at the level of the industrial floor.
As can be seen from Figure 4.8 the upper longitudinal reinforcing bars are continuous in the beam-column nodes, so the main beams are supposed fixed to the columns.
The seismic weights are obtained considering all structural and non-structural elements as well as live loads on the structures.
The infill walls are not considered for these analyses.
All chains of vault of three models are modelled as “truss” to transmit only axial force and they are made to act in the elastic-linear field.

All ribs of vault of three models are realised as technical design and they are modelled as “beam”; small steel bars of precast hollow bricks of the vault (joists) are not taken into account.
For Model one, the vault is realised with equivalent “beam” elements of concrete arches of C20/25 Class with a section of 0.77 x 0.20m positioned at every frame to simulate the real stiffness of the roof. These elements are considered without weight (Loads due to the proper weight of the vault assumed from technical design are applied to the main beams as linear loads).
For Model two, the vault is realised with bi-dimensional plate element of light-weight hollow brick with elastic modulus equal to 4500 N/mmq. The mesh size varies from a minimum of 1.66m (distance between the chains) to a maximum of 3.50m (half of the distance between two rib joints) with a thickness of 20cm. Loads due to the proper weight of the vault assumed from technical design are applied directly to the plate as pressure loads.
For Model three, the vault is realised with beam element of hollow light-weight brick with elastic modulus equal to 4500 N/mmq positioned at every frame with a dimension of 5.00x0.20mt. Loads due to the proper weight of the vault assumed from technical design are applied directly to the beam as linear loads.
All three models are reported in Figure 4.10.

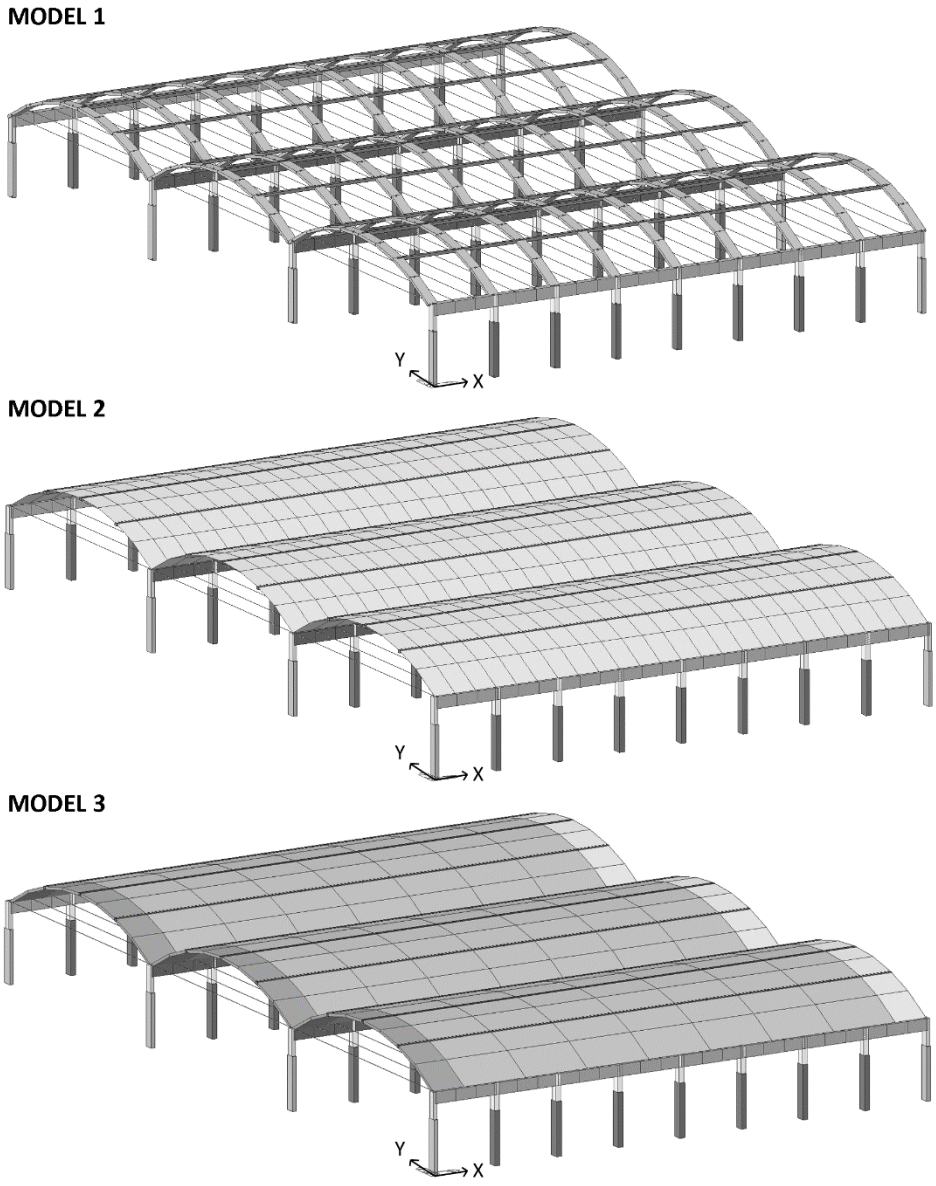

Figure 4.10 Numerical models of all three cases.

4.4 Intensity Measure (IM) and Damage Measure (DM)

In the fragility assessment, first of all, intensity measure and damage measure have to be defined.
A monotonic scalable ground motion intensity measure, or simply intensity measure (IM), is a non-negative scalar IM that constitutes a function $IM = f_{a_1}(\lambda)$ that depends on the unscaled accelerogram, a_1, which is increased monotonically with the scale factor λ. It could be defined as the desired input to subject a structure. The type of function used depends on the analysis performed: if fragility curves are derived from pushover analyses, the spectral acceleration Sa (T) (or spectral displacement Sd (T)) at the fundamental period is used. Instead, if incremental dynamic analysis [69] is performed, intensity measures can be PGA, Sa(T), PGV or on integral parameters as the Arias Intensity (IA) and the Housner Intensity (IH). Usually, the Peak Ground Acceleration (PGA) is commonly used since it is the simplest parameter extracted by the Ground Motion records.
Damage measure (DM), or Structural State Variable, is a non-negative scalar DM that characterises the additional response of the structural model due to a prescribed seismic loading defined by Intensity Measure (IM).
Intensity Measure (IM) and Damage Measure (DM) have to be a good correlation.
In this work, PGA is adopted as Intensity Measure while roof drifts associated at several Limit State (LS) in term of ductility ratio (chord rotation) is chosen as Damage Measures.
Threshold values for each LS, correspond to the local limit conditions, concerning bending or shear that first occurs in few elements, are determined through pushover analyses.

4.4.1 Modal Analysis

Tables 4.2-4.4 and Figures 4.11-4.16 show periods and modes shapes associated with the three models respectively.
Model one has periods and mode shapes different respect Model two and three because loads are applied on the main beams and not on the vaulted elements.

MODEL 1 - EIGENVALUE ANALYSIS AND MODAL PARTICIPATION MASSES

MODE N.	Period	TRAN-X		TRAN-Y	
	(sec)	MASS (%)	SUM (%)	MASS (%)	SUM (%)
1	0.5204	78.7926	78.7926	0	0
2	0.4838	0	78.7926	97.7083	97.7083
3	0.4768	0	78.7926	0	97.7083
4	0.4265	0	78.7926	0	97.7083
5	0.4152	20.6481	99.4408	0	97.7083

Table 4.2 Eigenvalue analysis and modal participation masses of Model 1.

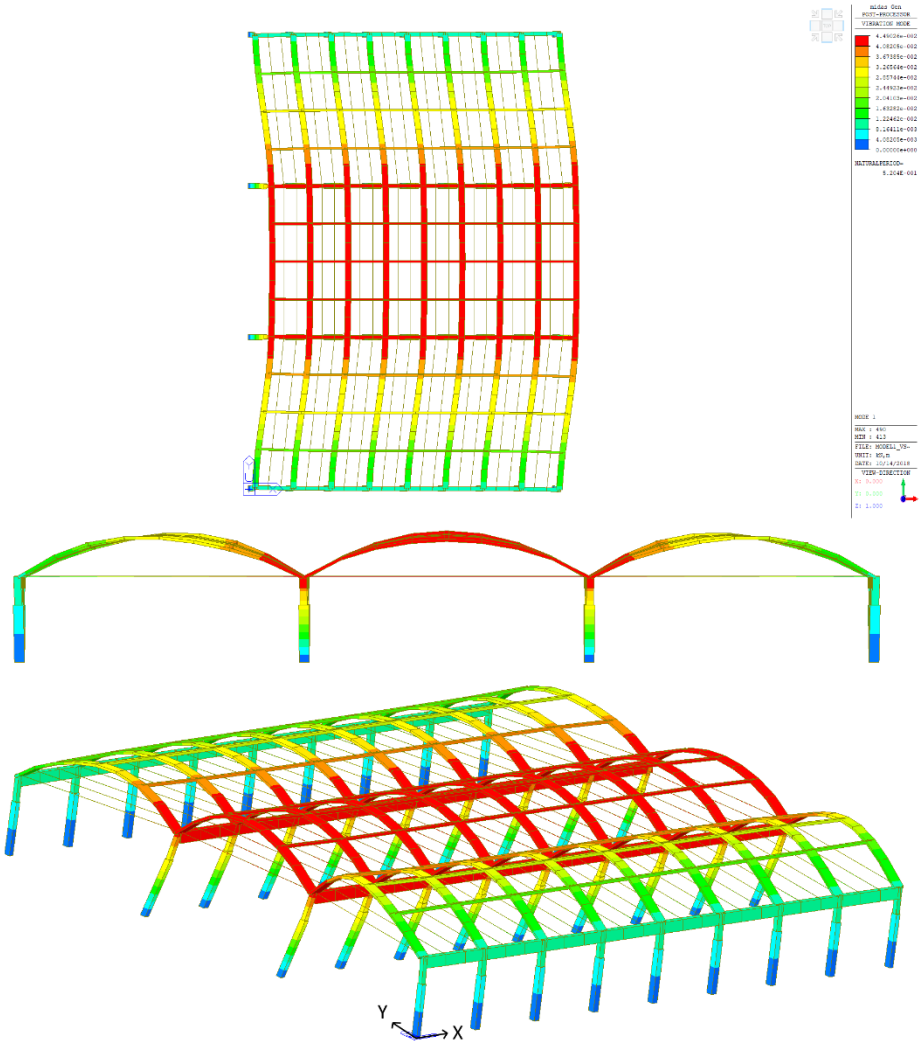

Figure 4.11 Model 1 – Mode 1 X direction (Mode Shape).

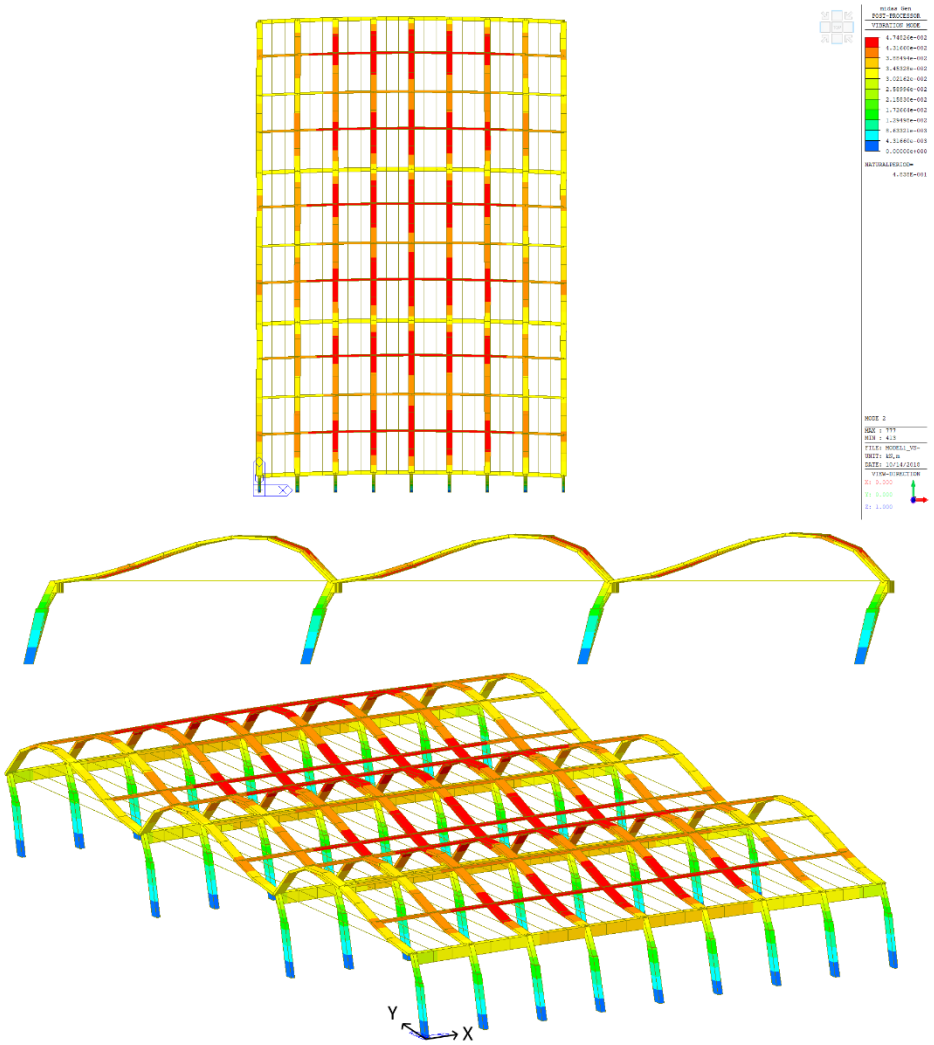

Figure 4.12 Model 1 – Mode 2 Y direction (Mode Shape).

MODEL 2 -EIGENVALUE ANALYSIS AND MODAL PARTICIPATION MASSES

MODE N.	Period	TRAN-X		TRAN-Y	
	(sec)	MASS (%)	SUM (%)	MASS (%)	SUM (%)
1	0.6047	0	0	95.2837	95.2837
2	0.5271	97.7677	97.7677	0	95.2837
3	0.4642	0	97.7677	0	95.2837
4	0.3106	1.6957	99.4634	0	95.2837
5	0.2942	0	99.4634	0	95.2837

Table 4.3 Eigenvalue analysis and modal participation masses of Model 2.

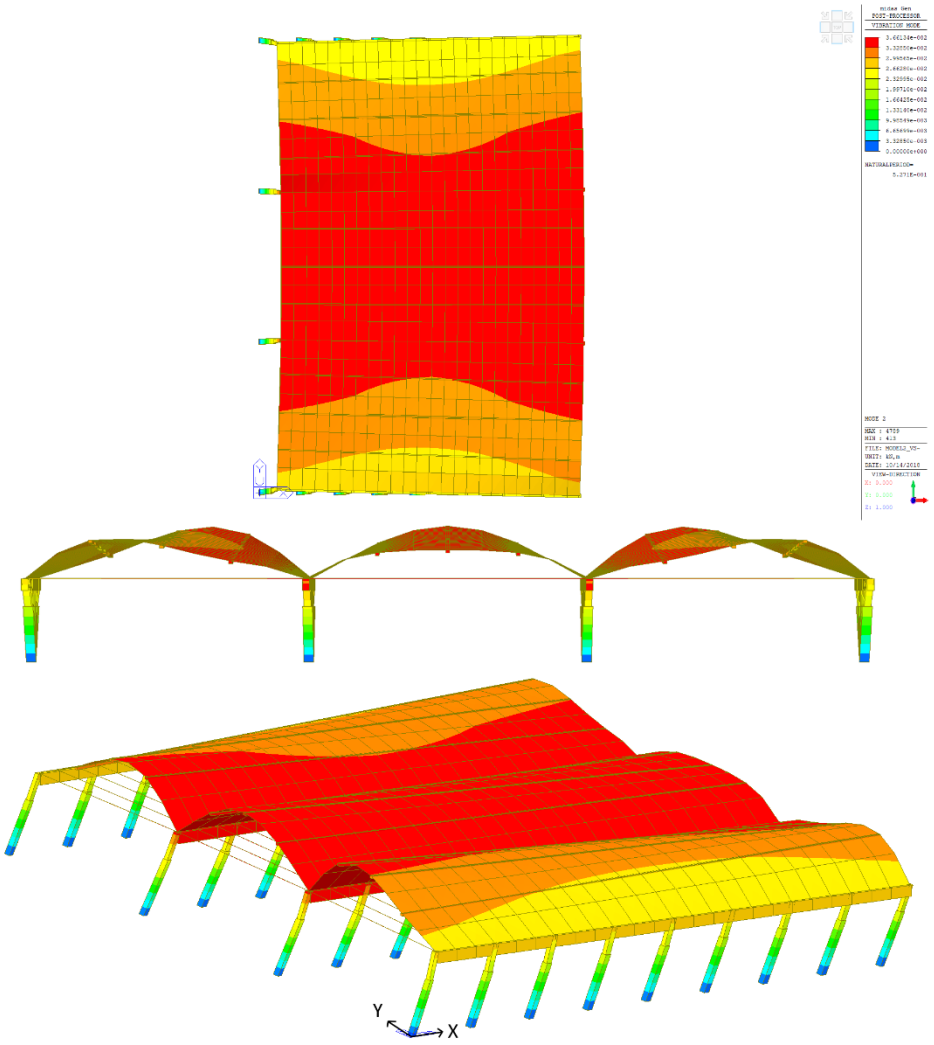

Figure 4.13 Model 2 – Mode 2 X direction (Mode Shape).

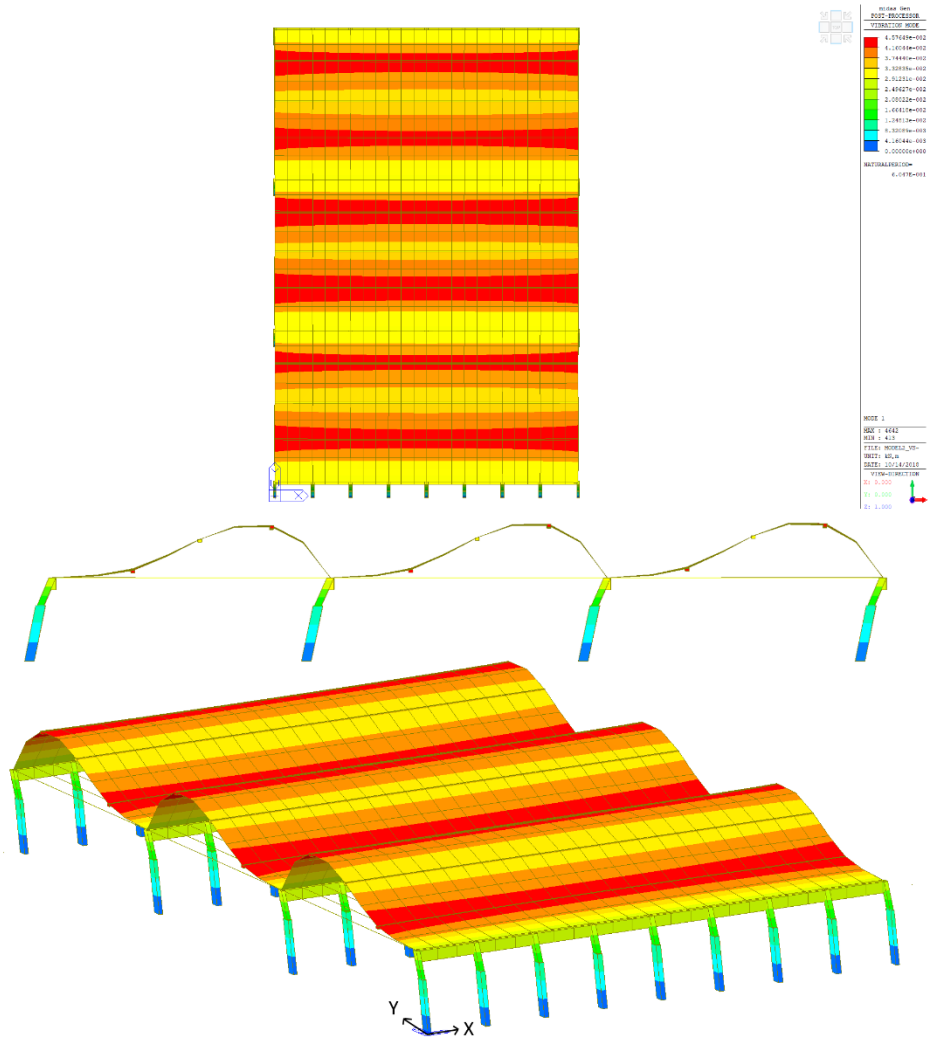

Figure 4.14 Model 2 – Mode 1 Y direction (Mode Shape).

MODEL 3 - EIGENVALUE ANALYSIS AND MODAL PARTICIPATION MASSES

MODE N.	Period	TRAN-X		TRAN-Y	
	(sec)	MASS(%)	SUM(%)	MASS(%)	SUM(%)
1	0.5974	0	0	95.442	95.442
2	0.5562	92.9586	92.9586	0	95.442
3	0.4981	0	92.9586	0	95.442
4	0.4392	0	92.9586	0	95.442
5	0.3595	6.1057	99.0643	0	95.442

Table 4.4 Eigenvalue analysis and modal participation masses of Model 3.

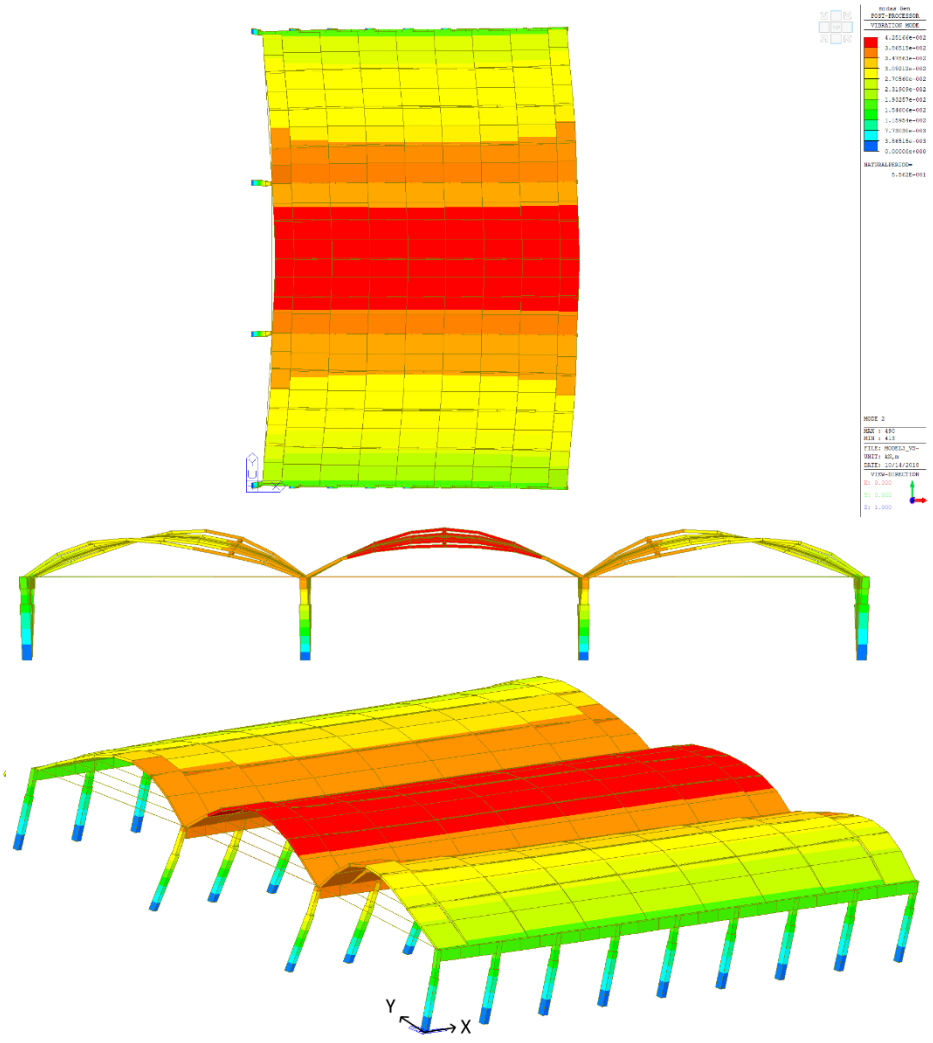

Figure 4.15 Model 3 – Mode 2 X direction (Mode Shape).

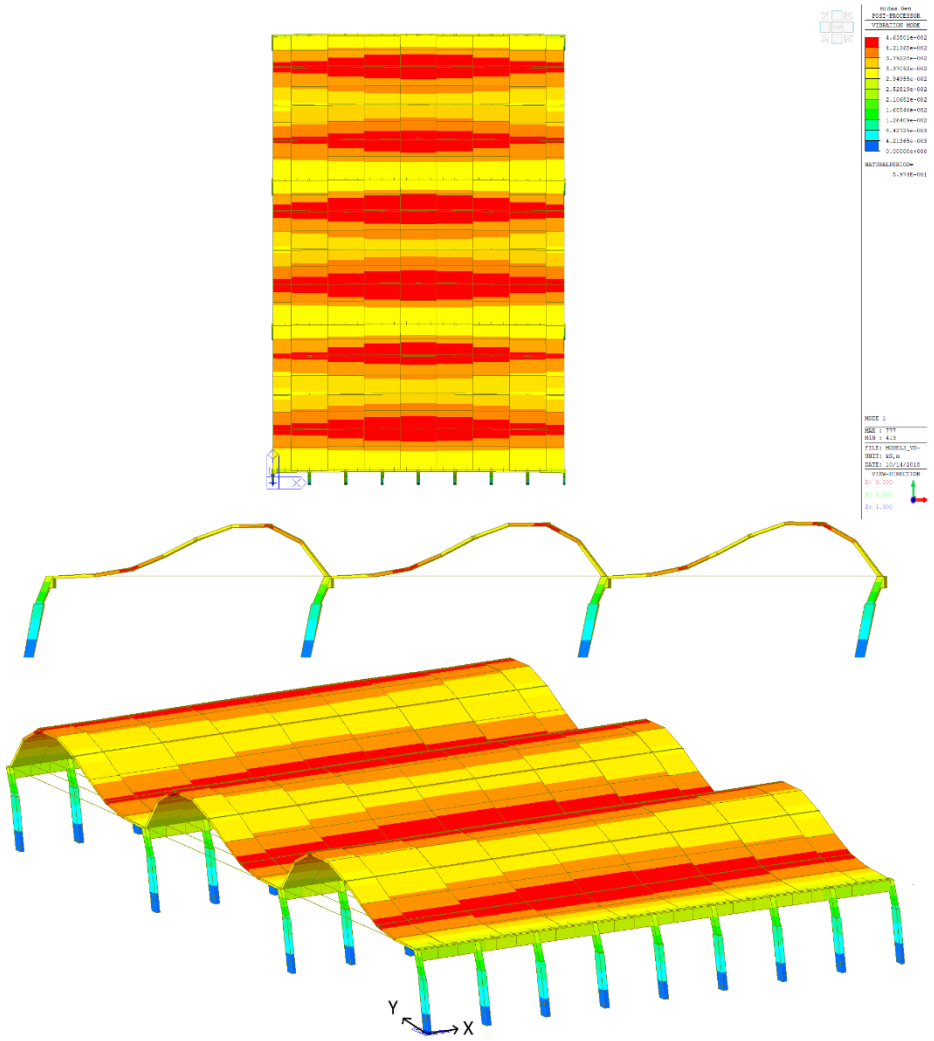

Figure 4.16 Model 3 – Mode 1 Y direction (Mode Shape).

4.4.2 Nonlinear static analysis

The nonlinear static analysis is performed with the aim to determine the LS thresholds for the three analysed models. Pushover analysis allows identifying nonlinear characteristics of system behaviour, i.e. elastic limit, redistribution of forces within the system subsequent to initial yielding and locations of plastic

hinges. As described previously, a lumped plasticity model is applied, and the nonlinear properties are assigned differently at every type of element for all three models.
Suggested by the Eurocode 8 provisions, elastoplastic behaviour for bending moments and shear failures with elastic-brittle behaviour with nonlinear constitutive laws are considered.
A-dimensional force-deformation relationship adopted are reported in Figure 4.17. The formulas proposed below are valid for each model analysed.
BENDING MOMENTS
SLD:

$$\theta_y = \phi_y \frac{L_y + a_y z}{3} + 0.0013\left(1 + 1.5\frac{h}{L_V}\right) + 0.13\phi_y \frac{d_b f_y}{\sqrt{f_c}} \tag{4.1}$$

SLV:

$$^3/_4 \ of\ ultimate\ chord\ rotation\ \theta_{um} \tag{4.2}$$

SLC:

$$\theta_{um} = \frac{1}{\gamma_{el}} 0.016(0.3^V)\left[\frac{max(0.01;\omega')}{max(0.01;\omega)} f_c\right]^{0.225}\left(\frac{L_V}{h}\right)^{0.35} 25^{\left(\alpha\rho_{sx}\frac{f_{yw}}{f_c}\right)}(1.25^{100\rho_d}) \tag{4.3}$$

SHEAR FAILURE
SLD, SLV, SLC:

$$V_{Rd} = max\left(V_{Rd,c}; V_{Rd,s}\right) \tag{4.4}$$

$V_{Rd,c}$ is given by:

$$V_{Rd,c} = \left[C_{Rd,c} k (100\rho_1 f_{ck})^{1/3} + k_1 \sigma_{cp}\right] b_w d \tag{4.5}$$

with a minimum of $V_{Rd,c} = (v_{min} + k_1\sigma_{cp}) b_w d$.
$V_{Rd,s}$ is the smallest value of:

$$V_{Rd,s} = \frac{A_{sw}}{s} z f_{ywd} \cot\theta$$
$$V_{Rd,max} = \alpha_{cw} b_w z v_1 \frac{f_{cd}}{(\cot\theta + \tan\theta)} \tag{4.6}$$

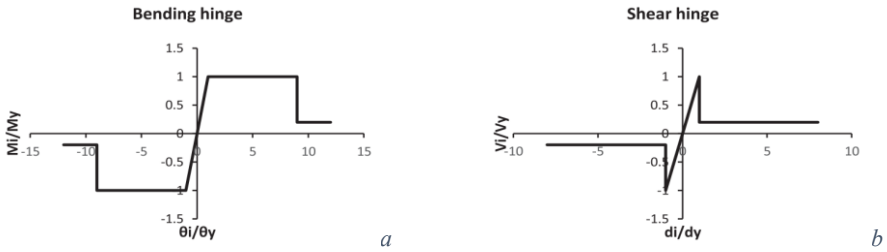

Figure 4.17 A-dimensional force-deformation relationship adopted for bending (a) and shear hinges (b) for beam elements.

The elastoplastic behaviour for bending moments and elastic-brittle behaviour for shear failures are taken into account for columns and main beams for Model one, only for columns for Model two and columns, main beams and ribs of the vault for Model three.
The analyses are performed following the N2 method proposed by Fajfar et al. [70] and adopted in some studies [71] [72] [73]. Two different horizontal load patterns for both X and Y directions are applied: the first one is proportional to the fundamental modes in the considered direction (PushMode), while the second one is proportional to the masses (PushMass); a total number of eight analyses are carried out for each model. The control node is chosen at the level of the roof, in the key of the central vault of models.
Figures 4.18-4.20 show the capacity curves provided by the three considered models. In X-direction, all three models provide capacity curves very similar because, being the direction perpendicular to the vault, the different representation of the vaults and the application of the plastic hinges to several elements does not affect the capacity of the structure.
Only model 2, which uses a modelling of the vault with shell elements, shows two different stiffnesses depending on the direction verified.
Generally, the curves display a high ductility, especially in the Y direction.
The roof drift thresholds for the three LSs considered (LD, SD, NC) are calculated. For each analysis and direction, the step on the capacity curve is considered for which, a little number of close plastic hinges reach the thresholds damage state regarding chord rotation or shear strength for each model taking into account where the plastic hinges are applied. In particular, limited damage (LD) state is achieved when the yielding threshold is exceeded; significant damage (SD) measure is observed when the ultimate condition is almost achieved, and the near collapse (NC) limit state is achieved when the columns and beams reach their ultimate capacity. For better comparison with subsequent IDA curves and for a unique threshold damage parameter for the considered LS, a minimum value of Roof Drift for the eight capacity curves is also reported in Table 4.5.

DAMAGE MEASURE (DM)	**RD (ROOF DRIFT)**		
	Model 1	Model 2	Model 3
	[m]	[m]	[m]
LD	0.0056	0.006	0.0026
SD	0.0462	0.0608	0.0481
NC	0.1008	0.1001	0.1001

Table 4.5 Minimum value of Roof Drift for the three limit states of Model 1,2 and 3.

A small scattering in roof drift threshold values between all three models is showed, especially for limit state near collapse that they are the same RDs.
For limited damage (LD) state Model three has minor RDs for the presence of plastic hinges also in a rib of the roof, while for SD damage state Model two has greater RDs because plastic hinges are only in the columns.

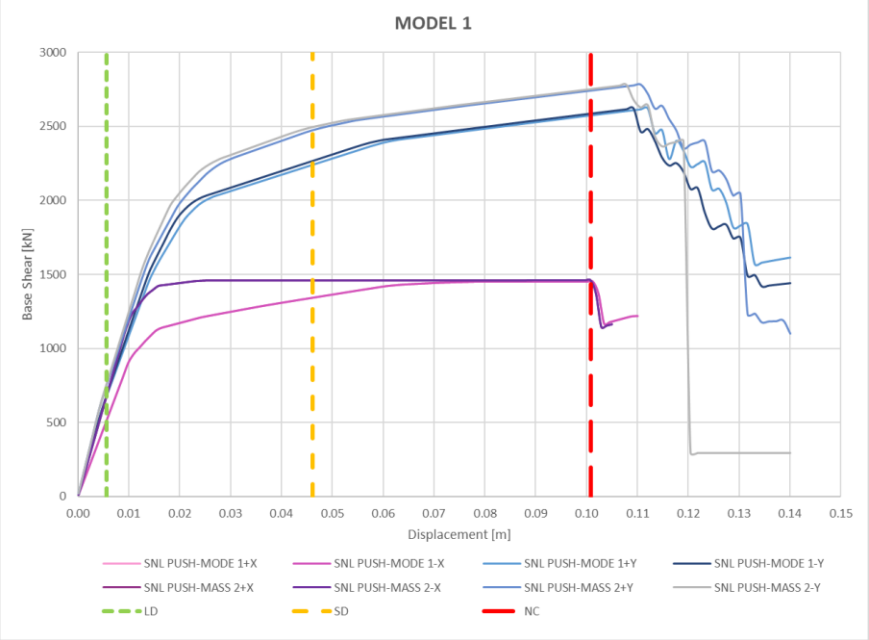

Figure 4.18 Model 1 – Capacity Curves.

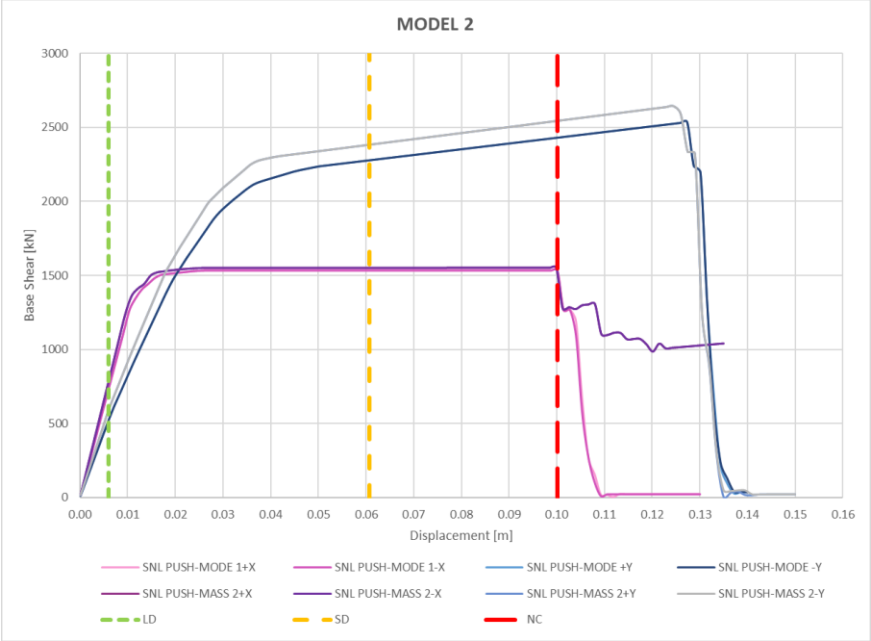

Figure 4.19 Model 2 – Capacity Curves.

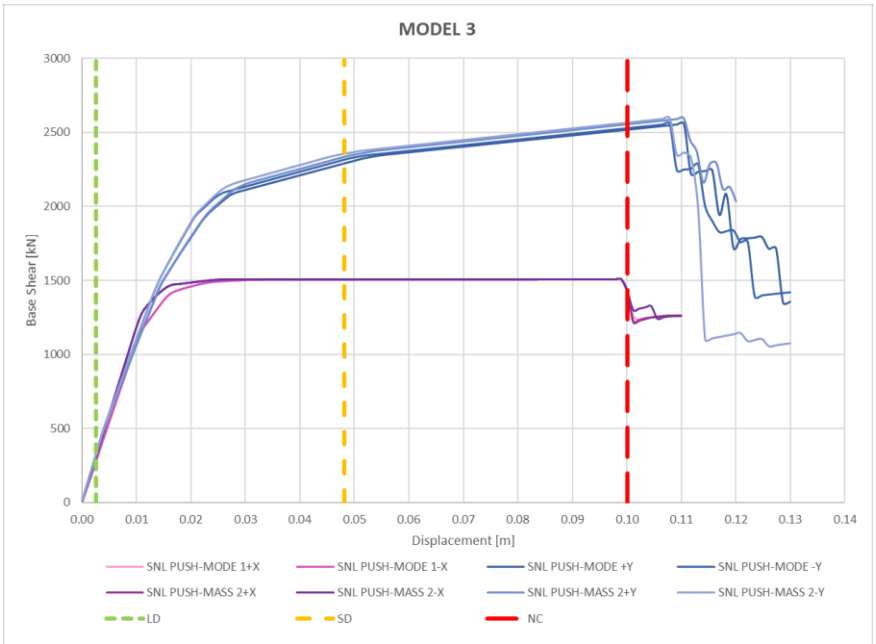

Figure 4.20 Model 3 – Capacity Curves.

4.5 Incremental Dynamic Analysis (IDA)

To realise the fragility curve, the statistical parameters θ and β of the normal cumulative distribution Φ are obtained by the Incremental Nonlinear Dynamic Analyses (IDA). A modified Takeda-type model [74] is used for columns, main beams and ribs, due to its ability to provide simple, numerically stable and sufficiently realistic hysteresis cycles. In the plane damage measure – intensity measure, the number of curves realised with this analysis are equal to the number of selected ground motions records (natural and artificial) scaled to multiple levels of intensity (λ) and compatible with the elastic response spectrum chosen as a reference for the considered hazard level (i.e. for a return period of 475 years). The knowledge of the LS thresholds derived from pushover analyses is used to realise dataset to estimate θ and β with Baker's methods [75].

4.5.1 Ground Motions selection

Incremental dynamic analysis is considered as the one of a most accurate numerical simulation method to evaluate the seismic risk of buildings. However, in addition to a suitable model that capture the cyclic behaviour of the structural elements, it requires a careful evaluation of the seismicity to which the site under examination is subjected and the choice of ground motions to be used in the analyses.
Several studies on the influence of ground motion spectral shape and duration on seismic collapse risk calculated with IDA and MSA are performed by Chandramohan et al. [76].
Three sets of spectral matching accelerograms for nonlinear dynamic analysis of structures regarding inelastic seismic response are taken into account: real records chosen by REXEL according to the site considered, real records of Emilia Romagna and Central Italy earthquake and artificial accelerograms. A comparison between artificial inputs and original real records is done by Iervolino et al. [77].
Their analysis shows that in some cases artificial accelerograms may underestimate the displacement response if compared to original real records, even if this conclusion does not seem to be statistically significant. Conversely, if the cyclic response is considered, artificial record classes show a significant overestimation of the demand.
According to Italian seismic code, selection of ground motions is based considering Ancona (AN) as geographic area, a C soil type and T1 topographic category; the functional type is "Class II" for precast building with a nominal life of 50 years and

with a Limit State of Significant Damage (SLSD or SLV in Italian) associated to a demand recurrence period $T_{R,D}$ of 475 years.
In the Probabilistic Seismic Hazard Assessment (PSHA), the aleatory uncertainty in seismic demand are considered with seven natural scaled ground motions, compatible with the reference SLSD spectrum and generated with the software REXEL [78]. Before this software, several studies are performed to time-history selection for nonlinear seismic analysis of structures by Iervolino et al. [79].
From Itaca database, ground motions that brought damage to the precast structures in Italy are also considered: Emilia Romagna earthquake in May 2012 in Mirandola and Central Italy earthquake in October 2016 in Norcia.
Time histories with the same class of site C are considered: real records of Mirandola and Castelsantangelo sul Nera are taken into account.
Table 4.6 lists all real ground motions considered.

Set of ground motion	Waveform ID	Earthquake ID	Station ID	Earthquake Name	Date	Mw	Fault Mechanism	Epicentral Distance [km]	EC8 Site class
REXEL	600	286	ST223	Umbria Marche	26/09/1997	6.0	normal	22	C
REXEL	170	81	ST46	Basso Tirreno	15/04/1978	6.0	oblique	18	C
REXEL	151	65	ST33	Friuli (aftershock)	15/09/1976	6.0	thrust	11	C
REXEL	1726	561	ST549	Adana	27/06/1998	6.3	strike slip	30	C
REXEL	335	158	ST121	Alkion	25/02/1981	6.3	normal	25	C
REXEL	141	65	ST12	Friuli (aftershock)	15/09/1976	6.0	thrust	46	C
REXEL	879	349	ST271	Dinar	01/10/1995	6.4	normal	8	C
ITACA	8	1	MRN	EMILIA_1ST_SHOCK	20/05/2012	6.1	thrust	16.1	C
ITACA	11	27	MRN	EMILIA_2ND_SHOCK	29/05/2012	6.0	thrust	4.1	C
ITACA	77	77	CNE	CENTRAL_ITALY	26/10/2016	5.4	normal	2.6	C
ITACA	95	142	CNE	CENTRAL_ITALY	26/10/2016	5.9	normal	2.5	C
ITACA	29	29	CNE	CENTRAL_ITALY	30/10/2016	6.5	normal	7.7	C

Table 4.6 Natural ground motions considered for IDA analysis.

The third set of artificial records is generated by Simqke software. This is the common method to generate synthetic ground motions compatible with an assigned design spectrum. This method is based on the simulation of stationary processes. The matching of the target spectrum may be improved using an iterative procedure. They fully respect the Italian code's provisions regarding the duration of both stationary and non-stationary parts (this software simulates non-stationary records and the user can choose how long to realise the beginning and the end of the non-stationary part).
Artificial accelerograms generated by Simqke software are reported in Figure 4.21.

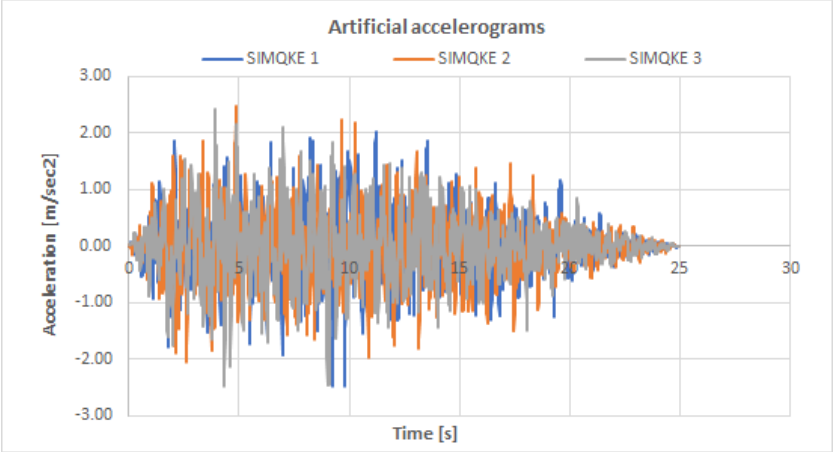

Figure 4.21 Artificial accelerograms considered for IDA analysis.

A total of twelve natural ground motions and three artificial seismic signals are applied to the all three models considered. Every ground motion is multiplied of the scale factor (λ) dependent on peak ground acceleration of every time-histories, to cover the range of roof drift values from 0 to the near collapse threshold.

4.5.2 IDA curves (Damage Measure-Intensity Measure)

Ida curves for all three models are reported in Figures 4.22-4.27 divided according to X-Y directions graphed in the plane damage measure – intensity measure with the threshold damage parameters previously obtained by push-over analyses.

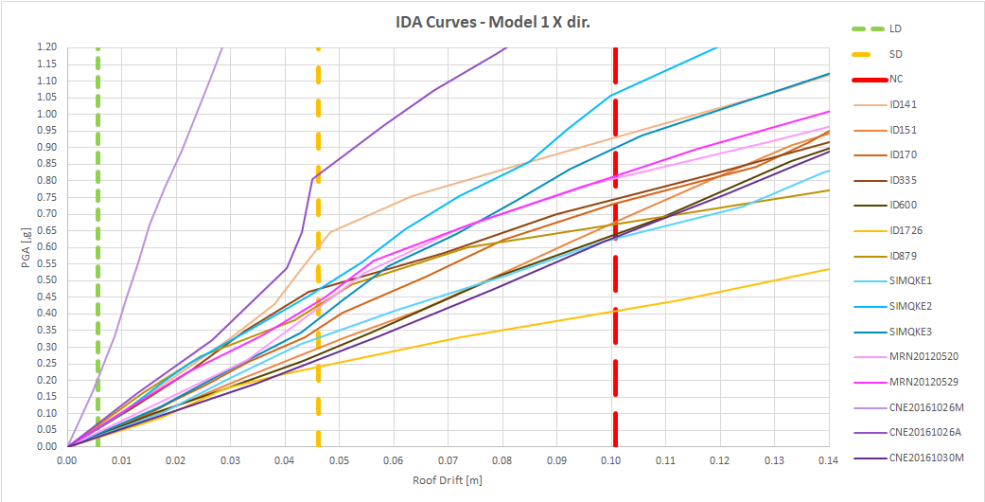

Figure 4.22 IDA curves for Model 1 X dir.

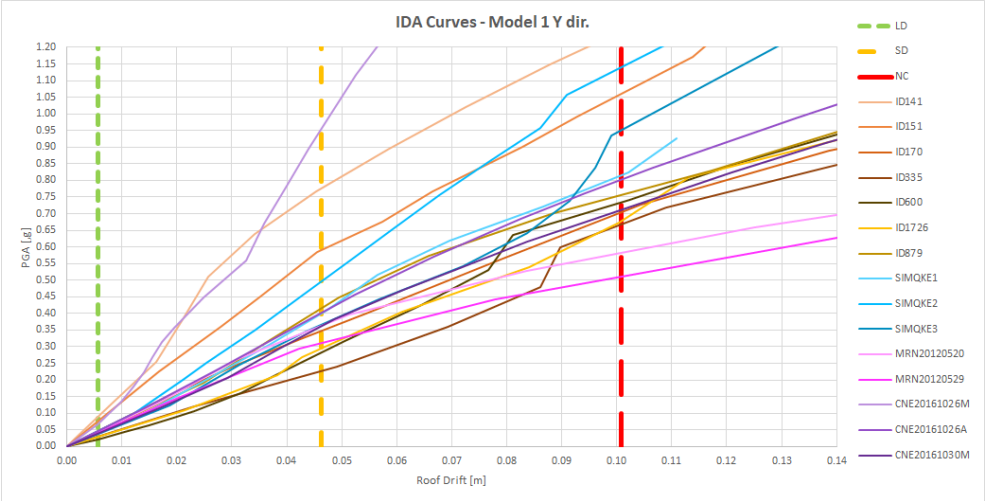

Figure 4.23 IDA curves for Model 1 Y dir.

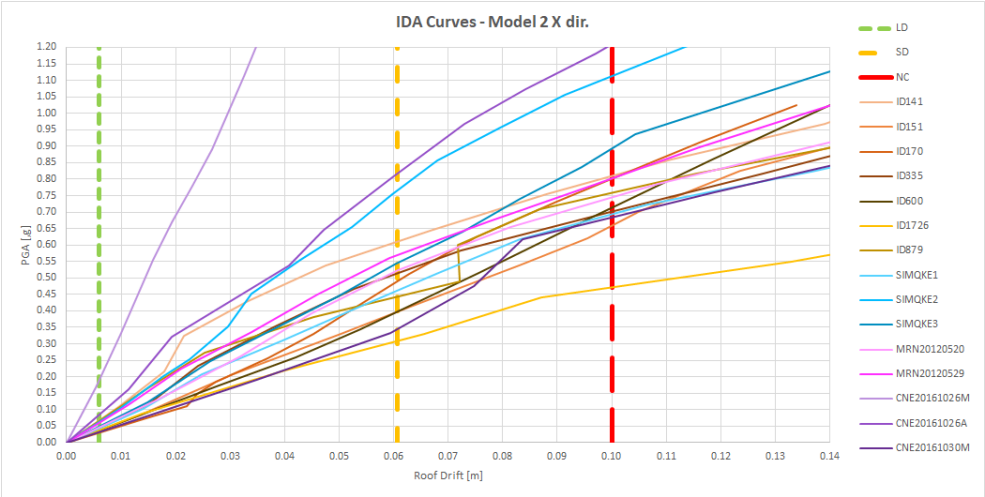

Figure 4.24 IDA curves for Model 2 X dir.

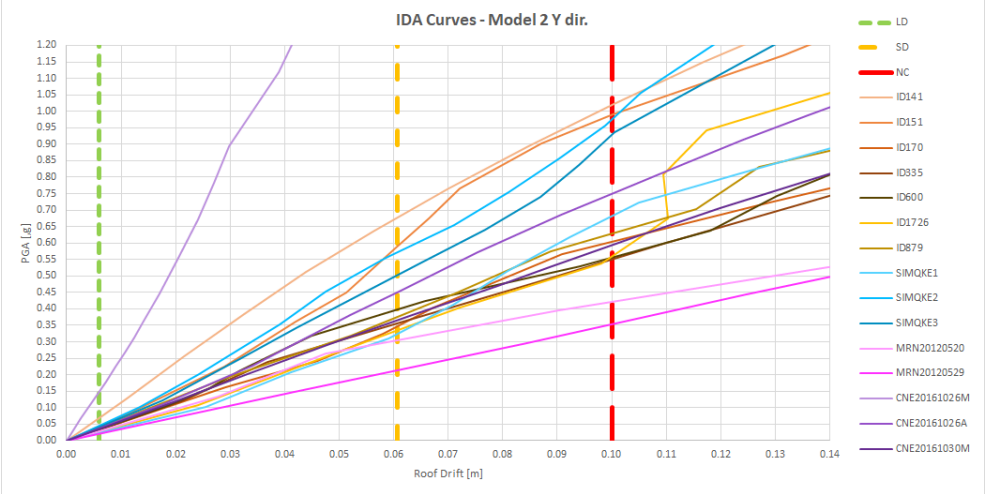

Figure 4.25 IDA curves for Model 2 Y dir.

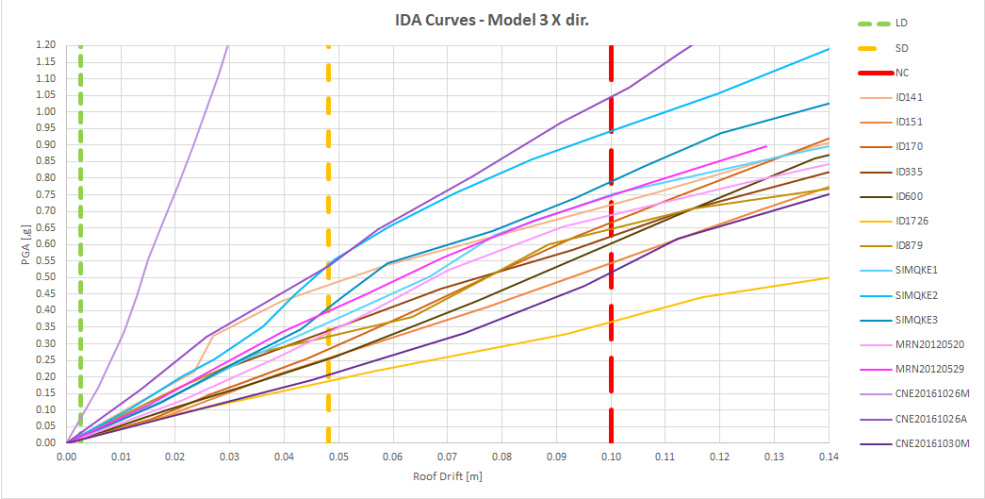

Figure 4.26 IDA curves for Model 3 X dir.

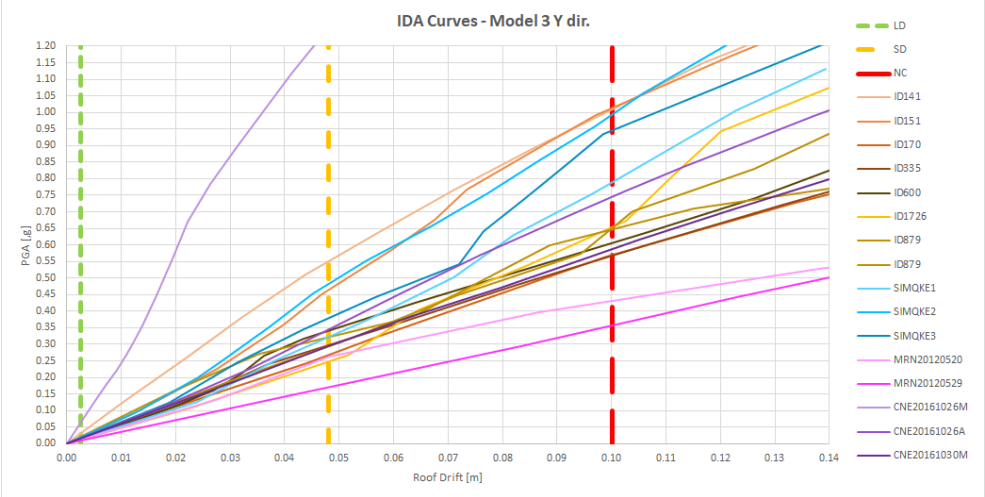

Figure 4.27 IDA curves for Model 3 Y dir.

Further results are reported in chapter 4.7, where IDA curves are plotted in terms of maximum displacements versus the corresponding base shear and they are compared with the relative pushover curves.

4.6 Fragility curves

There are some procedures to perform nonlinear dynamic analyses to collect the dataset to estimate a fragility function. One common approach is incremental dynamic analysis (IDA) [69], where a suite of ground motions is repeatedly scaled to find the IM level at which each ground motion causes collapse. A second common approach is multiple stripe analysis [80], where analysis is performed at a specified set of IM levels, each one has a unique ground motion set.
A fragility function is usually defined as a lognormal cumulative distribution function:

$$P(C|\mathrm{IM}=\mathrm{x})=\Phi\left(\frac{ln(x/\theta)}{\beta}\right) \tag{4.7}$$

where $P(C|\mathrm{IM}=\mathrm{x})$ is the probability that a ground motion with $\mathrm{IM}=\mathrm{x}$ will cause the collapse of the structure, $\Phi(\ \ )$ is the standard normal cumulative distribution function (CDF), θ is the median of the fragility function (the IM level with 50% probability of collapse) and β is the standard deviation of $\ln(IM)$ (sometimes referred to as the dispersion of IM). Equation 4.7 implies that the IM values of ground motions causing the collapse of a given structure are lognormally distributed; calibrating equation 4.7 for a given structure requires estimating θ and β from structural analysis results. All procedures are described by Baker [75]; all the analyses carried out are obtained from the Baker code implemented on MATLAB program [81].

4.6.1 A statistical procedure to fit fragility function

4.6.1.1 Recommended methods to process IDA dataset

In literature, three methods are available to calculate θ and β from IDA results.
The first fragility fitting approach is used widely to calibrate fragility functions for data other than structural collapse. With incremental dynamic analysis the probability of collapse at a given IM level, x, can then be estimated as the fraction of records for which collapse occurs at a level lower than x.
Fragility function parameters can be estimated from this data by taking logarithms of each ground motion's IM value associated with the onset of collapse and computing their mean and standard deviation.
This approach is called a method of "moments fit" (hat_mom) and it uses the following equations:

$$\ln\theta = \frac{1}{n}\sum_{i=1}^{n}\ln IM_i \tag{4.8}$$

$$\beta = \sqrt{\frac{1}{n-1}\sum_{i=1}^{n}\left(\ln\left({}^{IM_i}/_{\theta}\right)\right)^2} \tag{4.9}$$

where n is the number of ground motions considered and IM_i is the IM value associated with the onset of collapse for the i ground motion. This is a method of moments estimator, as $\ln\theta$ and β are the mean and standard deviation, respectively, of the normal distribution representing the $\ln IM$ values.

The second method is called "maximum likelihood fit for truncated IDA" (hat_trunc_alt) and it is based to perform incremental dynamic analysis only up to some level IM_{max} above which no further analyses are performed. If n ground motions are used in the analysis, there will be in general m ground motions that cause a collapse at IM levels less than IM_{max}, and n-m ground motions that do not cause collapse prior to the analyses being stopped.

For ground motions that are observed to cause collapse, their IM values at collapse (IM_i) are known. The likelihood that an arbitrary ground motion causes collapse at IM_i is the normal distribution probability density function (PDF)

$$Likelihood = \phi\left(\frac{ln\left({}^{IM_i}/_{\theta}\right)}{\beta}\right) \tag{4.10}$$

where $\phi(\ \ )$ denotes the standard normal distribution PDF. The n-m ground motions that do not cause a collapse at IM_{max} are called censored data. The likelihood that a given ground motion can be scaled to IM_{max} without causing collapse is the probability that IM_i is greater than IM_{max}

$$Likelihood = 1 - \Phi\left(\frac{ln\left({}^{IM_{max}}/_{\theta}\right)}{\beta}\right) \tag{4.11}$$

Making the reasonable assumption that the IM_i value for each ground motion is independent, the likelihood of the entire dataset being observed is the product of the individual likelihoods

$$Likelihood = \left(\prod_{i=1}^{m}\phi\left(\frac{ln\left({}^{IM_i}/_{\theta}\right)}{\beta}\right)\left(1 - \Phi\left(\frac{ln\left({}^{IM_{max}}/_{\theta}\right)}{\beta}\right)\right)\right)^{n-m} \tag{4.12}$$

where $\prod$ denotes a product over i values from 1 to m (corresponding to the m ground motions that cause a collapse at IM levels less than IM_{max}). Using this equation, the fragility function parameters are then obtained by varying the parameters until the likelihood function is maximised:

$$\{\theta,\beta\} = \arg max \sum_{j=1}^{m} \left\{ \ln \phi \left(\frac{ln\left(IM_i/\theta\right)}{\beta} \right) + (n-m) \ln \left(1 - \Phi \left(\frac{ln\left(IM_{max}/\theta\right)}{\beta} \right) \right) \right\} \quad (4.13)$$

The third method is called "maximum likelihood fit" (hat_mle) and it is usually used to process multiple stripe analysis data when structural analysis results provide the fraction of ground motions at each IM level that causes collapse. This method isn't theoretically correct for IDA, as the observations of collapse at each IM level are not independent, but in practice, it appears to produce often numerical results similar to the method of moments above (this approach is usually not recommended, but it is provided for comparison purposes).

At each intensity level $IM = x_j$, the structural analyses produce some number of collapses out of a total number of ground motions. Assuming that observation of collapse or no-collapse from each ground motion is independent of the observations from other ground motions, the probability of observing z_j collapses out of n_j ground motions with $IM = x_j$ is given by the binomial distribution:

$$P\left(z_j \text{ collapses out of } n_j \text{ ground motions}\right) = \binom{n_j}{z_j} p_j^{z_j} \left(1 - p_j\right)^{n_j - z_j} \quad (4.14)$$

where p_j is the probability that a ground motion with $IM = x_j$ will cause the collapse of the structure. Main goal is to identify the fragility function that will predict p_j, and the maximum likelihood approach identifies the fragility function that gives the highest probability of having observed the collapse data that is taken from the structural analysis. When analysis data is obtained at multiple IM levels, the product of the binomial probabilities is extracted (from equation 4.14) at each IM level to get the likelihood for the entire data set:

$$Likelihood = \prod_{j=1}^{m} \binom{n_j}{z_j} p_j^{z_j} \left(1 - p_j\right)^{n_j - z_j} \quad (4.15)$$

where m is the number of IM levels, and $\prod$ denotes a product over all levels. Replacing equation 4.7 for p_j, the fragility parameters are explicited in the likelihood function.

$$Likelihood = \prod_{j=1}^{m} \binom{n_j}{z_j} \Phi \left(\frac{ln\left(x_j/\theta\right)}{\beta} \right)^{z_j} \left(1 - \Phi \left(\frac{ln\left(x_j/\theta\right)}{\beta} \right) \right)^{n_j - z_j} \quad (4.15)$$

Estimates of the fragility function parameters are obtained by maximizing this likelihood function.

$$\{\theta,\beta\} = \arg max \sum_{j=1}^{m} \left\{ \ln \binom{n_j}{z_j} + z_j \ln \Phi \left(\frac{ln\left(x_j/\theta\right)}{\beta} \right) + \left(n_j - z_j\right) \ln \left(1 - \Phi \left(\frac{ln\left(x_j/\theta\right)}{\beta} \right) \right) \right\} \quad (4.16)$$

Tables 4.7-4.12 show the data processed to derive the fragility curves for all three models for X-Y direction and for three considered damage states for the three methods described above.

MODEL 1 - X DIR

LD			SD			NC		
IM_i	Cumulative number of collapses	Fraction causing collapse	IM_i	Cumulative number of collapses	Fraction causing collapse	IM_i	Cumulative number of collapses	Fraction causing collapse
0.03	1	0.0667	0.24	1	0.0667	0.41	1	0.0667
0.03	2	0.1333	0.265	2	0.1333	0.63	2	0.1333
0.034	3	0.2000	0.279	3	0.2000	0.632	3	0.2000
0.034	4	0.2667	0.298	4	0.2667	0.64	4	0.2667
0.038	5	0.3333	0.33	5	0.3333	0.67	5	0.3333
0.038	6	0.4000	0.359	6	0.4000	0.678	6	0.4000
0.04	7	0.4667	0.385	7	0.4667	0.735	7	0.4667
0.044	8	0.5333	0.42	8	0.5333	0.745	8	0.5333
0.055	9	0.6000	0.425	9	0.6000	0.81	9	0.6000
0.056	10	0.6667	0.44	10	0.6667	0.815	10	0.6667
0.057	11	0.7333	0.475	11	0.7333	0.9	11	0.7333
0.058	12	0.8000	0.475	12	0.8000	0.932	12	0.8000
0.065	13	0.8667	0.6	13	0.8667	1.07	13	0.8667
0.07	14	0.9333	0.82	14	0.9333	1.4	14	0.9333
0.208	15	1.0000						
Number of analyses:		15	Number of analyses:		15	Number of analyses:		15
IM_{max}		1	IM_{max}		1	IM_{max}		1
Number not collapsed for truncated IDA		0	Number not collapsed for truncated IDA		1	Number not collapsed for truncated IDA		3

Table 4.7 Dataset for recommended methods to process IDA results – Model 1 – X dir.

MODEL 1 - Y DIR

LD			SD			NC		
IM_i	Cumulative number of collapses	Fraction causing collapse	IM_i	Cumulative number of collapses	Fraction causing collapse	IM_i	Cumulative number of collapses	Fraction causing collapse
0.020	1	0.0667	0.228	1	0.0667	0.510	1	0.0667
0.030	2	0.1333	0.285	2	0.1333	0.582	2	0.1333
0.030	3	0.2000	0.295	3	0.2000	0.670	3	0.2000
0.038	4	0.2667	0.312	4	0.2667	0.680	4	0.2667
0.039	5	0.3333	0.348	5	0.3333	0.705	5	0.3333
0.040	6	0.4000	0.368	6	0.4000	0.712	6	0.4000
0.041	7	0.4667	0.368	7	0.4667	0.738	7	0.4667
0.042	8	0.5333	0.368	8	0.5333	0.758	8	0.5333
0.043	9	0.6000	0.400	9	0.6000	0.802	9	0.6000
0.044	10	0.6667	0.400	10	0.6667	0.818	10	0.6667
0.045	11	0.7333	0.415	11	0.7333	0.953	11	0.7333
0.046	12	0.8000	0.495	12	0.8000	1.060	12	0.8000
0.065	13	0.8667	0.592	13	0.8667	1.140	13	0.8667
0.078	14	0.9333	0.775	14	0.9333	1.250	14	0.9333
0.088	15	1.0000	0.958	15	1.0000			
Number of analyses:		15	Number of analyses:		15	Number of analyses:		15
IM_{max}		1	IM_{max}		1	IM_{max}		1
Number not collapsed for truncated IDA		0	Number not collapsed for truncated IDA		1	Number not collapsed for truncated IDA		4

Table 4.8 Dataset for recommended methods to process IDA results – Model 1 – Y dir.

MODEL 2 - X DIR

LD			SD			NC		
IM_i	Cumulative number of collapses	Fraction causing collapse	IM_i	Cumulative number of collapses	Fraction causing collapse	IM_i	Cumulative number of collapses	Fraction causing collapse
0.030	1	0.0667	0.310	1	0.0667	0.470	1	0.0667
0.030	2	0.1333	0.345	2	0.1333	0.660	2	0.1333
0.040	3	0.2000	0.398	3	0.2000	0.685	3	0.2000
0.040	4	0.2667	0.398	4	0.2667	0.695	4	0.2667
0.040	5	0.3333	0.445	5	0.3333	0.700	5	0.3333
0.045	6	0.4000	0.462	6	0.4000	0.715	6	0.4000
0.046	7	0.4667	0.490	7	0.4667	0.748	7	0.4667
0.047	8	0.5333	0.515	8	0.5333	0.760	8	0.5333
0.048	9	0.6000	0.525	9	0.6000	0.804	9	0.6000
0.060	10	0.6667	0.545	10	0.6667	0.804	10	0.6667
0.061	11	0.7333	0.568	11	0.7333	0.812	11	0.7333
0.062	12	0.8000	0.612	12	0.8000	0.895	12	0.8000
0.063	13	0.8667	0.768	13	0.8667	1.110	13	0.8667
0.085	14	0.9333	0.818	14	0.9333	1.190	14	0.9333
0.190	15	1.0000						
Number of analyses:		15	Number of analyses:		15	Number of analyses:		15
IM_{max}		1	IM_{max}		1	IM_{max}		1
Number not collapsed for truncated IDA		0	Number not collapsed for truncated IDA		1	Number not collapsed for truncated IDA		3

Table 4.9 Dataset for recommended methods to process IDA results– Model 2 – X dir.

MODEL 2 - Y DIR

LD			SD			NC		
IM_i	Cumulative number of collapses	Fraction causing collapse	IM_i	Cumulative number of collapses	Fraction causing collapse	IM_i	Cumulative number of collapses	Fraction causing collapse
0.020	1	0.0667	0.215	1	0.0667	0.352	1	0.0667
0.023	2	0.1333	0.305	2	0.1333	0.423	2	0.1333
0.026	3	0.2000	0.325	3	0.2000	0.55	3	0.2000
0.029	4	0.2667	0.335	4	0.2667	0.558	4	0.2667
0.035	5	0.3333	0.348	5	0.3333	0.56	5	0.3333
0.036	6	0.4000	0.358	6	0.4000	0.593	6	0.4000
0.037	7	0.4667	0.369	7	0.4667	0.603	7	0.4667
0.038	8	0.5333	0.378	8	0.5333	0.63	8	0.5333
0.039	9	0.6000	0.440	9	0.6000	0.682	9	0.6000
0.040	10	0.6667	0.452	10	0.6667	0.75	10	0.6667
0.041	11	0.7333	0.502	11	0.7333	0.93	11	0.7333
0.042	12	0.8000	0.572	12	0.8000	0.975	12	0.8000
0.043	13	0.8667	0.590	13	0.8667	0.99	13	0.8667
0.070	14	0.9333	0.680	14	0.9333	1.060	14	0.9333
0.150	15	1.0000	1.500	15	1.0000			
Number of analyses:		15	Number of analyses:		15	Number of analyses:		15
IM_{max}		1	IM_{max}		1	IM_{max}		1
Number not collapsed for truncated IDA		0	Number not collapsed for truncated IDA		1	Number not collapsed for truncated IDA		3

Table 4.10 Dataset for recommended methods to process IDA results – Model 2 – Y dir.

MODEL 3 - X DIR

LD			SD			NC		
IM_i	Cumulative number of collapses	Fraction causing collapse	IM_i	Cumulative number of collapses	Fraction causing collapse	IM_i	Cumulative number of collapses	Fraction causing collapse
0.012	1	0.0667	0.190	1	0.0667	0.368	1	0.0667
0.013	2	0.1333	0.208	2	0.1333	0.518	2	0.1333
0.014	3	0.2000	0.252	3	0.2000	0.544	3	0.2000
0.015	4	0.2667	0.256	4	0.2667	0.605	4	0.2667
0.016	5	0.3333	0.284	5	0.3333	0.618	5	0.3333
0.017	6	0.4000	0.299	6	0.4000	0.627	6	0.4000
0.018	7	0.4667	0.322	7	0.4667	0.648	7	0.4667
0.019	8	0.5333	0.337	8	0.5333	0.668	8	0.5333
0.020	9	0.6000	0.340	9	0.6000	0.690	9	0.6000
0.021	10	0.6667	0.398	10	0.6667	0.720	10	0.6667
0.022	11	0.7333	0.410	11	0.7333	0.750	11	0.7333
0.023	12	0.8000	0.480	12	0.8000	0.792	12	0.8000
0.024	13	0.8667	0.538	13	0.8667	0.943	13	0.8667
0.030	14	0.9333	0.540	14	0.9333	1.040	14	0.9333
0.075	15	1.0000						
Number of analyses:		15	Number of analyses:		15	Number of analyses:		15
IM_{max}		1	IM_{max}		1	IM_{max}		1
Number not collapsed for truncated IDA		0	Number not collapsed for truncated IDA		1	Number not collapsed for truncated IDA		2

Table 4.11 Dataset for recommended methods to process IDA results – Model 3 – X dir.

MODEL 3 - Y DIR

LD			SD			NC		
IM_i	Cumulative number of collapses	Fraction causing collapse	IM_i	Cumulative number of collapses	Fraction causing collapse	IM_i	Cumulative number of collapses	Fraction causing collapse
0.010	1	0.0667	0.172	1	0.0667	0.360	1	0.0667
0.011	2	0.1333	0.250	2	0.1333	0.430	2	0.1333
0.012	3	0.2000	0.266	3	0.2000	0.570	3	0.2000
0.013	4	0.2667	0.267	4	0.2667	0.570	4	0.2667
0.014	5	0.3333	0.268	5	0.3333	0.590	5	0.3333
0.015	6	0.4000	0.295	6	0.4000	0.608	6	0.4000
0.016	7	0.4667	0.295	7	0.4667	0.646	7	0.4667
0.017	8	0.5333	0.297	8	0.5333	0.654	8	0.5333
0.018	9	0.6000	0.345	9	0.6000	0.654	9	0.6000
0.019	10	0.6667	0.346	10	0.6667	0.745	10	0.6667
0.020	11	0.7333	0.380	11	0.7333	0.948	11	0.7333
0.021	12	0.8000	0.464	12	0.8000	0.993	12	0.8000
0.022	13	0.8667	0.482	13	0.8667	1.010	13	0.8667
0.030	14	0.9333	0.552	14	0.9333	1.012	14	0.9333
0.065	15	1.0000	1.240	15	1.0000			
Number of analyses:		15	Number of analyses:		15	Number of analyses:		15
IM_{max}		1	IM_{max}		1	IM_{max}		1
Number not collapsed for truncated IDA		0	Number not collapsed for truncated IDA		1	Number not collapsed for truncated IDA		3

Table 4.12 Dataset for recommended methods to process IDA results – Model 3 – Y dir.

4.6.1.2 Alternative methods to process IDA data set

Processing dataset as a number of IDA curves that cross the vertical lines representative of three damage states computed for IMs values from 0.05 to 1 g with increasing step of 0.05g, three other methods are available in the literature to derive fragility curves.

The first method is “maximum likelihood fit” (hat_mle), already described by equation 4.16 to process the data of IDA but in this case theoretically valid.

The second method is “maximum likelihood fit” and it uses a probit regression (hat_probit).

The third method minimizes the sum of squared errors (hat_sse) between the observed fractions of collapse and probabilities of collapse predicted by the fragility function:

$$\{\theta, \beta\} = \arg min \sum_{j=1}^{m} \left(\frac{z_j}{n_j} - \Phi\left(\frac{ln\left(x_j/\theta\right)}{\beta} \right) \right)^2 \quad (4.17)$$

where all variables are defined in the previous chapter.

Tables 4.13-4.18 show the data processed to derive the fragility curves for all three models for X-Y direction and for three considered damage states for the three methods described above.

MODEL 1 – X DIR

PGA [g]	Number of analysis	Number of collapses	Fraction causing collapse	Number of collapses	Fraction causing collapse	Number of collapses	Fraction causing collapse
IM		**LD**		**SD**		**NC**	
0.05	15	9	0.600	0	0.000	0	0.000
0.10	15	14	0.933	0	0.000	0	0.000
0.15	15	14	0.933	0	0.000	0	0.000
0.20	15	14	0.933	0	0.000	0	0.000
0.25	15	15	1.000	1	0.067	0	0.000
0.30	15	15	1.000	4	0.267	0	0.000
0.35	15	15	1.000	5	0.333	0	0.000
0.40	15	15	1.000	7	0.467	0	0.000
0.45	15	15	1.000	10	0.667	1	0.067
0.50	15	15	1.000	12	0.800	1	0.067
0.55	15	15	1.000	12	0.800	1	0.067
0.60	15	15	1.000	13	0.867	1	0.067
0.65	15	15	1.000	13	0.867	4	0.267
0.70	15	15	1.000	13	0.867	6	0.400
0.75	15	15	1.000	13	0.867	8	0.533
0.80	15	15	1.000	13	0.867	8	0.533
0.85	15	15	1.000	14	0.933	10	0.667
0.90	15	15	1.000	14	0.933	11	0.733
0.95	15	15	1.000	14	0.933	12	0.800
1.00	15	15	1.000	14	0.933	12	0.800
1.05	15	15	1.000	14	0.933	12	0.800
1.10	15	15	1.000	14	0.933	13	0.867
1.15	15	15	1.000	14	0.933	13	0.867
1.20	15	15	1.000	14	0.933	13	0.867
1.25	15	15	1.000	14	0.933	13	0.867
1.30	15	15	1.000	14	0.933	13	0.867
1.35	15	15	1.000	14	0.933	13	0.867
1.40	15	15	1.000	14	0.933	13	0.867
1.45	15	15	1.000	14	0.933	14	0.933
1.50	15	15	1.000	14	0.933	14	0.933

Table 4.13 Dataset for alternative methods to process IDA results – Model 1 – X dir.

MODEL 1 – Y DIR

PGA [g] IM	Number of analysis	LD Number of collapses	LD Fraction causing collapse	SD Number of collapses	SD Fraction causing collapse	NC Number of collapses	NC Fraction causing collapse
0.05	15	12	0.800	0	0.000	0	0.000
0.10	15	15	1.000	0	0.000	0	0.000
0.15	15	15	1.000	0	0.000	0	0.000
0.20	15	15	1.000	0	0.000	0	0.000
0.25	15	15	1.000	1	0.067	0	0.000
0.30	15	15	1.000	3	0.200	0	0.000
0.35	15	15	1.000	5	0.333	0	0.000
0.40	15	15	1.000	10	0.667	0	0.000
0.45	15	15	1.000	11	0.733	0	0.000
0.50	15	15	1.000	12	0.800	0	0.000
0.55	15	15	1.000	12	0.800	1	0.067
0.60	15	15	1.000	13	0.867	2	0.133
0.65	15	15	1.000	13	0.867	2	0.133
0.70	15	15	1.000	13	0.867	4	0.267
0.75	15	15	1.000	13	0.867	7	0.467
0.80	15	15	1.000	14	0.933	9	0.600
0.85	15	15	1.000	14	0.933	10	0.667
0.90	15	15	1.000	14	0.933	10	0.667
0.95	15	15	1.000	14	0.933	10	0.667
1.00	15	15	1.000	15	1.000	11	0.733
1.05	15	15	1.000	15	1.000	11	0.733
1.10	15	15	1.000	15	1.000	12	0.800
1.15	15	15	1.000	15	1.000	13	0.867
1.20	15	15	1.000	15	1.000	13	0.867
1.25	15	15	1.000	15	1.000	14	0.933
1.30	15	15	1.000	15	1.000	14	0.933
1.35	15	15	1.000	15	1.000	14	0.933
1.40	15	15	1.000	15	1.000	14	0.933
1.45	15	15	1.000	15	1.000	14	0.933
1.50	15	15	1.000	15	1.000	14	0.933

Table 4.14 Dataset for alternative methods to process IDA results – Model 1 – Y dir.

MODEL 2 – X DIR

PGA [g] IM	Number of analysis	Number of collapses	Fraction causing collapse	Number of collapses	Fraction causing collapse	Number of collapses	Fraction causing collapse
		LD		SD		NC	
0.05	15	9	0.600	0	0.000	0	0.000
0.10	15	14	0.933	0	0.000	0	0.000
0.15	15	14	0.933	0	0.000	0	0.000
0.20	15	15	1.000	0	0.000	0	0.000
0.25	15	15	1.000	0	0.000	0	0.000
0.30	15	15	1.000	0	0.000	0	0.000
0.35	15	15	1.000	2	0.133	0	0.000
0.40	15	15	1.000	4	0.267	0	0.000
0.45	15	15	1.000	5	0.333	0	0.000
0.50	15	15	1.000	7	0.467	1	0.067
0.55	15	15	1.000	10	0.667	1	0.067
0.60	15	15	1.000	11	0.733	1	0.067
0.65	15	15	1.000	12	0.800	1	0.067
0.70	15	15	1.000	12	0.800	5	0.333
0.75	15	15	1.000	12	0.800	7	0.467
0.80	15	15	1.000	13	0.867	8	0.533
0.85	15	15	1.000	14	0.933	11	0.733
0.90	15	15	1.000	14	0.933	12	0.800
0.95	15	15	1.000	14	0.933	12	0.800
1.00	15	15	1.000	14	0.933	12	0.800
1.05	15	15	1.000	14	0.933	12	0.800
1.10	15	15	1.000	14	0.933	12	0.800
1.15	15	15	1.000	14	0.933	13	0.867
1.20	15	15	1.000	14	0.933	14	0.933
1.25	15	15	1.000	14	0.933	14	0.933
1.30	15	15	1.000	14	0.933	14	0.933
1.35	15	15	1.000	14	0.933	14	0.933
1.40	15	15	1.000	14	0.933	14	0.933
1.45	15	15	1.000	14	0.933	14	0.933
1.50	15	15	1.000	14	0.933	14	0.933

Table 4.15 Dataset for alternative methods to process IDA results – Model 2 – X dir.

MODEL 2 - Y DIR

PGA [g]	Number of analysis	Number of collapses	Fraction causing collapse	Number of collapses	Fraction causing collapse	Number of collapses	Fraction causing collapse
IM		**LD**		**SD**		**NC**	
0.05	15	13	0.867	0	0.000	0	0.000
0.10	15	14	0.933	0	0.000	0	0.000
0.15	15	15	1.000	0	0.000	0	0.000
0.20	15	15	1.000	0	0.000	0	0.000
0.25	15	15	1.000	1	0.067	0	0.000
0.30	15	15	1.000	1	0.067	0	0.000
0.35	15	15	1.000	5	0.333	0	0.000
0.40	15	15	1.000	9	0.600	1	0.067
0.45	15	15	1.000	10	0.667	2	0.133
0.50	15	15	1.000	11	0.733	2	0.133
0.55	15	15	1.000	11	0.733	3	0.200
0.60	15	15	1.000	13	0.867	6	0.400
0.65	15	15	1.000	13	0.867	8	0.533
0.70	15	15	1.000	14	0.933	9	0.600
0.75	15	15	1.000	14	0.933	10	0.667
0.80	15	15	1.000	14	0.933	10	0.667
0.85	15	15	1.000	14	0.933	10	0.667
0.90	15	15	1.000	14	0.933	10	0.667
0.95	15	15	1.000	14	0.933	11	0.733
1.00	15	15	1.000	14	0.933	13	0.867
1.05	15	15	1.000	14	0.933	14	0.933
1.10	15	15	1.000	14	0.933	14	0.933
1.15	15	15	1.000	14	0.933	14	0.933
1.20	15	15	1.000	14	0.933	14	0.933
1.25	15	15	1.000	14	0.933	14	0.933
1.30	15	15	1.000	14	0.933	14	0.933
1.35	15	15	1.000	14	0.933	14	0.933
1.40	15	15	1.000	14	0.933	14	0.933
1.45	15	15	1.000	14	0.933	14	0.933
1.50	15	15	1.000	14	0.933	14	0.933

Table 4.16 Dataset for alternative methods to process IDA results – Model 2 – Y dir.

MODEL 3 – X DIR

PGA [g]	Number of analysis	Number of collapses	Fraction causing collapse	Number of collapses	Fraction causing collapse	Number of collapses	Fraction causing collapse
IM		**LD**		**SD**		**NC**	
0.05	15	14	0.933	0	0.000	0	0.000
0.10	15	15	1.000	0	0.000	0	0.000
0.15	15	15	1.000	0	0.000	0	0.000
0.20	15	15	1.000	1	0.067	0	0.000
0.25	15	15	1.000	3	0.200	0	0.000
0.30	15	15	1.000	6	0.400	0	0.000
0.35	15	15	1.000	9	0.600	0	0.000
0.40	15	15	1.000	10	0.667	1	0.067
0.45	15	15	1.000	11	0.733	1	0.067
0.50	15	15	1.000	12	0.800	1	0.067
0.55	15	15	1.000	14	0.933	3	0.200
0.60	15	15	1.000	14	0.933	3	0.200
0.65	15	15	1.000	14	0.933	7	0.467
0.70	15	15	1.000	14	0.933	9	0.600
0.75	15	15	1.000	14	0.933	11	0.733
0.80	15	15	1.000	14	0.933	12	0.800
0.85	15	15	1.000	14	0.933	12	0.800
0.90	15	15	1.000	14	0.933	12	0.800
0.95	15	15	1.000	14	0.933	13	0.867
1.00	15	15	1.000	14	0.933	13	0.867
1.05	15	15	1.000	14	0.933	14	0.933
1.10	15	15	1.000	14	0.933	14	0.933
1.15	15	15	1.000	14	0.933	14	0.933
1.20	15	15	1.000	14	0.933	14	0.933
1.25	15	15	1.000	14	0.933	14	0.933
1.30	15	15	1.000	14	0.933	14	0.933
1.35	15	15	1.000	14	0.933	14	0.933
1.40	15	15	1.000	14	0.933	14	0.933
1.45	15	15	1.000	14	0.933	14	0.933
1.50	15	15	1.000	14	0.933	14	0.933

Table 4.17 Dataset for alternative methods to process IDA results – Model 3 – X dir.

MODEL 3 – Y DIR

PGA [g]	Number of analysis	Number of collapses	Fraction causing collapse	Number of collapses	Fraction causing collapse	Number of collapses	Fraction causing collapse
IM		**LD**		**SD**		**NC**	
0.05	15	14	0.933	0	0.000	0	0.000
0.10	15	15	1.000	0	0.000	0	0.000
0.15	15	15	1.000	0	0.000	0	0.000
0.20	15	15	1.000	1	0.067	0	0.000
0.25	15	15	1.000	2	0.133	0	0.000
0.30	15	15	1.000	8	0.533	0	0.000
0.35	15	15	1.000	10	0.667	0	0.000
0.40	15	15	1.000	11	0.733	1	0.067
0.45	15	15	1.000	11	0.733	2	0.133
0.50	15	15	1.000	13	0.867	2	0.133
0.55	15	15	1.000	14	0.933	2	0.133
0.60	15	15	1.000	14	0.933	5	0.333
0.65	15	15	1.000	14	0.933	9	0.600
0.70	15	15	1.000	14	0.933	9	0.600
0.75	15	15	1.000	14	0.933	10	0.667
0.80	15	15	1.000	14	0.933	10	0.667
0.85	15	15	1.000	14	0.933	10	0.667
0.90	15	15	1.000	14	0.933	10	0.667
0.95	15	15	1.000	14	0.933	11	0.733
1.00	15	15	1.000	14	0.933	12	0.800
1.05	15	15	1.000	14	0.933	14	0.933
1.10	15	15	1.000	14	0.933	14	0.933
1.15	15	15	1.000	14	0.933	14	0.933
1.20	15	15	1.000	14	0.933	14	0.933
1.25	15	15	1.000	14	0.933	14	0.933
1.30	15	15	1.000	14	0.933	14	0.933
1.35	15	15	1.000	14	0.933	14	0.933
1.40	15	15	1.000	14	0.933	14	0.933
1.45	15	15	1.000	14	0.933	14	0.933
1.50	15	15	1.000	14	0.933	14	0.933

Table 4.18 Dataset for alternative methods to process IDA results – Model 3 – Y dir.

4.6.1.3 θ and β

The statistical parameters θ (median value) and β (standard deviation value) of cumulative density functions Φ are reported in Tables 4.19-4.21.
Values described for alternative methods about "maximum likelihood fit" and "maximum likelihood fit" using a probit regression are the same for all models so only fragility curves for alternative methods "maximum likelihood fit" are listed in next paragraph.

		MODEL 1											
		LD				SD				NC			
		DIR X		DIR Y		DIR X		DIR Y		DIR X		DIR Y	
		β	ϴ	β	ϴ	β	ϴ	β	ϴ	β	ϴ	β	ϴ
Main methods	mle	0.351	0.044	0.357	0.041	0.316	0.372	0.361	0.381	0.213	0.690	0.165	0.696
	mom	0.474	0.049	0.371	0.043	0.334	0.393	0.393	0.412	0.216	0.702	0.168	0.712
	trunc_alt	0.530	0.049	0.542	0.045	0.322	0.393	0.379	0.412	0.210	0.703	0.207	0.719
Alternative methods	mle	0.792	0.040	0.092	0.049	0.453	0.416	0.426	0.404	0.352	0.801	0.303	0.832
	probit	0.792	0.040	0.071	0.049	0.453	0.416	0.426	0.404	0.352	0.801	0.303	0.832
	sse	0.712	0.041	0.139	0.048	0.413	0.401	0.377	0.387	0.321	0.779	0.305	0.812

Table 4.19 Statistical parameters ϑ (median value) and ϐ – Model 1 – X e Y dir.

		MODEL 2											
		LD				SD				NC			
		DIR X		DIR Y		DIR X		DIR Y		DIR X		DIR Y	
		β	ϴ	β	ϴ	β	ϴ	β	ϴ	β	ϴ	β	ϴ
Main methods	mle	0.346	0.048	0.354	0.036	0.271	0.477	0.306	0.385	0.156	0.715	0.318	0.607
	mom	0.455	0.052	0.476	0.039	0.275	0.496	0.305	0.402	0.161	0.721	0.307	0.634
	trunc_alt	0.521	0.053	0.556	0.040	0.265	0.496	0.294	0.402	0.205	0.729	0.295	0.634
Alternative methods	mle	0.655	0.042	0.484	0.045	0.350	0.519	0.388	0.421	0.295	0.811	0.384	0.697
	probit	0.655	0.042	0.486	0.045	0.350	0.519	0.388	0.421	0.295	0.811	0.384	0.698
	sse	0.635	0.042	0.540	0.044	0.349	0.507	0.356	0.407	0.253	0.790	0.377	0.684

Table 4.20 Statistical parameters ϑ (median value) and ϐ – Model 2 – X e Y dir.

		MODEL 3											
		LD				SD				NC			
		DIR X		DIR Y		DIR X		DIR Y		DIR X		DIR Y	
		β	ϴ	β	ϴ	β	ϴ	β	ϴ	β	ϴ	β	ϴ
Main methods	mle	0.298	0.018	0.345	0.016	0.340	0.316	0.302	0.306	0.216	0.627	0.285	0.600
	mom	0.441	0.020	0.460	0.018	0.327	0.330	0.305	0.320	0.228	0.638	0.284	0.624
	trunc_alt	0.633	0.021	0.648	0.019	0.316	0.330	0.304	0.321	0.221	0.639	0.272	0.624
Alternative methods	mle	0.092	0.049	0.092	0.049	0.492	0.348	0.498	0.336	0.349	0.697	0.382	0.704
	probit	0.071	0.049	0.071	0.049	0.492	0.348	0.498	0.336	0.349	0.697	0.381	0.704
	sse	0.139	0.048	0.139	0.048	0.417	0.337	0.386	0.322	0.268	0.680	0.374	0.690

Table 4.21 Statistical parameters ϑ (median value) and ϐ – Model 3 – X e Y dir.

4.6.2 Result

All fragility curve analysed are itemised below. A comparison between damage measures and between X-Y directions of three models are done in next paragraphs.

4.6.2.1 Comparison between fragility curves for all three models

In the first part, a comparison is made between the fragility curves concerning the different damage limit states of the three different models. All fragility curves calculated using the statistical method of “maximum likelihood fit for truncated IDA”, have more probability of collapse respect the other main methods to process IDA dataset (curves are less flattened). Another characteristic is those main statistical methods have more probability of collapse than alternative methods suitable for other types of analysis. Overall small differences depending on a statistical method to achieve fragility curves are observed.
Modelling precast reinforced hollow brick vault as Model one, the nonlinear structural behaviour is overestimated. In both X and Y directions, it is also observed that the slope of the fragility curves varies with damage state considered; as a consequence, there is also the variety of relationships between fragility curves.
Specific conclusions for X and Y directions are reported below.

4.6.2.1.1 X direction

According to X direction perpendicular to the vault, for limited damage fragility curves of the Model one and two overlap and the Model three has a greater probability of collapse than the previous ones regarding all the statistical methods considered (especially with the curve calculated with the statistical method of the moments fit).
For significant damage, all fragility curves are very distinct from each other and Model three shows the greatest probability of collapse, then Model one and two. For the probability of collapse close to 0.9, fragility curves of Models one and two coincide considering alternative statistical methods not proper suitable for IDA dataset.
For near collapse damage state, fragility curve of Model three is the one with the probability of major collapse. With the exception of the curves obtained with statistical method of likelihood fit for truncated IDA where Model one has greater probability of collapse than Model two, in other comparisons obtained with main statistical methods, Model one has a greater probability of collapse than Model two until a peak ground acceleration equal to 0.75g (after that probability of collapse seems to be perfectly exchanges each other). For alternative method the same behaviour of Model one and two is displayed with a point of exchange equal to 0.60g and more difference in probability of collapse of the three models is shown.
For all the damage states considered, it can be observed how the model three with a vault made of beam elements and with plastic hinges arranged on the ribs is the one with the highest probability of collapse in X-direction.
All fragility curves in X-direction calculated with main (Figures 4.28-4.30) and alternative (Figures 4.31-4.33) methods are reported below.

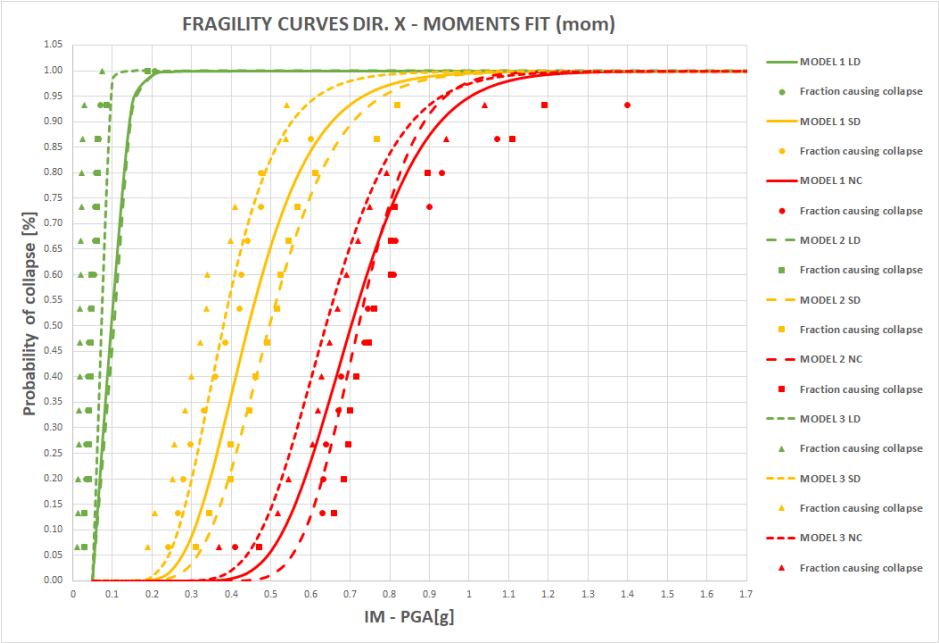

Figure 4.28 Fragility Curves DIR. X MODEL 1,2,3 – Moment fit main method.

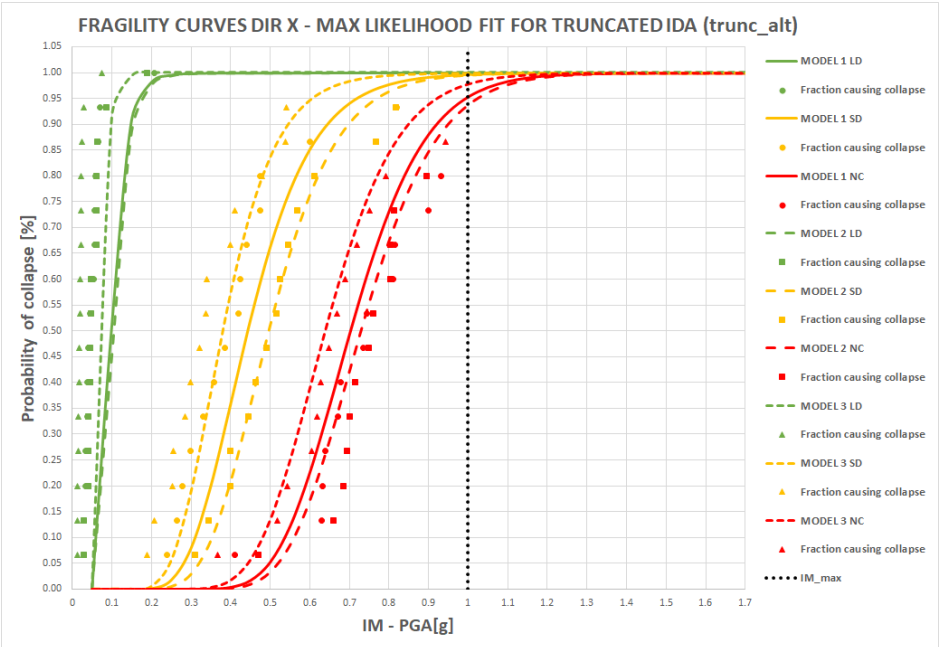

Figure 4.29 Fragility Curves DIR. X MODEL 1,2,3 – Max likelihood fit for truncated IDA main method.

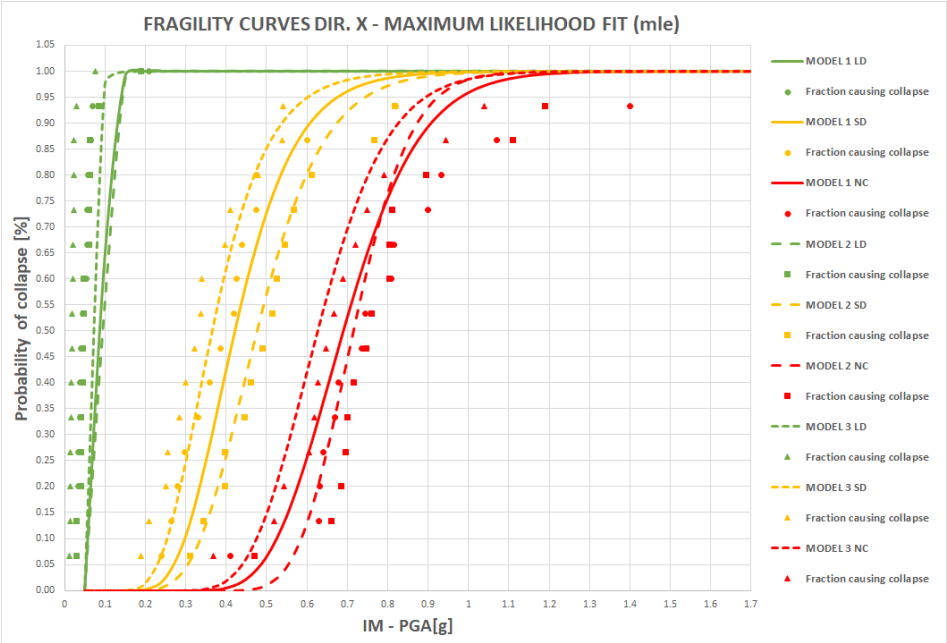

Figure 4.30 Fragility Curves DIR. X MODEL 1,2,3 – Maximum likelihood fit main method.

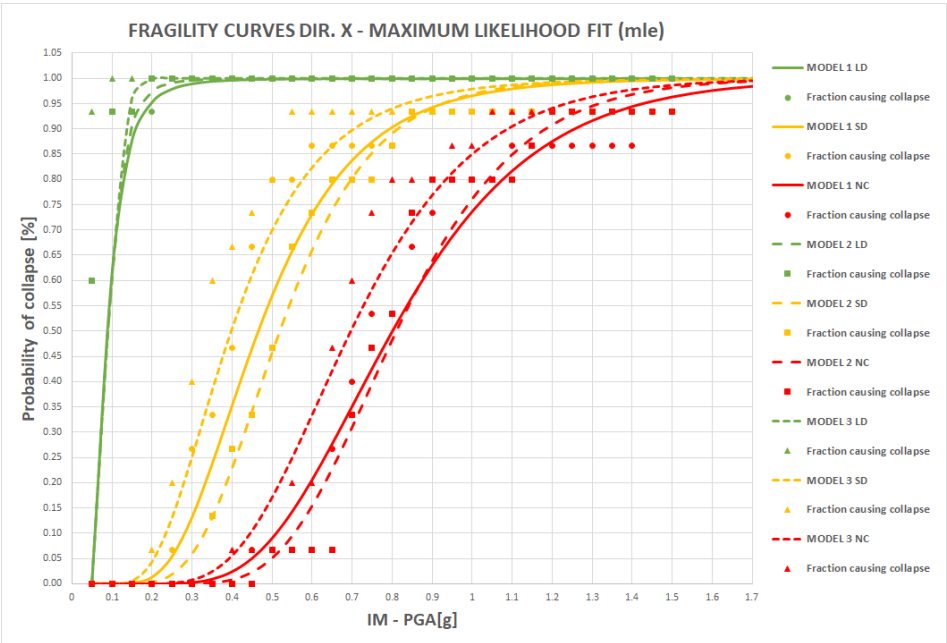

Figure 4.31 Fragility Curves DIR. X MODEL 1,2,3 – Maximum likelihood fit alternative method.

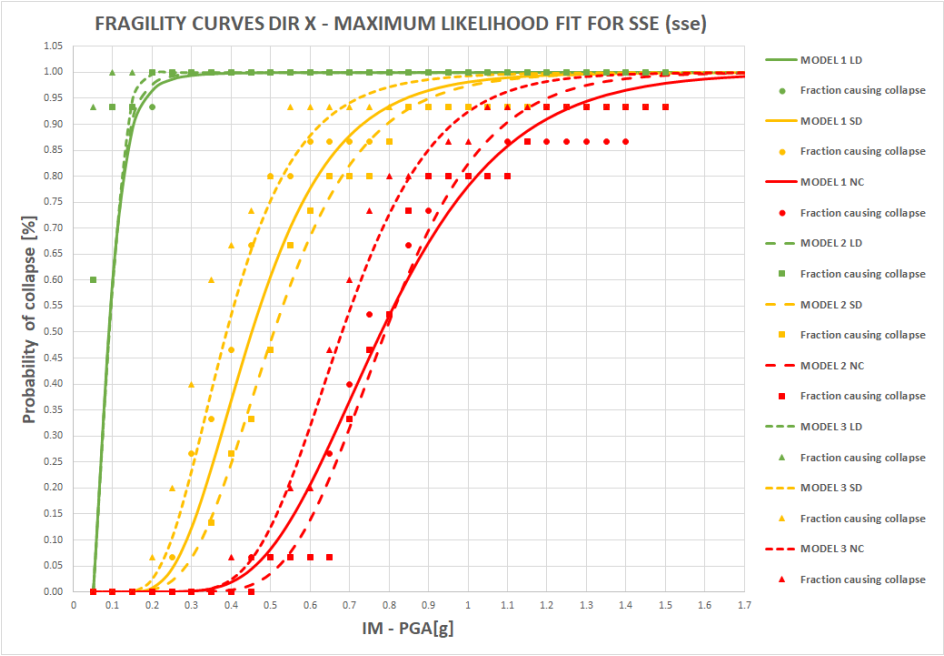

Figure 4.32 Fragility Curves DIR. X MODEL 1,2,3 – Max likelihood fit for SSE alternative method.

4.6.2.1.2 Y direction

According to Y direction parallel to the vault, for limited damage fragility curves derived from main statistical methods for Models one and two overlaps, while fragility curves for Model three have a major probability of collapse.
All fragility curves of all three models overlap each other taking into account alternative statistical methods.
For significant damage, for all statistical methods, the probability of collapse increases considering in order Model one, two and three. Fragility curves realised with main methods have a greater detachment each other with the increase of the PGA (major differences are observed with fragility curves realised with "maximum likelihood fit for truncated IDA"). If the probability of collapse achieved by alternative methods is considered, fragility curves are very close to each other.
For near collapse damage state with alternative probabilistic models, fragility curves of Models two and three overlaps for all cases and the Model one has the lowest probability of collapse, in particular at lesser PGA levels. For fragility curves realised with the main statistical methods, the description of their behaviour is more complex because for fragility curves of Models two and three there is no clear distinction because the probabilities of collapse are more or less the same.
Model one is less probability of collapsing than Model two and three for PGA values below 0.85g; once this value is exceeded, Model one is more probability of collapsing than Model two and three.
Using a maximum likelihood fit for truncated IDA of main statistical method, for PGA values greater than one the curves of the three models overlap.
In conclusion, even for Y direction, Model three has the major probability of collapse for all three damage measures respect other models even if there is less difference between fragility curves in Y-direction respect X-direction due to the fact that all minimum of threshold values in pushover analysis considered are in X-direction.
All fragility curves calculated in Y-direction with main (Figures 4.33-4.35) and alternative (Figures 4.36-4.38) methods are reported below.

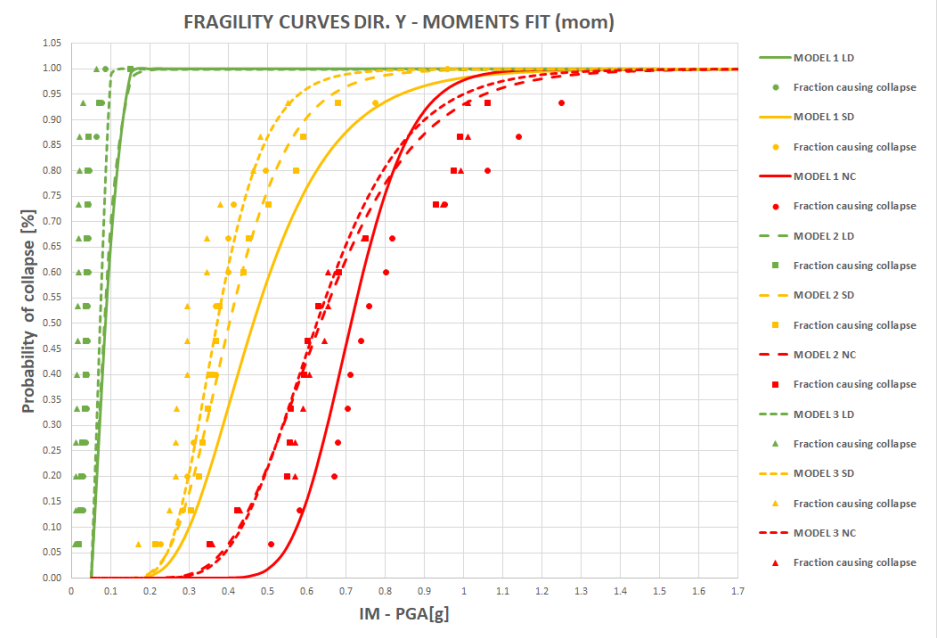

Figure 4.33 Fragility Curves DIR. Y MODEL 1,2,3 – Moment fit main method.

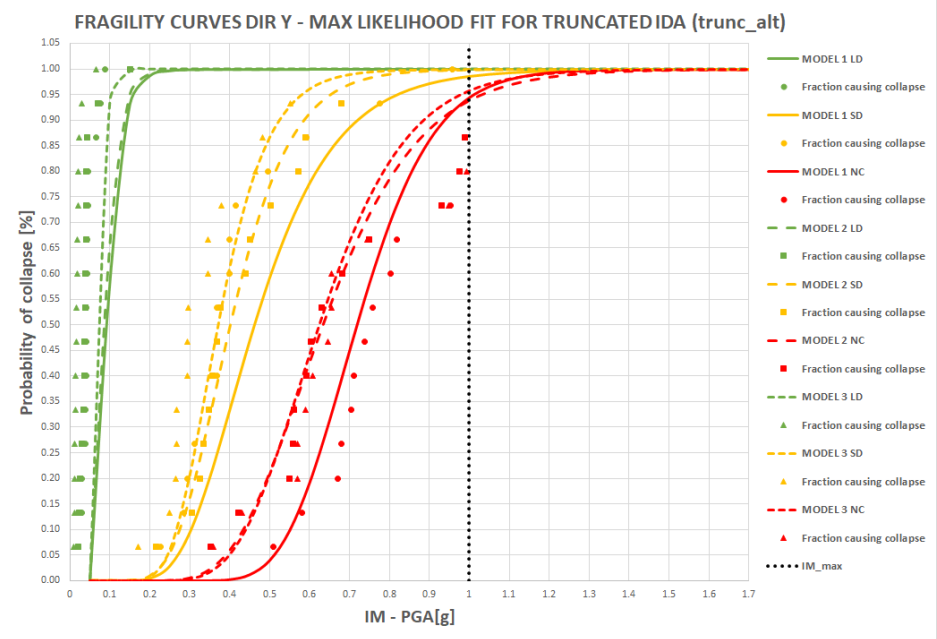

Figure 4.34 Fragility Curves DIR. Y MODEL 1,2,3 – Max likelihood fit for truncated IDA main method.

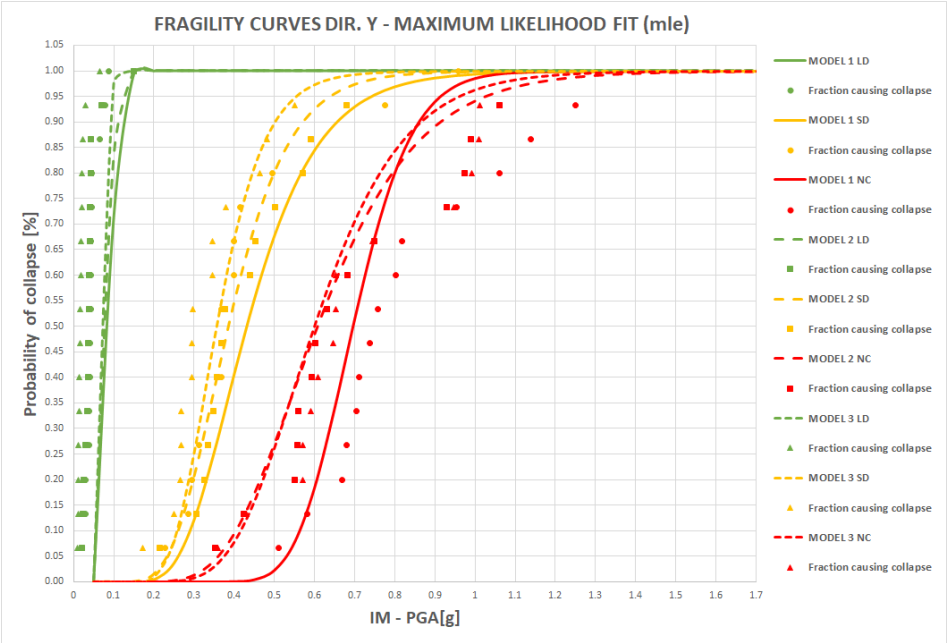

Figure 4.35 Fragility Curves DIR. Y MODEL 1,2,3 – Maximum likelihood fit for main method.

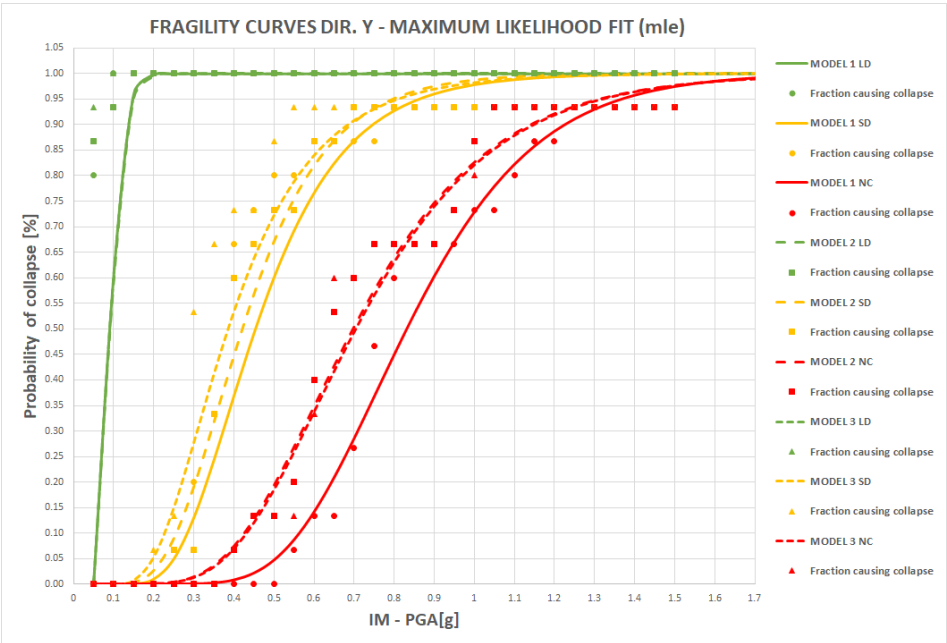

Figure 4.36 Fragility Curves DIR. Y MODEL 1,2,3 – Maximum likelihood fit for alternative method.

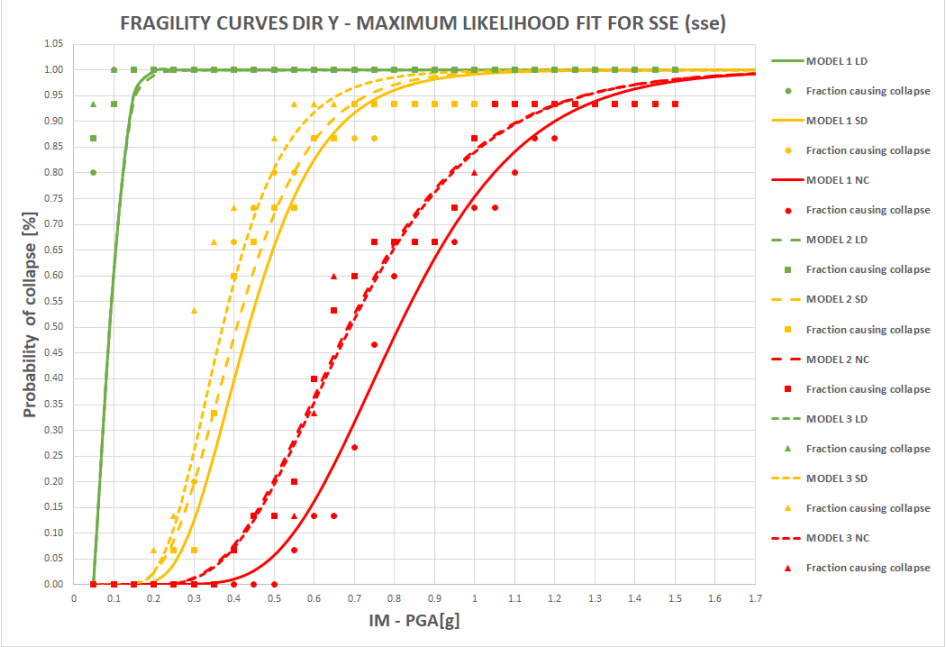

Figure 4.37 Fragility Curves DIR. Y MODEL 1,2,3 – Max likelihood fit for SSE for alternative method.

4.6.2.2 Comparison between X-Y directions for all models

X-direction describes the probability of collapse parallel to the vault while y-direction evaluates the structural behaviour of the vault and how much it influences the different type of modelling chosen for all models.
As already mentioned previously, precast reinforced hollow brick light-weight vaults were built from the thirties up to around the mid-sixties and section, material and details of reinforced bars of main structural elements such as columns and beams reflect the constructive practices of these years. The X-direction also assumes a fundamental role since the vulnerability of this type of building depends not only on the secondary structural elements such as the vault but also on the main building elements that are usually not adequately designed.
For all three models, considering significant damage level the Y-direction is the one that gives a greater probability of collapse while considering near collapse damage level fragility curves of X-direction have a higher slope than fragility curve of Y direction. All detailed evaluations carried out separately for the three types of models are shown in the following paragraphs.

4.6.2.2.1 Model 1

For limited damage for main statistical methods probabilities of collapse for X and Y directions are the same while for alternative statistical methods fragility curves in Y direction have a major probability of collapse respect X direction. For significant damage, fragility curves overlap each other in case of the main statistical method while for alternative method fragility curves in Y direction shows major probability of collapse for lower intensity measure (PGA) than X direction with a clear distinction between them. For near collapse for all statistical method fragility curves show similar behaviour in all directions (for maximum likelihood fit for truncated IDA curves fragility curves are the same). In conclusion, for all cases there is no clear distinction between curves except those of significant damage limit state.

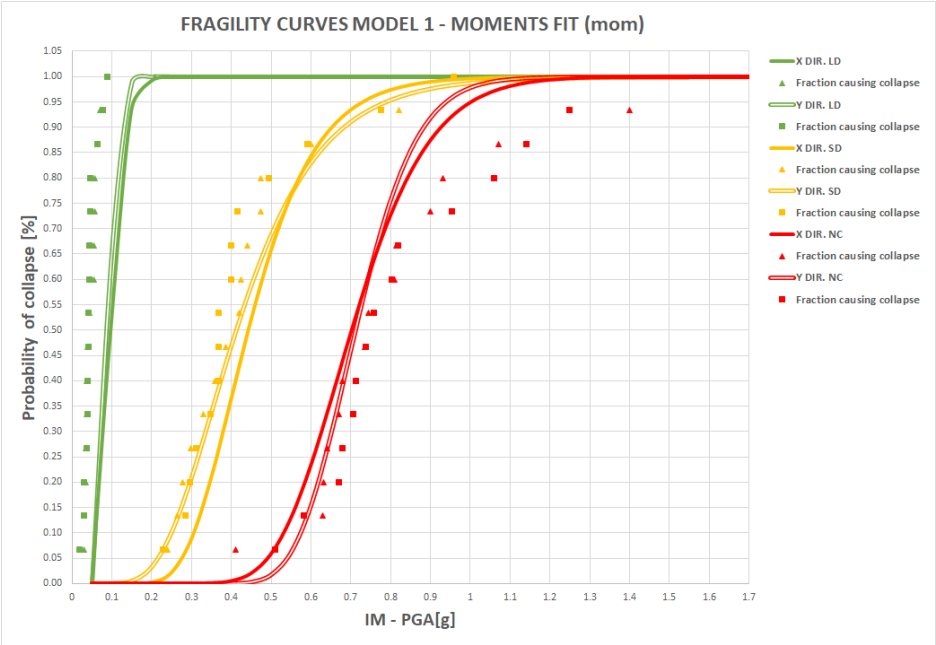

Figure 4.38 Fragility Curves MODEL1 X-Y dir. – Moment fit main method.

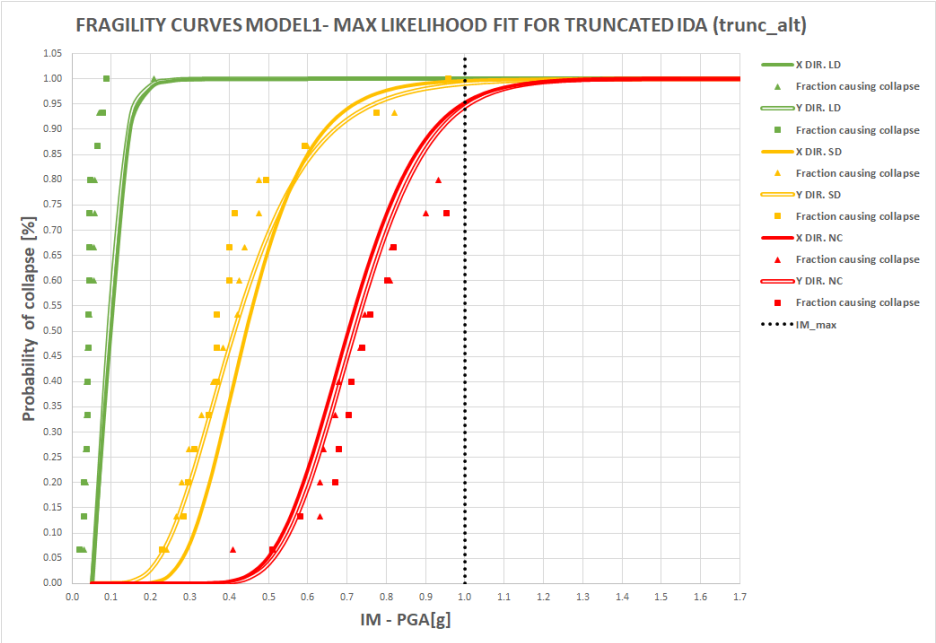

Figure 4.39 Fragility Curves MODEL1 X-Y dir. – Max likelihood fit for truncated IDA main method.

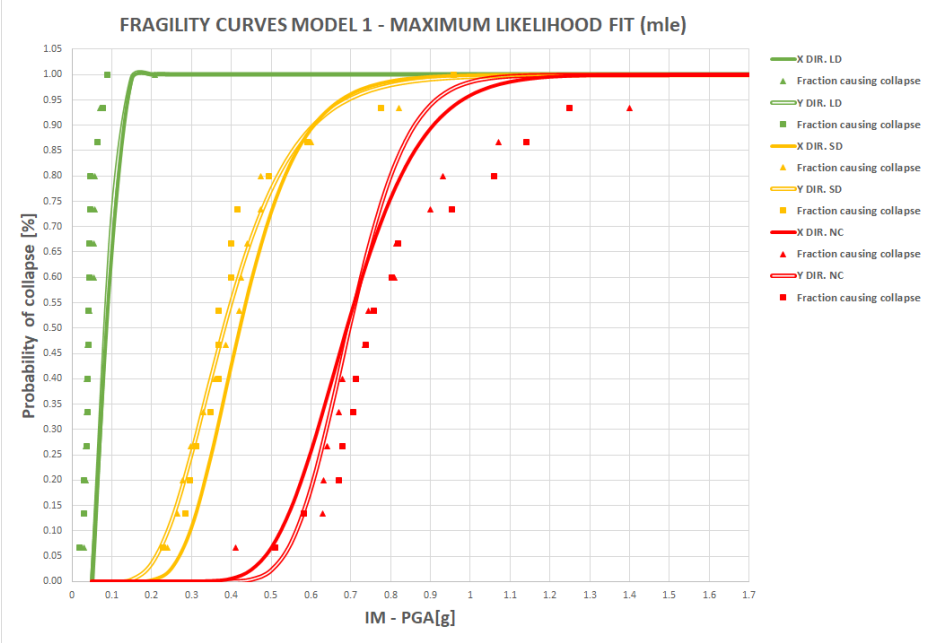

Figure 4.40 Fragility Curves MODEL1 X-Y dir. – Maximum likelihood fit for main method.

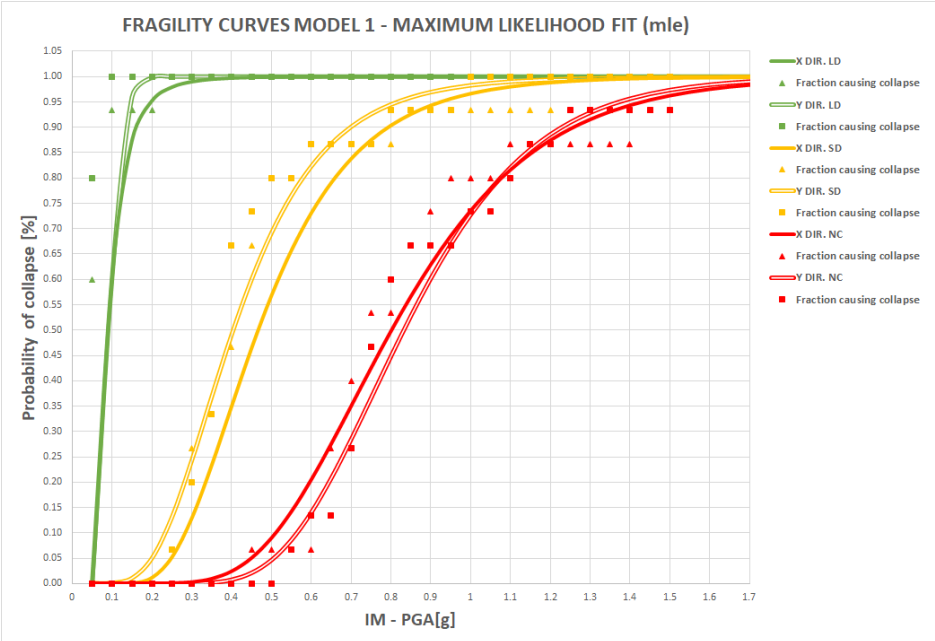

Figure 4.41 Fragility Curves MODEL1 X-Y dir. – Maximum likelihood fit for alternative method.

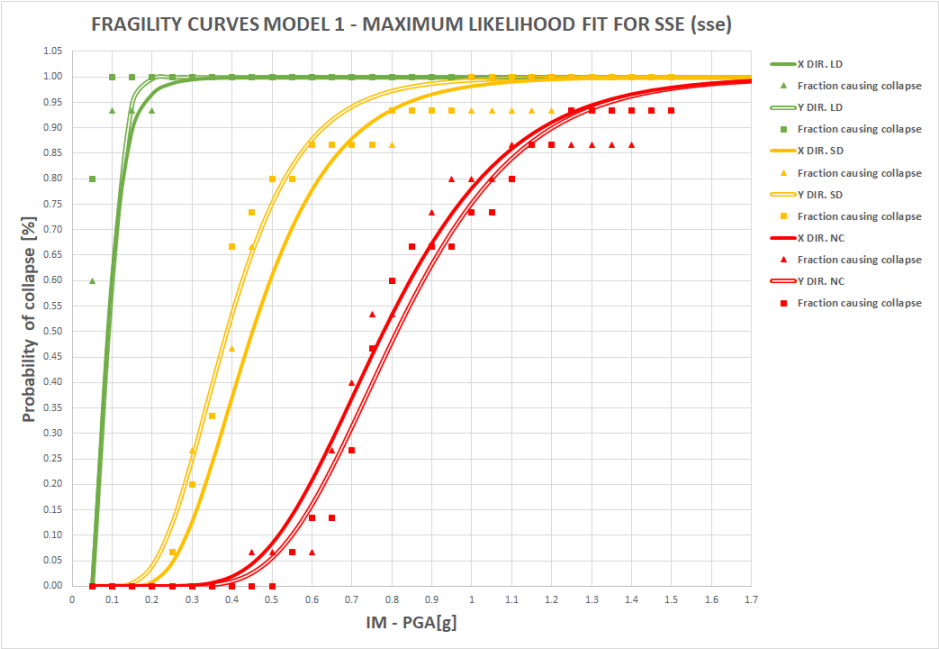

Figure 4.42 Fragility Curves MODEL1 X-Y dir. – Max likelihood fit for SSE for alternative method.

4.6.2.2.2 Model 2

The behaviour of the fragility curves of the Model two does not depend on the type of statistical method considered. For limited damage and for all statistical methods fragility curve in X and Y directions perfectly overlap. For significant damage and for all statistical cases, Model two in the Y direction is more vulnerable than X direction and these fragility curves have the same slope. For near collapse and for main statistical method fragility curves in X direction have a lower slope than Y direction and until PGA of 0.85g X direction have a minor probability of collapse respect Y direction; after this value, the structural behaviour is exchanged. For maximum likelihood fit for truncated IDA method fragility curves overlap each other. Fragility curves realised with alternative method have the same behaviour showed in moment fit main method but the ratio between curves vary for 1.3g with maximum likelihood method and for 1.05g with maximum likelihood method for sse.

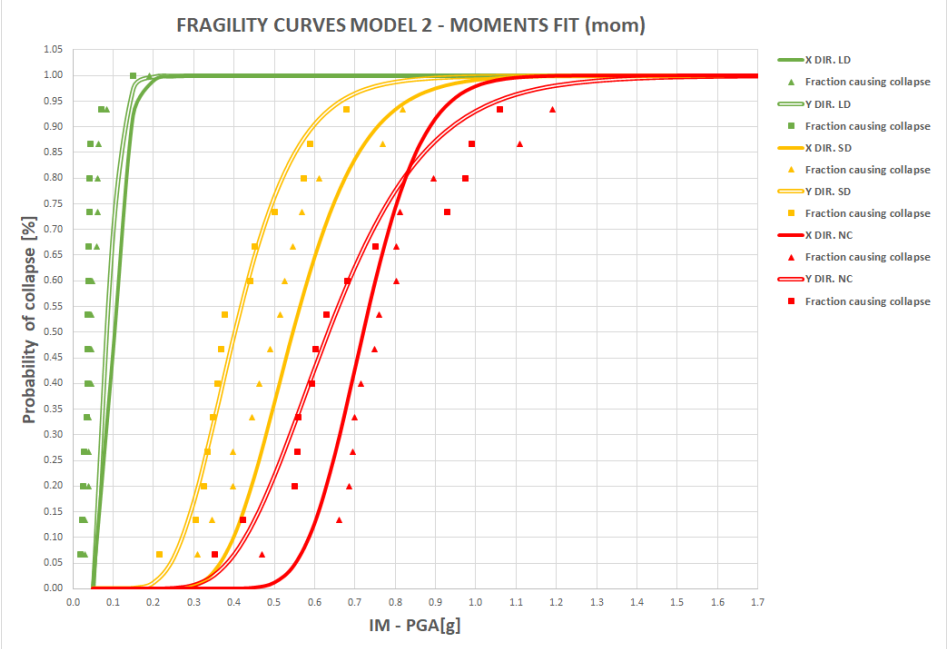

Figure 4.43 Fragility Curves MODEL 2 X-Y dir. – Moment fit main method.

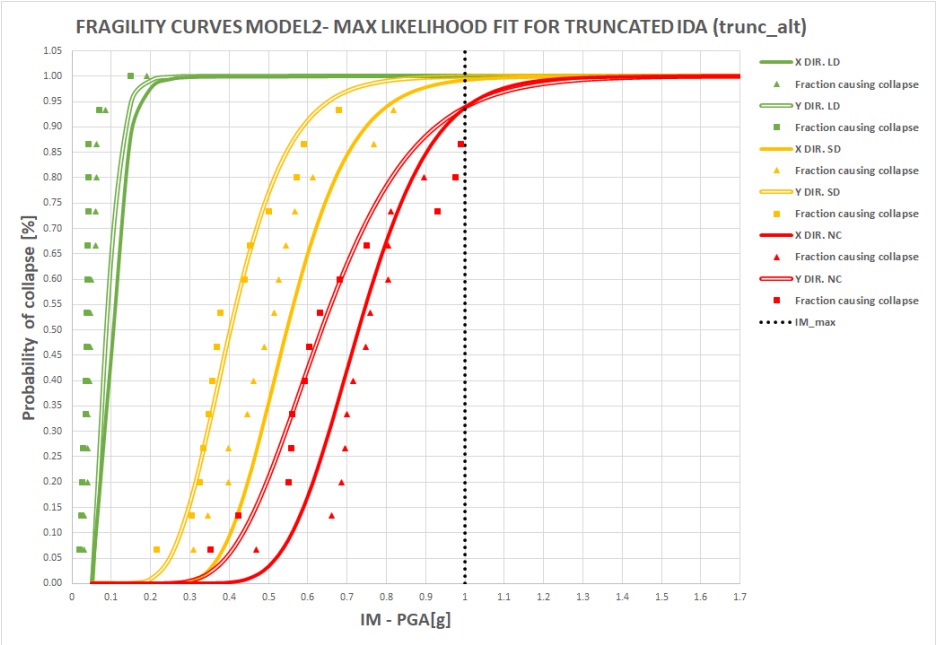

Figure 4.44 Fragility Curves MODEL2 X-Y dir. – Max likelihood fit for truncated IDA main method.

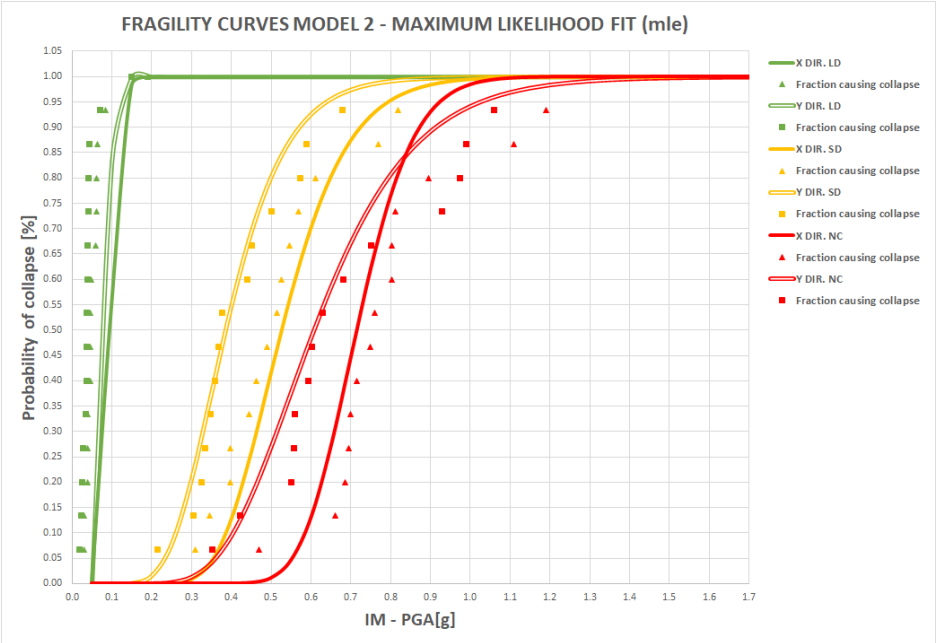

Figure 4.45 Fragility Curves MODEL2 X-Y dir. – Maximum likelihood fit for main method.

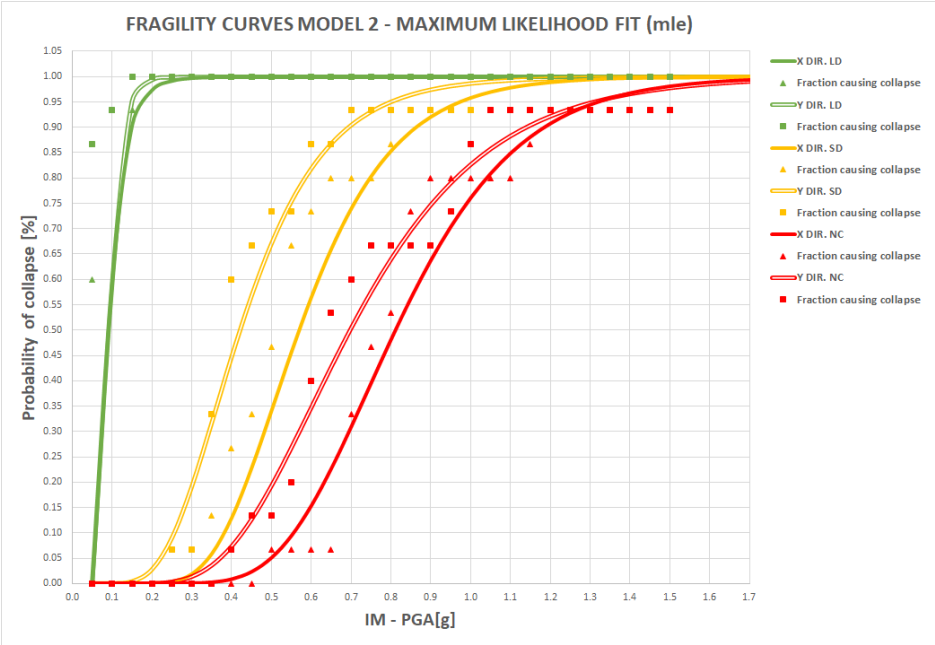

Figure 4.46 Fragility Curves MODEL2 X-Y dir. – Maximum likelihood fit for alternative method.

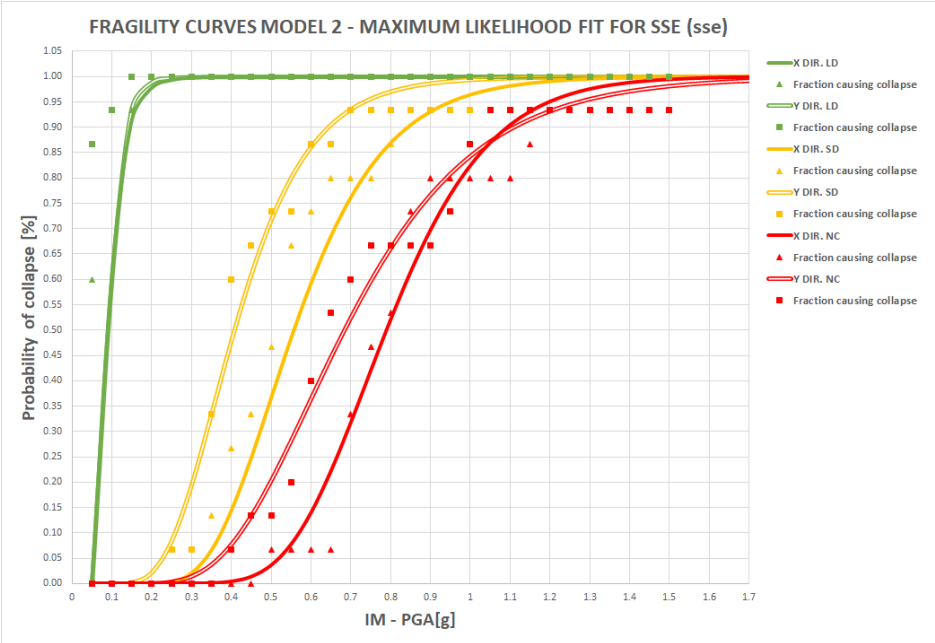

Figure 4.47 Fragility Curves MODEL2 X-Y dir. – Max likelihood fit for SSE for an alternative method.

4.6.2.2.3 Model 3

For limited damage and for all statistical methods fragility curves in X and Y directions perfectly overlap. For significant damage, like the behaviour of Model two but with less detachment between curves, Model three in the Y direction is more vulnerable than X direction. Even for near collapse damage state, fragility curves of Model three show the same behaviour of fragility curves of Model two. Until a value of 0.7g of PGA, fragility curves in X direction have less probability of collapse respect Y direction; after this value, X-direction becomes the weak direction.

Fragility curves are significantly different if "maximum likelihood fit for sse" as an alternative statistical method is considered; in the other cases there is only a slight gap between the curves except for significant limit damage state threshold cases.

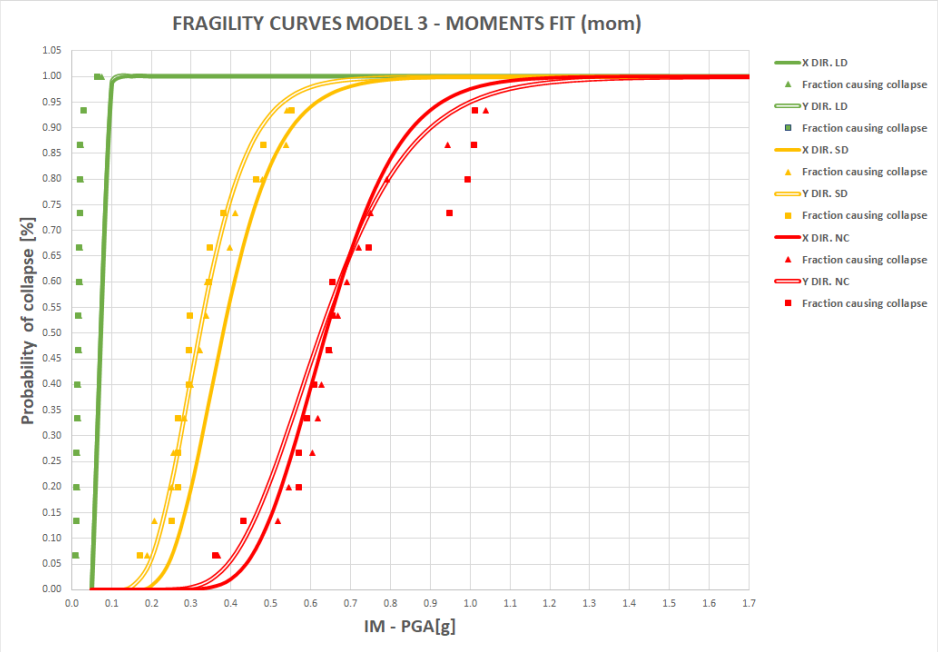

Figure 4.48 Fragility Curves MODEL 3 X-Y dir. – Moment fit main method.

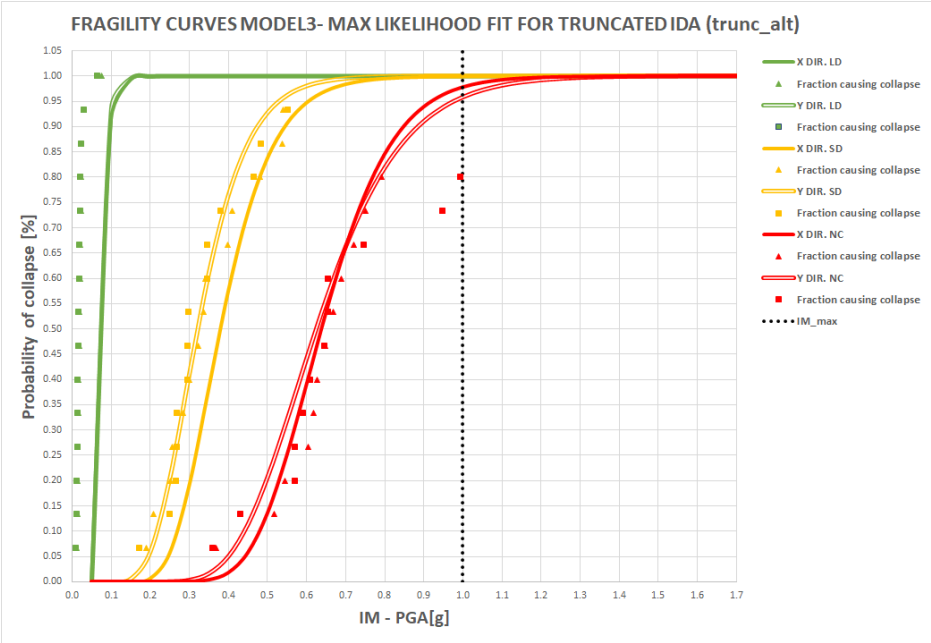

Figure 4.49 Fragility Curves MODEL 3 X-Y dir. – Max likelihood fit for truncated IDA main method.

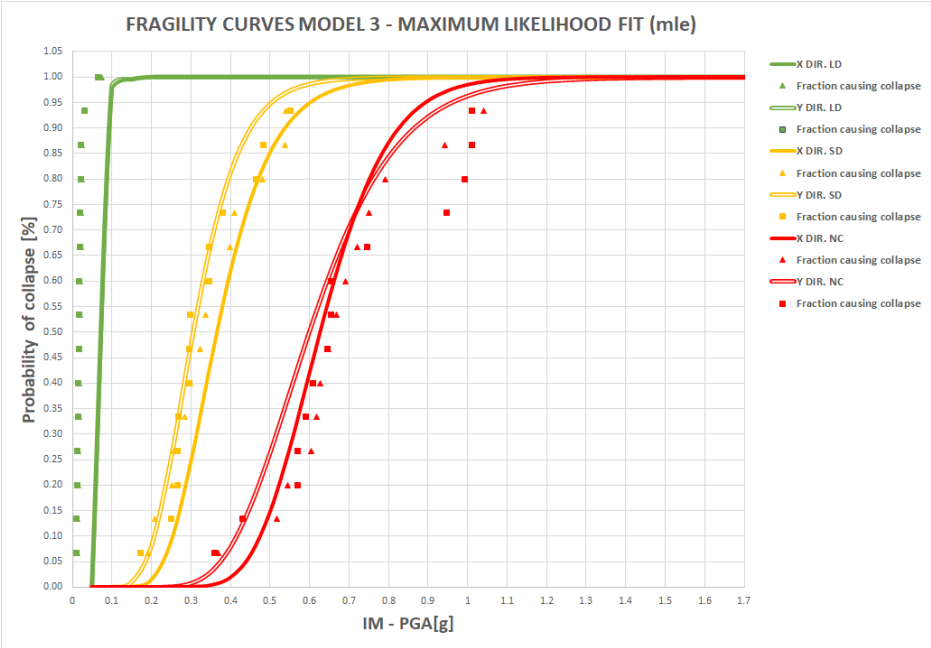

Figure 4.50 Fragility Curves MODEL 3 X-Y dir. – Maximum likelihood fit for main method.

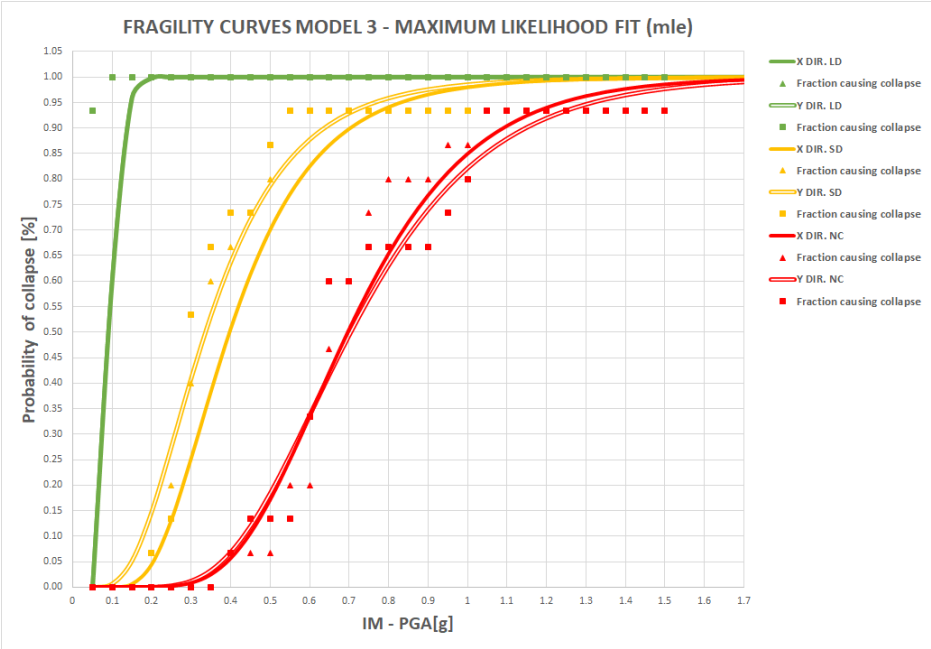

Figure 4.51 Fragility Curves MODEL 3 X-Y dir. – Maximum likelihood fit for alternative method.

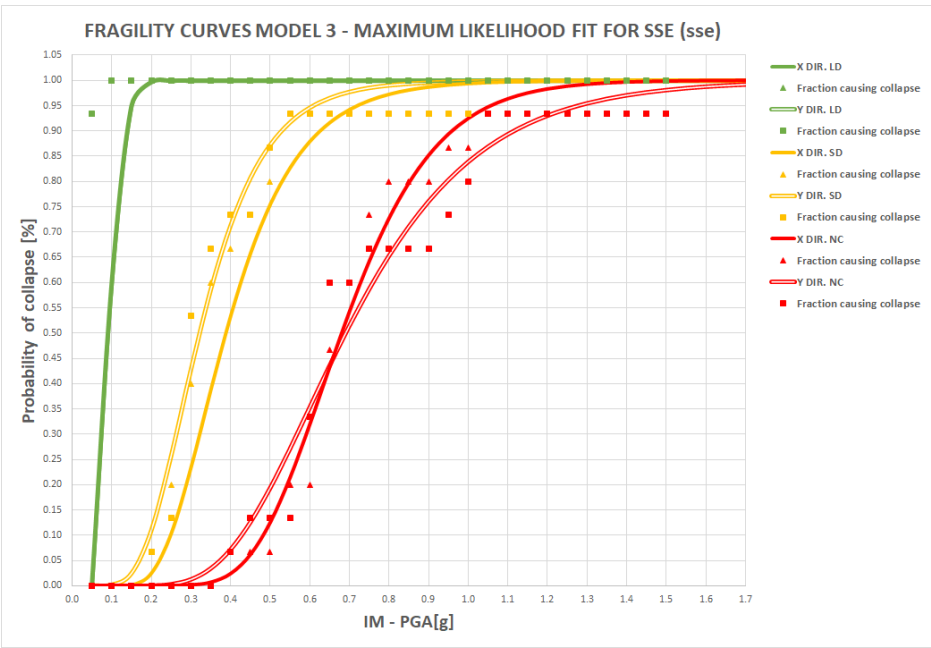

Figure 4.52 Fragility Curves MODEL 3 X-Y dir. – Max likelihood fit for SSE for alternative method.

4.7 IDA versus Nonlinear static analysis capacity curves

A comparison between the capacity curves obtained from both the nonlinear analyses performed (IDA and push-over) for all three models is carried out.
Main conclusions are reported below:

- The pushover analysis provides a good result if compared to the IDA global response at varying ground motions;
- The pushover curves of all models are in most cases above the IDA curves. This means that, except in X-direction in Model one and two where there are some IDA curves with base shears and displacements less than those deriving from curves of nonlinear static analysis, the two pushover curves are not upper and lower bounds for the more realistic IDA curves (This situation is very difficult to obtain);
- The push-over curves underestimate base shear but, in some cases, overestimate the displacement;
- In Model three for all directions the capacity curves created with incremental dynamic analysis have a lower stiffness than the capacity curves realized with nonlinear static analysis;
- In Model one for all directions the slope of the elastic part of IDA curves is positioned in the middle of push mode and push mass curves of the nonlinear static analysis;
- For + and - y directions, fragility curves of Model one and two assume the same stiffness in the elastic field.

All capacity curves grouped by the direction considered are shown below.

4.7.1 Capacity Curves +X direction

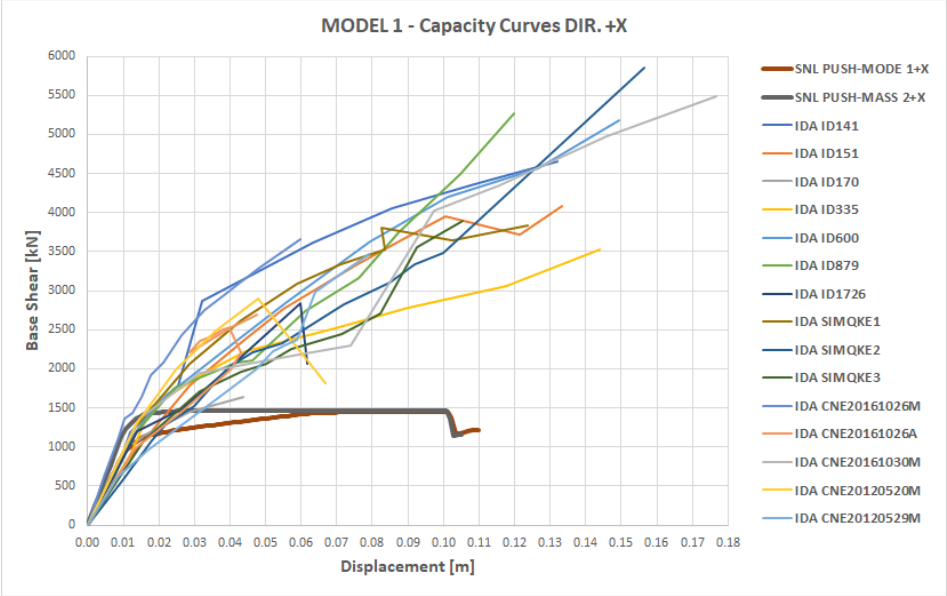

Figure 4.53 Capacity Curves MODEL 1 direction +X.

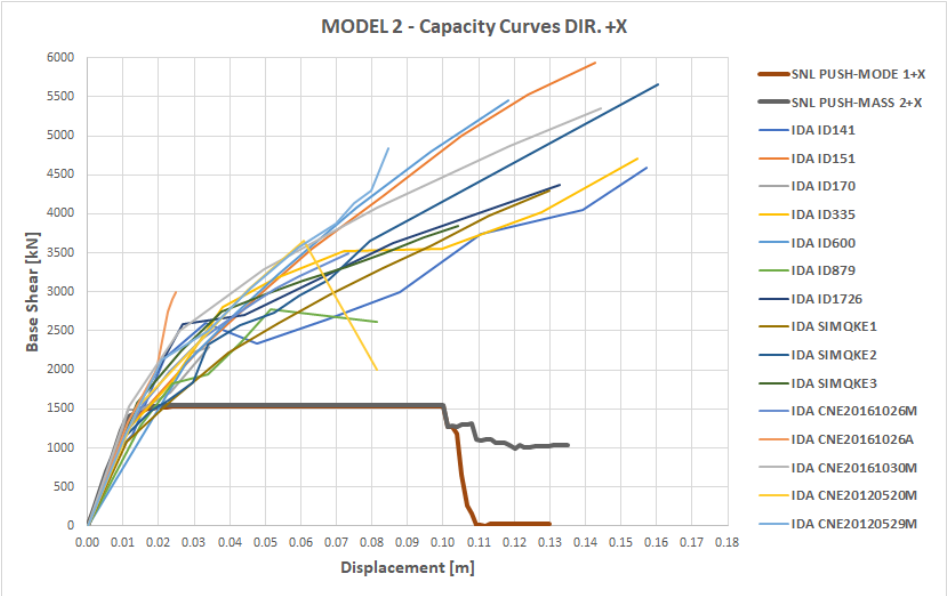

Figure 4.54 Capacity Curves MODEL 2 direction +X.

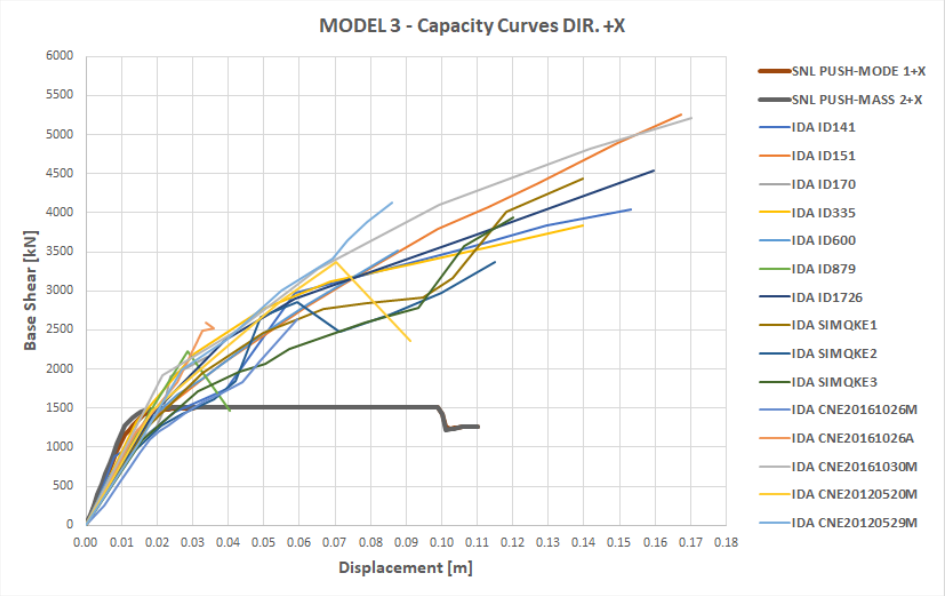

Figure 4.55 Capacity Curves MODEL 3 direction +X.

4.7.2 Capacity Curves direction -X

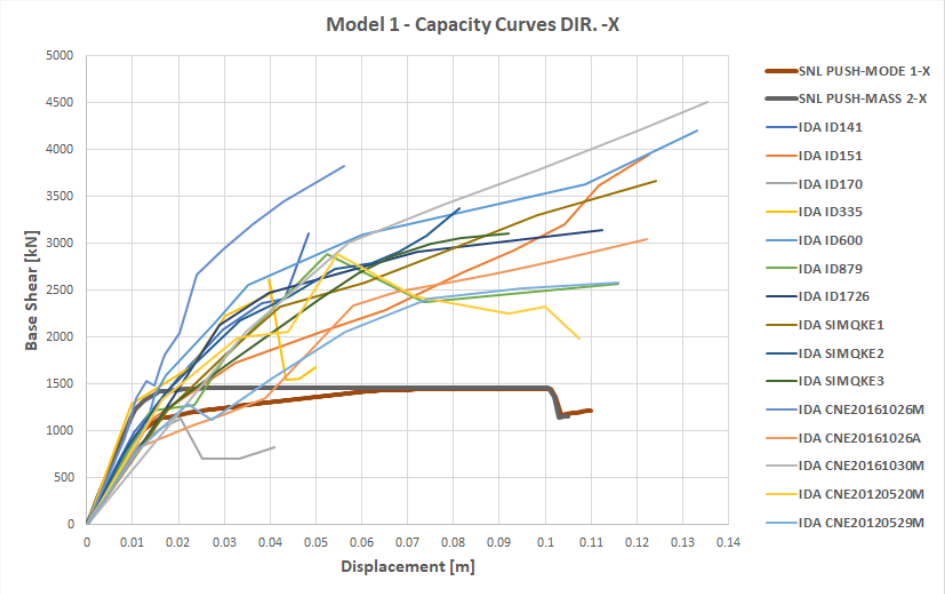

Figure 4.56 Capacity Curves MODEL 1 direction -X.

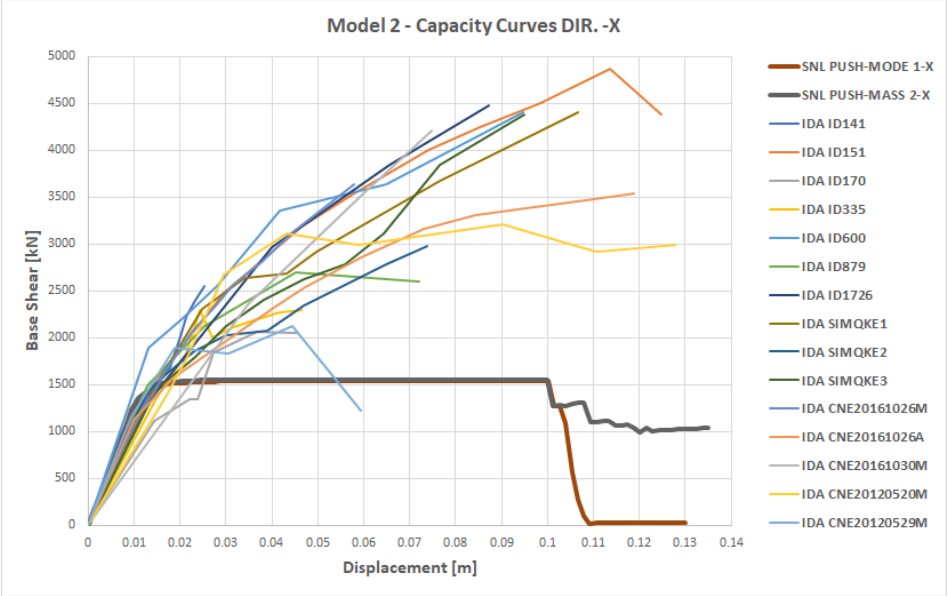

Figure 4.57 Capacity Curves MODEL 2 direction -X.

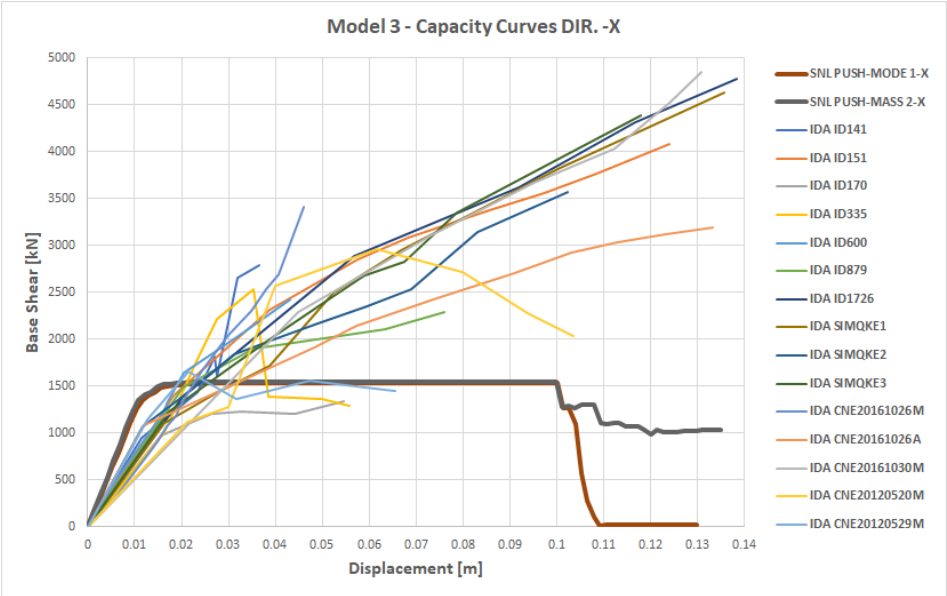

Figure 4.58 Capacity Curves MODEL 3 direction -X.

4.7.3 Capacity Curves direction +Y

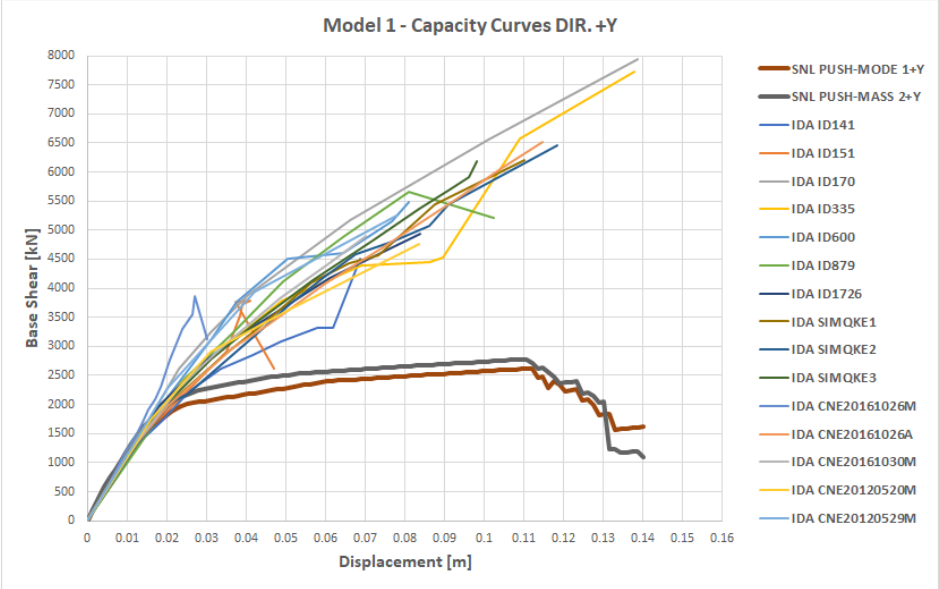

Figure 4.59 Capacity Curves MODEL 1 direction +Y.

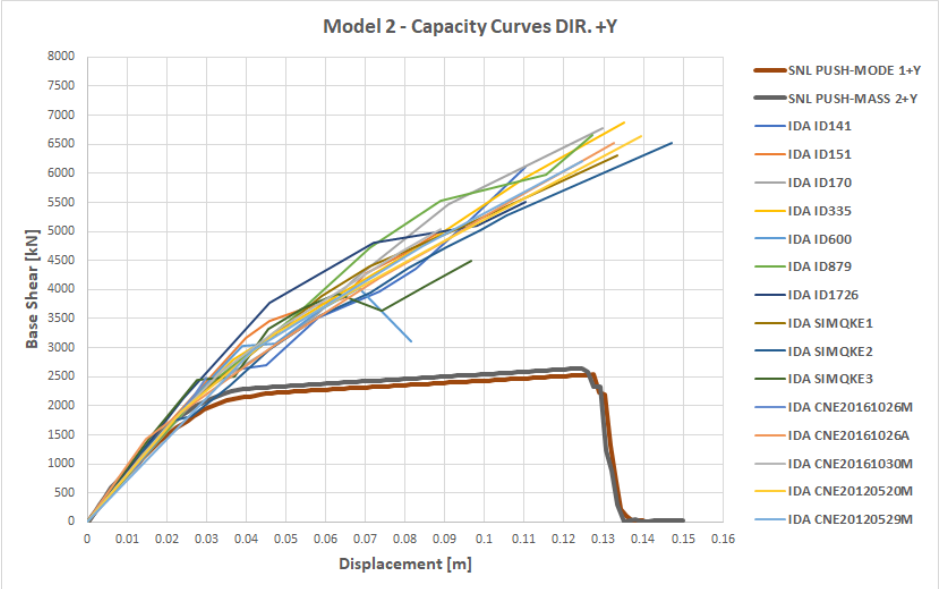

Figure 4.60 Capacity Curves MODEL 2 direction +Y.

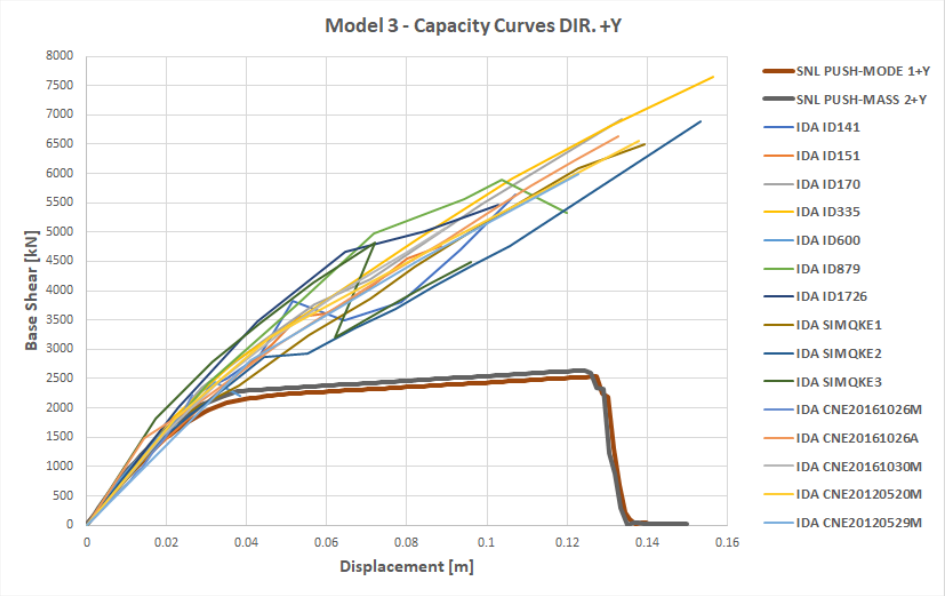

Figure 4.61 Capacity Curves MODEL 3 direction +Y.

4.7.4 Capacity Curves -Y direction

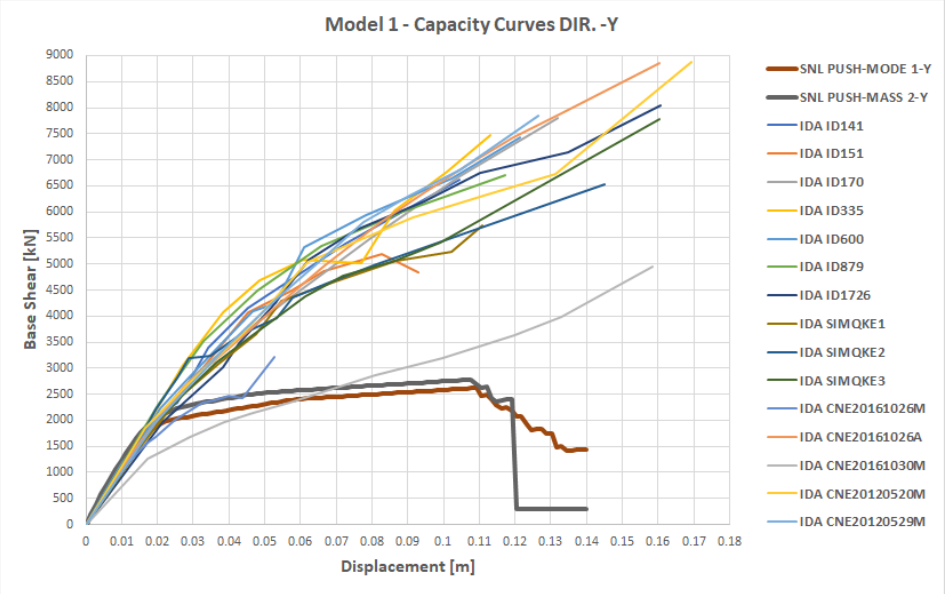

Figure 4.62 Capacity Curves MODEL 1 direction -Y.

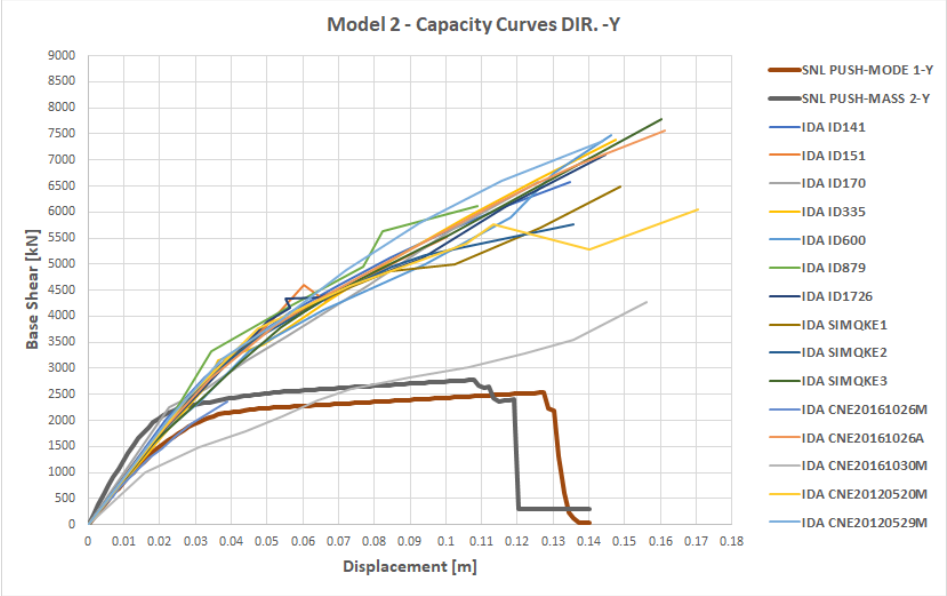

Figure 4.63 Capacity Curves MODEL 2 direction -Y.

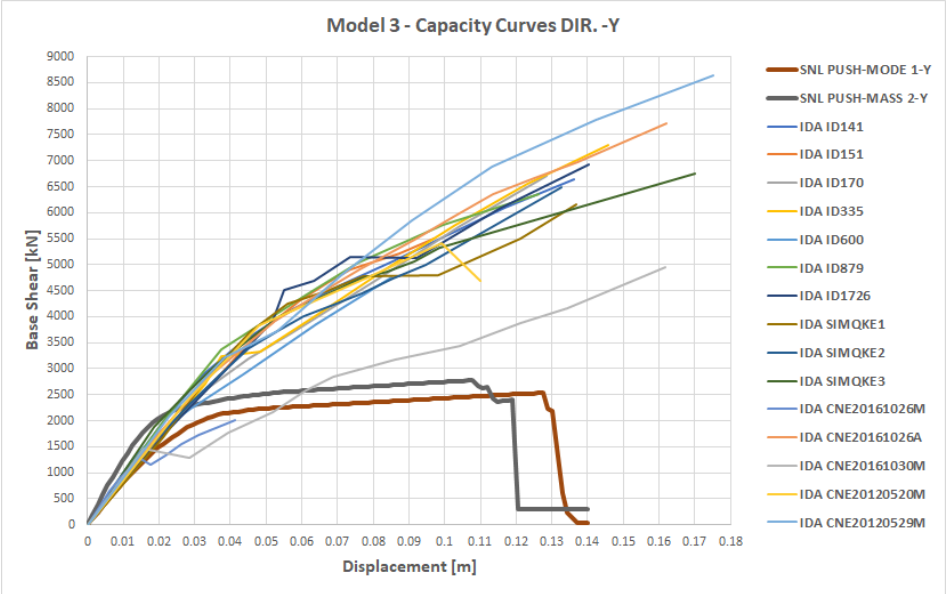

Figure 4.64 Capacity Curves MODEL 3 direction -Y.

4.8 Future works

A Multiple Stripe Analysis (MSA) will be carried out to implement some statistical methods suitable for this analysis (called alternative methods in previous paragraphs). This analysis will be performed with different sets of ground motions chosen at each intensity level (with IDA the same set of ground motions is scaled at different intensity level).
As observed previously, dataset of MSA is different than IDA dataset because MSA structural analysis results provide the fraction of ground motions at each IM level that cause collapse instead of IMi values associated with the onset of collapse for a given ground motion (For the fragility curves realized in the previous paragraphs, the data obtained from the IDA curves are evaluated in both ways).
Multiple stripe analysis approach also allows for different ground motions to be used for analyses at varying intensity levels, to represent the differing characteristics of low intensity and high intensity shaking.
A comparison with fragility curves realised with IDA curve and with MSA will be done to understand nonlinear analysis that better captures the behaviour of industrial buildings cast in place with precast reinforced hollow brick light-weight vaults as studies proposed by Banerjee et al. [82].

5 Chapter - Seismic sequence effects on the fragility analysis and damage of RC industrial structures cast in place with SAP vault

Observations from field investigations have shown that a structure may be subjected to more than one earthquake in a relatively short period. Since after every single earthquake, a structure faces a stiffness and strength degradation, it may not be able to withstand subsequent shaking especially when seismic retrofits are not an option due to the short time intervals between the successive earthquakes. In this chapter, the effect of mainshock-aftershock sequence is analysed to evaluate the response of the existing industrial buildings.
The most vulnerable model derived from previous fragility analysis (Model three) is taken into account and it is subjected to a large number of mainshock-aftershock sequences to quantify the vulnerability of aftershock damage with double incremental dynamic analysis.
To investigate the capacity of building to resist a seismic sequence, aftershock fragility curves of near collapse limit state and ductility damage indices of all nonlinear dynamic analysis are calculated.
Aftershock building fragility curves, representing the probability of experiencing a specified level of damage, are conditioned on the level of mainshock damage.
The result of the aftershock fragility assessment is then used to examine the relationship between the mainshock physical damage indicators and the capacity of building to withstand subsequent shaking.
Ductility damage indices are also another method to evaluate the damage from mainshock intensity until near collapse damage state.
These assessments are important to investigate post-earthquake industrial building tagging procedures that identify buildings that are significant life safety risks.

5.1 Analytical studies of mainshock-aftershock phenomena

The basic approach for the seismic design of structures utilised a single loading scenario and a single performance criterion but, usually, structures are affected by more than one earthquake within a relatively short period due to their special seismic-tectonic setting.

Major earthquakes that are considered “mainshock” are typically followed by smaller magnitude earthquakes known as “aftershock” with originating at or near the rupture zone of the larger earthquake.
Cascading shakings have been observed in recent earthquakes like L’Aquila (Italy, 2009), Tohoku (Japan, 2011), Christchurch (New Zealand, 2010–2011), Chile (2010), Nepal (2015), Kumamoto (Japan, 2016).
A typical and recent example of several mainshock-aftershock sequences is 2016 Central Italy earthquakes: the seismic events, which hit Central Italy on 24th August 2016, 26th and 30th October 2016 and 18th January 2017, have caused casualties and significant damage mostly to buildings of the Italian regions of Marche, Lazio, Abruzzo and Umbria.
The mainshock occurred on 24th August at 3:36 am (local time) with an epicentre close to Accumoli (Rieti province) and with a magnitude Mw= 6.2; it was followed, at 4.33 am, by an aftershock with an epicentre close to Norcia (Perugia province) and with a magnitude Mw= 5.5. On 26th October, there were two strong aftershocks with 5.6 and 6.1 Mw. The earthquake of 30th October, which happened at 07:40 am with Mw 6.5, is the largest event in terms of released energy occurred in Italy since the Mw 6.9 in 1980 during the Irpinia earthquake with the succession of strong aftershock throughout the day. Finally, on 18th January 2017 took place a new sequence of four strong shocks of Mw=5 and epicentres located between the cities of Montereale, Capitignano and Cagnano Amiterno.
As a result of these phenomena, the building may be damaged by the mainshock and there may not be time to repair between strong events, damage induced by the main event modifies the overall strength and stiffness and consequently dynamic response to aftershock signals.
Several studies are performed to quantify the aftershock vulnerabilities. Some brief descriptions of these studies are reported below considering nonlinear static and dynamic analysis pointing out permanent displacements observed after mainshock occurred.
In 2010 Hatzigeorgiou et al. [83] show an extensive parametric study on the inelastic response of eight reinforced concrete planar frames under forty-five seismic sequence (five real and forty artificial records) employing for the first time as-recorded seismic sequences to determine the nonlinear behaviour of RC framed structures with incremental dynamic analysis. They underline that the multiplicity of earthquakes strongly influences the permanent displacements that should be taken into account for the seismic design of structures.

Di Sarno [84] analyses the effects of multiple earthquakes on inelastic structural response thank to an exceptionally rich set of records obtained from earthquake sequence of Tohoku (Japan) starting on March 2011.
He selects a short list of earthquake response parameters and the records are treated in two different manners: inelastic constant ductility spectra for acceleration response are examined alongside force reduction factor spectra. His studies not only confirm that multiple earthquakes deserve extensive and urgent studies, but also give indications of the levels of lack of conservatism in the safety of conventionally-designed structures when subjected to multiple earthquakes.
Hatzivassiliou et al. [85] investigate maximum displacements, inter-storey drift ratio, damage indices and ductility demands of several three dimensional reinforced concrete structures subjected to five real seismic sequences where their two horizontal components, as well as the vertical one, are taken into account. They underline that structures subjected to strong motions show permanent displacements, which are accumulated during oncoming earthquakes and therefore the maximum displacements appear to be increased for the case of seismic sequences in comparison with the case of single earthquakes.
Furtado et al. [86] assess the mainshock-aftershock effects on an eight-storey RC building with different numerical models considering several infill masonry panels modelling strategies subjected to nonlinear dynamic analyses with different intensity levels of aftershock-mainshock. Their research shows that model which consider infills masonry with in-plane and out-of-plane behaviour increase the vulnerability of building. In a subsequent analysis, Furtado et al. [87] propose a fragility analysis considering a damaged structure with a certain mainshock PGA (respect of collapse identified by IDA analysis previous realised) subjected to a scaled aftershock. Between mainshock and aftershock, a period of 10 sec is inserted. Six damage state are taking into account (slight, light, moderate, extensive, partial collapse and collapse) with the realization of comparison of respective fragility curves.
Oyguc et al. [88] investigate the degrading behaviour of irregularly built reinforced concrete structures subjected to the Tohoku ground motion sequences with the creation of models with appropriate damage features that capture both the irregularity and material deterioration effects using N2 and extended N2 methods. Their results underline that irregularity effects increase the dispersed damage under these excitation sequences.
Zhai et al. [89] analyse the influence of aftershocks with different durations on the additional accumulative damage considering the post-mainshock damage state:

their results indicate that aftershocks with longer durations can cause more severe accumulative damage and have a significant effect on the damage pattern.
Recently fragility assessment of RC structures under seismic sequence is done.
Raghunandan et al. [90] describe a probabilistic methodology to quantify building fragility considering sequences of earthquakes. They realise the fragility curve with incremental dynamic analysis using a set of 30 ground motion applied as both mainshock and aftershock. The intensity of the scaled aftershock ground motion in the sequence quantifies the collapse capacity of the mainshock-damaged building. They underline that aftershock building fragility curves are conditioned on the level of mainshock damage.
Hosseinpour et al. [91] realise fragility curves for three reinforced concrete buildings with a different number of stories under multiple earthquakes with real recorded sequences from a different part of the world. Their fragility curves are derived from four cases based on mainshock only, mainshock aftershocks sequence and aftershock only with considering or not the damage due to the previous event: results indicate that considering damage from previous events significantly affect fragility curves. With a previous article [92], the same authors indicate that earthquake direction, structure irregularity and vertical earthquake component have a considerable effect on the response of structures subjected to multiple earthquakes.
Di Trapani et al. [93] evaluate seismic fragility and residual capacity of masonry infilled reinforced concrete frames subject to artificial mainshock/aftershock sequences using a double incremental dynamic analysis (D-IDA) approach based on the combination of a mainshock signal at different intensities with a set of spectrum-compatible aftershock scaled in amplitude with respect to peak ground acceleration. Their conclusions are that aftershock capacity of bare and infilled frames depends on mainshock intensity and infilled frame aftershock fragilities are lower if compared with that of the intact bare frame.

5.2 Case study

For this topic, it is considered the same case study analysed in chapter four, an industrial structure cast in place with SAP vault: this choice is due to the fact that new analysis will be based on previously processed data always with the idea to treat industrial building never tested in the scientific literature.
In paragraph 4.3 the main features of this building are reported.

5.2.1 Numerical Models

According to the result of fragility analysis of the prior chapter, Model three is taken into account as it reports the major vulnerability of all three previously analysed models. All the assumptions made in paragraph 4.3.1 are also valid in this case. The main features of the model investigated are shown below.
Using a commercial calculation code and according to Mezzapelle et al. [62], in nonlinear-field lumped plasticity is considered. A modified Takeda-type model [74] is implemented for the plastic hinge of columns and beams, due to its ability to provide simple numerically stable and sufficiently realistic hysteresis cycles.
The main structural elements, used for the spatial discretization of beams and columns, are modelled as "beam" and they are made to act both in the elastic-linear and plastic field. The structure is fixed at the base at the level of the industrial floor. The seismic weights are obtained considering all structural and non-structural elements as well as live loads on the structures.
All chains of the vault are modelled as “truss” and they are made to act in the elastic-linear field to transmit only axial force.
All ribs of the vault are realised as technical design and they are modelled as “beam”; steel bars of joists are not taken into account.
SAP vault is realised with beam element of hollow light-weight brick with elastic modulus equal to 4500 N/mmq positioned at every frame with a dimension of 5.00x0.20mt. Loads due to the proper weight of the vault assumed from technical design are applied directly to the beam as linear loads.
The numerical model chosen for the analysis is reported in Figure 5.1.

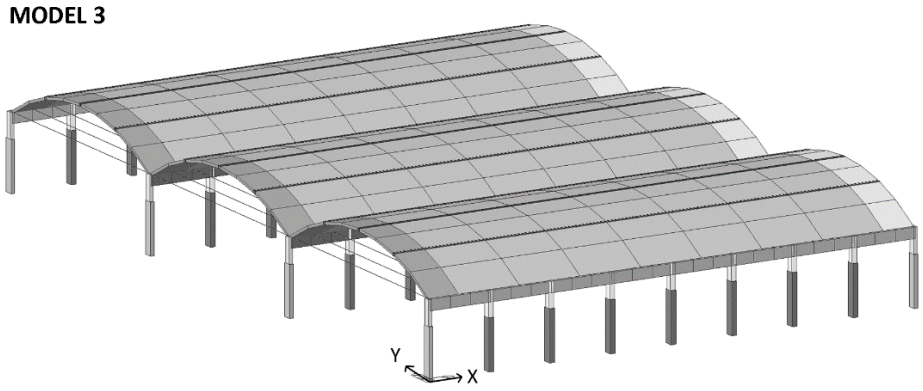

Figure 5.1 Numerical model chosen from previous cases (model three).

5.3 Double Incremental Dynamic Analysis (D-IDA)

A summary of the results of the previous chapter is done, necessary to set up a double incremental dynamic analysis to realise aftershock fragility curves.
For this work, the same Intensity Measure (PGA) and Damage Measure (Roof Drift) of previous analysis are taken into account.
Only threshold value of Near Collapse (NC) of Model three defined with nonlinear static analysis of paragraph 4.4.2 is considered.
Ground motions selection described in paragraph 4.5.1 is used as mainshock and aftershock.
In this type of analysis, IDA curves of Model three reported in paragraph 4.5.2 are considered as the case of pre-damage (only mainshock - intact structure) carrying out a standard IDA procedure to define the range of PGA scaling intensities to adopt for mainshock and aftershocks. There is substantial variation in structural response as a function of ground motion intensity among the 30 records in X-Y direction, due to differences in frequency content, duration and other ground motion characteristics. In Double Incremental Dynamic Analysis, the building is subjected to a mainshock-aftershock sequence. The mainshock record is scaled, the response of the structure is recorded and a scaled aftershock record is applied to the mainshock damaged structure. The scale factor on the mainshock record is varied to represent different levels of damage in the building: the structure is subjected to the cases of pre-damage with IDA realised in Chapter four (only mainshock - intact structure), 40%NC PGA, 60%NC PGA and 80%NC PGA mainshocks with scaled aftershock (it is necessary to define NC PGA of every ground motion in X and Y directions and it is important to underline that it depends of threshold limit of push-over analysis in X-direction). PGA collapse of every ground motion took from previous analysis and the respective percentages used for mainshock of D-IDAs are reported in Table 5.1.

		NEAR COLLAPSE PGA (IDA)	MAINSHOCK + SCALED AFTERSHOCK (D-IDA)		
			MS with 40%NC PGA	MS with 60%NC PGA	MS with 80%NC PGA
		[g]	[g]	[g]	[g]
ID 600	X dir.	0.605	0.242	0.363	0.484
	Y dir.	0.608	0.243	0.365	0.486
ID 170	X dir.	0.668	0.267	0.401	0.534
	Y dir.	0.570	0.228	0.342	0.456
ID 151	X dir.	0.544	0.218	0.326	0.435
	Y dir.	1.012	0.405	0.607	0.810
ID 1726	X dir.	0.368	0.147	0.221	0.294
	Y dir.	0.654	0.262	0.392	0.523
ID 335	X dir.	0.627	0.251	0.376	0.502
	Y dir.	0.570	0.228	0.342	0.456
ID 141	X dir.	0.720	0.288	0.432	0.576
	Y dir.	1.010	0.404	0.606	0.808
ID 879	X dir.	0.648	0.259	0.389	0.518
	Y dir.	0.654	0.262	0.392	0.523
MRN_20120520	X dir.	0.690	0.276	0.414	0.552
	Y dir.	0.430	0.172	0.258	0.344
MRN_20120529	X dir.	0.750	0.300	0.450	0.600
	Y dir.	0.360	0.144	0.216	0.288
CNE_20161026M	X dir.	2.000	0.800	1.200	1.800
	Y dir.	2.000	0.800	1.200	1.800
CNE_20161026A	X dir.	1.040	0.416	0.624	0.832
	Y dir.	0.745	0.298	0.447	0.596
CNE_20161030	X dir.	0.518	0.207	0.311	0.414
	Y dir.	0.590	0.236	0.354	0.472
SIMQKE1	X dir.	0.760	0.304	0.456	0.608
	Y dir.	0.780	0.312	0.468	0.624
SIMQKE2	X dir.	0.940	0.376	0.564	0.752
	Y dir.	0.980	0.392	0.588	0.784
SIMQKE3	X dir.	0.790	0.316	0.474	0.632
	Y dir.	0.950	0.380	0.570	0.760

Table 5.1 Near Collapse PGA and respective percentages used for mainshock of D-IDAs.

The PGA levels of following aftershocks are outlined between mainshocks PGA previous defined and Near Collapse PGA of every curve. A period of five seconds is added between the mainshock and aftershock ground motions to represent the situation in which the structure comes to rest after the first event but is not repaired. The aftershock analysis is repeated considering the same structure and mainshock-aftershock sequence, increasing the intensity of the aftershock ground motions (by scaling the aftershock record) until the mainshock-aftershock sequence reached the NC collapse threshold. The intensity of the scaled aftershock ground motion in the sequence quantifies the collapse capacity of the mainshock-damaged building.

Figure 5.2 illustrates seismic sequence realised for ID335 X-direction with 40%NC PGA mainshock + scaled aftershock.

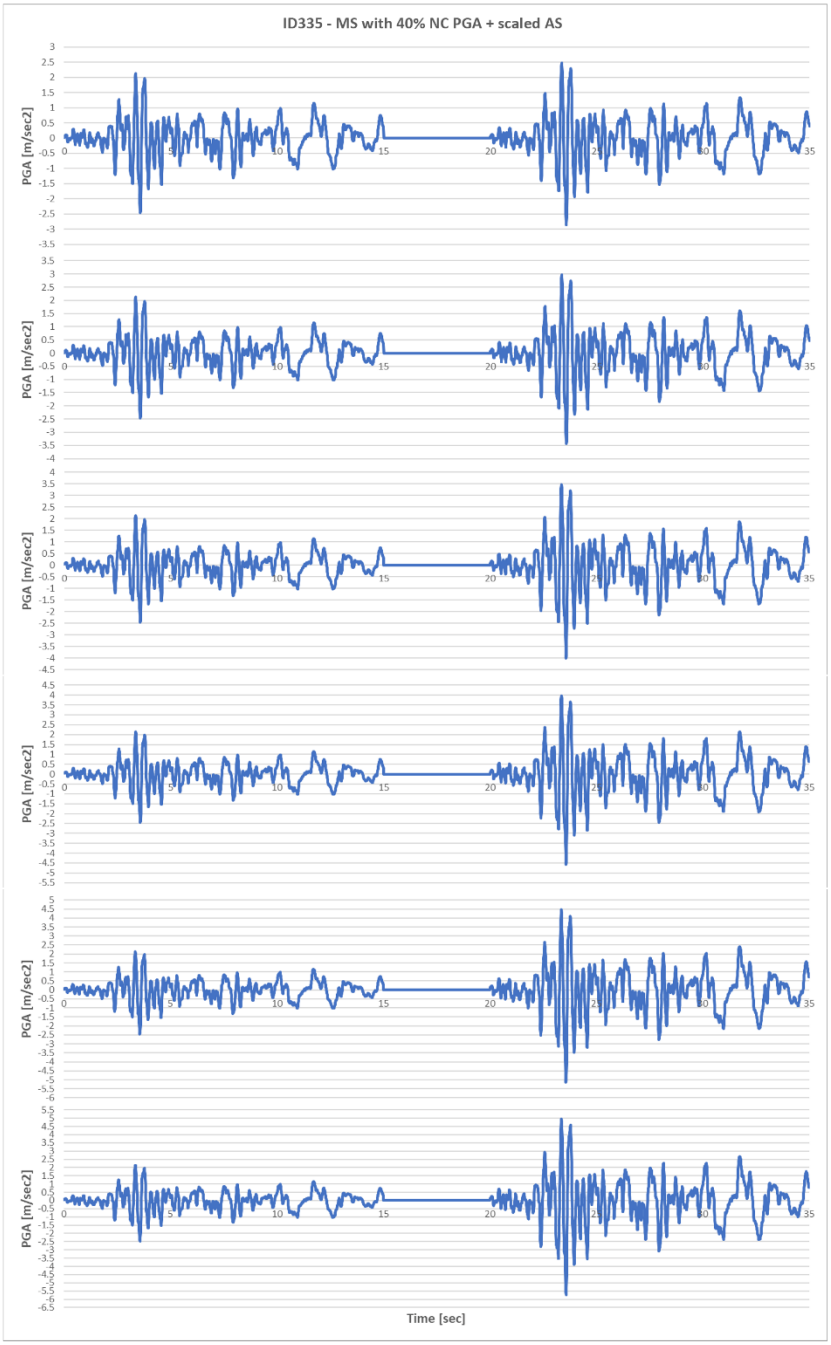

Figure 5.2 Seismic sequence realised for ID335 X-direction -MS with 40%NC PGA + scaled AS.

A comparison between IDA (-only mainshock – intact structure) and D-IDA (seismic sequences composed by MS with 40%,60% and 80% NC PGA + scaled AS) divided for every ground motion in X-Y direction are reported in Figures 5.3-5.17. Every IDA and D-IDA curves are completed by relative roof drifts with the same PGA level that reach the NC threshold value of all considered cases.

The polarity of the aftershock concerning the mainshock is important for cases in which the residual drift (or called as permanent displacements) after a mainshock is high (the structure is leaning to one side or another). 'Polarity' refers to the direction of the aftershock with respect to the mainshock and, depending on the polarity, the aftershock tends to amplify or reduce mainshock residual drift. In this study, the polarity of the mainshock is randomized to represent the realistic scenario in which the polarity of mainshock to the aftershock is random and unknown. To satisfy the targeted performance levels under predefined seismic hazard levels, the permanent displacements should be accurately estimated: the multiplicity of earthquakes strongly influences the residual drifts and therefore multiple earthquakes phenomena should be taken into account to achieve a dependable estimation of permanent displacements. The accumulation of residual drifts is obvious, in any case under consideration.

Figure 5.7 (ID335, X-direction), Figure 5.8 (ID141, X-direction) and Figure 5.13 (X-Y directions) show a residual drifts that produce an increase of drifts of aftershock while Figure 5.6 (ID1726, X-direction), Figure 5.9 (ID879, X-direction) and Figure 5.11 (MRN20120529, X-direction) underline a reduction of roof displacements of aftershock always due to polarity of mainshock.

Moreover, in some cases, a period of five seconds added between the mainshock and aftershock ground motions is not sufficient to stabilise residual drifts, particularly visible in Figure 5.7 (ID335, X-Y directions), Figure 5.9 (ID879, X-Y directions) and Figure 5.17 (SIMQKE3, Y direction).

Figure 5.3 Comparison between IDA and D-IDA and relative roof drift of NC threshold - ID 600 dir. X-Y.

Figure 5.4 Comparison between IDA and D-IDA and relative roof drift of NC threshold - ID 170 dir. X-Y.

Figure 5.5 Comparison between IDA and D-IDA and relative roof drift of NC threshold - ID 151 dir. X-Y.

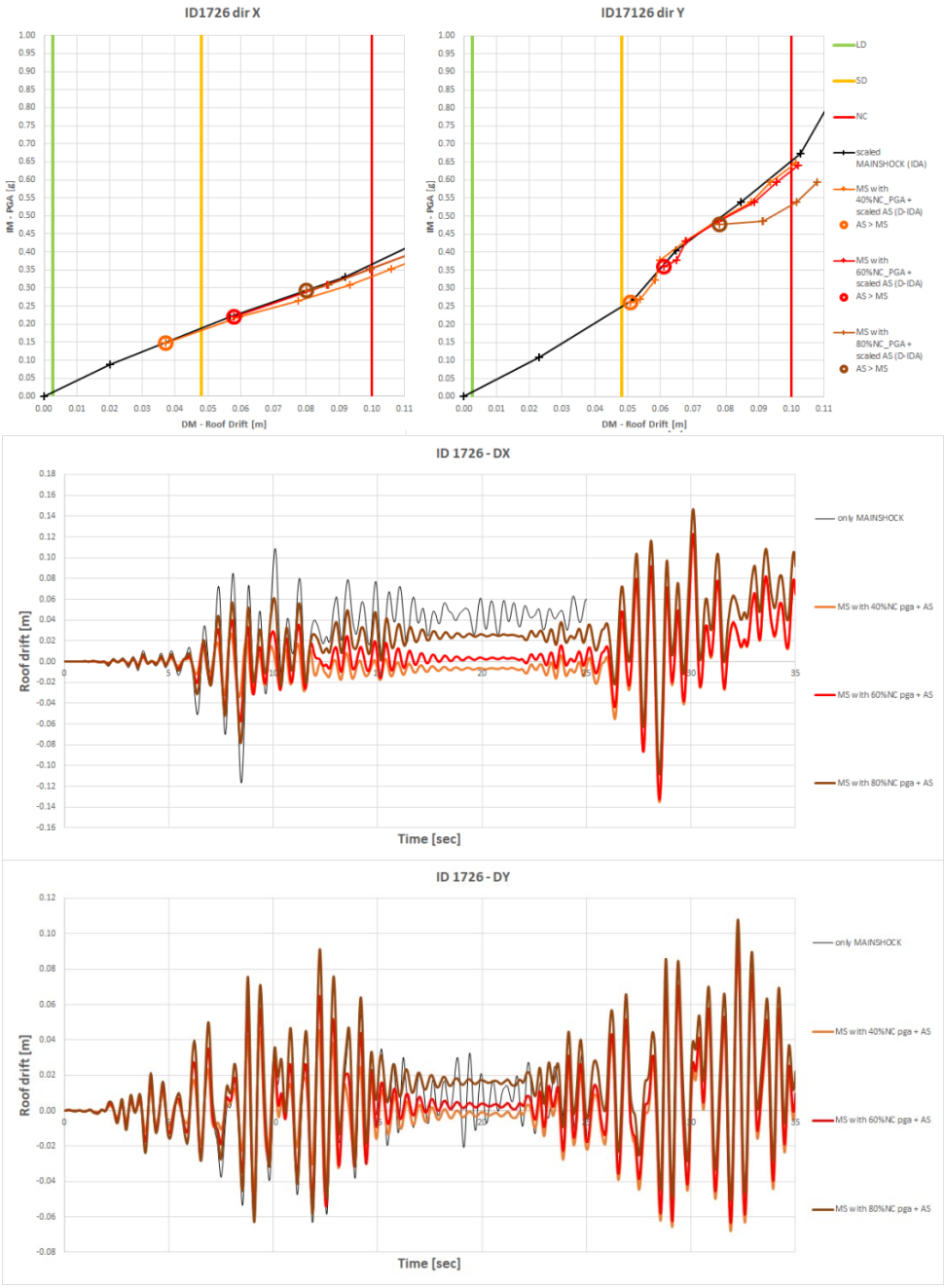

Figure 5.6 Comparison between IDA and D-IDA and relative roof drift of NC threshold – ID 1726 dir. X-Y.

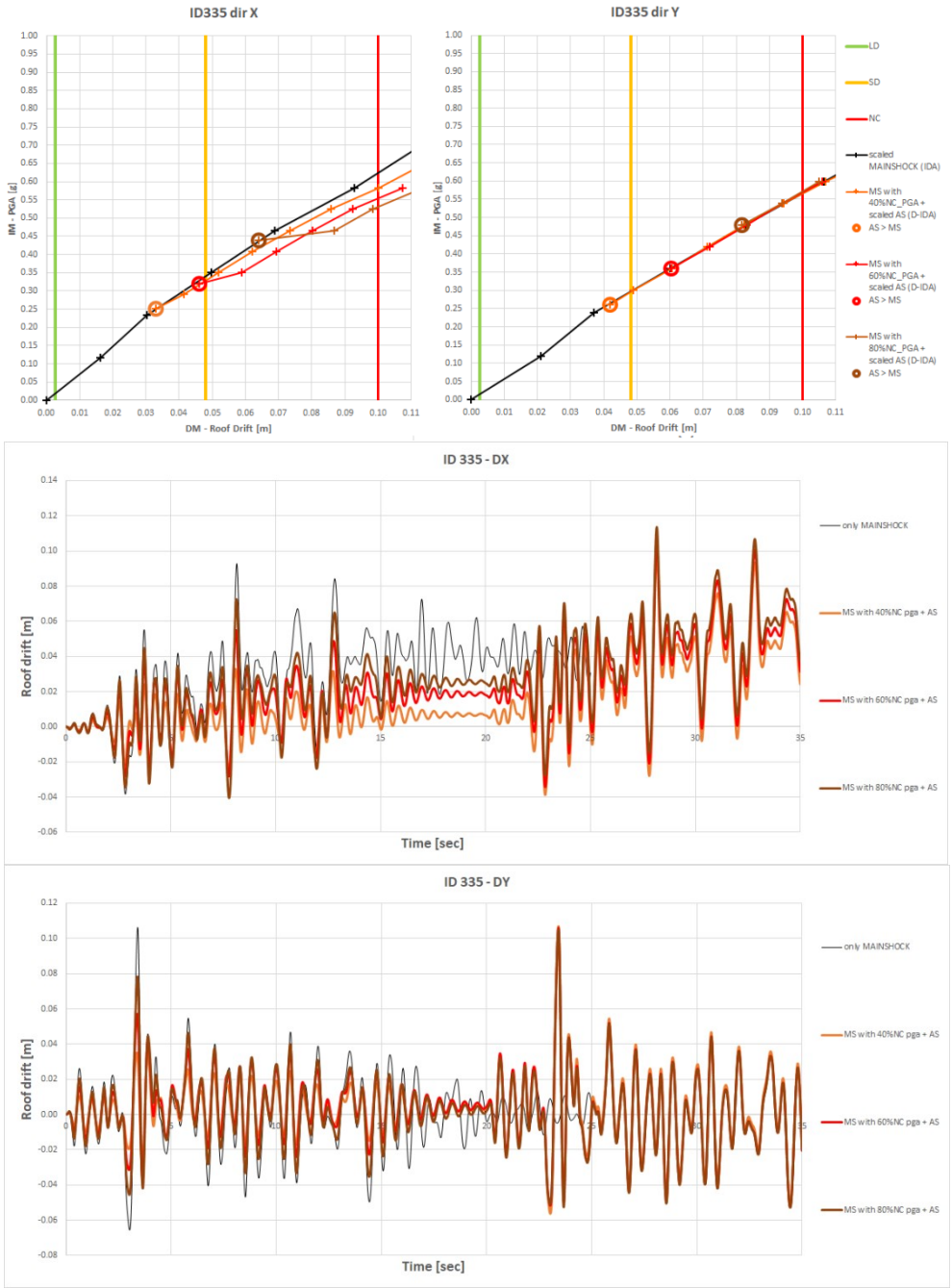

Figure 5.7 Comparison between IDA and D-IDA and relative roof drift of NC threshold - ID 335 dir. X-Y.

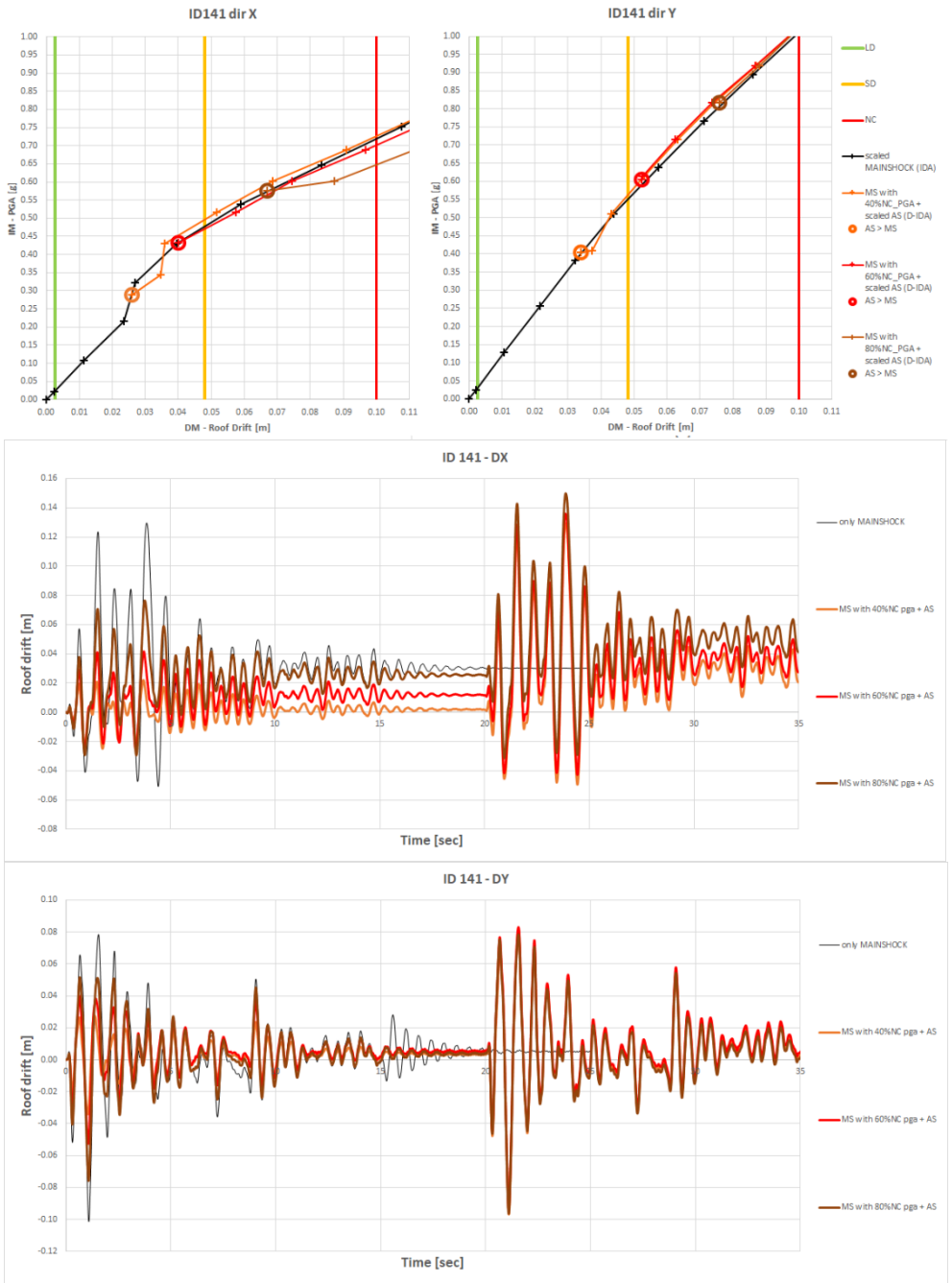

Figure 5.8 Comparison between IDA and D-IDA and relative roof drift of NC threshold - ID 141 dir. X-Y.

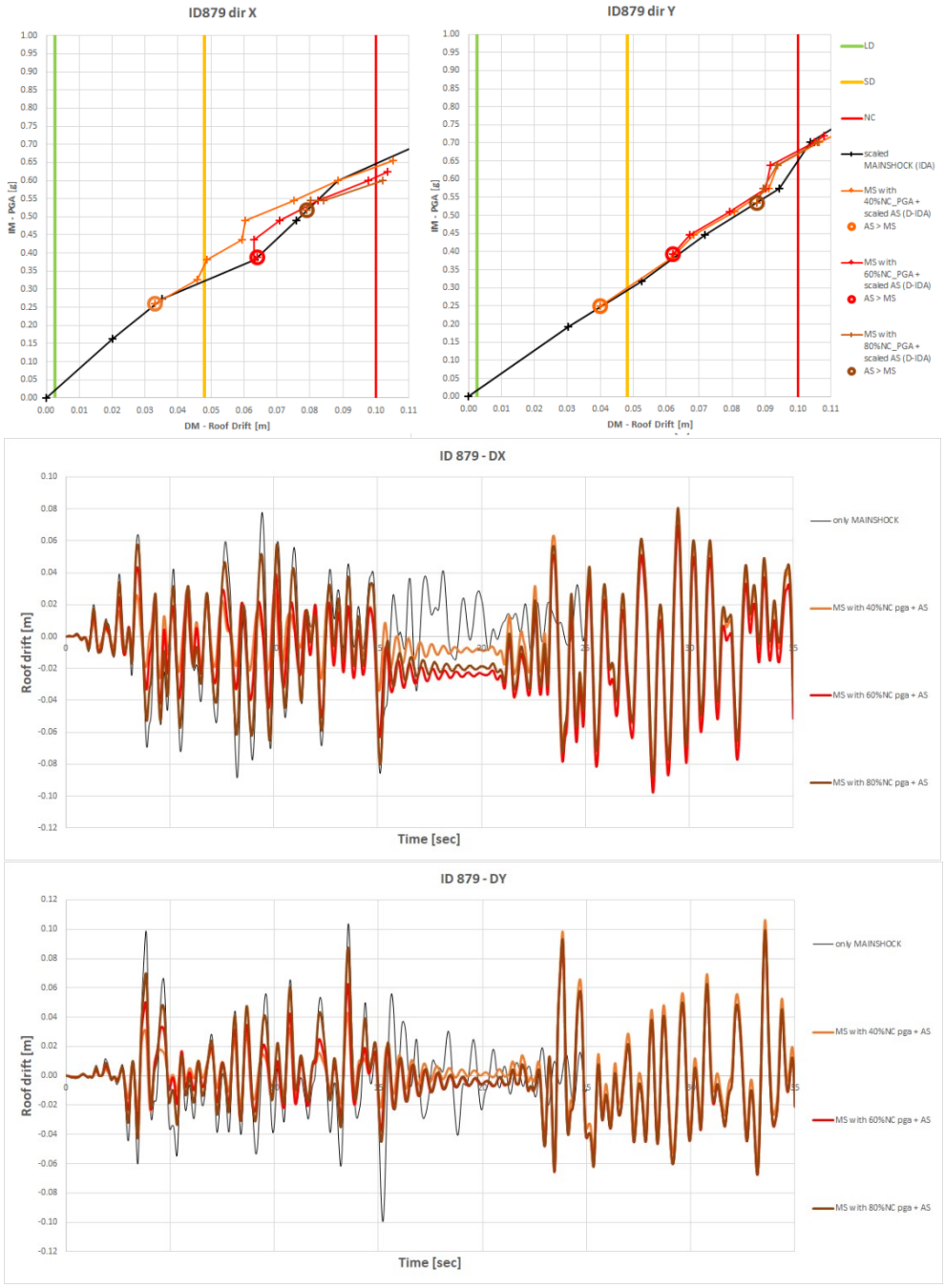

Figure 5.9 Comparison between IDA and D-IDA and relative roof drift of NC threshold - ID 879 dir. X-Y.

Figure 5.10 Comparison between IDA and D-IDA and relative roof drift of NC threshold – MRN20120520 dir. X-Y.

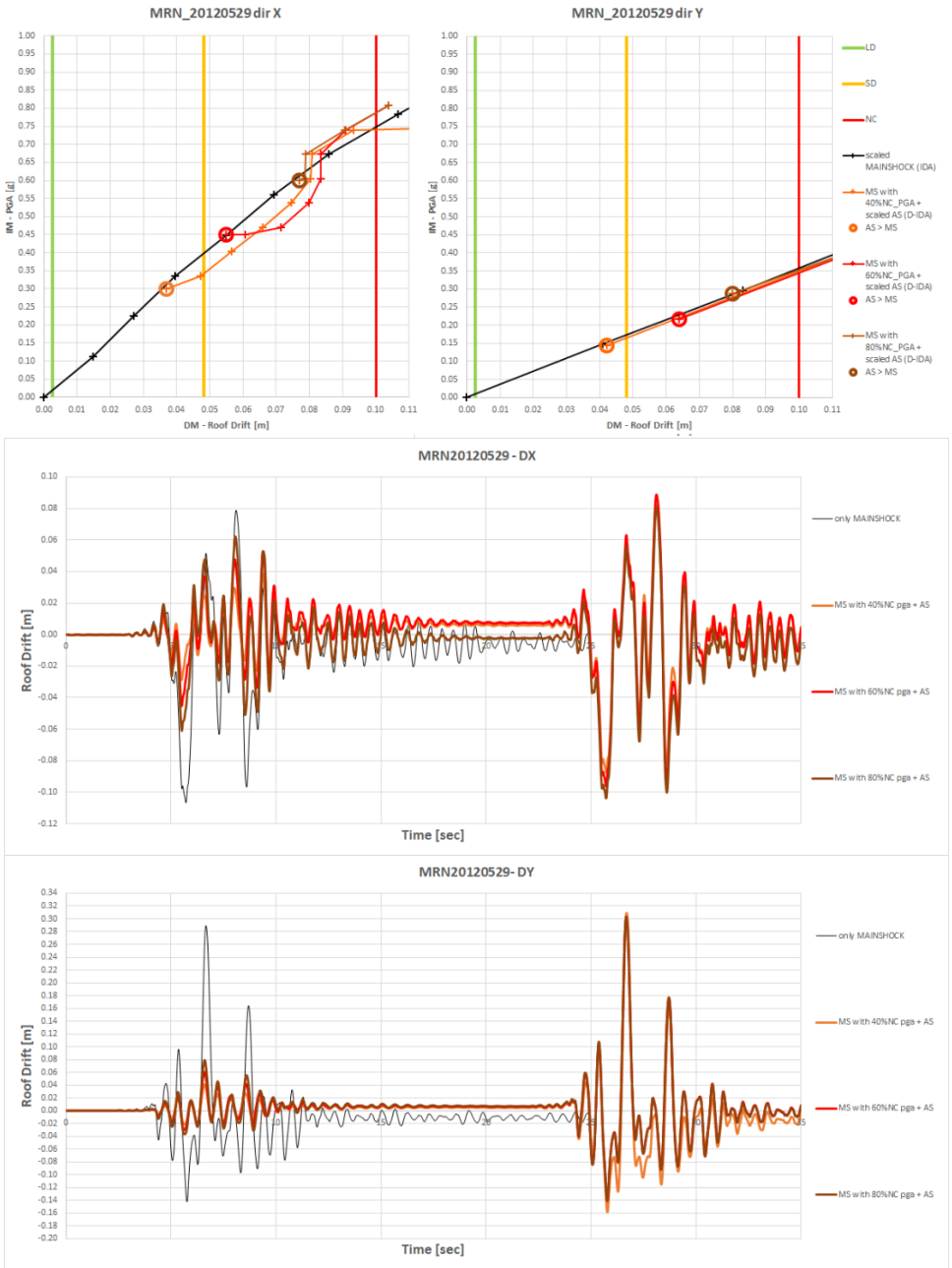

Figure 5.11 Comparison between IDA and D-IDA and relative roof drift of NC threshold – MRN20120529 dir. X-Y.

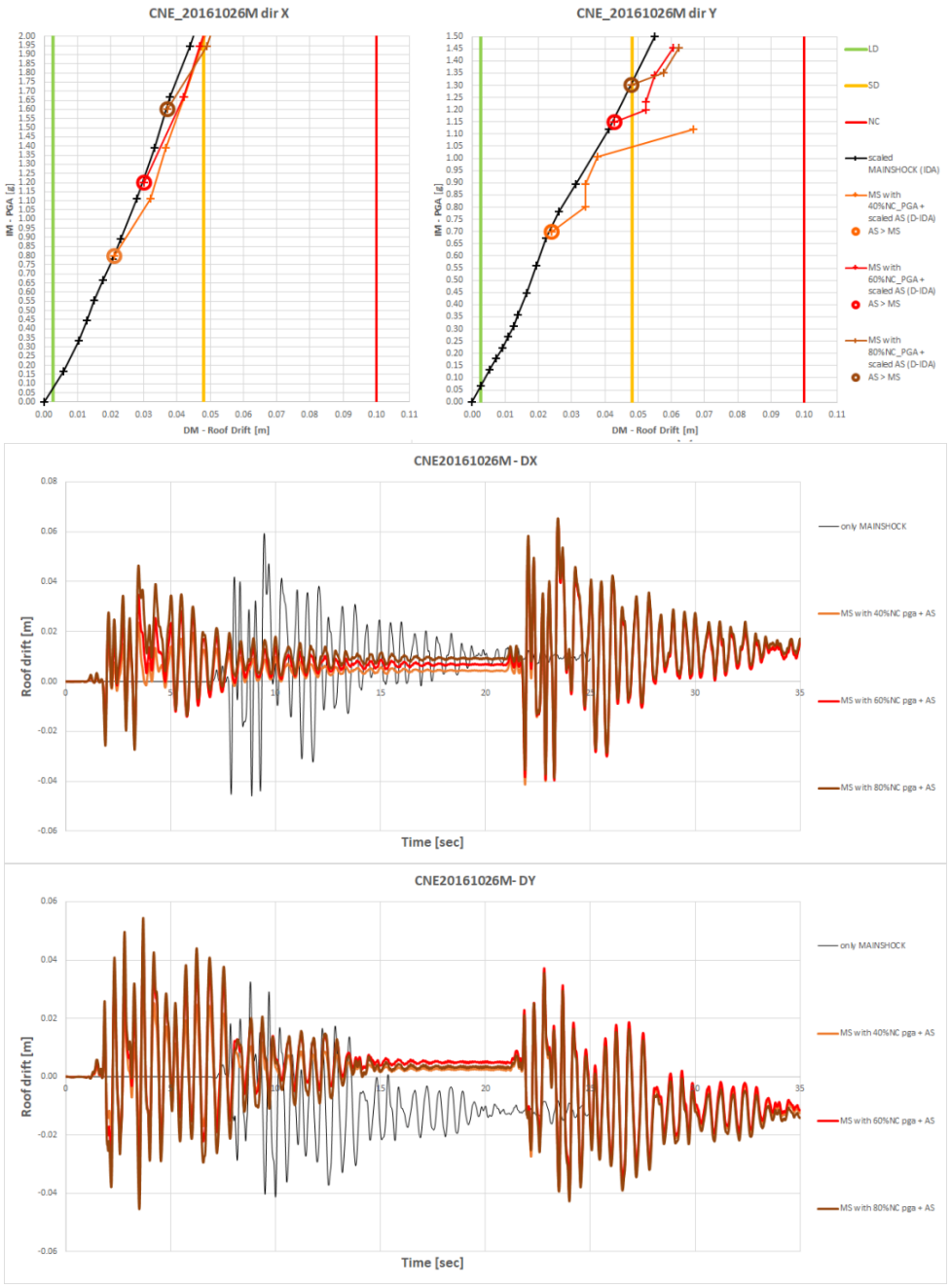

Figure 5.12 Comparison between IDA and D-IDA and relative roof drift of NC threshold – CNE20161026M dir. X-Y.

Figure 5.13 Comparison between IDA and D-IDA and relative roof drift of NC threshold – CNE20161026A dir. X-Y.

Figure 5.14 Comparison between IDA and D-IDA and relative roof drift of NC threshold – CNE20161030 dir. X-Y.

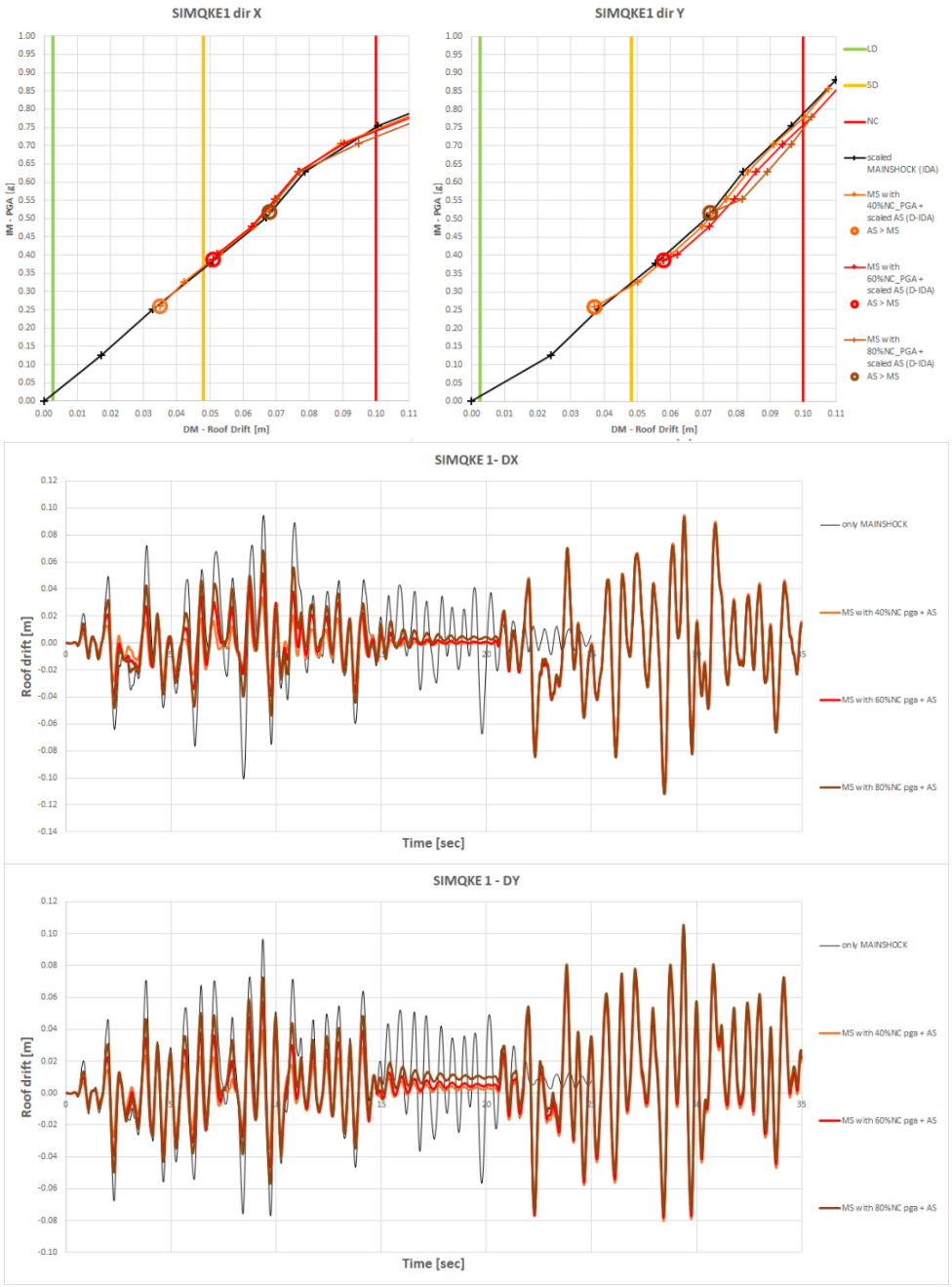

Figure 5.15 Comparison between IDA and D-IDA and relative roof drift of NC threshold – SIMQKE1 dir. X-Y.

Figure 5.16 Comparison between IDA and D-IDA and relative roof drift of NC threshold – SIMQKE2 dir. X-Y.

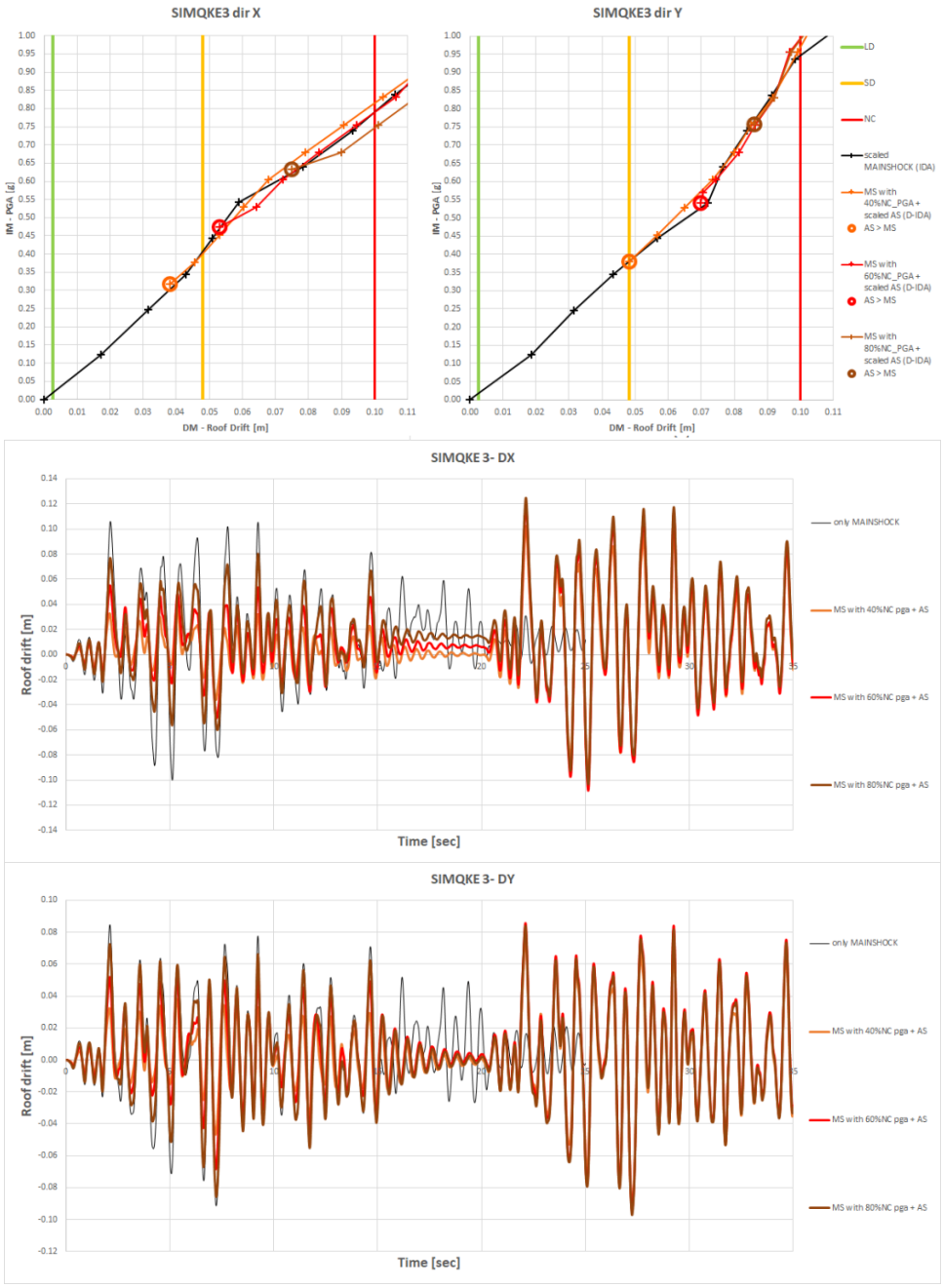

Figure 5.17 Comparison between IDA and D-IDA and relative roof drift of NC threshold – SIMQKE3 dir. X-Y.

5.3.1 D-IDA curves (Damage Measure-Intensity Measure)

D-IDA curves for mainshocks of 40%, 60% and 80%NC PGA with scaled aftershocks of all ground motions are reported in Figures 5.18-5.23 divided according to X-Y directions graphed in the plane damage measure – intensity measure with the same threshold damage parameters. IDA curves considering scaled mainshock (intact structure) are the same reported in paragraph 4.5.2 Figures 4.26-4.27.
Only threshold limit of near collapse is considered here in this type of analysis.

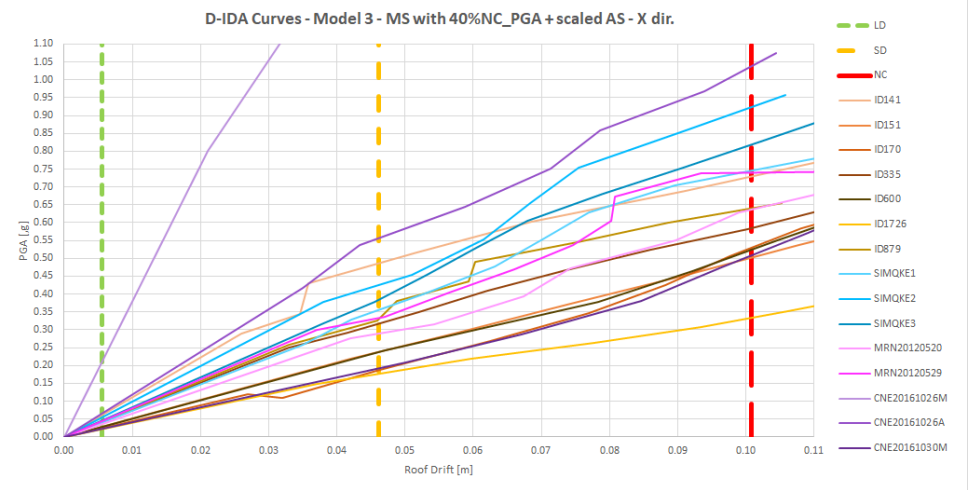

Figure 5.18 D-IDA curves with MS of 40%NC PGA with scaled AS - X dir.

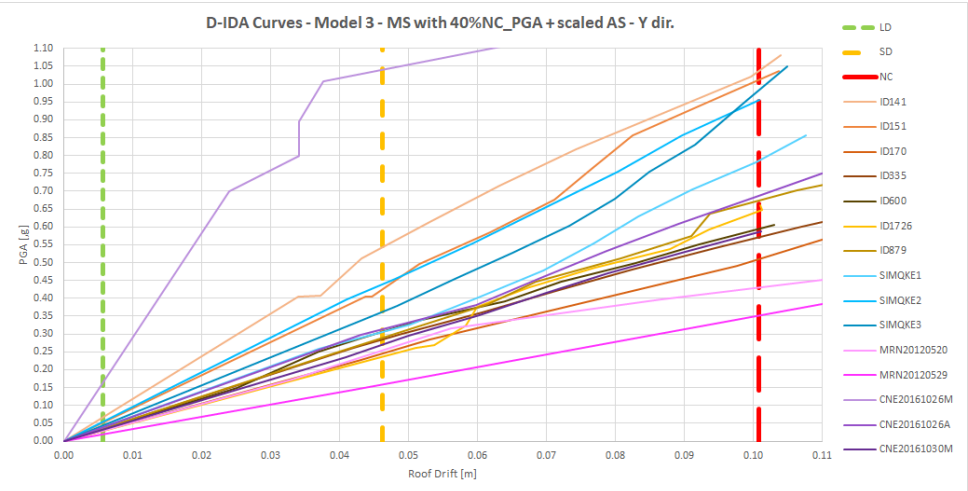

Figure 5.19 D-IDA curves with MS of 40%NC PGA with scaled AS - Y dir.

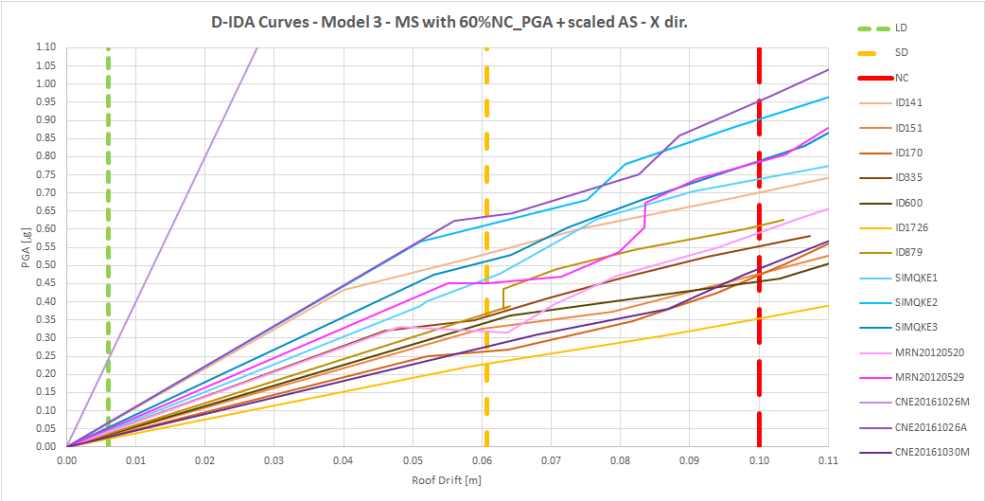

Figure 5.20 D-IDA curves with MS of 60%NC PGA with scaled AS - X dir.

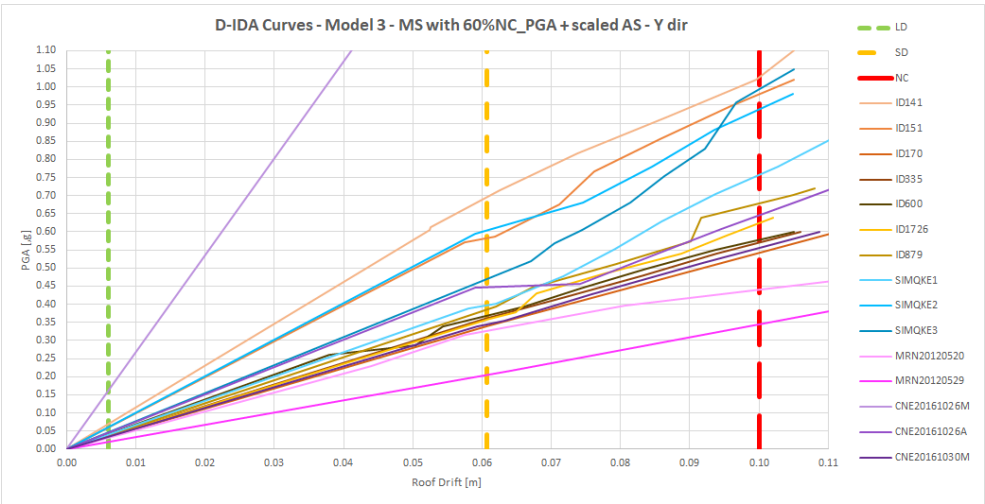

Figure 5.21 D-IDA curves with MS of 60%NC PGA with scaled AS - Y dir.

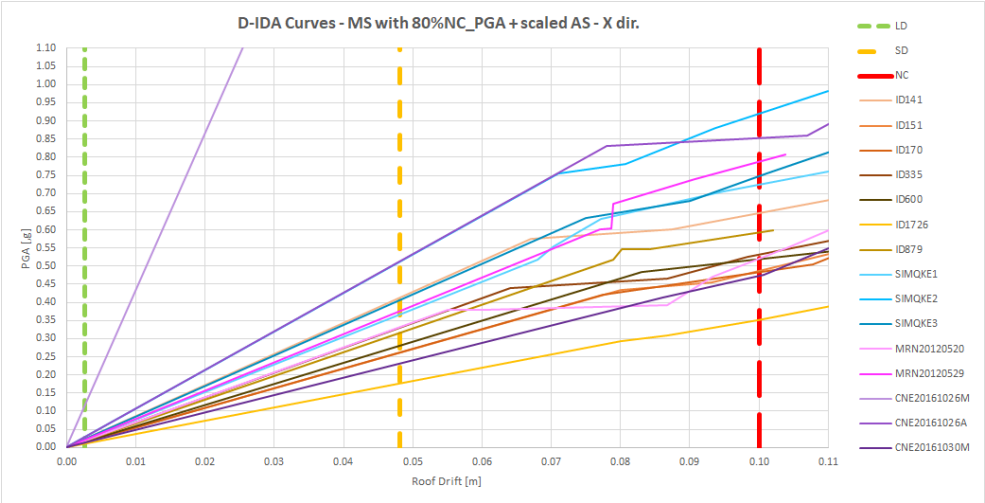

Figure 5.22 D-IDA curves with MS of 80%NC PGA with scaled AS - X dir.

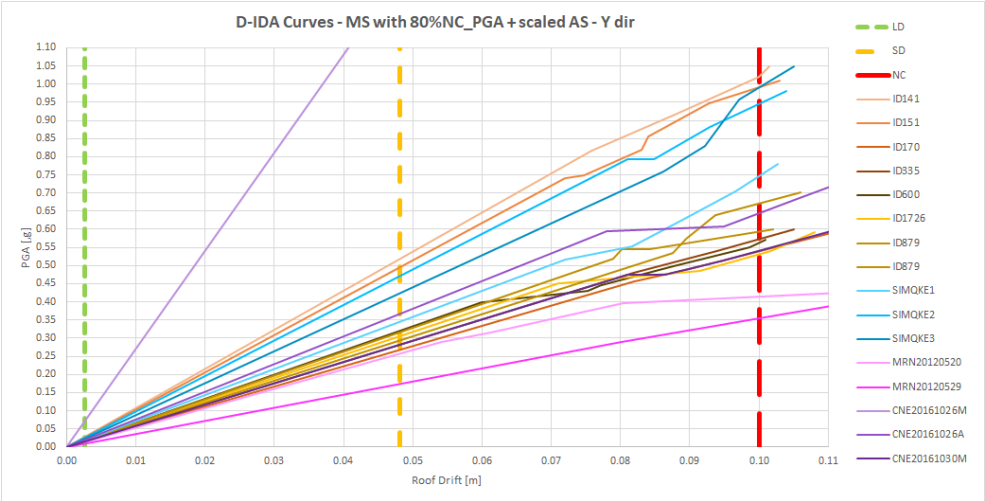

Figure 5.23 D-IDA curves *with MS of 80%NC PGA with scaled AS - Y dir.*

5.4 Fragility curves

The statistical procedures to realise fragility curves are previously described in paragraph 4.6.1. In this work, only recommended methods to process IDA dataset are used because more precautionary results are observed and also there is no huge difference of behaviour between curves implemented with recommended or alternative methods.
Tables 5.2 and 5.3 show the data processed to derive the fragility curves for mainshock of 40%, 60% and 80%NC PGA and scaled aftershock of D-IDA curves for X-Y directions and Near Collapse damage state.

MODEL 3 NC damage level - X DIR

D-IDA MS 40%NC PGA + scaled AS		
IM_i	Cumulative number of collapses	Fraction causing collapse
0.332	1	0.0667
0.502	2	0.1333
0.510	3	0.2000
0.520	4	0.2667
0.530	5	0.3333
0.585	6	0.4000
0.638	7	0.4667
0.640	8	0.5333
0.730	9	0.6000
0.740	10	0.6667
0.748	11	0.7333
0.820	12	0.8000
0.920	13	0.8667
1.038	14	0.9333
Number of analyses:		15
IM_{max}		1
Number not collapsed for truncated IDA		2

D-IDA MS 60%NC PGA + scaled AS		
IM_i	Cumulative number of collapses	Fraction causing collapse
0.354	1	0.0667
0.455	2	0.1333
0.476	3	0.2000
0.478	4	0.2667
0.492	5	0.3333
0.556	6	0.4000
0.592	7	0.4667
0.610	8	0.5333
0.702	9	0.6000
0.740	10	0.6667
0.788	11	0.7333
0.790	12	0.8000
0.902	13	0.8667
0.954	14	0.9333
Number of analyses:		15
IM_{max}		1
Number not collapsed for truncated IDA		1

D-IDA MS 80%NC PGA + scaled AS		
IM_i	Cumulative number of collapses	Fraction causing collapse
0.354	1	0.0667
0.472	2	0.1333
0.484	3	0.2000
0.490	4	0.2667
0.520	5	0.3333
0.520	6	0.4000
0.530	7	0.4667
0.592	8	0.5333
0.648	9	0.6000
0.724	10	0.6667
0.748	11	0.7333
0.786	12	0.8000
0.852	13	0.8667
0.930	14	0.9333
Number of analyses:		15
IM_{max}		1
Number not collapsed for truncated IDA		1

Table 5.2 Dataset for recommended methods to process D-IDA results – Model 3 for mainshocks of 40%, 60% and 80%NC PGA with scaled aftershocks– X dir.

MODEL 3 NC damage level - Y DIR

D-IDA MS 40%NC PGA + scaled AS		
IM_i	Cumulative number of collapses	Fraction causing collapse
0.352	1	0.0667
0.430	2	0.1333
0.508	3	0.2000
0.570	4	0.2667
0.588	5	0.3333
0.592	6	0.4000
0.642	7	0.4667
0.672	8	0.5333
0.688	9	0.6000
0.785	10	0.6667
0.954	11	0.7333
0.980	12	0.8000
1.010	13	0.8667
1.038	14	0.9333

Number of analyses:	15
IM_{max}	1
Number not collapsed for truncated IDA	3

D-IDA MS 60%NC PGA + scaled AS		
IM_i	Cumulative number of collapses	Fraction causing collapse
0.344	1	0.0667
0.440	2	0.1333
0.540	3	0.2000
0.555	4	0.2667
0.568	5	0.3333
0.578	6	0.4000
0.628	7	0.4667
0.648	8	0.5333
0.679	9	0.6000
0.758	10	0.6667
0.938	11	0.7333
0.980	12	0.8000
0.992	13	0.8667
1.028	14	0.9333

Number of analyses:	15
IM_{max}	1
Number not collapsed for truncated IDA	1

D-IDA MS 80%NC PGA + scaled AS		
IM_i	Cumulative number of collapses	Fraction causing collapse
0.352	1	0.0667
0.412	2	0.1333
0.532	3	0.2000
0.540	4	0.2667
0.540	5	0.3333
0.560	6	0.4000
0.574	7	0.4667
0.648	8	0.5333
0.672	9	0.6000
0.748	10	0.6667
0.948	11	0.7333
0.990	12	0.8000
0.990	13	0.8667
1.020	14	0.9333

Number of analyses:	15
IM_{max}	1
Number not collapsed for truncated IDA	2

Table 5.3 Dataset for recommended methods to process D-IDA results – Model 3 for mainshocks of 40%, 60% and 80%NC PGA with scaled aftershocks– Y dir.

The statistical parameters θ (median value) and β (standard deviation value) of cumulative density functions Φ of all cases are reported in Table 5.4.

		MODEL 3											
		MS 40%NC PGA + scaled AS				MS 60%NC PGA + scaled AS				MS 80%NC PGA + scaled AS			
		DIR X		DIR Y		DIR X		DIR Y		DIR X		DIR Y	
		β	ϴ	β	ϴ	β	ϴ	β	ϴ	β	ϴ	β	ϴ
Main methods	hat_mle	0.2926	0.6161	0.3478	0.6421	0.3090	0.5883	0.3416	0.6337	0.2844	0.5750	0.3603	0.6181
	hat_mom	0.2932	0.6360	0.3286	0.6673	0.2910	0.6109	0.3240	0.6592	0.2713	0.5972	0.3340	0.6466
	hat_trunc_alt	0.2825	0.6360	0.3167	0.6673	0.2804	0.6109	0.3122	0.6591	0.2615	0.5972	0.3219	0.6466

Table 5.4 Statistical parameters ϑ (median value) and β – Model 3 for mainshocks of 40%, 60% and 80%NC PGA with scaled aftershocks – X e Y dir.

Fragility curves of Model 3 for mainshocks of 40%, 60% and 80%NC PGA with scaled aftershocks in X-Y directions are shown in next paragraph; a comparison with the case of only scaled mainshock (intact structure) is also realised.

5.4.1 X direction

Fragility curves for X direction for all cases are displayed below: all main methods to calculate fragility functions show the same behaviour each other.
Aftershock IDA fragility curves, obtained with double-IDA, are dependent on the mainshock intensity.
All curves have different slopes each other due to the polarity of aftershocks respect mainshocks that in some ground motions do not bring an increase of roof drifts (This phenomenon is particularly visible in the comparison of only mainshock and MS of 40%NC PGA with scaled AS fragility curves, where the probability of collapse of intact structure is slightly major of the probability of collapse of MS of 40%NC PGA with scaled AS for PGA greater than 0.7g).
For low levels of mainshock damage, there is not much difference between the collapse capacity of the damage and the intact building. For these cases, the level of mainshock damage is low enough that significant failure modes have not started to develop, so the presence of this damage before the aftershock does not make collapse more likely.
Starting at MS with 60%NC PGA, probability of collapse of aftershock fragility curves increases with the growing of mainshock PGA: the aftershock collapse capacity becomes more distinct from the intact building because the irrecoverable damage has begun to occur. For PGA less than 0.55g, aftershock fragility curves of MS of 60% and 80%NC PGA overlap each other.

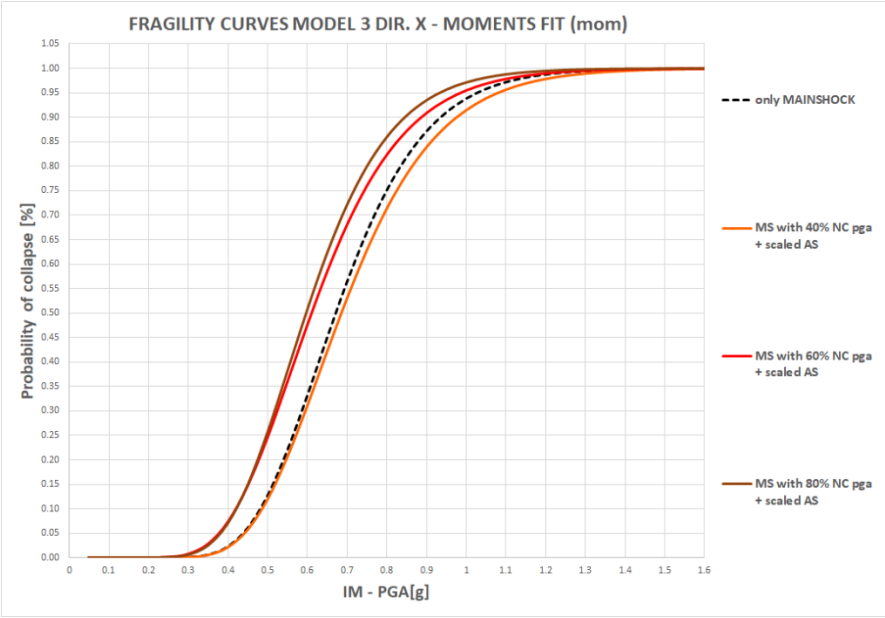

Figure 5.24 Fragility Curves Model 3 only mainshock (intact structure), MS with 40%, 60%, 80% NC PGA + scaled AS X-dir. – Moment fit main method.

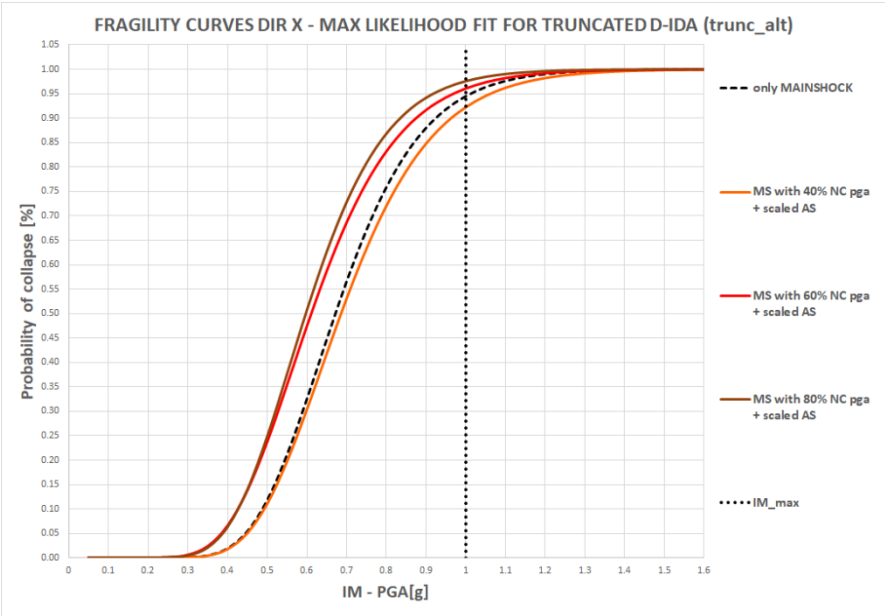

Figure 5.25 Fragility Curves Model 3 only mainshock (intact structure), MS with 40%, 60%, 80% NC PGA + scaled AS X-dir. – Max likelihood fit for truncated D-IDA main method.

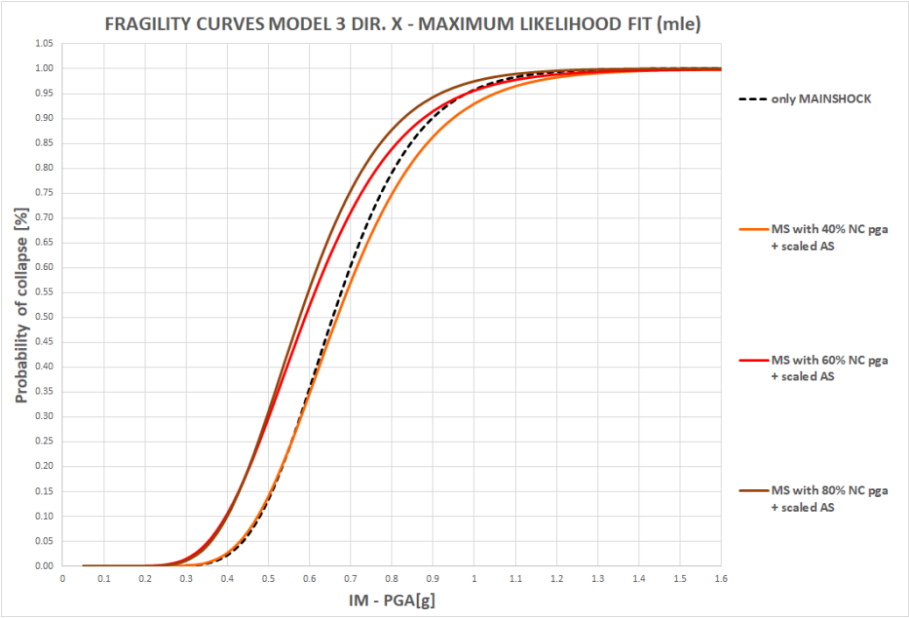

Figure 5.26 Fragility Curves Model 3 only mainshock (intact structure), MS with 40%, 60%, 80% NC PGA + scaled AS X-dir. – Maximum likelihood fit main method.

5.4.2 Y direction

Fragility curves for Y direction for all cases are shown below. There is no significant difference between curves because threshold limit of Near Collapse considered to estimate a percentage of mainshocks in D-IDA analysis is taken from the minimum drift between X-Y directions of push-over analysis (for Model three minimum drift is reached in the X-direction). All fragility curves show the same slope calculated with moment fit and maximum likelihood method; small differences are visible for maximum likelihood method for truncated D-IDA.

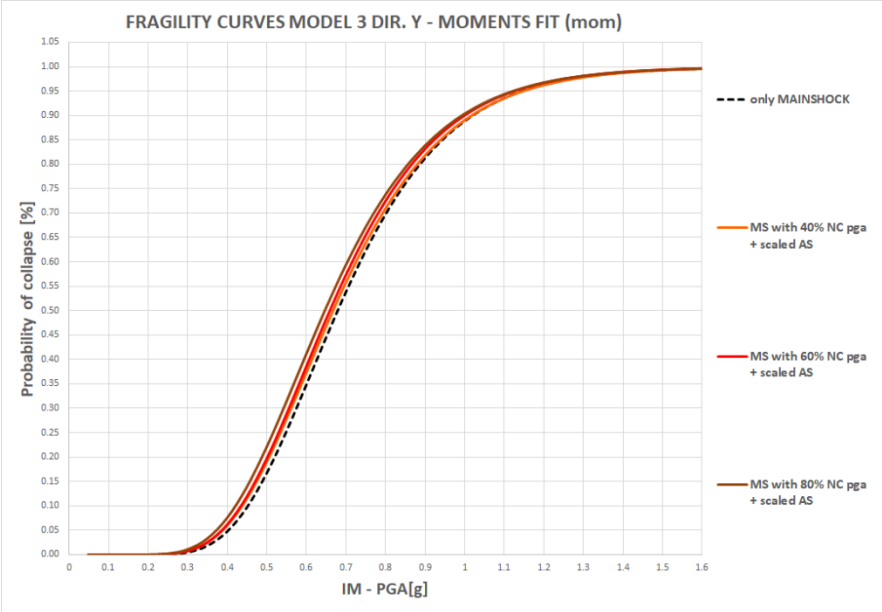

Figure 5.27 Fragility Curves Model 3 only mainshock (intact structure), MS with 40%, 60%, 80% NC PGA + scaled AS Y-dir. – Moment fit main method.

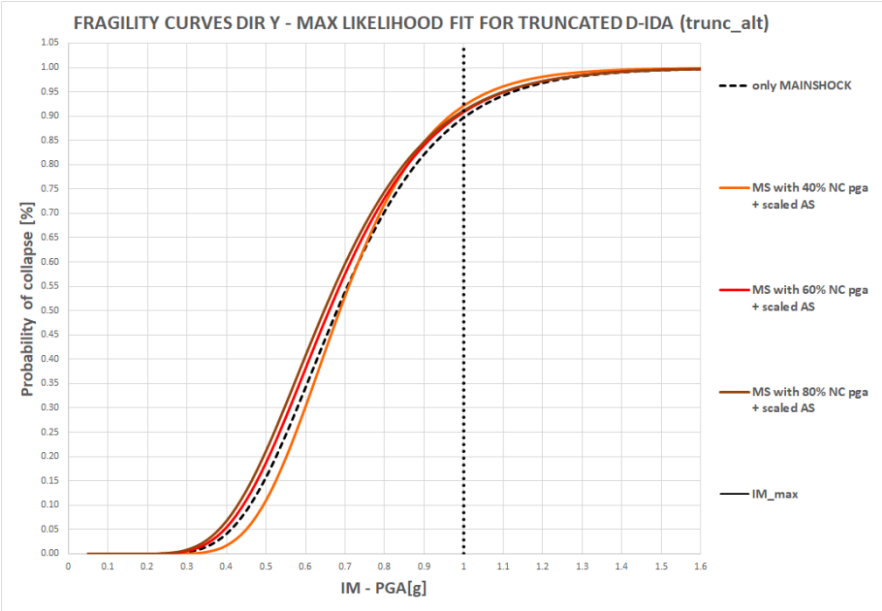

Figure 5.28 Fragility Curves Model 3 only mainshock (intact structure), MS of 40%, 60%, 80% NC PGA + scaled AS Y-dir. – Max likelihood fit for truncated D-IDA main method.

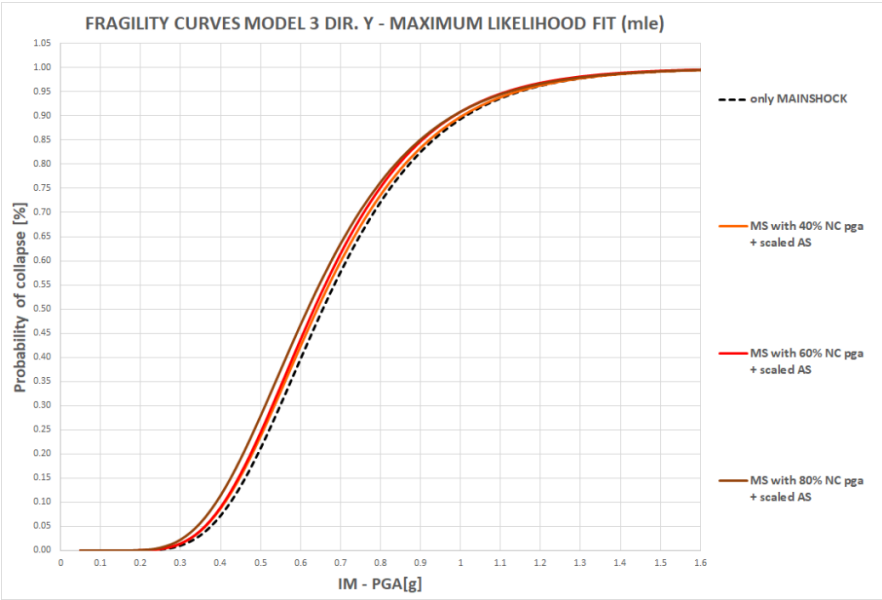

Figure 5.29 Fragility Curves Model 3 only mainshock (intact structure), MS of 40%, 60%, 80% NC PGA + scaled AS Y-dir. – Maximum likelihood fit main method.

5.5 Damage Index

5.5.1 State of Art

Damage accumulation of seismic sequence analysed is also estimated in term of damage index. In the first instance, the damage can be classified as ‘‘local” when it refers to a single member, as ‘‘intermediate” if it concerns a portion of the overall structure or as ‘‘global” if it regards the whole structure.
Researchers propose several methods to calculate this index concerning structural entities (force, displacement, deformation, or energy dissipation) versus the corresponding structural capacity. Currently, available Damage Indices (DIs) have their own merits and limitations and in some cases fail to reflect the state of damage appropriately. The most drawbacks identified as part of the current research are that the DI is not 0 when a structure operates within elastic range and that the magnitude of DI often exceeds 1 (there is no specific upper limit to define the state of collapse): Table 5.5 reports the common interpretation of the damage index according to the scientific literature.

Degree of damage	Damage index	State of structure
Minor	0.0-0.2	Serviceable
Moderate	0.2-0.5	Repairable
Severe	0.5-1.0	Irreparable
Collapse	>1.0	Loss of storey of buildings

Table 5.5 Interpretation of the damage index according to the scientific literature.

A brief description of DI widely used in literature is provided.
A comparison and numerical calibration of damage indices are reported in Mitropoulou et al. [94].
For local damage index, one of the widely used is the Park and Ang index [95], defined as the linear combination of the maximum displacement and the dissipated energy:

$$DI_{PA} = \frac{\delta_M}{\delta_u} + \frac{\beta}{Q_y \delta_u} \int dE \tag{5.1}$$

where δ_M is the maximum deformation obtained under the earthquake loading, δ_u is the ultimate deformation achieved under a monotonic loading, Q_y is the calculated yield strength and E is the incremental absorbed hysteretic energy (β is a non-negative parameter calibrated from tests).
The damage proposed by Kunnath et al. [96] is a modification of DI_{PA} for the case of damage of structural element end-section:

$$DI_{PA} = \frac{\theta_m - \theta_r}{\theta_u - \theta_r} + \frac{\beta}{M_y \theta_u} \int dE \quad (5.2)$$

In this case, deformation is replaced by the rotation: θ_m is the maximum rotation attained during the loading history, θ_u is the ultimate rotation capacity of the critical region, θ_r is the recoverable rotation after unloading, $M_y$is the yield moment and E is the dissipated energy in the critical region. The element damage is selected as the largest damage index of the end critical region.

For a global index, numerous formulations are proposed in literature depending on parameters considered.

Di Pasquale et al. [97] develop two damage indices based on the combined effect of stiffness degradation and plastic deformation concerning the evolution of the natural period of a time-varying linear system to the actual nonlinear system for a series of non-overlapping time windows and the final state of the building:

$$DI_{MS} = 1 - \frac{(T_0)_{initial}}{(T_0)_{max}} \quad (5.3)$$

$$DI_{FS} = 1 - \frac{(T_0)_{initial}}{(T_0)_{final}} \quad (5.4)$$

where $(T_0)_{initial}$, $(T_0)_{max}$ and $(T_0)_{final}$ correspond to the initial, maximum and final fundamental period computed for the total duration of the seismic event.

In this work, the ductility damage index DI_μ is used as observed in research of Pierdicca et al. [98].

This index is proposed by Powell et al. [99] and it is representative of the conditions of the entire structure:

$$DI_\mu = \frac{\delta - \delta_y}{\delta_u - \delta_y} = \frac{\mu - 1}{\mu_u - 1} \quad (5.5)$$

where δ is the maximum inelastic displacement during an earthquake, δ_y is the yielding displacement and δ_u the ultimate displacement computed with a preliminary nonlinear static (pushover) analysis.

5.5.2 Result

All ductility damage index calculated for X and Y directions are reported below. Same cases of fragility curve regarding the maximum inelastic displacements of intact structure (only mainshock, simple IDA) and the maximum inelastic displacements of MS of 40%NC, 60%NC and 80%NC pga with scaled aftershocks (D-IDA) are considered. The values of yielding and ultimate displacements used are computed from a minimum of bilinear curves of nonlinear static analysis previous described in paragraph 4.4.2 (In X-direction $\delta_y = 0.013m$ and $\delta_u = 0.1001m$ are used while $\delta_y = 0.03m$ and $\delta_u = 0.1280m$ are utilised for Y-direction).

In all directions, a more marked and distinct behaviour of damage index is observed compared with no great difference of fragility curves regarding only Near Collapse situation.

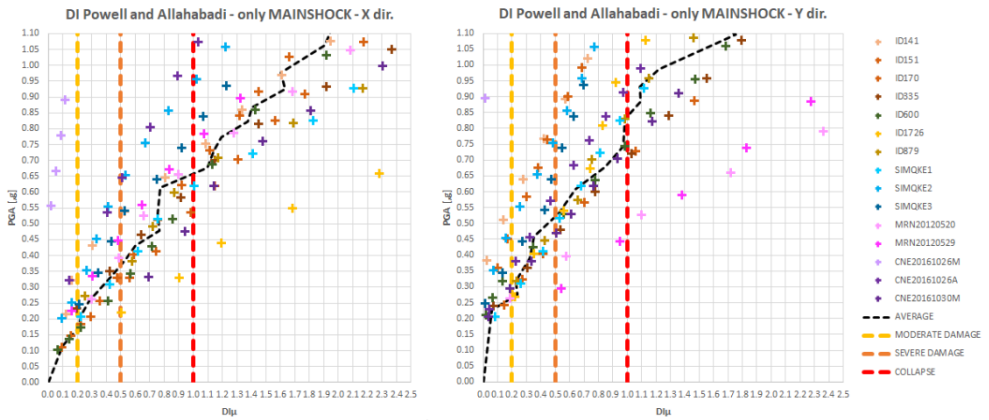

Figure 5.30 Ductility damage index concerning drifts of IDA dataset (only mainshock -intact structure).

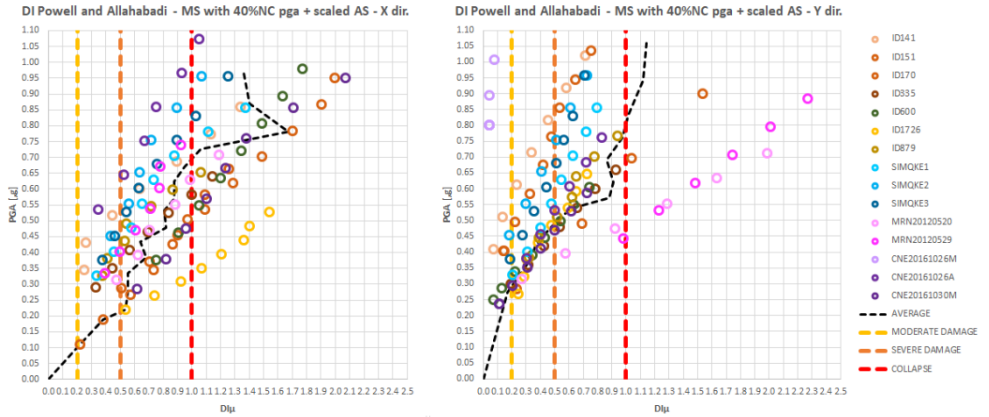

Figure 5.31 Ductility damage index concerning drifts of D-IDA dataset (MS with 40%NC PGA + scaled AS).

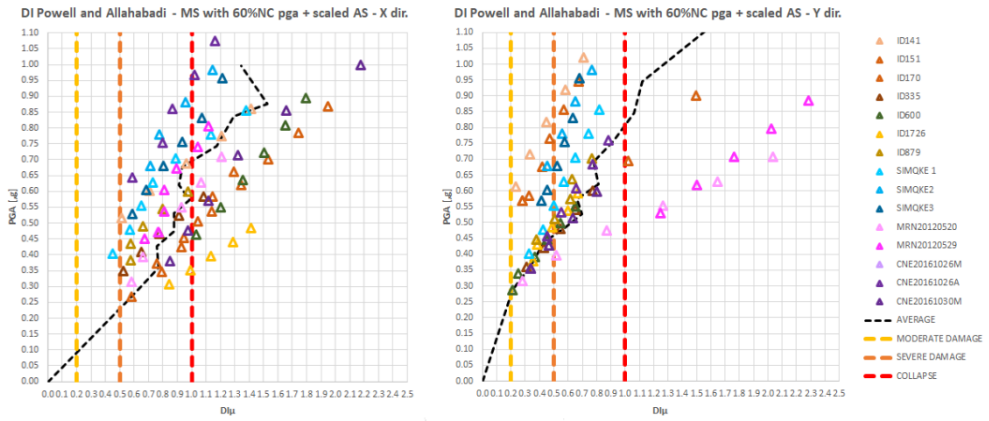

Figure 5.32 Ductility damage index concerning drifts of D-IDA dataset (MS with 60%NC PGA + scaled AS).

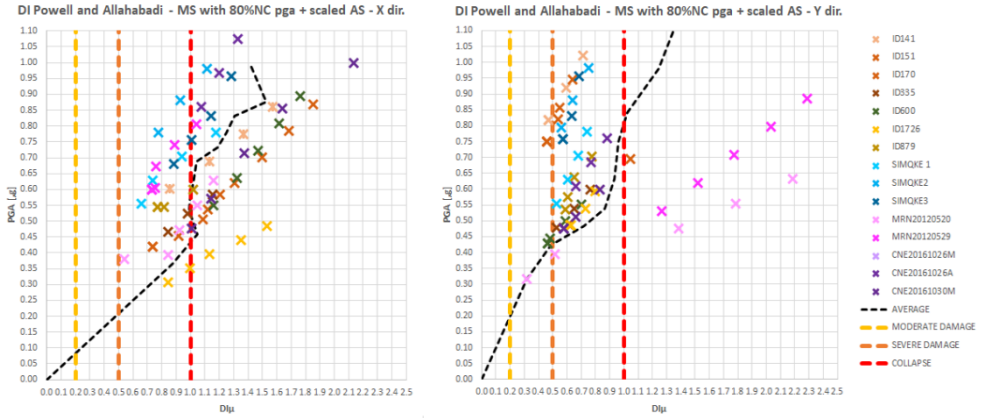

Figure 5.33 Ductility damage index concerning drifts of D-IDA dataset (MS with 80%NC PGA + scaled AS).

Comparisons in X-Y directions between all cases are reported in Figures 5.34-5.35. Averages curves of all cases demonstrate that there are more differences between damage indices in X-direction respect Y-direction in accordance with the behaviour of fragility curves. Mayor variances of damage indices respect of intact structure are visible for DI<1; after this value, the behaviour of DI average curves is similar.

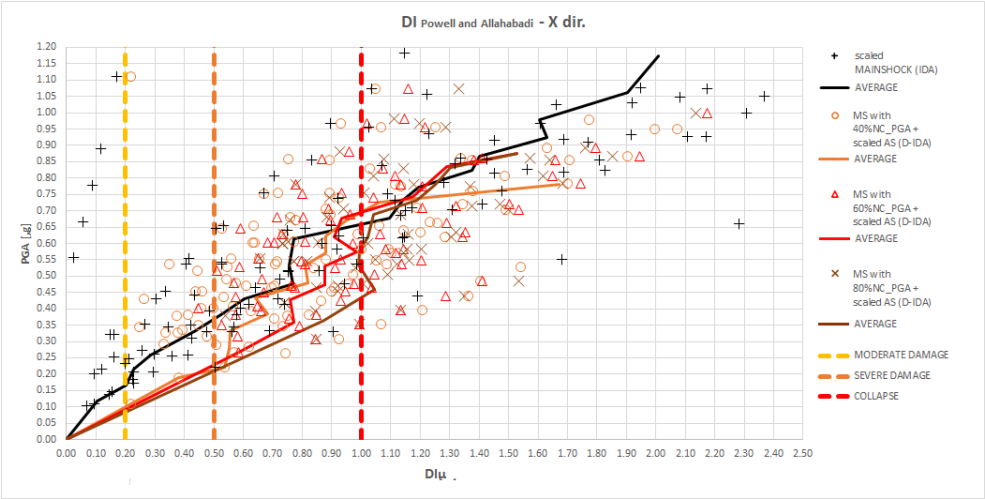

Figure 5.34 Comparison between ductility damage index of all cases – X direction.

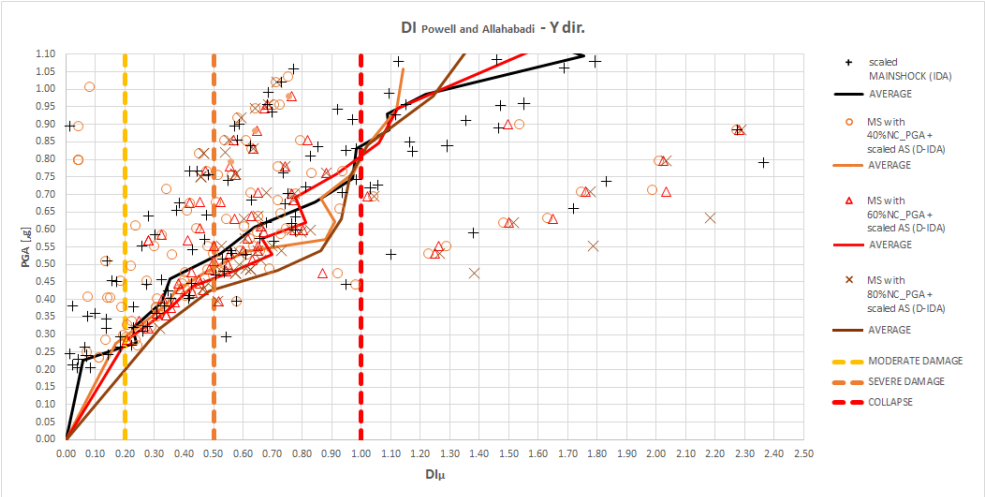

Figure 5.35 Comparison between ductility damage index of all cases – Y direction.

5.6 Future works

Several hypotheses are done to continue this work.
A diffuse plasticity model as realised in Di Trapani et al. [93] could be implemented to compare the roof drift results, especially for the behaviour of the polarity of aftershocks that influence in a significant manner D-IDA curves and consequently fragility curves as observed in the result.
It could also be interesting the use of real mainshock-aftershock sequences as reported in Di Sarno [84] but with 2016 Central Italy seismic sequences to evaluate seismic response of a structure.
Moreover, a comparison with several damage indices is suitable to understand which is the type of index that best represents the real situation.

6 Chapter - Influence of cladding panels in the first period of precast frame structures

This chapter investigates the influence of cladding panels on the fundamental period of the precast industrial frame buildings.
During the Emilia-Romagna earthquake, the problem of considering non-structural element in the linear and nonlinear analysis was already taken into account, but now it is more evident with NTC2018 that also requires the design and the verification of these nonstructural elements.
Bare frame precast structure has a fundamental period very close to steel structure (low seismic forces but very high displacements), now if it is considered the high influence of the cladding panels-to-structure interaction the elastic period change in a significant manner.
After an introduction to the typologies of cladding panels and their static scheme, scientific literature formulas to calculate fundamental period are analysed and compared to a preliminary first case study, for the small size not characteristic of the real period of a precast structure but necessary to understand how to implement the different cases into a numerical model.
Subsequently, a more representative case study is realised.

6.1 The SAFECLADDING research project: design criteria and experimental campaign to connect frame and panels

For existing building, design practice of precast buildings is based on a bare frame, where cladding panels are considered only as masses without any stiffness. The panels are then connected to the structure with fastenings devices dimensioned with a local calculation on the basis of their mass to anchorage orthogonal forces in the plane of the panels.
The Emilia Romagna earthquake has demonstrated that the panels come to be an integral part of the resisting system and they condition its seismic response. The high stiffness of this resisting system leads to forces much higher than those calculated from the frame model. These forces are related to the global mass of the floors and are primarily directed in the plane of the structures.
So the design of these connections cannot rely on the seismic reduction factor used to design of the bare structure.

The research project SAFECLADDING wants to investigate the seismic behaviour of precast structures with cladding panels to develop innovative connection devices and novel design approaches for a correct conception and dimensioning of the fastening system supported by the experimental results of the testing campaigns and numerical simulations performed within the project. Joint Research Centre realises two design guidelines for precast structures with cladding panels [24,25].
In these guidelines, three design criteria are assessed defined as an isostatic, integrated and dissipative solutions in addition to the existing solution found in existing precast structures.
For an isostatic criterion, the frame deformation demand is allowed by relative fastening devices that uncouple the motion of frame and panels. The two systems are kinematically uncoupled, except for the out-of-plane displacements (Figure 6.1a).
Integrated solution assumes that integrated panels and frame have a coupled motion: the system is kinematically paired. Panels become part of the seismic resisting system, and they act as the main limitations in the horizontal direction thanks to their higher stiffness. As a consequence, the connections must be over-proportioned to carry the higher loads transferred by the frame, according to capacity design rules (Figure 6.1b).
Existing solutions show a behaviour partly isostatic and partly integrated depending on fastening devices adopted by the company.
As isostatic configuration, the dissipative systems are kinematically uncoupled, but they are also constrained by inelastic links, like friction or yielding devices. The joints between structure and panels, or between panels, have to be designed to dissipate energy during the earthquake shock. Dissipative specific devices can balance the overall building response, reducing the displacement and keeping the load below an imposed threshold, determined by the connections themselves (Figure 6.1c). Several experimental tests of dissipative solutions with structure and panels are performed by Negro et al. [100]. A further dissipative system of panel-to-panel connections that allow to control the level of forces and limit the displacements is studied by Dal Lago et al. [101].

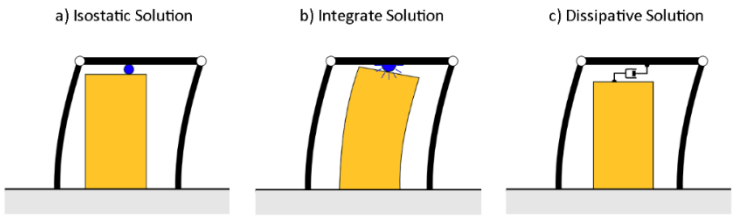

Figure 6.1 Design criteria to connect frame and panels: a) Isostatic Solution, b) Integrate Solution, c) Dissipative Solution [100].

In the following paragraph the static scheme and the coupling systems of the existing, integrated and the isostatic solution will be discussed. Dissipative solution is not taken into account in this work.
A summary of result of full-scale experimentation of cladding panel connection systems performed at ELSA (Laboratory of the European Joint Research Centre of Ispra) is reported in Toniolo et al. [102]. The main conclusions of this experimental campaign are that isostatic solution is the one that can be applied from now on in the simplest of ways provided that some acceptance checks are made of the chosen connection devices, the integrated solution leads to very high joint forces all over the structure and technological problems have to be overcome for the proportioning of the related connection devices and the dissipative solution is presently out of the consolidated applicative experience, but it shows very promising features only for application in new constructions.

6.1.1 Existing Solution

For the seismic analysis, the old design practice of the precast structures is often based on a bare frame model where the peripheral cladding panels enter only as masses without any stiffness. The panels are then connected to the structure with fixed or pinned fastenings dimensioned with a local calculation on the base of their single mass to anchorage forces orthogonal to the plane of the panels.
Emilia Romagna and Central Italy earthquakes demonstrated that this approach is not correct.
The panels, depending on the actual degree of stiffness of the connectors, may come to be an integral part of the resisting system, conditioning its seismic response as of a dual wall-frame system of lower energy dissipation capacity. The high stiffness of this resisting system leads to much higher forces than those calculated from the frame model. These forces are related to the global mass of the floors and they are primarily directed in the plane of the walls. The unexpected

intensity and direction of the forces bring many fastenings to failure with the consequent fall of panels that can have up to 10 tons of weight.

6.1.1.1 Static schemes

Both vertical and horizontal connection systems failed with a brittle rupture in many precast structures during recent earthquakes due to an inadequate resistance concerning the longitudinal force received and to the lack of ductility capacity.

6.1.1.1.1 Vertical Panel

The matrix below proposed by Colombo et al. [24] is a very common connection system used many years for vertical panels: the unit is simply supported on the foundation beam without mechanical connectors; it is connected to the top beam through vertical channel bars and headed fasteners giving a bilateral out-of-plane y restraint and an unintended "weak" bilateral restraint with limited movement allowance in the horizontal X-direction (Figure 6.2).

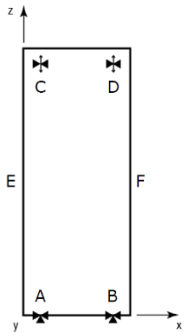

	A	B	C	D	E	F
x	f*	f*	f	f	0	0
y	f	f	f	f	0	0
z	f⁻	f⁻	s	s	0	0

f* restrain due to friction

- f = fixed (bilateral)
- f+= fixed (unilateral in + direction)
- f-= fixed (unilateral in - direction)
- s = sliding (bilateral)
- i = indifferent
- d = dissipative
- 0 = absent
- / = omitted

Figure 6.2 Vertical panel existing solution static scheme.

6.1.1.1.2 Horizontal Panel

Figure 6.3 gives the arrangement matrix and the graphics scheme of one of the connection systems used many years for horizontal panels: the unit is connected to the two lateral columns; the two lower connections consist of steel corbels protruding from the columns proportioned to give the vertical -z support to the panel; the two upper connections consist of shear dowels that ensure the bilateral horizontal x restraint; all the four connections provide the bilateral horizontal y restraint.

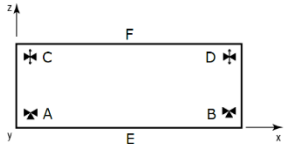

	A	B	C	D	E	F
x	f*	f*	f	f	0	0
y	f	f	f	f	0	0
z	f⁻	f⁻	s	s	0	0

f* restrain due to friction

- f = fixed (bilateral)
- f+= fixed (unilateral in + direction)
- f-= fixed (unilateral in - direction)
- s = sliding (bilateral)
- i = indifferent
- d = dissipative
- 0 = absent
- / = omitted

Figure 6.3 Horizontal panel existing solution static scheme.

6.1.1.2 Fastening devices

The fastening devices usually utilised are hammer-head strap connections, cantilever connections and steel angle connections. All fastening systems are described in detail.

6.1.1.2.1 Hammer-head strap connections

The connection consists of a special steel strap (a hammer-head strap), a toothed washer, a bolt and two steel channels with anchors, which are installed before casting of the elements. One of the channels is cast into the panel, whereas the other is cast into the structural element (beam or column) to which the panel is to be fixed. The strap is fastened to the channel which is cast into the structural element using a toothed washer and a bolt. Finally, the head of the strap is fixed inside the channel which is cast into the panel. In this way, between the panel and the structural element is created a connection (Figure 6.4). Hammer-head strap connections are most often used for fastening of vertical panels to the beams. Usually, at the base of the vertical panel to allow sliding, there is an L-shaped steel profile (panels are not anchored but only seated on the foundation beam).

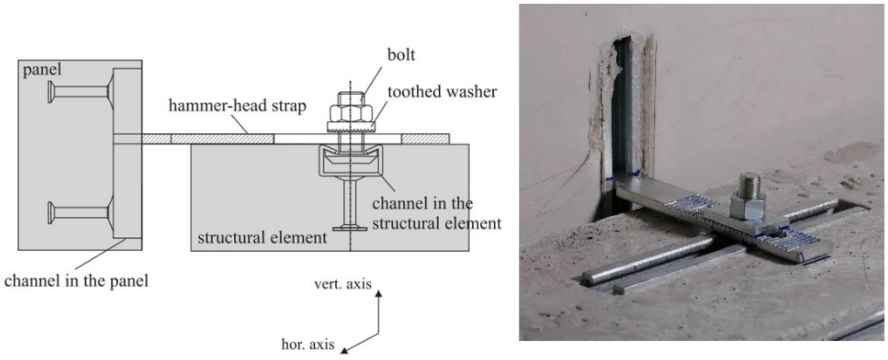

Figure 6.4 Schematic presentation of hammer-head strap connection.

Hammer-head strap connections could be provided with channels of different strength.

Mainly two different types of channels should be recognized: strong (hot rolled) channel, when the connection fails for the failure of the strap (Figure 6.5a), and weak (cold formed) channel, when the connection fails for the failure of the channel (Figure 6.5b).

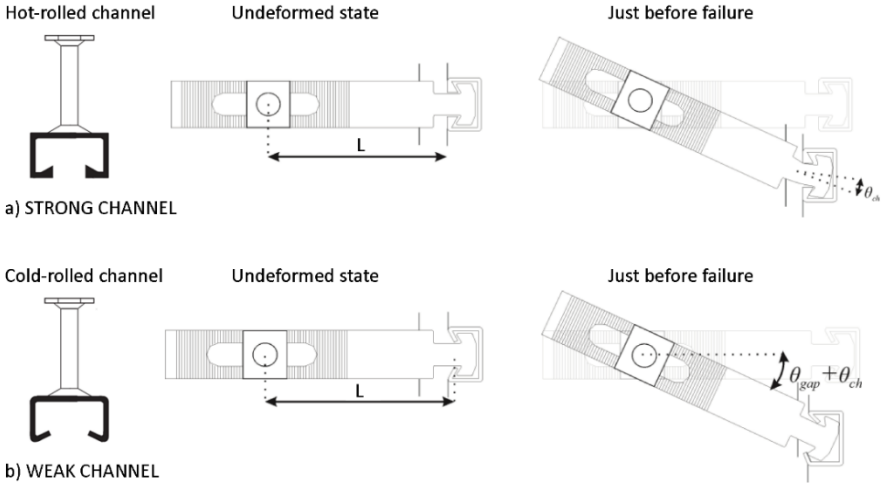

Figure 6.5 Scheme of failure of hammer-head strap connection: a) strong channel, b) weak channel.

Zoubek et al. [103] realise sixteen cyclic tests on hammer-head strap connections with the weak and strong channels. Three different types of tests are performed: uniaxial and biaxial shear tests and uniaxial sliding tests. The result of shear test is that the displacement capacity of a connection can increases if the tightening

torque is very low (The strap can then not only rotate but also move along the channel which is cast into the beam).
Another experimental result also shows that the size of the gap between the beam and the panel should be sufficient to permit full utilization of the displacement capacity of the connections. If the gap is too small, panels and beam come in contact, which induces additional friction forces between the elements and the behaviour is much more complex and more difficult to predict.
They also underline that another important parameter which influences the response of hammer- head strap connections is the type of channels used. When cold-formed channels are used in the performed experiments, failure of the connection occur in the channel, whereas in the case of hot-rolled channels the strap fail. Although the type of failure is different, the response is qualitatively as well as quantitatively the same because they observe similar hysteresis loops, displacement and strength capacities.

6.1.1.2.2 Cantilever box connections

Cantilever box connections consist of a vertical channel, which is mounted in the columns, and a special steel element, which is collocated in the panel: these two components are then connected using a single bolt. Cantilever connections are most often used as fastening devices of horizontal panels to the beams at the top corners of a panel.

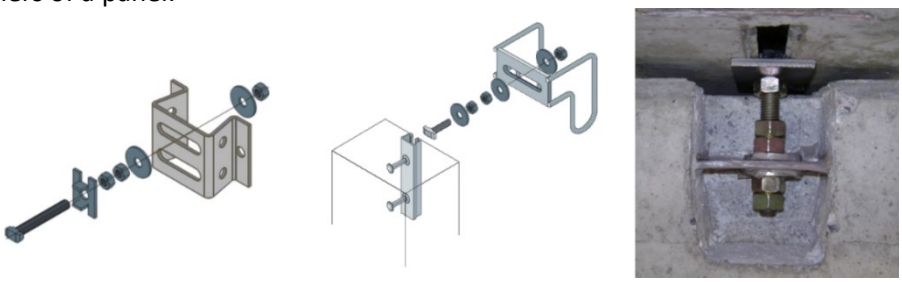

Figure 6.6 Schematic presentation of the cantilever connection assembly.

The behaviour of the cantilever connections, when loaded in shear, is schematically presented in Figure 6.7. At first, the bolt slides along the profile until it reaches the end of the profile (The resistance of the connection is equal to the friction force between the components). At that point the stiffness of the connection increases, the channel fails, and the bolt is pulled out of the channel.

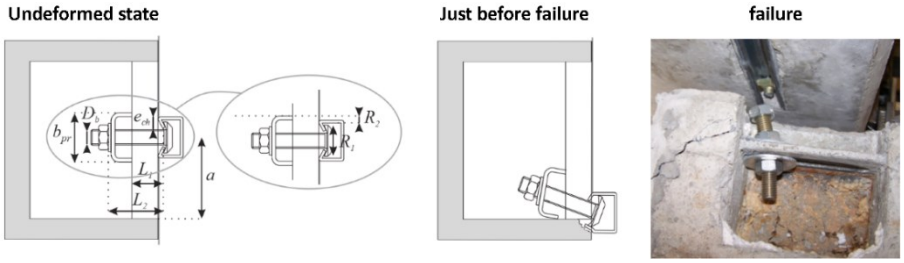

Figure 6.7 Scheme of failure of the cantilever connection.

Belleri et al. [104] conduct an experimental campaign on four full-scale horizontal cladding panel to column subassemblies with typical connections adopted in the Italian territory. The experimental results highlight failure mechanisms associated with the top connections. In case of uncontrolled anchor bolt tightening, the sliding capacity can be inhibited and an anticipated connection failure is recorded leading to possible panel out of plane overturning. The inclusion of a steel ring placed inside the slotted connection depth avoids uncontrolled tightening of the connecting bolts.

6.1.1.2.3 Steel angle connections

The steel angle connection consists of two steel channels which are mounted in a beam (or column) and in a panel and a steel angle which is fastened to the channels using bolts (Figure 6.8).

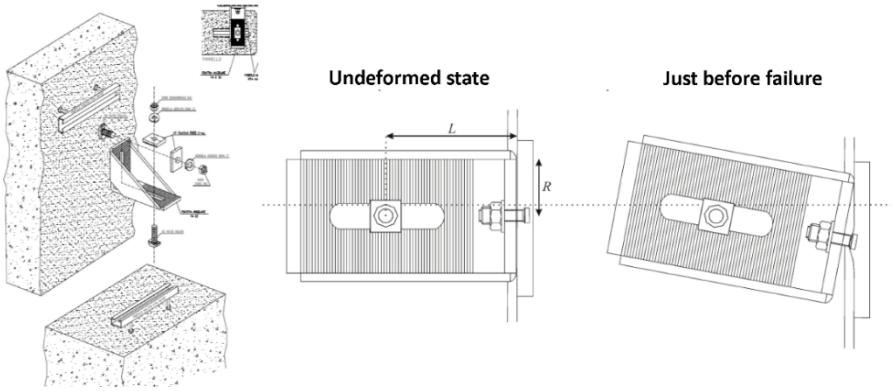

Figure 6.8 Schematic presentation and scheme of failure of steel angle connections.

6.1.2 Isostatic Solution

To ensure the pure frame behaviour of the resisting structure, the isostatic connection system of the wall panels allows without reaction the large displacements of the frame structure under seismic action, except for possible minor reaction effects due to friction or sealing. In this case, there is the adoption of sliding connection devices with adequate capacities (such as ±150 mm or greater) or pinned connectors for free rotations.
There are five available solutions for an isostatic connection, three for the vertical panel and two for horizontal panel. In the typical structural arrangements, the connections of the panels are therefore designed to resist the panel out-of-plane seismic only.
Within an isostatic connection system, silicone sealant is a natural completion material of precast panels used to fill and to close the joints between panels and other components. It is not a structural product and it allows free drifts of the joint without damages, keeping its waterproof function.
However, a reaction of the long silicone sealant strips to the relevant drifts under seismic action arises, affecting at a certain level the response of the structure. Dal Lago et al. [105] investigate the role of the silicone sealant on the seismic response of precast structures with cladding panels. Authors conclude that the silicone sealant influences the seismic performance at the serviceability limit state and increase the load demand on the panel connections. However, it is worth noting that the stiffening contribution is limited and not reliable since the variability of the mechanical characteristics of this type of product is large and silicone is not suitable to sustain the large drifts typically associated with the ultimate limit state. Therefore, they recommend to disregard the influence of the silicone sealant when it involves possible beneficial effects on the seismic performance of the structure.

6.1.2.1 Static schemes

6.1.2.1.1 Vertical panel

In the structural scheme of vertical panels, non-structural components are placed over the foundation beam, to which they transmit their weight, and they are supported horizontally by the roof beam with connections placed close to the top to obtain an isostatic connection system. The first solution adopts hinged lower and upper supports so to have a pendulum behaviour for any single panel (see Figure 6.9). The second solution adopts fixed (pinned) supports at the base of the panels

and one or two sliding connections to the structure at the upper position so to have a cantilever behaviour uncoupled from the structure (see Figure 6.10). The third solution adopts a simple seating of the panels on bearings placed at the two edges of the base side together with a hinged connection to the structure at the upper position so to have a rocking behaviour for large displacements (see Figure 6.11). For all the three solutions, in the out-of-plane direction, the panels are supported with an isostatic pendulum scheme.

Pendulum Solution

In the pendulum arrangement, for a given top displacement d, the adjacent vertical sides of the panels display a relative slide of b/h where h is the height of the upper support and b is the width of the panels. In the meantime, the two adjacent sides get closer by a minor quantity that requires, in any case, a free spacing between the panels (few millimeters) closed by the sealant. Since only vertical compression forces are expected at the base supports, connections consist of simple seatings able to provide only a unilateral restraint in the z-direction.
The arrangement matrix and structural scheme are given in Figure 6.9.

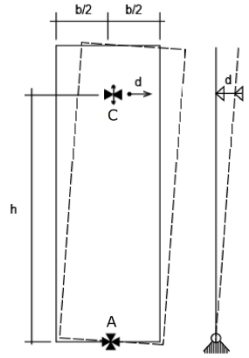

	A	B	C	D	E	F
x	f	/	f	/	0	0
y	f	/	f	/	0	0
z	f	/	s	/	0	0

- f = fixed (bilateral)
- f+= fixed (unilateral in + direction)
- f-= fixed (unilateral in - direction)
- s = sliding (bilateral)
- i = indifferent
- d = dissipative
- 0 = absent
- / = omitted

Figure 6.9 Vertical panel Pendulum Isostatic Solution static scheme.

Cantilever Solution

The cantilever solution or isostatic sliding frame (Figure 6.10) keeps the panels still during the motion of the structure because of the horizontal slide channel bars placed at the upper position. Sensible friction effects may arise due to the contemporary orthogonal forces caused by the biaxial vibratory motion. The base support of the panels can be provided with reinforcing bars protruding from the

bottom and anchored by bond within corrugated sleeves inserted in the foundation and filled with no-shrinking mortar.

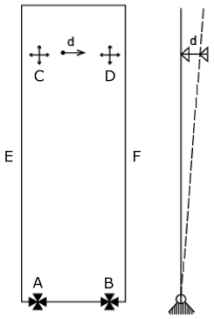

	A	B	C	D	E	F
x	f	f	s	s	0	0
y	f	f	f	f	0	0
z	f	f	s	s	0	0

f* restrain due to friction

- f = fixed (bilateral)
- f+= fixed (unilateral in + direction)
- f-= fixed (unilateral in - direction)
- s = sliding (bilateral)
- i = indifferent
- d = dissipative
- 0 = absent
- / = omitted

Figure 6.10 Vertical panel Cantilever Isostatic Solution static scheme.

<u>Rocking Solution</u>

The rocking arrangement (Figure 6.11) consists of the seating of the panels on the foundation through unilateral bearings that work only in compression. The two edges of the base side of the panel alternatively rise during the rocking motion and should be properly reinforced against spalling. In this condition, the panels behave as integrated into the structure that becomes a dual wall-frame system with a much higher global stiffness. Under seismic action, therefore, the reacting system receives an initial high horizontal impulsive force that decreases when that limit is overcome and the panels begin to rock, behaving as an isostatic system. In the rotated position the panel, seated in its edge active bearing, provides a stabilizing constant horizontal force. At the reverse motion the panel seats back again on the two base lateral bearings restoring its initial stable equilibrium.

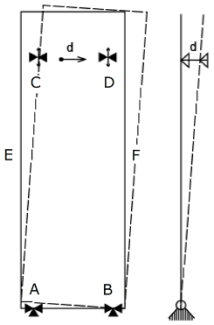

	A	B	C	D	E	F
x	f*	f*	f	f	0	0
y	f	f	f	f	0	0
z	f`	f`	s	s	0	0

*working alternatively

- f = fixed (bilateral)
- f+= fixed (unilateral in + direction)
- f-= fixed (unilateral in - direction)
- s = sliding (bilateral)
- i = indifferent
- d = dissipative
- 0 = absent
- / = omitted

Figure 6.11 Vertical panel Rocking Isostatic Solution static scheme.

6.1.2.1.2 Horizontal panel

The horizontal panels are connected externally to the adjacent columns to which they transmit their weight, being restrained horizontally by the same connections. The lower panels can be seated directly with their weight on the foundation elements.
Following alternative solutions, the horizontal panels can be seated one over the other, taking all their weights directly to the foundation and transmitting to the adjacent columns only the horizontal orthogonal actions due to their mass. In this case, one has a lower reliability of the model because of the higher uncertainties of the longitudinal friction behaviour of the mutual joints under seismic conditions.

Hanging Solution

The superimposed panels have a free spacing at the joint between the adjacent sides to allow the relative slide motion without friction. This joint is sealed with proper material (silicone) that may introduce a minor reaction effect. Any single panel is provided by two upper vertical supports placed at the ends and fixed to the columns. One of them also provides the horizontal restraint in the plane of the panel. At the opposite lower side, two couples of sliding connections are placed allowing the free horizontal and vertical displacements. All the four corner connections provide a fixed horizontal support orthogonal to the panel (Figure 6.12).

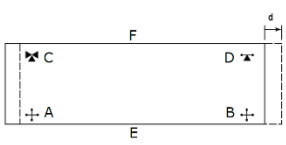

	A	B	C	D	E	F
x	s	s	f	s	0	0
y	f	f	f	f	0	0
z	s	s	f	f	0	0

- f = fixed (bilateral)
- f+= fixed (unilateral in + direction)
- f-= fixed (unilateral in - direction)
- s = sliding (bilateral)
- i = indifferent
- d = dissipative
- 0 = absent
- / = omitted

Figure 6.12 Horizontal panel Hanging Isostatic Solution static scheme.

Seated Solution

Seated solution is equivalent from a kinematic point of view to hanging solution; the only difference is to exchange of upper and lower connections. Figure 6.13 reports structural scheme and the arrangement matrix.

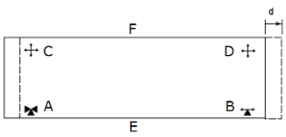

	A	B	C	D	E	F
x	f	s	S	s	0	0
y	f	f	F	f	0	0
z	f	f	S	s	0	0

- f = fixed (bilateral)
- f+= fixed (unilateral in + direction)
- f-= fixed (unilateral in - direction)
- s = sliding (bilateral)
- i = indifferent
- d = dissipative
- 0 = absent
- / = omitted

Figure 6.13 Horizontal panel Seated Isostatic Solution static scheme.

6.1.2.2 Rotating devices

Rotating connections are mainly used at the base of vertical panels in pendulum arrangement. Figure 6.14 shows the mechanical device to be used when a resultant vertical lifting action is expected on the panel so to require a downward reaction from the connection. The quoted one is an ordinary hinge, common in steel construction, that relays its resistance on the shear strength of the pin and to the bearing action of the lateral plates.

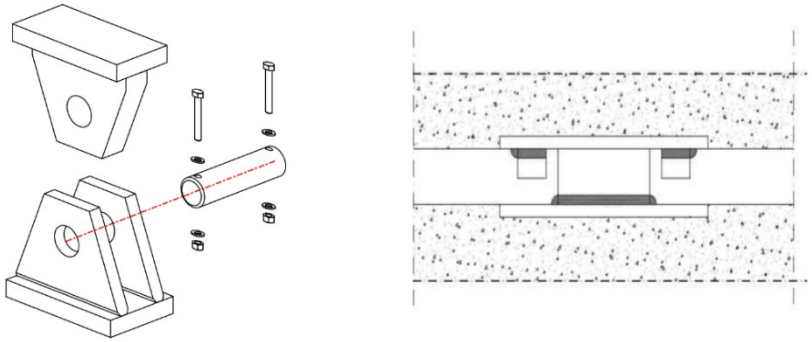

Figure 6.14 Schematic presentation of the rotating device.

Negro et al. [100] implement this device to an experimental test to create the double-hinged panel solution and they demonstrate that it is the most proper way to connect panels to frame without affecting the global stiffness.

6.1.2.3 Sliding devices

The sliding devices, such as fixed channel bars with internal moving head slides, allow the free longitudinal alternate displacements without reactions and they have to provide an effective connection between panel and structure in the direction orthogonal to the panel without excessive out of the plane. In the overall arrangement of the panels, all possible hammering phenomena between adjacent panels and panels to structure have to be prevented.
Figure 6.15 shows a sliding device to connect a vertical panel to the upper beam. The channel bar is fixed to the beam, a fixing gear is attached to the panel in a special pocket, bolted to counter-plate, and a fastener is placed to connect the two parts, where its grooved head slide is inserted in the lips of the channel bar to provide a bilateral transverse support while it remains free to slide in the longitudinal direction.

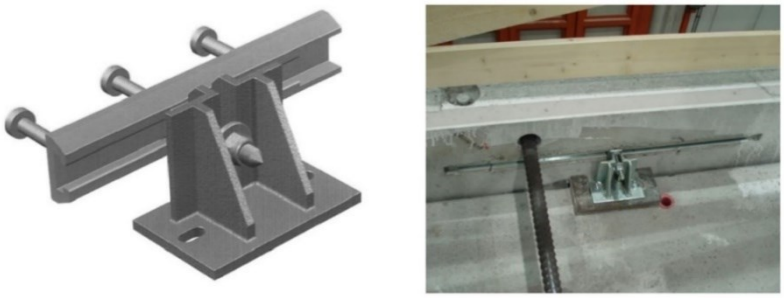

Figure 6.15 Schematic presentation of the sliding device.

Dal Lago et al. [106] investigate the correct kinematics of this connection within a uniaxial experimental test, imposing displacement histories with the application of constant normal force. A cyclic test on a full-scale precast prototype equipped with sliding panel connections is carried out, checking the global behaviour of cantilever system for the vertical panel and seated and hanged solution for horizontal panel. The connection can slide in all tests for ten imposed cycles, showing a typical friction hysteresis. The experimental tests with axial out-of-plane loading are characterised by relatively low friction and total absence of damage to the connection. The tests with shear out-of-plane loading describe slightly larger values of friction and permanent deformation on the slider after the tests with the high out-of-plane load.

6.1.2.4 Supports with steel brackets

Strong steel brackets are conceived to support the horizontal suspended panels connecting them to the columns: they are made with traditional steel profiles and usually filled with concrete to increase their stiffness. Bracket connections are conceived to carry the gravity load of the panel and they are usually placed in two positions in a row. A recess in the panel or/and an inclined contact surface prevent out-of-plane displacement of the panel.
Figure 6.16 shows a bearing bracket device provided with an adjustable steel bolt for the support of horizontal panels, connected to the column. The bracket is inserted in a recess left in the column and the panel, which is provided with a hosting groove, it is placed on top of the bolt.

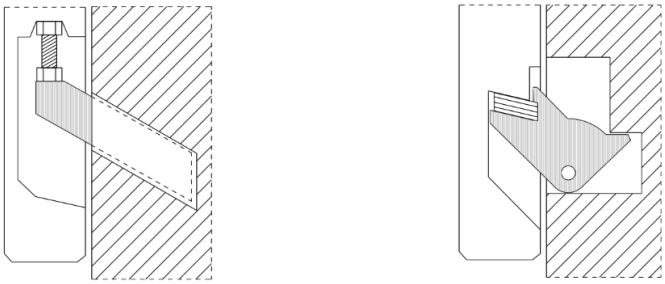

Figure 6.16 Schematic presentation of support with steel brackets.

6.1.3 Integrated Solution

In the integrated system, the connections of each panel are arranged with a hyperstatic set of fixed supports (connections with restrains in displacements only). With this arrangement of connections, the panels participate to the seismic response of the structure within a dual wall-frame system which has much higher stiffness and a lower energy dissipation capacity compared to a pure frame and this leads to a structural seismic response with higher forces and lower displacements.

6.1.3.1 Static schemes

6.1.3.1.1 Vertical panel

For vertical panel four fixed fastenings are used, one for each corner, the lower two attached to the bottom beam, the upper two attached to the top beam. In such cases, thermal forces must be considered in the design of the panels to prevent local damages and consequently the rupture. The corresponding arrangement matrix and the structural scheme is given in Figure 6.17.

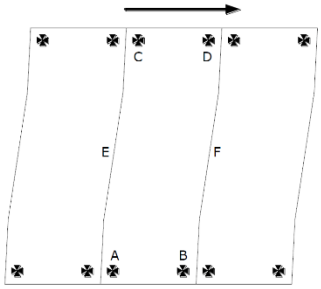

	A	B	C	D	E	F
x	F	f	f	f	0	0
y	F	f	f	f	0	0
z	F	f	f	f	0	0

- f = fixed (bilateral)
- f+= fixed (unilateral in + direction)
- f-= fixed (unilateral in - direction)
- s = sliding (bilateral)
- i = indifferent
- d = dissipative
- 0 = absent
- / = omitted

Figure 6.17 Vertical panel Integrated solution static scheme.

6.1.3.1.2 Horizontal panel

Figure 6.18 shows a hyperstatic arrangement of connections for horizontal panels. Four fixed fastenings are used, one for each corner, attached to the contiguous columns. In the case of horizontal panels, the fixed connections applied to the columns affect their deformation during earthquakes with the development of high local forces.

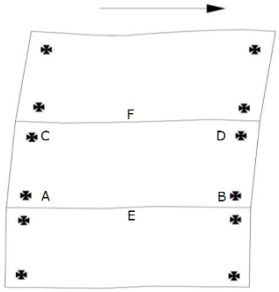

	A	B	C	D	E	F
x	F	f	f	f	0	0
y	F	f	f	f	0	0
z	F	f	f	f	0	0

- f = fixed (bilateral)
- f+= fixed (unilateral in + direction)
- f-= fixed (unilateral in - direction)
- s = sliding (bilateral)
- i = indifferent
- d = dissipative
- 0 = absent
- / = omitted

Figure 6.18 Horizontal panel Integrated solution static scheme.

6.1.3.2 Base supports

There are three types of base fixed connecting mechanisms: connections with protruding bars, with bolted shoes and with bolted plates.
Independently from the type of connection, a gap is typically left during construction between the panel and the supporting beam, which is filled with high strength, non-shrinking grout after mounting the panels to realise a uniform contact necessary to ensure friction and prevent sliding.
Panels with integrated connections behave as clamped at their ends. For this reason, taking under consideration their large in-plane stiffness, significant internal forces can develop during strong earthquakes.
Within the framework of the FP7 European project SAFECLADDING, Psycharis et al. [107] investigate the behaviour of several types of connections materialised with vertical reinforcement bars, referred to 'protruding bars' connections, or steel mechanisms of two types: 'wall shoe' and 'steel plate'. In all three types of the connections tested under monotonic loading, reverse monotonic loading and cyclic excitation, the overall behaviour, in terms of initial stiffness and ultimate strength, is similar and the overall failure is determined by the failure of the connectors and not by the deformation of the panel.
Another conclusion of their experiments is that wall shoe and steel plate connections do not dissipate as much energy as those with rebar connections, due to the larger pinching that characterised their response.

6.1.3.2.1 Connections with protruding bars

This type of connections can be executed using steel bars (reinforcement rebars) protruding from the panels into the beams or vice versa. In both cases, waiting corrugated sleeves are provided in the opposite element for the insertion of the bars. These sleeves are filled with high strength, non-shrinking fluid mortar after erection (the use of epoxy resins in combination with the smooth surface of in-situ drilled holes proved to be insufficient as reported experimental test of Psycharis et al. [107]). In Figure 6.19 the typical connection in case of bars protruding from the panel into the supporting beam is shown. In case that the connecting bars are protruding from the supporting beam into the panel, the corrugated sleeves are placed in the panels and must have holes for the injection of the grout.
The same type of connection can be used at the upper side of the panel to fix it to a superimposed element of the structure.
The possible failure modes of this system are pull-out of the tension bars, break of the bars, permanent elongation of the bars due to large strains developed, failure of the concrete in the compression zone (not probable except in case of very high forces) and sliding shear failure of the panel (not probable except in case of yielded connecting bars).

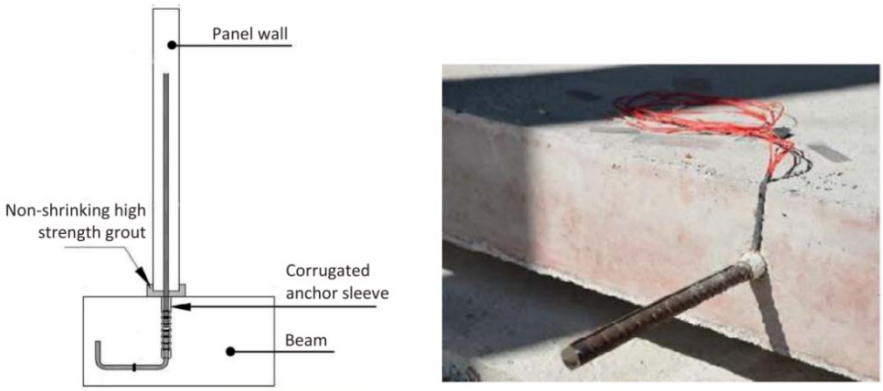

Figure 6.19 Schematic presentation of the protruding bars connections.

6.1.3.2.2 Connections with wall shoes

A typical wall shoe is shown in Figure 6.20: it consists of a steel nest with a strong bottom plate which is cast into the bottom part of the upper wall and fixed with anchor bars, an anchor bolt which is cast into the upper part of the lower wall or beam and a washer and a nut used to fasten the bolt to the bottom plate.
The possible failure modes associated with the resisting mechanism are pull-out or break of the anchor bolts, permanent elongation of the anchor bolts due to large strains developed, warping of the plate, failure of the concrete in the tension zone (not probable except in case of very high forces) and sliding shear failure of the panel (not probable except in case of yielded anchor bolts). In general, all parts of the wall shoes are over-proportioned, except the anchor bolt that is allowed to yield. Only wall shoe systems experimentally qualified can be used.

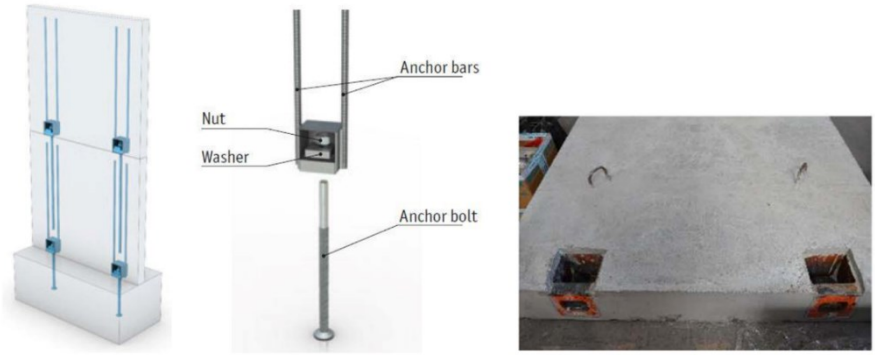

Figure 6.20 Schematic presentation of the wall shoe connections.

6.1.3.2.3 Connections with bolted plates

This type of connection can be executed using steel plates connected to waiting nests fixed to the supporting beam and the panel by an adequate number of bolts. The steel nests are embedded in the concrete and they welded to reinforcing rebars, so the connection forces are gradually transferred to the concrete.
A typical configuration of this connection is shown in Figure 6.21.
The advantage of this connection is that the steel plate can be easily substituted in case of damage and it does not pose any difficulties in the installation of the panels.
The possible failure modes associated with the resisting mechanism are shear failure of the connecting bolts, permanent distortion of the bolts and/or the plate due to large strains developed, loosening of the connection due to the permanent

distortion of the bolt holes, failure of the connecting plate, failure of the concrete in the compression zone and sliding shear failure of the panel.

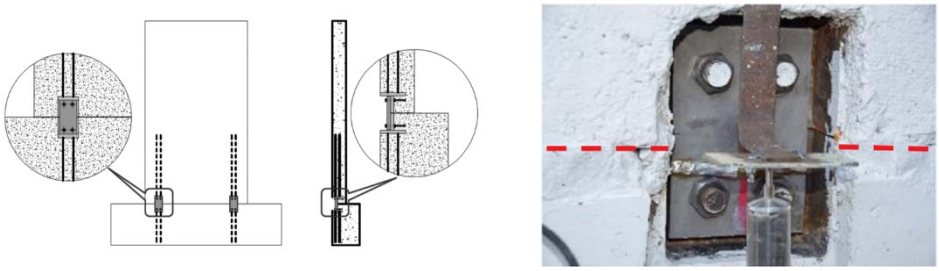

Figure 6.21 Schematic presentation of the bolted plate connections.

6.2 Evaluation of the period in the technical literature

The fundamental period of oscillation, dependent from mass, stiffness and the system of constraints applied of the structure, is influenced by several factors including the structural regularity, the number of planes, the geometric characteristics, the presence of non-structural components like infill masonry or cladding panels and the soil-structure interaction. This parameter provides indications on the overall behaviour of the building-ground system and strongly depends also on the type of dynamics exhibited by the structure as well as on the design criteria used and the construction practice utilised during the construction phase. In recent years, several experimental studies are carried out, calibrated on data from buildings monitored during relevant seismic events, which led to the development of simplified formulations to estimate the elastic period. The vast majority of regulatory codes at international level propose simplified reports for the assessment of the elastic period of structures according to height, the number of floors and, in some cases, plan extension. However, most of these relationships are designed according to modern seismic design criteria, different from those that characterise existing buildings, especially for precast frame structures.

In recent years, to propose simplified reports, several numerical and experimental campaigns are carried out on reinforced concrete structures in different geographical areas.

For precast frame structure several studies are performed by Magliulo et al. [108] and Ercolino et al. [109] to evaluate the first period in a linear analysis of one-storey precast buildings, both in the case of bare buildings and of buildings with cladding

system (Except this, there isn't a specific technical literature concerning the evaluation of period in precast frame buildings with cladding panels).
The main formulas to estimate the fundamental period of a structure regarding reinforced concrete framed structures with and without infills masonry are reported below.
One of the first formulations concerning the calculation of the period existing in the scientific and technical literature is ***FORMULA USCGS*** (United States Coast and Geodetic Survey of 1949) for building with the framed structure:

$$T = 0.11\frac{H}{\sqrt{B}} \tag{6.1}$$

where B is the length of the structure in the direction perpendicular of the earthquake.
Two other formulations of the same typology are reported in code DM LLPP 24.05.1982 and DM LLPP 24.1.1986 about RC frame structure:

$$T = 0.09\frac{H}{\sqrt{B}} \tag{6.2}$$

$$T = 0.1\frac{H}{\sqrt{B}} \tag{6.3}$$

(6.1), (6.2) and (6.3) are the first formulations to identify the period also with the length of the structure because most of the relationships existing in literature are a function of only total height H that, more than any other parameter, summarises the relationship between the stiffness and the mass of the building.
The calibration of these relationships is generally performed numerically by experimental data. The traditional numerical approach is based on the analysis of a set of buildings united by the same structural typology and on the consequent derivation of an interpolating curve. The experimental approach, in analogy to the previous case, defines this relationship by periods derived from the analysis of the data recorded by the monitoring of buildings subjected to seismic actions, even repeated.
The traditionally adopted simplified formulation relates the elastic period to the height H of the building in the following form:

$$T = \alpha H^{\beta} \tag{6.4}$$

where α is a coefficient depending on the structural type.
It appears for the first time in ATC3-06 [110] assuming β = 0.75, while the coefficient α, calibrated from the periods measured during the earthquake of San Fernando in 1971, is set at 0.06 (if H is expressed in meters). The expression (6.4) can be obtained numerically through the Rayleigh method, as reported in Chopra [111], with the following assumptions: seismic forces distributed linearly along the height,

distribution of the masses of plane constant along the height, linear deformed along the height and finally base shear proportional to $1/T^{\gamma}$.
In these hypotheses, the period can be expressed as:

$$T = C_1 H^{1/(2-\gamma)} \quad (6.5)$$

If the base shear is proportional to $1/T^{2/3}$ it can be obtained:

$$T = C_1 H^{0.75} \quad (6.6)$$

formulation adopted by *Eurocode 8* and *NTC2008* with $\alpha = C_1 = 0.075$ for RC frame structures (C_1 depends on the structural system).
At first, the calibration of the α and β coefficients of the relation (6.4) is performed directly on an experimental database. However, it is evident how this approach assesses of the period reliant on the level of the seismic excitation. In this sense, in 1997, *Goel and Chopra* [112] collect an experimental database of thirty-seven RC buildings, designed seismically and of variable height between ten and one hundred meters. The buildings are subjected to eight earthquakes in Californian territories of different sizes. In particular, twenty-two buildings are subject to a base acceleration of less than 0.15g while the remaining ones are accelerated by more than 0.15g. Database analysis allows to make a series of considerations. Firstly, buildings subject to high acceleration are characterised, for the same height, by a longer period. This circumstance is due to the lower stiffness that characterises the structural elements subject to a greater seismic demand caused by the cracking. Furthermore, the comparison between the observational results and those deriving from the relation (6.6) show how, in general, the code formulation tends to underestimate the period of the building and in particular for heights greater than 50m. This aspect is further amplified for buildings subject to accelerations greater than 0.15g. After these considerations, the authors propose, as an alternative to (6.6), the following relations:

$$T = 0.53 H^{0.9} \quad (6.7)$$

for accelerations lower than 0.15g

$$T = 0.047 H^{0.9} \quad (6.8)$$

for accelerations greater than 0.15g.
Similarly, *Hong and Hwang* [113], on the basis of the results recorded on twenty-one RC buildings, seismically designed, built on the territory of Taiwan and subjected to four events of moderate size that do not violate the elastic behavior of the structure, propose as a period-height relation the following expression:

$$T = 0.029 H^{0.804} \quad (6.9)$$

Furthermore, the authors also highlight the non-secondary role of the dimensions in the plan on the evaluation of the period.

In the last decade, the calibration of the α and β coefficients of the relation (6.4) is performed with a numerical approach.

In *Crowley and Pinho* [114] a numerical analysis are performed on eleven RC structures located in different European countries; the presence of infill masonry is considered using a macro-model that represents the infill panels as diagonal. The buildings are analysed by modelling 2D representative frames; to take into account the three-dimensional behaviour a simplified procedure is adopted. 2D bare frames, fully infilled frames and infilled frames with openings are analysed. Finally, averaging the data of bare and infill frames, the authors suggest using the relationship (6.4) with α = 0.038 and β =1:

$$T = 0.038H \tag{6.10}$$

Ricci et. Al [115] carry out a parametric numerical analysis on structural models varying the number of storeys, the plan dimensions, the bay lengths, the infill characteristics and the presence of the openings. The simulated buildings are low-rise to mid-rise in height with regular plans and they are designed under gravity loads only. The numerical modelling of the infills is simulated using two distinct approaches taken from the literature in terms of uncracking and cracking infills. They state that the correlation of the period with the height and dimension of buildings in the evaluated direction does not largely influence the prediction. Regression analyses are done by the authors to obtain equations able to take into account all the analysed parameters:

$$T = 0.026H^{0.86} \tag{6.11}$$

All the formulations presented so far concern RC framed structures considered with and without infill masonry.

For precast structures, until DM2018 [3], the design approach aimed to isolate the cladding panels from the resistant structure, employing flexible connections, that had slots and gaps between structural and non-structural components. According to this approach, these elements were considered as non-loading bearing precast concrete panels (claddings) that were defined as “panels (structural or architectural) which resist only wind, (or seismic loads) and their weight”.

As already mentioned at the beginning of the paragraph, *Magliulo et al.* [108] investigate the influence of vertical cladding panels on the first vibration period of one-storey precast concrete buildings, with a rigid floor in its plane with some numerical models. At this purpose, a bare structural elastic model and an innovative elastic model with cladding system are implemented and a parametric study is performed. Panel-to-beam connections are designed to allow large drifts expected under dynamic actions and the vertical panels are modelled as vertical pendulums. To take into account such interaction, the authors propose as model of

the panel-to-structure connections two hinge connections at the bottom of each panel and two constraints that allow rotations but avoid the sliding of the panel concerning the beam, at the top of the panel.
Panels are modelled using shell elements.
They also realise a parametric study to evaluate the first period of 288 realistic buildings, designed according to EC8 and for different seismic zones. The considered variables are some geometrical characteristics of the structures: columns height, the width of the transversal bays and number of the bays in both the main directions of the building.
From the analysis of the first period values, authors list the following conclusions: first of all, the first vibration period is significantly influenced by the presence of the cladding system, presenting large variations concerning the case of bare buildings (reduction up to 80%).
Concern the simplified Eurocode 8 formula (6.6), it strongly underestimates the first periods of the analysed bare one-storey precast buildings and overestimates the first periods of the same buildings with cladding system. With reference to the analysed bare one-storey precast buildings, they propose a different formulation, similar to the current Eurocode 8 formula and easily implemented:

$$T = 0.026H^{0.86} \tag{6.12}$$

In the case of one-storey precast buildings with cladding system, authors obtain a relationship between the first period and a proposed function, that depends on a plan dimension of the building and its height. The new formula, proposed to evaluate the first vibrational period of one-storey precast buildings with cladding system, is:

$$T = 0.00088H^{3/2}{L_x}^{1/2} \tag{6.13}$$

where L_x represents the long side length of the building in meters and H is its total height in meters. This formula is valid for vertical panels with pendulum isostatic solution and with precast structures with rigid diaphragm.
Finally, the formula described in the NTC2018 to calculate the period is also reported:

$$T = 2\sqrt{d} \tag{6.14}$$

where d is the lateral elastic displacement of the highest point of the building, expressed in meters, due to the combination of loads applied in the horizontal direction.

In Table 6.1 all formulations previously described for the calculation of the elastic period are reported.

Author	Year	Formula		Results derives from
FORMULA USCGS	1949	$T = 0.11\frac{H}{\sqrt{B}}$		Experimental test
Goel and Chopra	1997	$T = 0.53H^{0.9}$	for $a_g < 0.15$	Experimental test
		$T = 0.047H^{0.9}$	for $a_g > 0.15$	
Hong and Hwang	2000	$T = 0.029H^{0.804}$		Experimental test
Crowley and Pinho	2006	$T = 0.038H$		Numerical test
Ricci et al.	2011	$T = 0.026H^{0.86}$		Numerical test
Magliulo et al.	2014	$T = 0.026H^{0.86}$	bare frame	Numerical test
		$T = 0.00088H^{3/2}{L_x}^{1/2}$	frame with cladding panel	
NTC 2008 EUROCODE 8	2008	$T = 0.075H^{0.75}$		Code
NTC 2018	2018	$T = 2\sqrt{d}$		Code

Table 6.1 Formulas previously described to calculate the fundamental period of a structure.

6.3 Preliminary case study

The variability of the first vibration period of the precast structures considering the different types of connections of the panels defined in the technical summary documents drafted by Joint Research Center [25] reported in paragraph 6.1 is investigated and compared with the simplified formulas for the calculation of the period provided by the literature. First of all, the connection types of the panels are applied to a small case, not representative of the enormous planimetric dimensions characterising precast frame structures, but useful to check the assumed modelling hypotheses.

From the analysis of the technical documents of the preliminary case study, necessary information for a correct definition of the numerical models as regards the main structural elements, containing details on the connections roofing tiles/beams and column-foundation are extrapolated.

All the characteristics of the structure taken into consideration are shown below.

This structure is a RC one-storey precast structure made in 1985 with 9.40x9.90 m square shaped and a height under Y-beam of 5.30 m, consisting of columns with forks and prestressed Y-beams and tiles.

The concrete Class is C40/50 for columns and beams with elastic modulus equal to 32111 MPa; the steel Class is FeB38K. All the four columns have a square cross-section with side width of 60 cm and they are reinforced with 4Ø14 mm longitudinal bars and stirrups of Ø6/25cm.
The Y-beams/columns with fork connections have 4 Ø16 pins connection described only in the technical report. The drawing and the technical reports do not describe the type of connections between the roof tiles and the Y-shaped beams, probably of friction type. The precast structure has a socket foundation with 15 cm of concrete slab with an electro-welded net (industrial floor).
The height considered to calculate the period with analytical formulas is the medium value of the intrados of the roof.
Some drawings concerning the project are reported in Figures 6.22- 6.24.

Type of precast structures	One-storey RC PRECAST FRAME STRUCTURE
Year of construction:	1985
Plan dimensions:	9.40x9.90m
Height under main beam:	5.30m
Dimension of columns:	60x60cm
Type of main beam:	Prestressed Y-beam
Type of roof:	Tiles
Type of connection beam-column:	Double pin
Concrete Class:	C40/50
Steel Class:	FeB38k

Table 6.2 Main features of the preliminary case study.

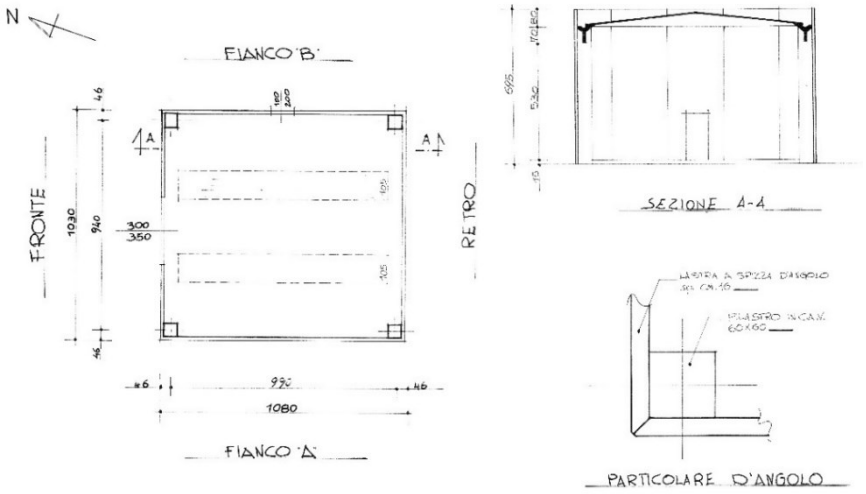

Figure 6.22 Plan and section of the preliminary case study.

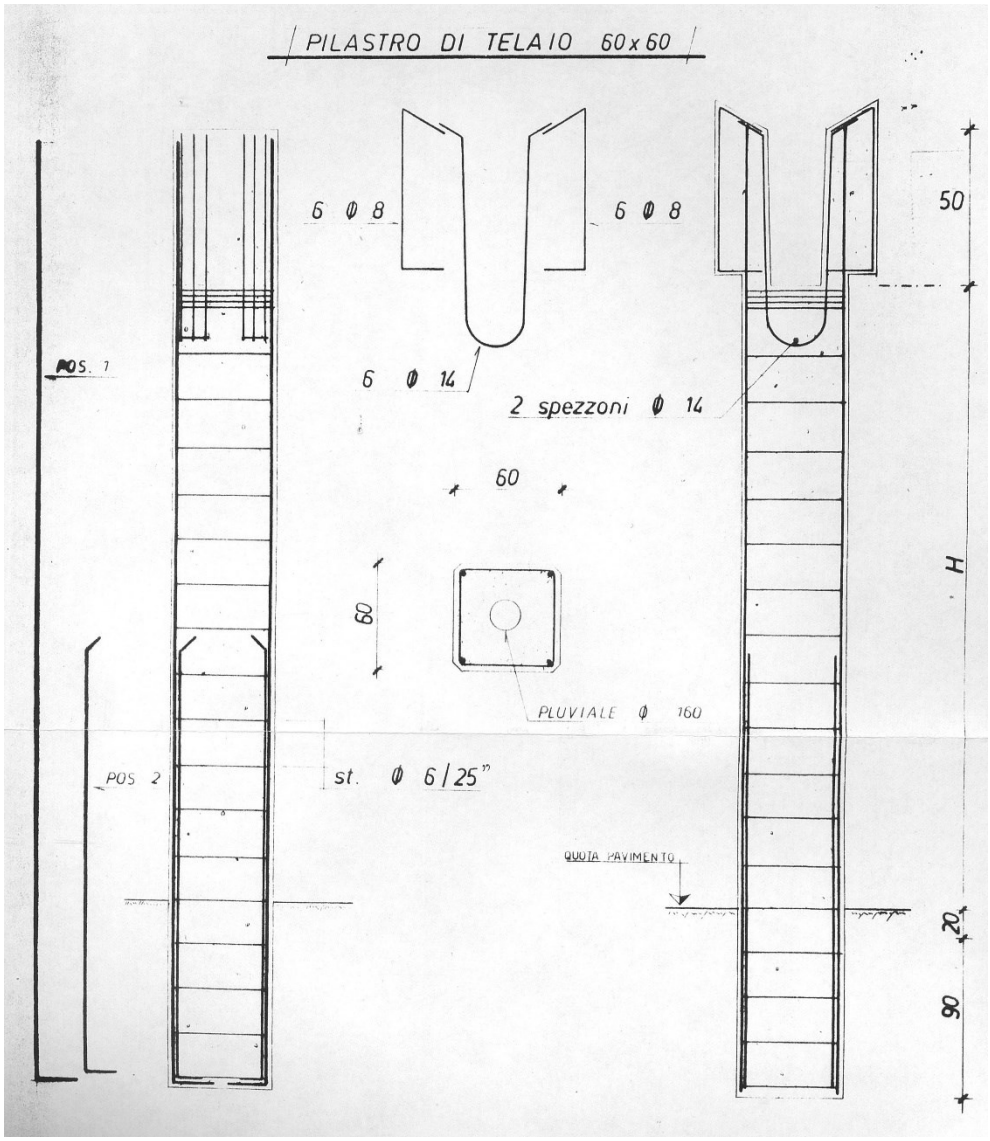

Figure 6.23 Details concerning reinforcement of columns of the preliminary case study.

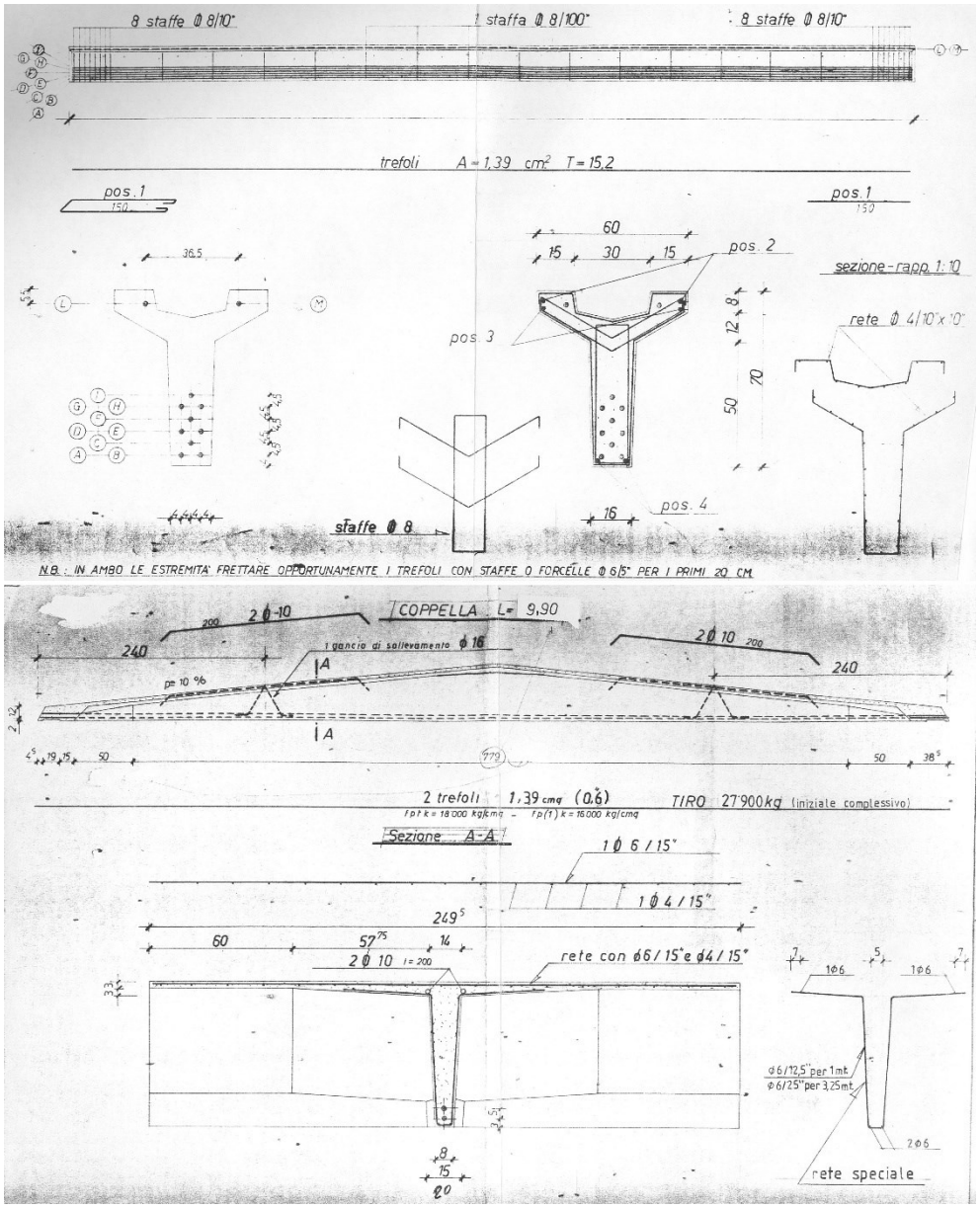

Figure 6.24 Details concerning reinforcement of prestressed beams and tiles of the preliminary case study.

6.3.1 Numerical Models

Using a commercial calculation code, three-dimensional models are defined.
The elements used for the spatial discretization are of a single-dimensional "beam" type with two nodes.
The main structural elements, such as columns, are modelled as "beam" and they are made to act both in the elastic-linear and plastic field.
The structure is supposedly fixed at the base at the level of the industrial floor; heights are defined at the intrados of the main beam.
The main Y-shaped beams are linked to the columns using a cylindrical hinge constraint, considering the beam-column connection described in the technical report. The double slope roof tiles are connected to the main beams using a spherical hinge, assumed that there is no mechanical connection between elements. In the numerical model, only the tiles are modelled, the roof is added only as a load, made up of Eternit sheets screwed to the wooden strips embedded in the roofing panes.
The seismic weights are obtained considering all structural and non-structural elements (panels) as well as live loads on the structures.
In the bare structure, the panel weights are inserted as seismic masses in X-Y directions.
Vertical and Horizontal panels are placed along the two major sides of the building with an equivalent concrete thickness of 15 cm, leading to a weight of 3.0 kN/mq.
Cladding panels are modelled taking into account all details of the fastening devices described in the cases of existing, isostatic and integrated solutions and in the numerical model these panels are represented with beam, wall and shell elements (the mesh discretization is chosen according to the thickness of the panel) to analyse the effect of several types of finite elements. In case of fixed connections, a linking made with infinite stiffness are considered according to Biondini et al. [116]. To simulate frictions, some springs are inserted with different stiffness. Figure 6.25 reports the models analysed; for now, an infinite stiffness is set for out of the plane mechanism to evaluate the influence in the plane of the different types of connection of the panels as reported in the structural schemes of paragraph 6.1.
During analysis, the height and the stiffness of roof (rigid or deformable roof) are changed for all cases analysed (Models with the reduced height of one meter are also considered). Similar studies based on parametric linear analysis with different levels of interaction among frame, panels and diaphragm system are reported in Dal Lago et al. [117].

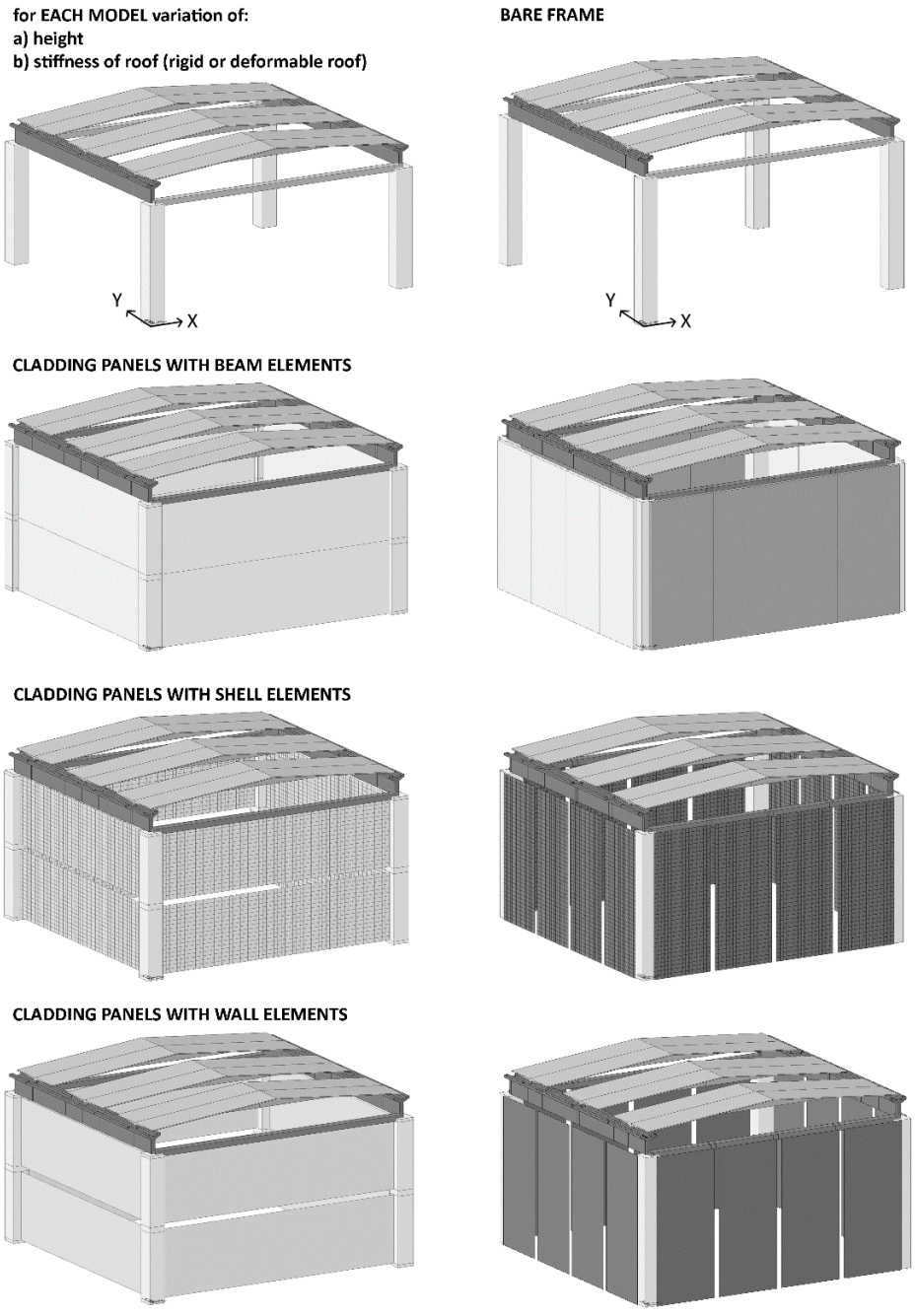

Figure 6.25 Numerical models concerning bare frame and cladding panels.

6.3.2 Results

First periods for bare frame and for a precast structure with all types of cladding panels realised with the different elements are shown in Tables 6.3-6.5.

		BEAM					
		DEFORMABLE ROOF			RIGID ROOF		
		Dir.	h=5.00m	h=6.00m	Dir.	h=5.00m	h=6.00m
			[sec]	[sec]		[sec]	[sec]
BARE FRAME		X	0.2445	0.3305	Y	0.2390	0.3278
EXISTING SOLUTION	HORIZONTAL PANEL	X	0.1429	0.1510	X	0.1069	0.1154
	VERTICAL PANEL	Y	0.2429	0.3244	Y	0.2428	0.3244
INTEGRATED SOLUTION	HORIZONTAL PANEL	X	0.1425	0.1500	X	0.1049	0.1134
	VERTICAL PANEL	X	0.2190	0.2776	Y	0.2190	0.2776
ISOSTATIC SOLUTION	HORIZONTAL PANEL HANGED SOLUTION	X	0.2152	0.2966	Y	0.2035	0.2895
	HORIZONTAL PANEL SEATED SOLUTION	X	0.1943	0.2551	Y	0.1769	0.2448
	VERTICAL PANEL CANTILEVER SOLUTION	Y	0.2290	0.2971	Y	0.2289	0.2971
	VERTICAL PANEL PENDULUM SOLUTION	Y	0.2874	0.3814	X	0.2874	0.3814
	VERTICAL PANEL ROCKING SOLUTION	Y	0.2191	0.2778	Y	0.2288	0.2778

Table 6.3 First periods of models with cladding panels realised with beam elements.

		SHELL					
		DEFORMABLE ROOF			RIGID ROOF		
		Dir.	h=5.00m	h=6.00m	Dir.	h=5.00m	h=6.00m
			[sec]	[sec]		[sec]	[sec]
BARE FRAME		X	0.2445	0.3305	X	0.2390	0.3278
EXISTING SOLUTION	HORIZONTAL PANEL	Y	0.1405	0.1461	X	0.0948	0.1010
	VERTICAL PANEL	Y	0.1964	0.2545	Y	0.194	0.2544
INTEGRATED SOLUTION	HORIZONTAL PANEL	Y	0.1402	0.1455	X	0.0942	0.1004
	VERTICAL PANEL	X	0.1752	0.2202	X	0.1752	0.2202
ISOSTATIC SOLUTION	HORIZONTAL PANEL HANGED SOLUTION	Y	0.1578	0.1834	X	0.1284	0.1622
	HORIZONTAL PANEL SEATED SOLUTION	X	0.1576	0.1689	X	0.1221	0.1357
	VERTICAL PANEL CANTILEVER SOLUTION	Y	0.1849	0.2382	Y	0.1848	0.2382
	VERTICAL PANEL PENDULUM SOLUTION	X	0.2605	0.3299	X	0.2605	0.3299
	VERTICAL PANEL PENDULUM SOLUTION + PANEL TO PANEL LINK	X	0.2201	0.2776	X	0.2201	0.2776
	VERTICAL PANEL PENDULUM SOLUTION + PANEL TO COLUMN LINK	X	0.1824	0.2254	X	0.1823	0.2253
	VERTICAL PANEL ROCKING SOLUTION	X	0.1804	0.2325	X	0.1803	0.2325

Table 6.4 First periods of models with cladding panels realised with shell elements.

		WALL					
		DEFORMABLE ROOF			RIGID ROOF		
		Dir.	h=5.00m	h=6.00m	Dir.	h=5.00m	h=6.00m
			[sec]	[sec]		[sec]	[sec]
BARE FRAME		X	0.2445	0.3305	X	0.239	0.3278
EXISTING SOLUTION	HORIZONTAL PANEL	X	0.1412	0.1492	X	0.1026	0.1119
	VERTICAL PANEL	X	0.2976	0.3526	X	0.2976	0.3525
INTEGRATED SOLUTION	HORIZONTAL PANEL	X	0.1407	0.1482	X	0.1015	0.1099
	VERTICAL PANEL	X	0.2287	0.289	X	0.2287	0.289
ISOSTATIC SOLUTION	HORIZONTAL PANEL HANGED SOLUTION	Y	0.2141	0.296	Y	0.2023	0.2894
	HORIZONTAL PANEL SEATED SOLUTION	X	0.1955	0.258	X	0.1784	0.2485
	VERTICAL PANEL CANTILEVER SOLUTION	Y	0.2359	0.3039	Y	0.2359	0.3039
	VERTICAL PANEL PENDULUM SOLUTION	X	0.2867	0.3794	X	0.2867	0.3794
	VERTICAL PANEL ROCKING SOLUTION	X	0.2288	0.2892	X	0.2288	0.2892

Table 6.5 First periods of models with cladding panels realised with wall elements.

As observed from the results, first periods of models are not comparable to those of industrial precast structure that, according to the extensive parametric study provided by Magliulo et al. [108] on single-storey precast structures designed with the current Italian code in low-to-high seismic zones, the bare precast structures usually exhibit an elastic fundamental period ranging from 0.54sec to 1.45sec, while infilled precast structures range from 0.09sec to 0.40sec, due to the presence of cladding panels.

This preliminary case needs only to define more precisely the various types of connection and how to model them most appropriately.

The main conclusions are listed below:

- No first period is similar to the formula of Magliulo et al., based on a study of the precast structure with cladding panels (in this formula the length of the structure plays a fundamental role);
- In all considered cases, there aren't any huge differences in first periods between rigid and deformable roofs due to the small dimensions of the structure in the plan;
- First periods of the existing solution vertical panels and bare frame are very similar each other especially with beam elements, in accordance with the practice of considering only seismic masses of panels in the numerical model of existing precast buildings;
- Horizontal panels give greater stiffness to the structure than the vertical ones as underlined by the low periods reported, due to the fact that the panels are hooked to the columns of the structure and not fixed to the upper edge beam;
- Regarding the isostatic solution of the horizontal panels, the seated solution leads to first periods lower than the hanged solution case;

- The use of shell elements over the others (beam and wall) lead to lower periods for each type of connection;
- Vertical panel existing solution with wall and deformable roof has an identical value to the period calculated with NTC2018 formula;
- Horizontal panel existing solution has similar first periods to horizontal panel integrated solution;
- Vertical panel pendulum isostatic solution report greater periods than those realized with the bare frame structure, except for the case with shell elements that has a period equal to the model with no cladding panels. The problem is probably due to the particular case considered. Indeed, in the main case presented in the next paragraph, the increase of stiffness deriving from the modelling of cladding panels lead to a decrease in the period even for isostatic pendulum solution realised with the same assumption of preliminary case study.

Figures 6.28-6.66 show a comparison between the periods concerning the same type of solution of cladding panels realised with different elements (beam, shell and wall) evaluating the overall increase of stiffness of the structure and a comparison between the different types of solution of cladding panels represented (existing solution vertical and horizontal panels, integrated solution with vertical and horizontal panels etc.) with the same elements in the numerical model, always evaluating the overall increase of stiffness of the structure.

The modal shapes corresponding to the first period for the cases analysed with a rigid roof with a height structure equal to 6m are also reported.

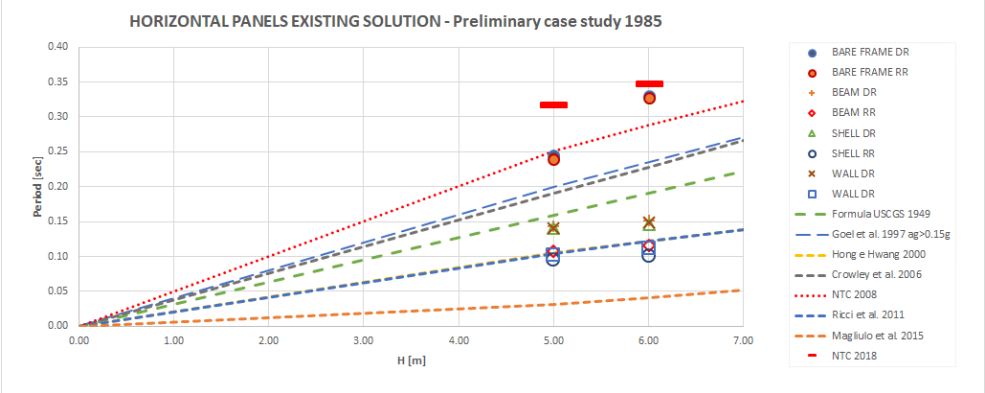

Figure 6.26 First periods of a preliminary case study with horizontal panels existing solution.

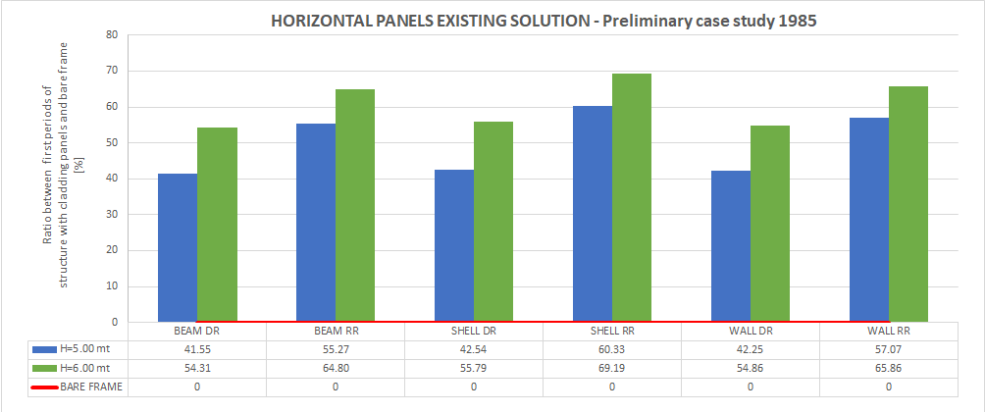

	BEAM DR	BEAM RR	SHELL DR	SHELL RR	WALL DR	WALL RR
H=5.00 mt	41.55	55.27	42.54	60.33	42.25	57.07
H=6.00 mt	54.31	64.80	55.79	69.19	54.86	65.86
BARE FRAME	0	0	0	0	0	0

Figure 6.27 Ratio [%] between first periods of the structure with horizontal panels existing solution and bare frame.

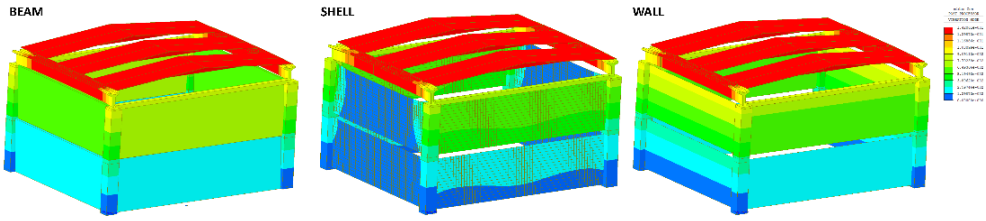

Figure 6.28 First periods mode shapes of horizontal panels existing solution with rigid roof.

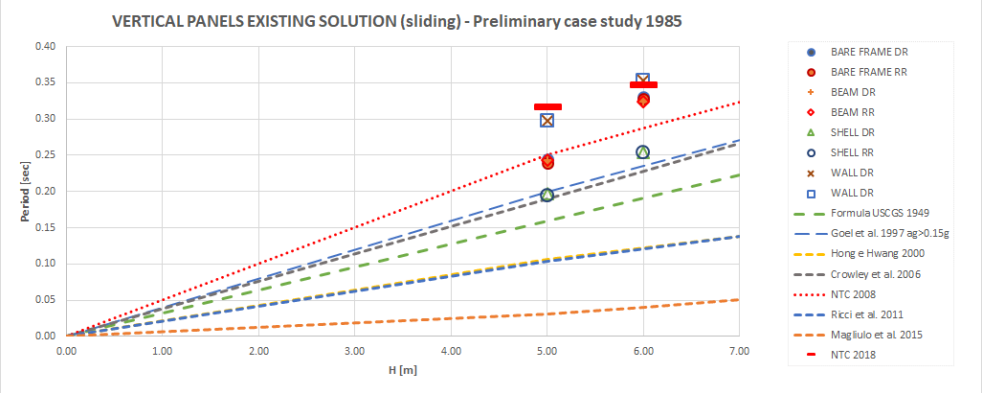

Figure 6.29 First periods of a preliminary case study with vertical panels existing solution.

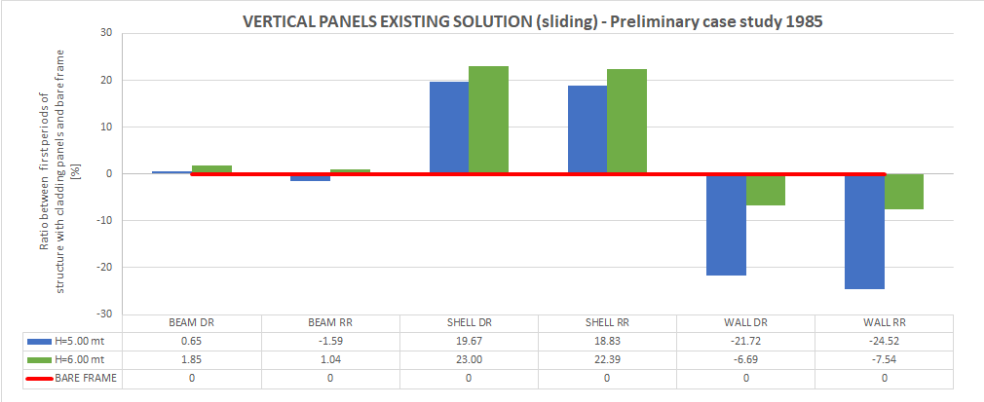

	BEAM DR	BEAM RR	SHELL DR	SHELL RR	WALL DR	WALL RR
H=5.00 mt	0.65	-1.59	19.67	18.83	-21.72	-24.52
H=6.00 mt	1.85	1.04	23.00	22.39	-6.69	-7.54
BARE FRAME	0	0	0	0	0	0

Figure 6.30 Ratio [%] between first periods of the structure with vertical panels existing solution and bare frame.

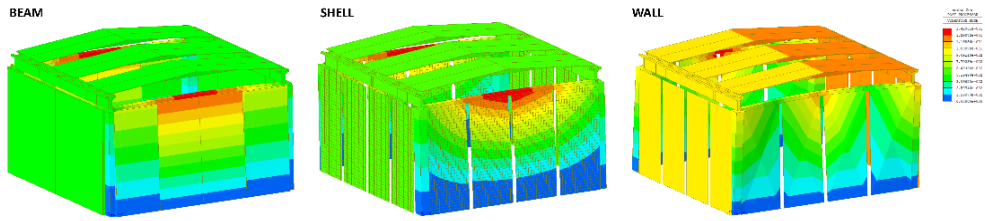

Figure 6.31 First periods mode shapes of vertical panels existing solution with rigid roof.

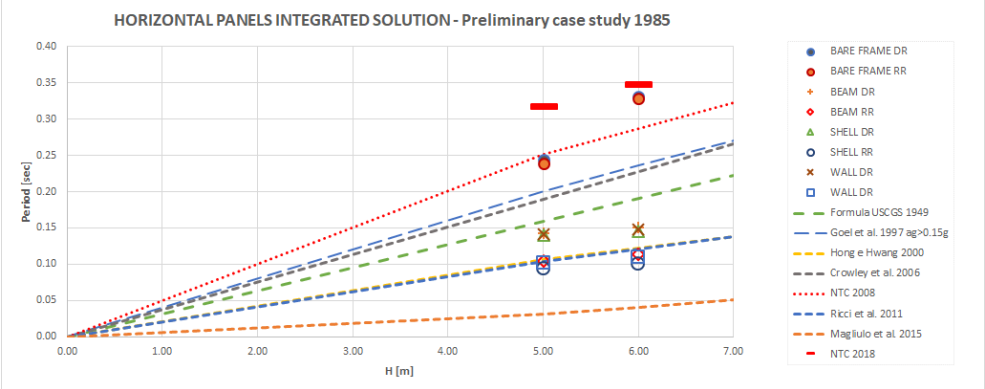

Figure 6.32 First periods of a preliminary case study with horizontal panels integrated solution.

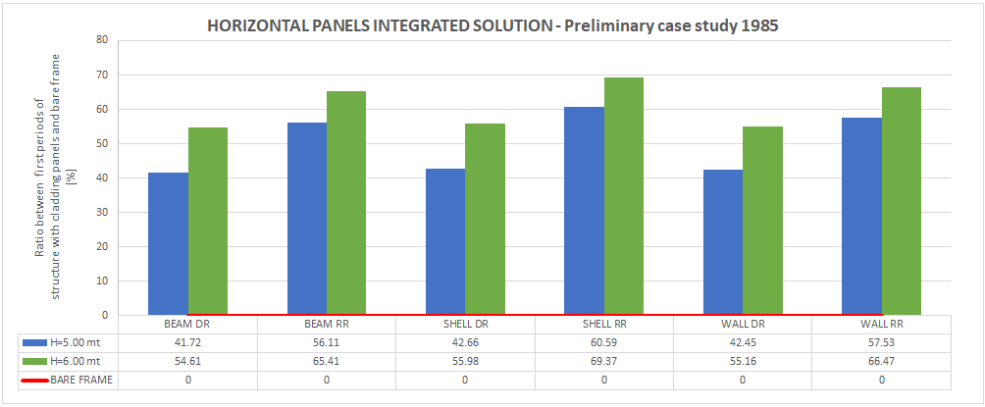

	BEAM DR	BEAM RR	SHELL DR	SHELL RR	WALL DR	WALL RR
H=5.00 mt	41.72	56.11	42.66	60.59	42.45	57.53
H=6.00 mt	54.61	65.41	55.98	69.37	55.16	66.47
BARE FRAME	0	0	0	0	0	0

Figure 6.33 Ratio [%] between first periods of the structure with horizontal panels integrated solution and bare frame.

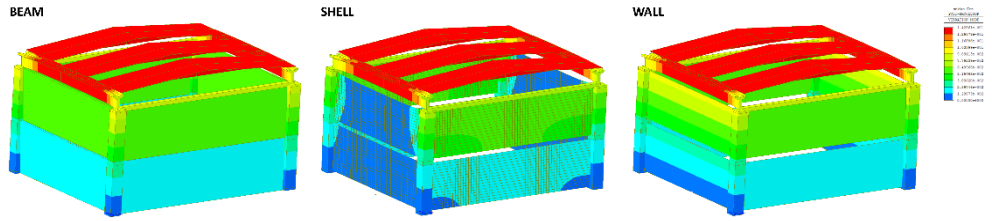

Figure 6.34 First periods mode shapes of horizontal panels integrated solution with rigid roof.

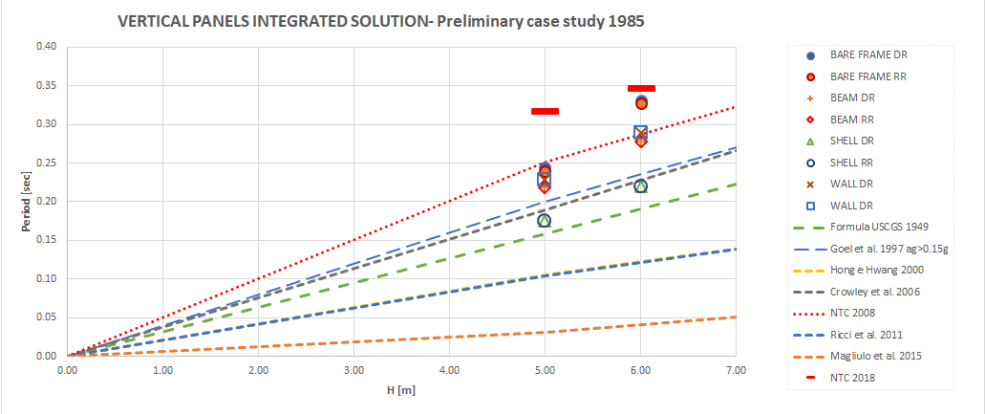

Figure 6.35 First periods of a preliminary case study with vertical panels integrated solution.

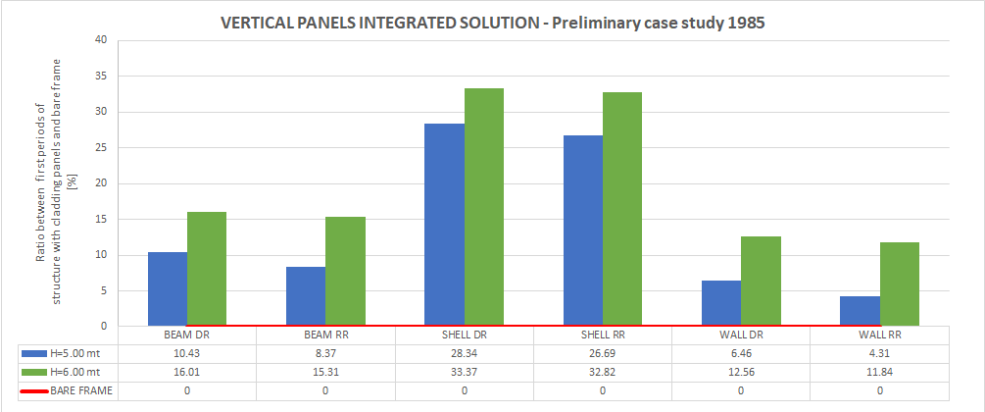

Figure 6.36 Ratio [%] between first periods of the structure with vertical panels integrated solution and bare frame.

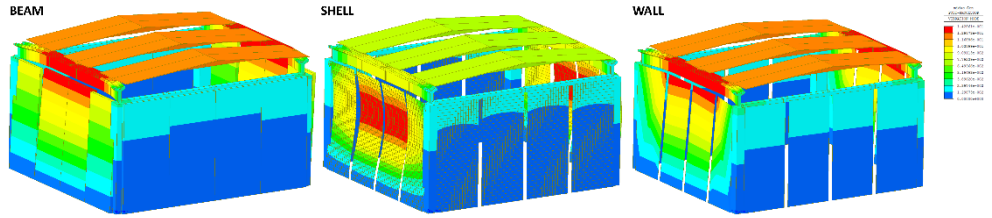

Figure 6.37 First periods mode shapes of vertical panels integrated solution with rigid roof.

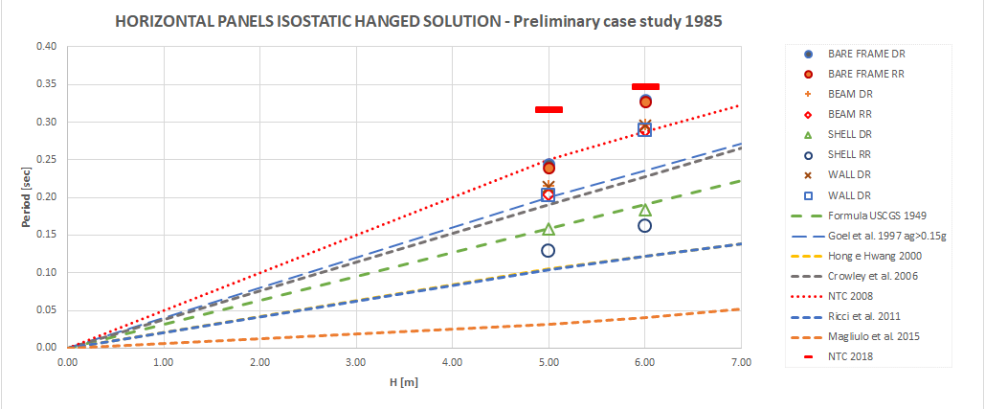

Figure 6.38 First periods of a preliminary case study with horizontal panels isostatic hanged solution.

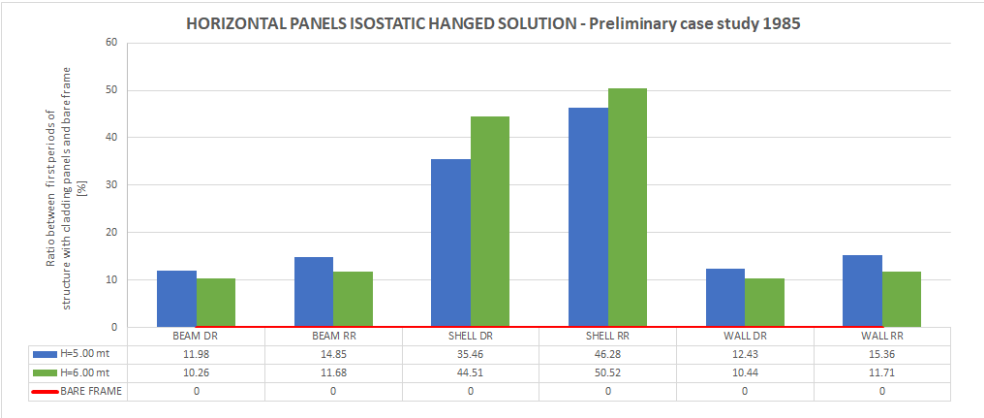

Figure 6.39 Ratio [%] between first periods of the structure with horizontal panels isostatic hanged solution and bare frame.

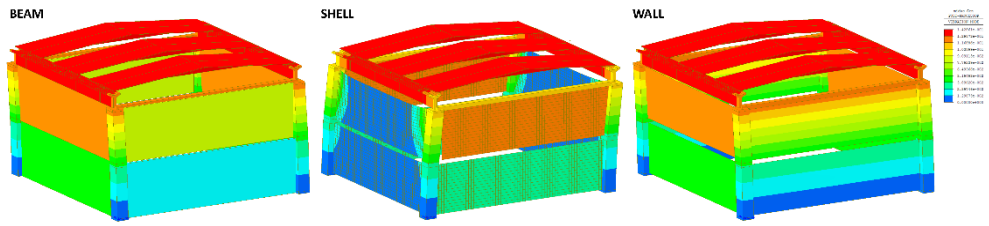

Figure 6.40 First periods mode shapes of horizontal panels isostatic hanged solution with rigid roof.

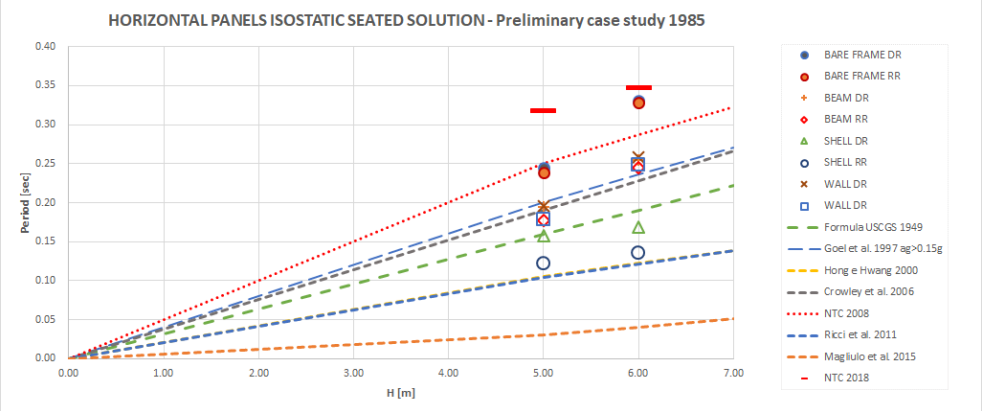

Figure 6.41 First periods of a preliminary case study with a horizontal panels isostatic seated solution.

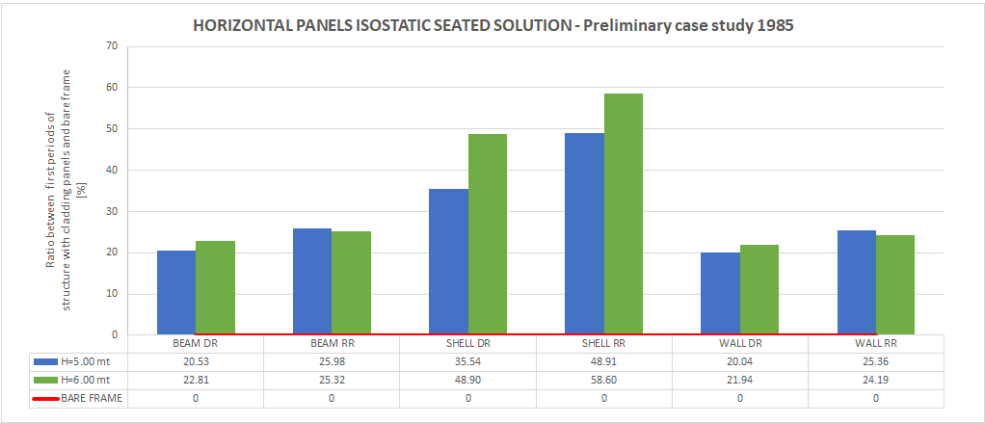

	BEAM DR	BEAM RR	SHELL DR	SHELL RR	WALL DR	WALL RR
H=5.00 mt	20.53	25.98	35.54	48.91	20.04	25.36
H=6.00 mt	22.81	25.32	48.90	58.60	21.94	24.19
BARE FRAME	0	0	0	0	0	0

Figure 6.42 Ratio [%] between first periods of the structure with a horizontal panels isostatic seated solution and bare frame.

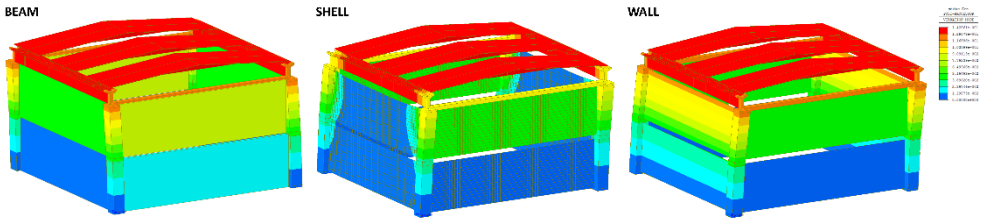

Figure 6.43 First periods mode shapes of horizontal panels isostatic seated solution with rigid roof.

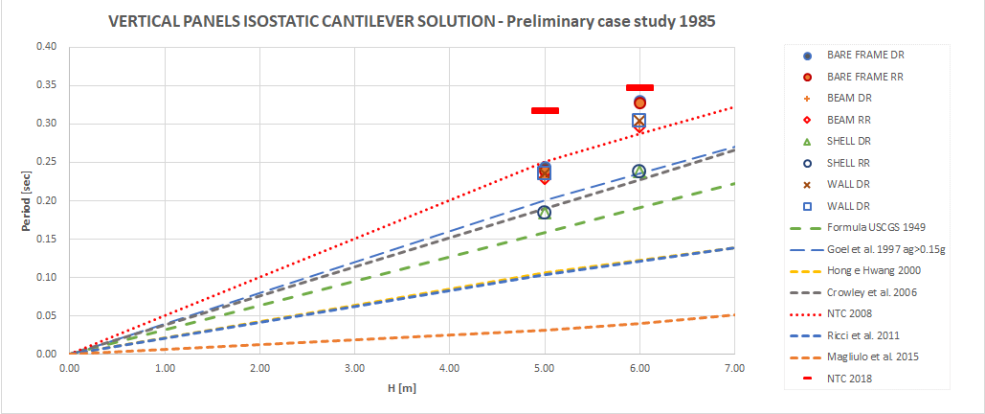

Figure 6.44 First periods of a preliminary case study with vertical panels isostatic cantilever solution.

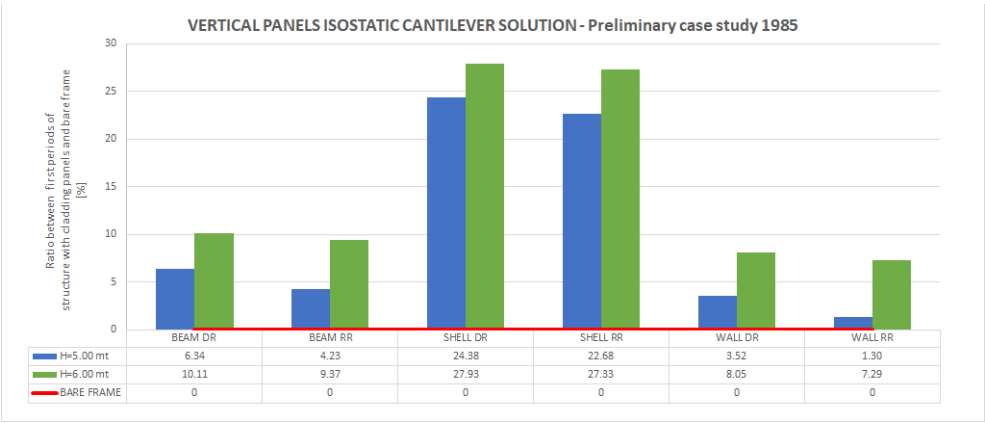

	BEAM DR	BEAM RR	SHELL DR	SHELL RR	WALL DR	WALL RR
H=5.00 mt	6.34	4.23	24.38	22.68	3.52	1.30
H=6.00 mt	10.11	9.37	27.93	27.33	8.05	7.29
BARE FRAME	0	0	0	0	0	0

Figure 6.45 Ratio [%] between first periods of the structure with vertical panels isostatic cantilever solution and bare frame.

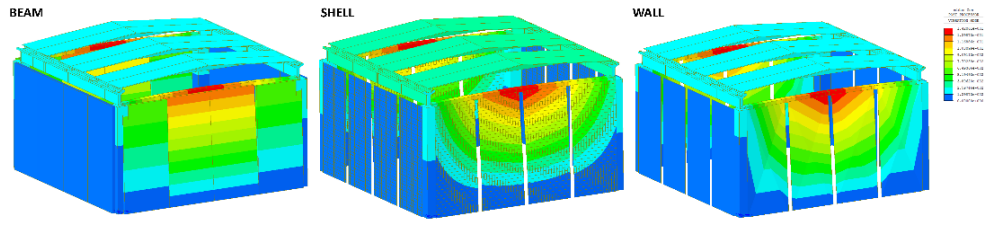

Figure 6.46 First periods mode shapes of vertical panels isostatic cantilever solution with rigid roof.

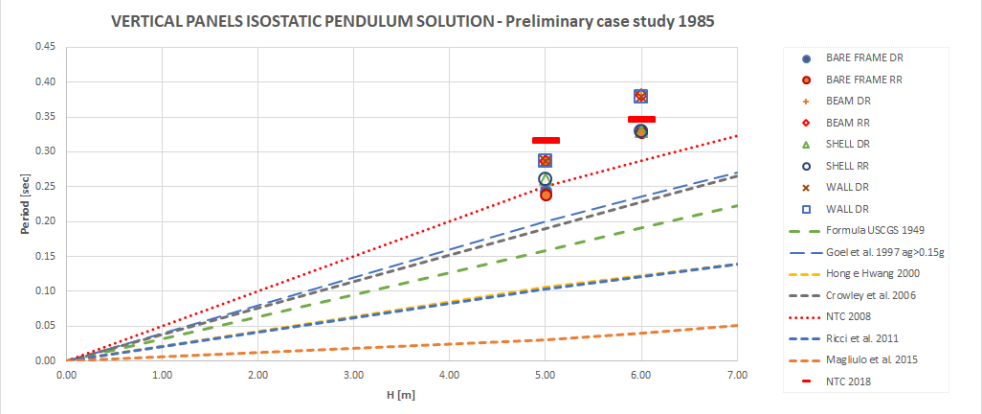

Figure 6.47 First periods of a preliminary case study with vertical panels isostatic pendulum solution.

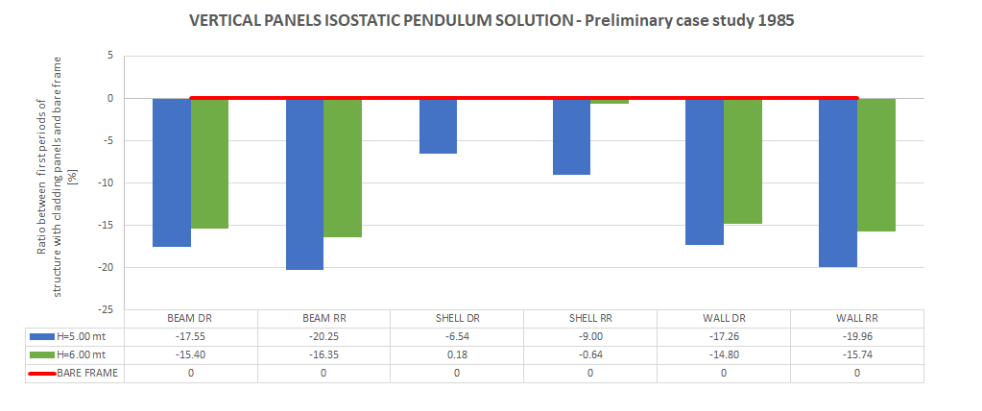

	BEAM DR	BEAM RR	SHELL DR	SHELL RR	WALL DR	WALL RR
H=5.00 mt	-17.55	-20.25	-6.54	-9.00	-17.26	-19.96
H=6.00 mt	-15.40	-16.35	0.18	-0.64	-14.80	-15.74
BARE FRAME	0	0	0	0	0	0

Figure 6.48 Ratio [%] between first periods of the structure with vertical panels isostatic pendulum solution and bare frame.

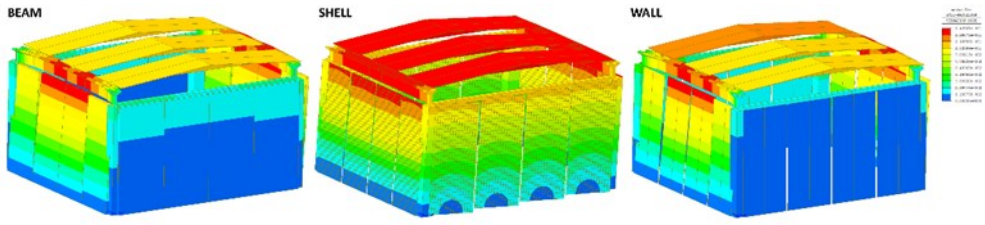

Figure 6.49 First periods mode shapes of vertical panels isostatic pendulum solution with rigid roof.

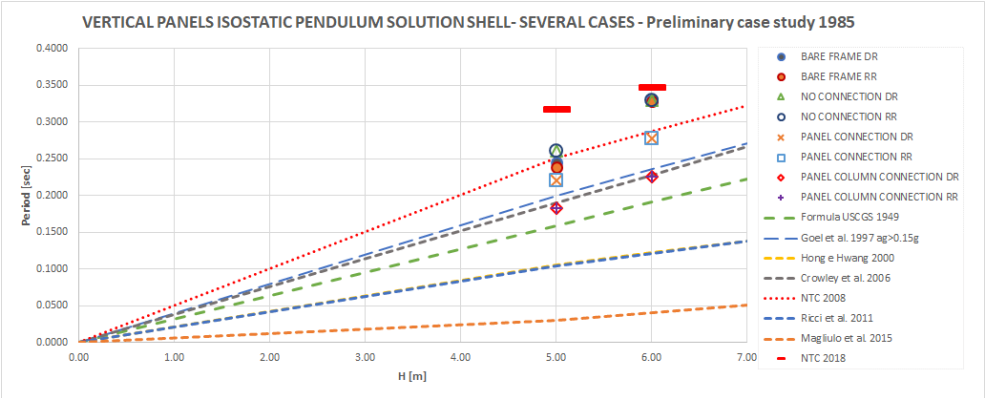

Figure 6.50 First periods of a preliminary case study with vertical panels isostatic pendulum solution SHELL elements – several cases considering or not the interaction between panels and panels-columns.

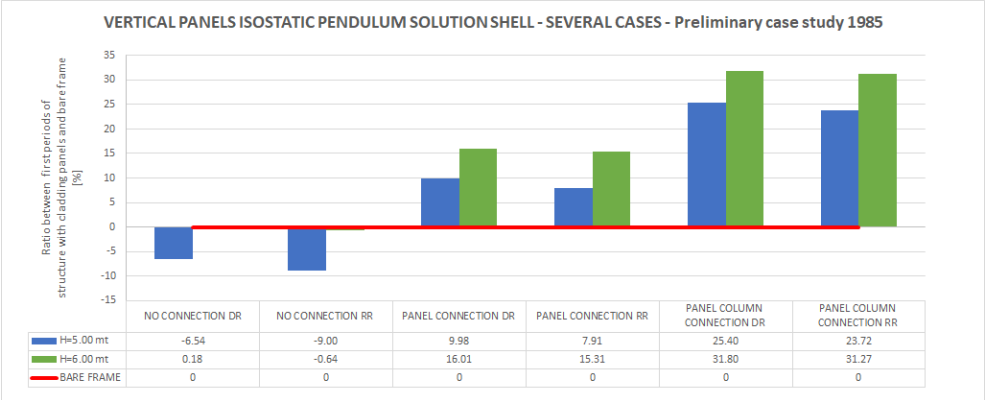

	NO CONNECTION DR	NO CONNECTION RR	PANEL CONNECTION DR	PANEL CONNECTION RR	PANEL COLUMN CONNECTION DR	PANEL COLUMN CONNECTION RR
H=5.00 mt	-6.54	-9.00	9.98	7.91	25.40	23.72
H=6.00 mt	0.18	-0.64	16.01	15.31	31.80	31.27
BARE FRAME	0	0	0	0	0	0

Figure 6.51 Ratio [%] between first periods of the structure with vertical panels isostatic pendulum solution SHELL elements (several cases considering or not the interaction between panels and panels-columns) and bare frame.

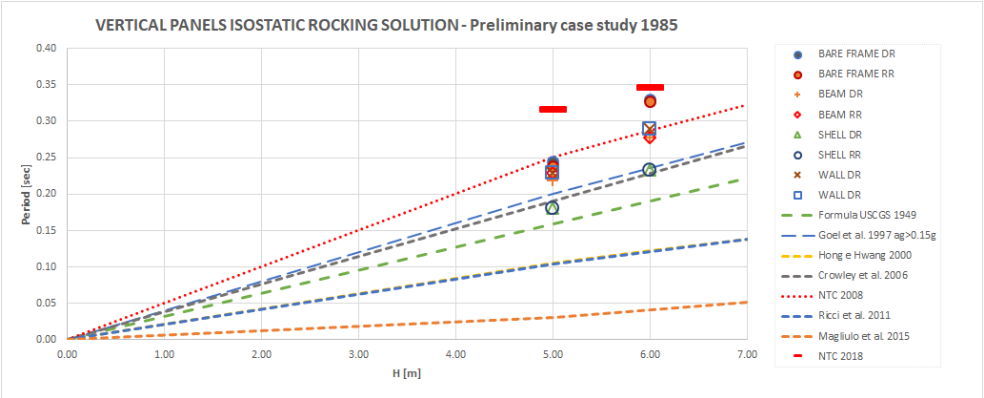

Figure 6.52 First periods of a preliminary case study with vertical panels isostatic rocking solution.

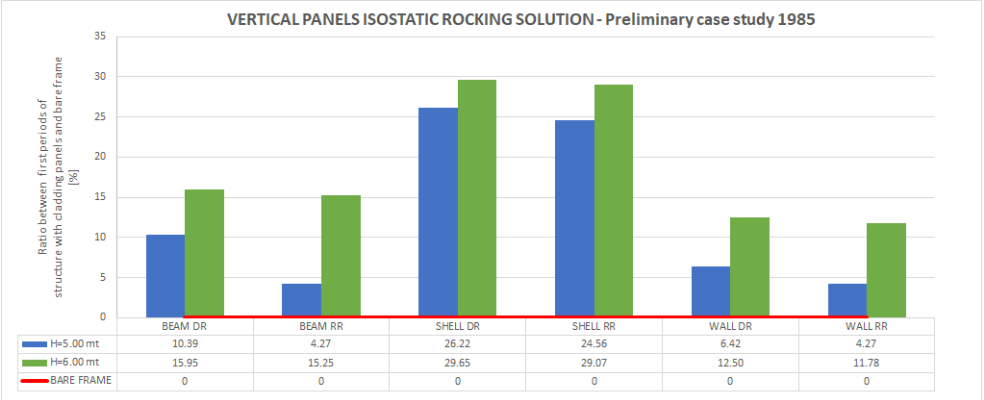

	BEAM DR	BEAM RR	SHELL DR	SHELL RR	WALL DR	WALL RR
H=5.00 mt	10.39	4.27	26.22	24.56	6.42	4.27
H=6.00 mt	15.95	15.25	29.65	29.07	12.50	11.78
BARE FRAME	0	0	0	0	0	0

Figure 6.53 Ratio [%] between first periods of the structure with vertical panels isostatic rocking solution and bare frame.

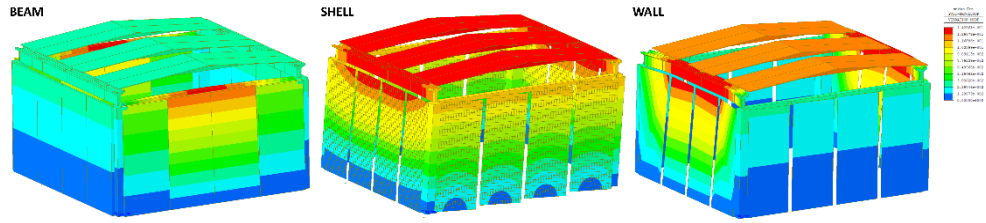

Figure 6.54 First periods mode shapes of vertical panels isostatic rocking solution with rigid roof.

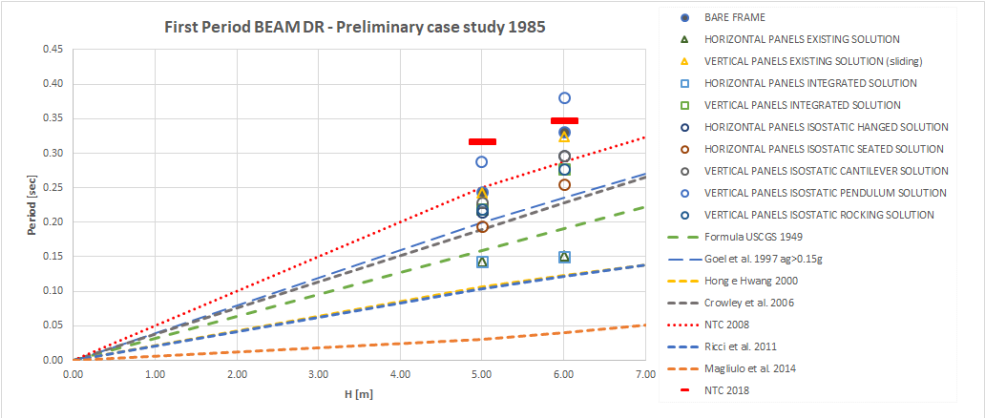

Figure 6.55 First periods of a preliminary case study with panels realised with BEAM - Deformable Roof.

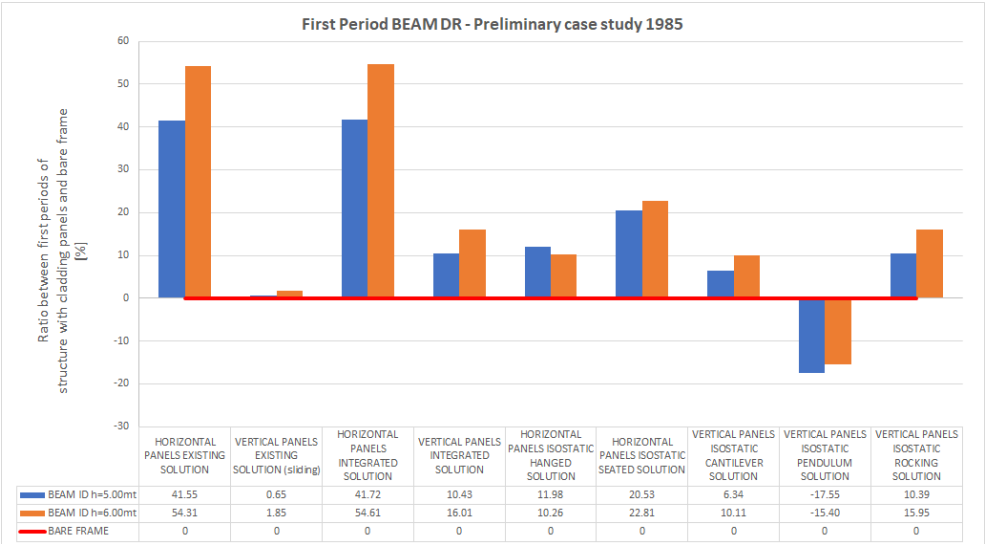

	HORIZONTAL PANELS EXISTING SOLUTION	VERTICAL PANELS EXISTING SOLUTION (sliding)	HORIZONTAL PANELS INTEGRATED SOLUTION	VERTICAL PANELS INTEGRATED SOLUTION	HORIZONTAL PANELS ISOSTATIC HANGED SOLUTION	HORIZONTAL PANELS ISOSTATIC SEATED SOLUTION	VERTICAL PANELS ISOSTATIC CANTILEVER SOLUTION	VERTICAL PANELS ISOSTATIC PENDULUM SOLUTION	VERTICAL PANELS ISOSTATIC ROCKING SOLUTION
BEAM ID h=5.00mt	41.55	0.65	41.72	10.43	11.98	20.53	6.34	-17.55	10.39
BEAM ID h=6.00mt	54.31	1.85	54.61	16.01	10.26	22.81	10.11	-15.40	15.95
BARE FRAME	0	0	0	0	0	0	0	0	0

Figure 6.56 Ratio [%] between first periods of the structure with cladding panels realised with BEAM and bare frame – Deformable Roof.

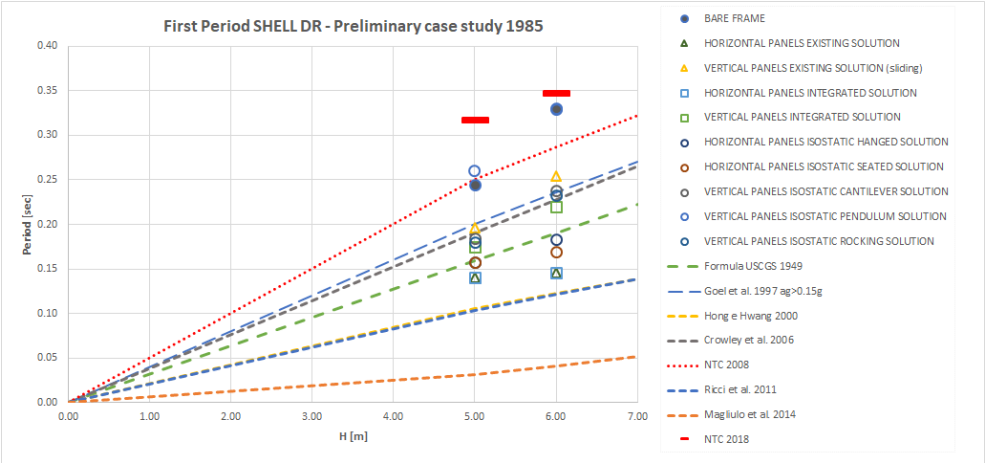

Figure 6.57 First periods of a preliminary case study with panels realised with SHELL - Deformable Roof.

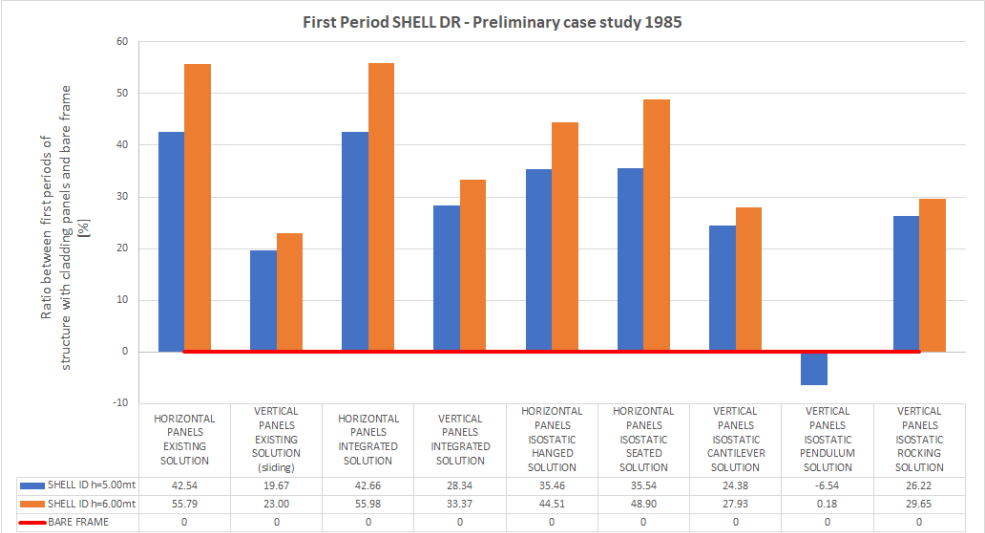

	HORIZONTAL PANELS EXISTING SOLUTION	VERTICAL PANELS EXISTING SOLUTION (sliding)	HORIZONTAL PANELS INTEGRATED SOLUTION	VERTICAL PANELS INTEGRATED SOLUTION	HORIZONTAL PANELS ISOSTATIC HANGED SOLUTION	HORIZONTAL PANELS ISOSTATIC SEATED SOLUTION	VERTICAL PANELS ISOSTATIC CANTILEVER SOLUTION	VERTICAL PANELS ISOSTATIC PENDULUM SOLUTION	VERTICAL PANELS ISOSTATIC ROCKING SOLUTION
SHELL ID h=5.00mt	42.54	19.67	42.66	28.34	35.46	35.54	24.38	-6.54	26.22
SHELL ID h=6.00mt	55.79	23.00	55.98	33.37	44.51	48.90	27.93	0.18	29.65
BARE FRAME	0	0	0	0	0	0	0	0	0

Figure 6.58 Ratio [%] between first periods of the structure with cladding panels realised with SHELL and bare frame – Deformable Roof.

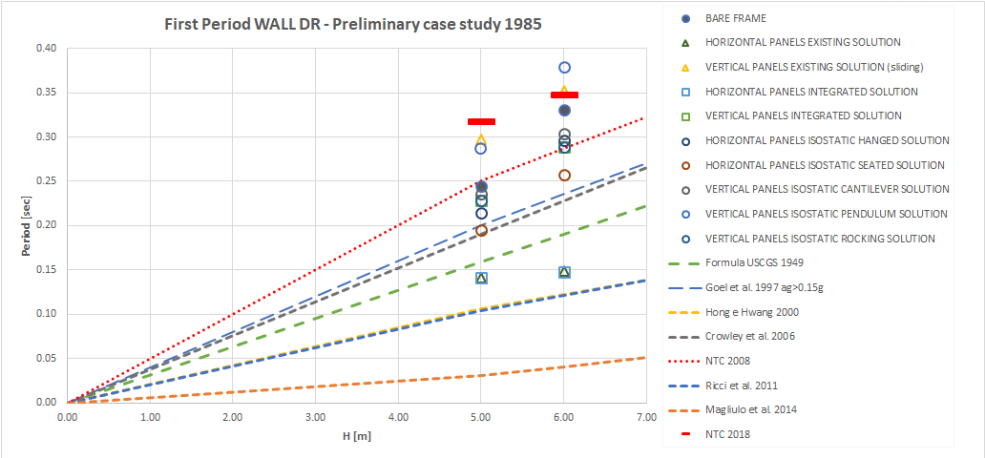

Figure 6.59 First periods of a preliminary case study with panels realised with WALL - Deformable Roof.

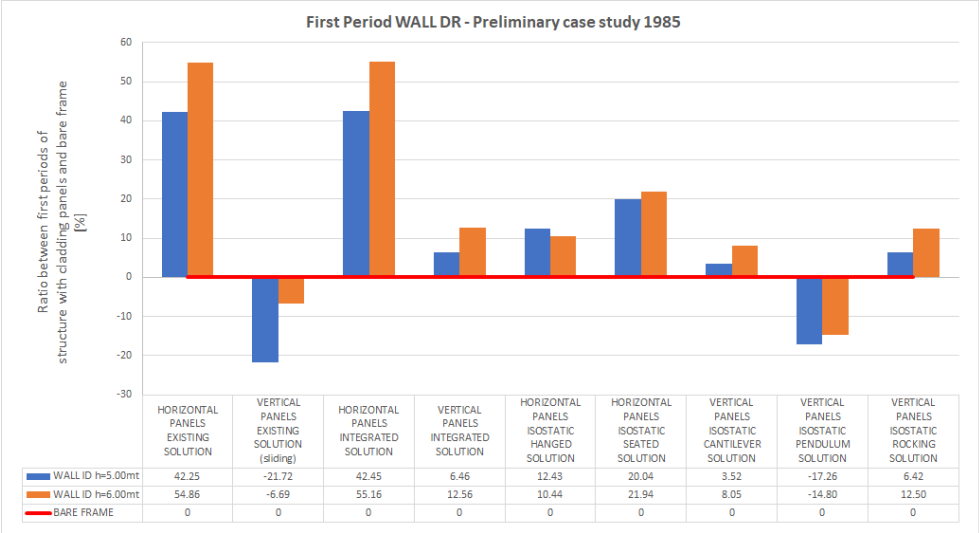

	HORIZONTAL PANELS EXISTING SOLUTION	VERTICAL PANELS EXISTING SOLUTION (sliding)	HORIZONTAL PANELS INTEGRATED SOLUTION	VERTICAL PANELS INTEGRATED SOLUTION	HORIZONTAL PANELS ISOSTATIC HANGED SOLUTION	HORIZONTAL PANELS ISOSTATIC SEATED SOLUTION	VERTICAL PANELS ISOSTATIC CANTILEVER SOLUTION	VERTICAL PANELS ISOSTATIC PENDULUM SOLUTION	VERTICAL PANELS ISOSTATIC ROCKING SOLUTION
WALL ID h=5.00mt	42.25	-21.72	42.45	6.46	12.43	20.04	3.52	-17.26	6.42
WALL ID h=6.00mt	54.86	-6.69	55.16	12.56	10.44	21.94	8.05	-14.80	12.50
BARE FRAME	0	0	0	0	0	0	0	0	0

Figure 6.60 Ratio [%] between first periods of the structure with cladding panels realised with WALL and bare frame – Deformable Roof.

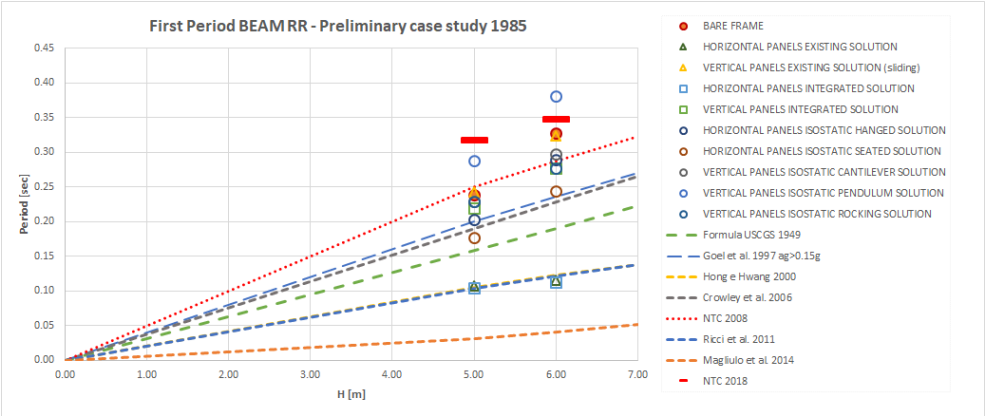

Figure 6.61 First periods of a preliminary case study with panels realised with BEAM - Rigid Roof.

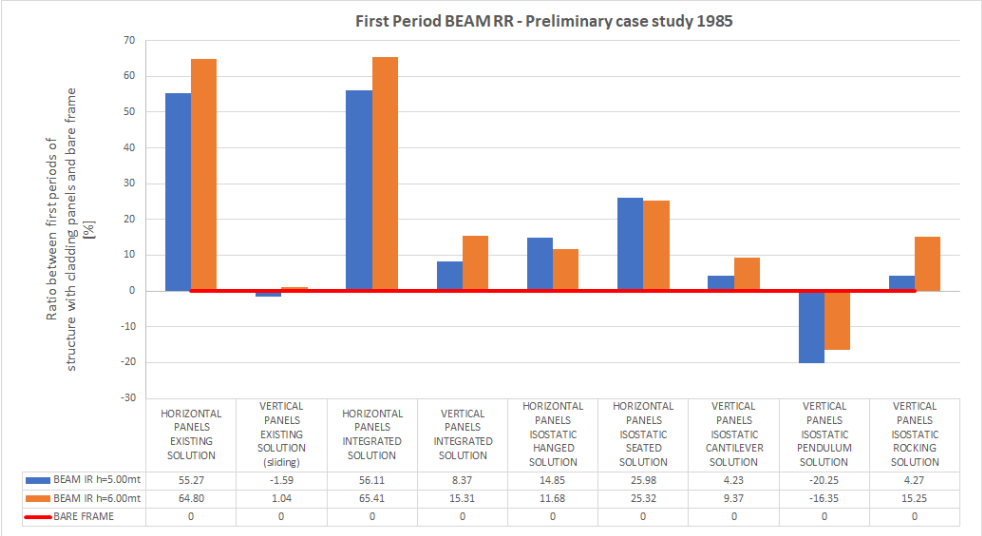

	HORIZONTAL PANELS EXISTING SOLUTION	VERTICAL PANELS EXISTING SOLUTION (sliding)	HORIZONTAL PANELS INTEGRATED SOLUTION	VERTICAL PANELS INTEGRATED SOLUTION	HORIZONTAL PANELS ISOSTATIC HANGED SOLUTION	HORIZONTAL PANELS ISOSTATIC SEATED SOLUTION	VERTICAL PANELS ISOSTATIC CANTILEVER SOLUTION	VERTICAL PANELS ISOSTATIC PENDULUM SOLUTION	VERTICAL PANELS ISOSTATIC ROCKING SOLUTION
BEAM IR h=5.00mt	55.27	-1.59	56.11	8.37	14.85	25.98	4.23	-20.25	4.27
BEAM IR h=6.00mt	64.80	1.04	65.41	15.31	11.68	25.32	9.37	-16.35	15.25
BARE FRAME	0	0	0	0	0	0	0	0	0

Figure 6.62 Ratio [%] between first periods of the structure with cladding panels realised with BEAM and bare frame – Rigid Roof.

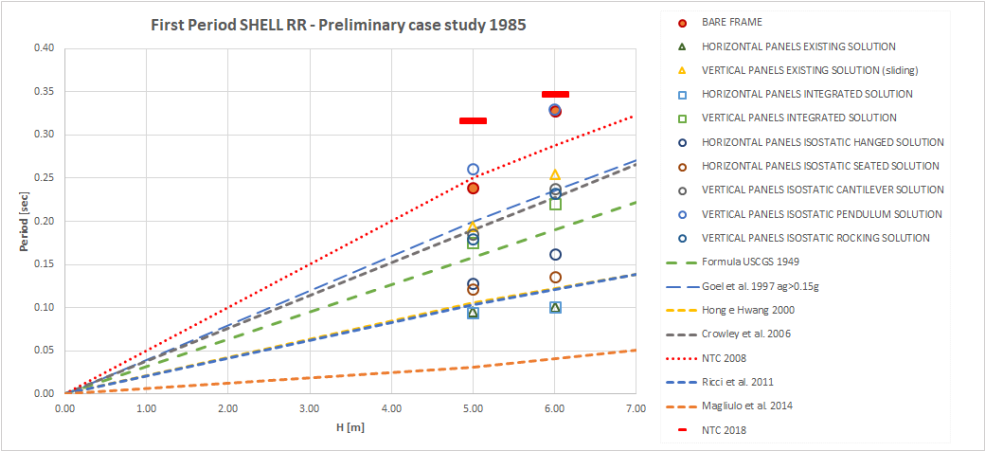

Figure 6.63 First periods of a preliminary case study with panels realised with SHELL - Rigid Roof.

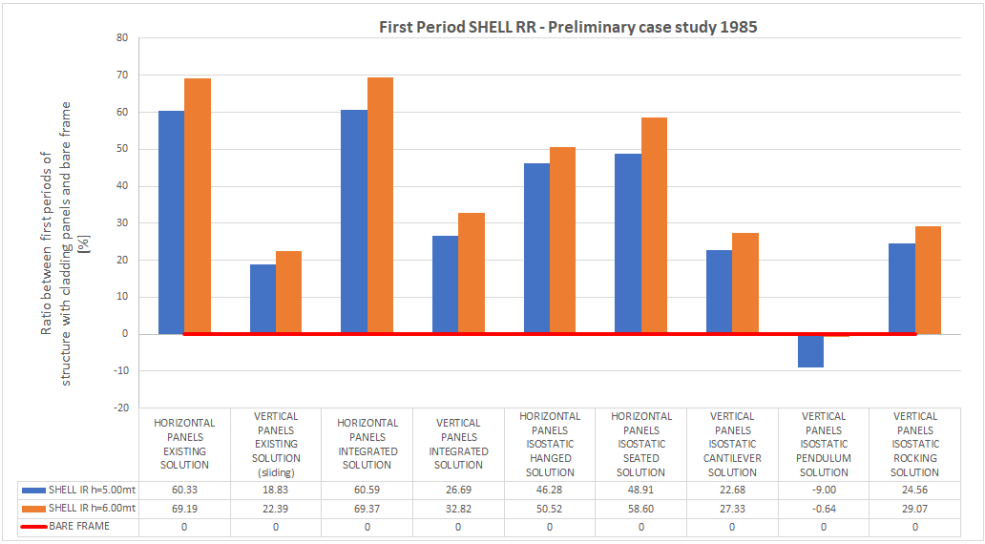

	HORIZONTAL PANELS EXISTING SOLUTION	VERTICAL PANELS EXISTING SOLUTION (sliding)	HORIZONTAL PANELS INTEGRATED SOLUTION	VERTICAL PANELS INTEGRATED SOLUTION	HORIZONTAL PANELS ISOSTATIC HANGED SOLUTION	HORIZONTAL PANELS ISOSTATIC SEATED SOLUTION	VERTICAL PANELS ISOSTATIC CANTILEVER SOLUTION	VERTICAL PANELS ISOSTATIC PENDULUM SOLUTION	VERTICAL PANELS ISOSTATIC ROCKING SOLUTION
SHELL IR h=5.00mt	60.33	18.83	60.59	26.69	46.28	48.91	22.68	-9.00	24.56
SHELL IR h=6.00mt	69.19	22.39	69.37	32.82	50.52	58.60	27.33	-0.64	29.07
BARE FRAME	0	0	0	0	0	0	0	0	0

Figure 6.64 Ratio [%] between first periods of the structure with cladding panels realised with SHELL and bare frame – Rigid Roof.

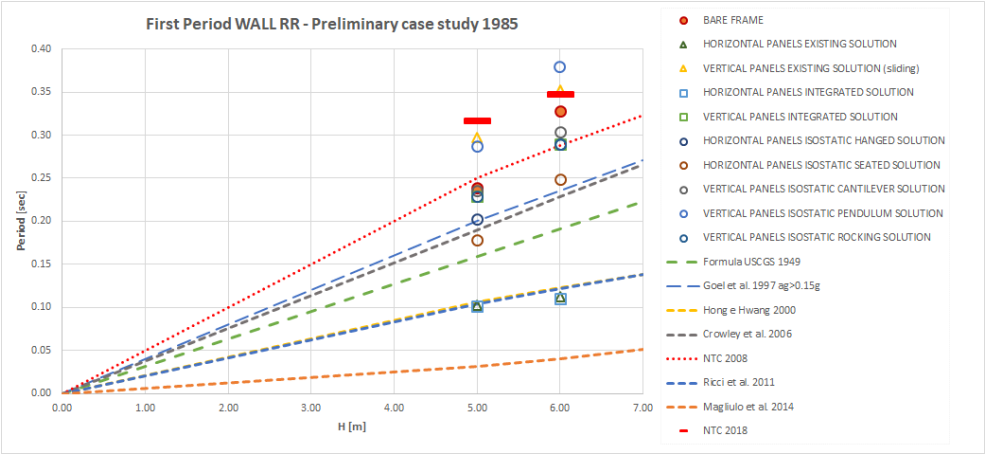

Figure 6.65 First periods of a preliminary case study with panels realised with WALL - Rigid Roof.

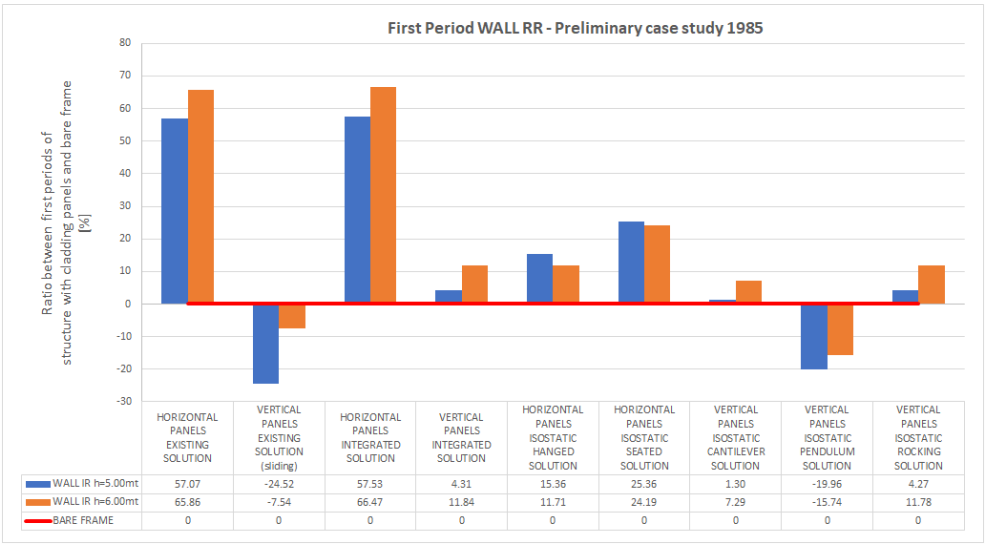

	HORIZONTAL PANELS EXISTING SOLUTION	VERTICAL PANELS EXISTING SOLUTION (sliding)	HORIZONTAL PANELS INTEGRATED SOLUTION	VERTICAL PANELS INTEGRATED SOLUTION	HORIZONTAL PANELS ISOSTATIC HANGED SOLUTION	HORIZONTAL PANELS ISOSTATIC SEATED SOLUTION	VERTICAL PANELS ISOSTATIC CANTILEVER SOLUTION	VERTICAL PANELS ISOSTATIC PENDULUM SOLUTION	VERTICAL PANELS ISOSTATIC ROCKING SOLUTION
WALL IR h=5.00mt	57.07	-24.52	57.53	4.31	15.36	25.36	1.30	-19.96	4.27
WALL IR h=6.00mt	65.86	-7.54	66.47	11.84	11.71	24.19	7.29	-15.74	11.78
BARE FRAME	0	0	0	0	0	0	0	0	0

Figure 6.66 Ratio [%] between first periods of the structure with cladding panels realised with WALL and bare frame – Rigid Roof.

6.4 Main case study

A typical example of Italian precast frame structure is now considered. From the analysis of the technical documents of the main case study, necessary information for a correct definition of the numerical models as regards the main structural elements, containing details on the connections shed/tapered beams, tapered beams/columns and columns/foundation are extrapolated. All the characteristics of the structure considered are reported below.

The main structure is a part of RC one-storey precast structure made in 1973 with 55x72 m rectangular shaped composed by three spans and height under the tapered beam of 5.90 m, consisting of columns with forks, prestressed tapered beams and shed roof with reinforced concrete prestressed panels.

For columns and beams, the concrete Class is C28/35 with elastic modulus equal to 28853 MPa and the steel Class is AQ60. All columns have dimensions 40x50cm. The main beams are of 17.90 m length with a variable section and double slope in the Y-direction (in the plan) with a horizontal lower profile and the upper inclined of about six degrees.

The roof is realised with reinforced prestressed panels of 8 cm thick laid on the beams and presumably tuned with friction connections to the main beams.

The precast structure has a socket foundation with 25 cm of concrete slab with an electro-welded net (industrial floor).

The height considered to calculate the period with analytical formulas is the medium value of the intrados of the roof.

Principal features of the main case study are summarised in Table 6.6 while some drawings concerning the project are reported in Figures 6.26- 6.28.

Type of precast structures	One-story RC PRECAST FRAME STRUCTURE
Year of construction:	1973
Plan dimensions:	55x72m
Height under the main beam:	5.90m
Dimension of columns:	40x50cm
Type of the main beam:	Prestressed tapered beam
Type of roof:	Shed roof with RC concrete panels
Type of connection beam-column:	Pin-dowel
Concrete Class:	C28/35
Steel Class:	AQ 60

Table 6.6 Principal features of the main case study.

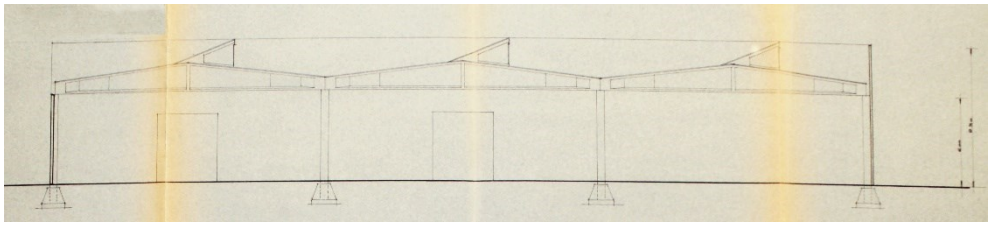

Figure 6.67 Section of the main case study.

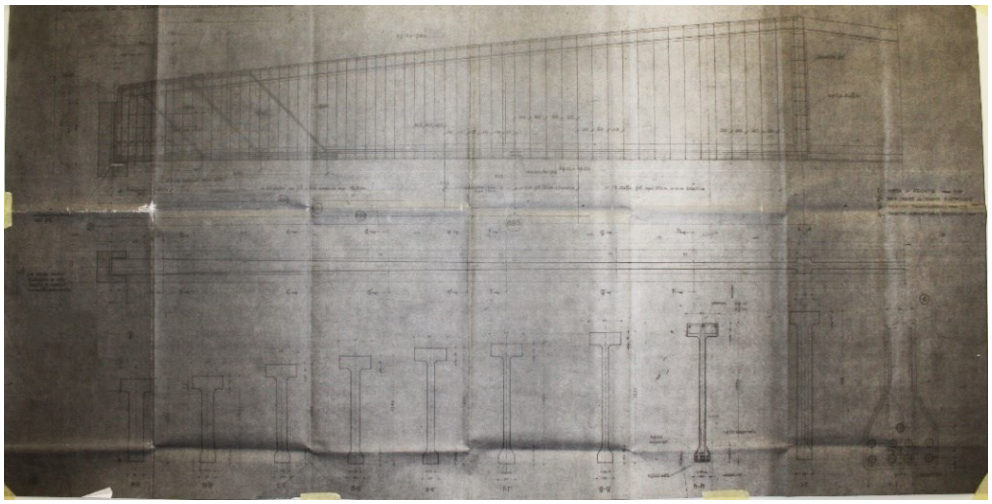

Figure 6.68 Details of the tapered beam of the main case study.

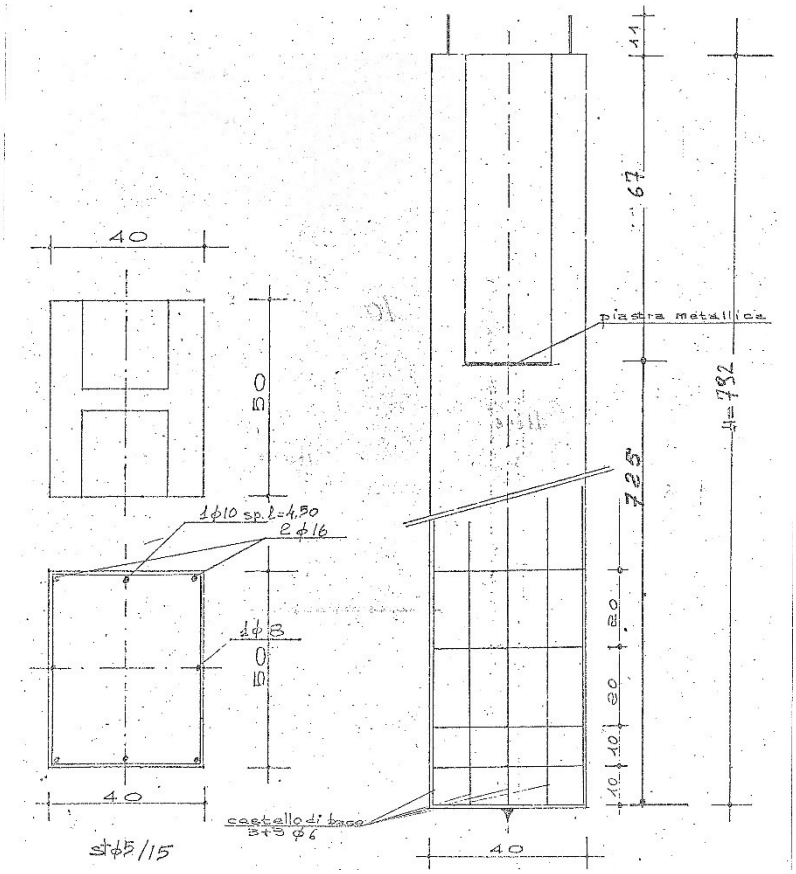

Figure 6.69 Longitudinal and transversal bars of columns of the main case study.

6.4.1 Numerical Models

Using a commercial calculation code, three-dimensional models are defined. The elements used for the spatial discretization are of a single-dimensional "beam" type with two nodes and bi-dimensional “plate” elements.
The main structural elements, such as columns, are modelled as "beam". The structure is supposedly fixed at the base at the level of the industrial floor; height is defined at the intrados of the main beam.
The main tapered beams are connected to the columns using spherical hinges because it is assumed the presence of a single pin for beam-column connections.
The transverse gutter beams are connected to the columns with cylindrical hinges, as observed by the presence of pins and bolts described in the technical report attached to the original project.
The sheds of the roof are inserted as weight in the numerical model. The seismic weights are obtained considering all structural and non-structural elements (panels) as well as live loads on the structures.
In the bare structure, the panel weights are inserted as seismic masses in X-Y directions.
Only vertical panels are placed along two major sides of the building with an equivalent concrete thickness of 15 cm, leading to a weight of 3.0 kN/mq.
In this case, horizontal panels are not analysed because, due to the size of the structure in one direction (17.90mt), they could not be inserted without the help of other columns that modify the original dynamic behaviour and stiffness of the structure.
Cladding panels are modelled taking into account all details of the fastening devices described in the cases of existing, isostatic and integrated solutions and in the numerical model these panels are represented with beam, wall and shell elements (the mesh discretization is chosen according to the thickness of the panel) to analyse the effect of several types of finite elements. In the case of fixed connections, a linking made with infinite stiffness are considered according to [116]. To simulate frictions, some springs are inserted with different stiffness in the interface between elements.
Figure 6.28 reports the models analysed; first of all, like the previous case, an infinite stiffness is set for out of the plane mechanism to evaluate the influence in the plane of the different types of connection of the panels as reported in the structural schemes of paragraph 6.1.
During analysis, the height, the length and the stiffness of roof (deformable or rigid roof) are changed of symmetrical and asymmetrical models of all typologies of

vertical cladding panels (The variability in length of the structure is considered because, according to Magliulo et al. [108], it is a fundamental parameter to be included to estimate the first period of precast structure).
For the original model, the behaviour of out of the plane of the panel is evaluated, assigning a stiffness to the connection according to Belleri et al. [118].

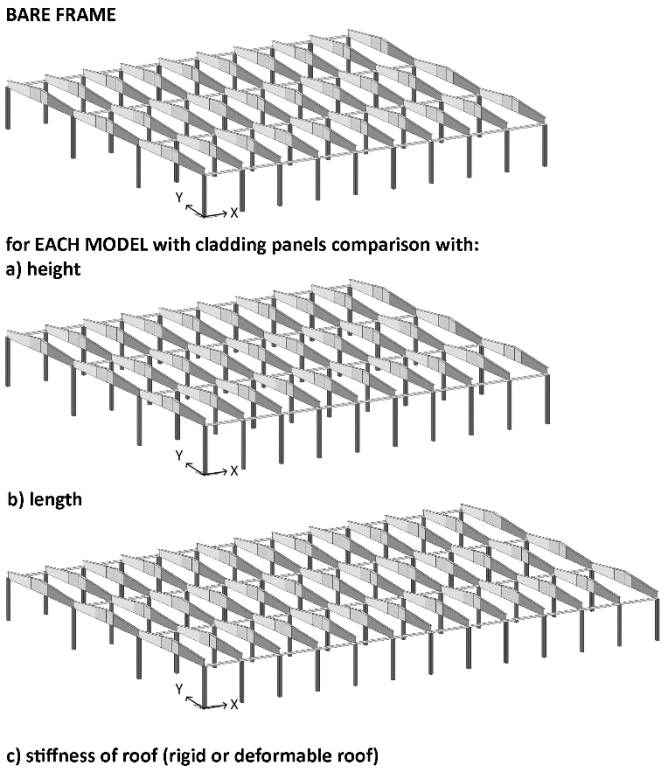

Figure 6.70 Variation of the height, length and stiffness of roof for main case study.

Another model is created to evaluate the influence of an asymmetrical structure on the first period: while the original model is made as symmetrical as possible respect to the two axes in terms of stiffness (construction elements geometry; all columns are taken with a dimension of 40x50cm) and load applied, in the asymmetical one are applied some differences in terms of the geometry of the construction elements and load applied between the various beams (see Figure 6.71).

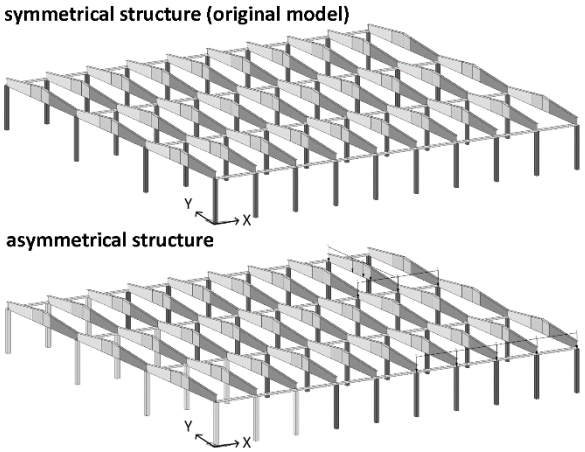

Figure 6.71 Comparison with symmetrical and asymmetrical models.

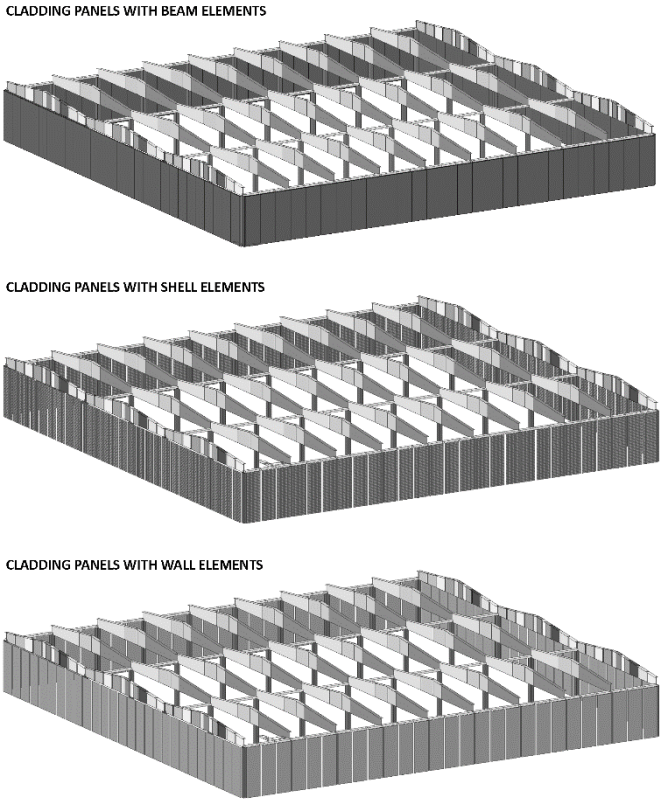

Figure 6.72 Cladding panels with beam, shell and wall elements for the main case study.

6.4.2 Result

6.4.2.1 Comparison with different heights and lengths

First periods for bare frame and frame with all types of vertical cladding panels realised with the different elements are shown in Tables 6.7-6.9. As for the preliminary case study, even here in the pendulum solution case with shell elements, three cases considering or not the infinite stiffness of the connections between panels and between panels and structure are evaluated.

	BEAM							
	DEFORMABLE ROOF				RIGID ROOF			
	Dir.	h=7.76mt l=54mt	h=8.76mt l=54mt	h=7.76mt l=72mt	Dir.	h=7.76mt l=54mt	h=8.76mt l=54mt	h=7.76mt l=72mt
		[sec]	[sec]	[sec]		[sec]	[sec]	[sec]
BARE FRAME	X	1.9771	2.1225	1.9900	X	1.1411	1.4475	1.1391
EXISTING SOLUTION	X	1.8154	1.8958	1.8694	X	0.5895	0.6725	0.5896
INTEGRATED SOLUTION	X	1.8121	1.8920	1.8659	Y	0.1389	0.1704	0.1519
ISOSTATIC CANTILEVER SOLUTION	X	1.8128	1.8948	1.8686	X	0.5024	0.5615	0.5016
ISOSTATIC PENDULUM SOLUTION	X	1.8155	1.8965	1.8671	X	0.1652	0.2048	0.1779
ISOSTATIC ROCKING SOLUTION	X	1.8122	1.8920	1.8659	X	0.1589	0.1997	0.1721

Table 6.7 First periods of models with vertical cladding panels realised with beam elements.

	SHELL							
	DEFORMABLE ROOF				RIGID ROOF			
	Dir.	h=7.76mt l=54mt	h=8.76mt l=54mt	h=7.76mt l=72mt	Dir.	h=7.76mt l=54mt	h=8.76mt l=54mt	h=7.76mt l=72mt
		[sec]	[sec]	[sec]		[sec]	[sec]	[sec]
BARE FRAME	X	1.9771	2.1225	1.9900	X	1.1411	1.4475	1.1391
EXISTING SOLUTION	X	1.8133	1.8948	1.8661	Y	0.3916	0.4636	0.4038
INTEGRATED SOLUTION	X	1.8152	1.8979	1.8674	X	0.161	0.1975	0.1735
ISOSTATIC CANTILEVER SOLUTION	X	1.7964	1.9008	1.8701	X	0.478	0.5555	0.4963
ISOSTATIC PENDULUM SOLUTION	X	1.8557	1.9679	1.9031	X	0.8129	1.0244	0.8136
ISOSTATIC PENDULUM SOLUTION + PANEL TO PANEL LINK	X	1.8346	1.9317	1.8821	X	0.4234	0.5047	0.4177
ISOSTATIC PENDULUM SOLUTION + PANEL TO COLUMN LINK	X	1.7803	1.8404	1.8323	X	0.2232	0.2711	0.2418
ISOSTATIC ROCKING SOLUTION	X	1.8178	1.902	1.8675	X	0.5192	0.6375	0.2027

Table 6.8 First periods of models with vertical cladding panels realised with shell elements.

	WALL							
	DEFORMABLE ROOF				RIGID ROOF			
	Dir.	h=7.76mt l=54mt	h=8.76mt l=54mt	h=7.76mt l=72mt	Dir.	h=7.76mt l=54mt	h=8.76mt l=54mt	h=7.76mt l=72mt
		[sec]	[sec]	[sec]		[sec]	[sec]	[sec]
BARE FRAME	X	1.9771	2.1225	1.9900	X	1.1411	1.3084	1.1391
EXISTING SOLUTION	X	1.8166	1.8989	1.8690	X	0.4786	0.5236	0.4766
INTEGRATED SOLUTION	X	1.8149	1.8969	1.8671	X	0.0667	0.0716	0.0705
ISOSTATIC CANTILEVER SOLUTION	X	1.8174	1.8997	1.8698	X	0.4965	0.5479	0.4944
ISOSTATIC PENDULUM SOLUTION	X	1.8165	1.9017	1.8681	X	0.0902	0.1061	0.0902
ISOSTATIC ROCKING SOLUTION	X	1.8149	1.8969	1.8149	X	0.0669	0.0718	0.0669

Table 6.9 First periods of models with vertical cladding panels realised with wall elements.

As can be seen from the tables listed above, the first periods of the symmetrical models for the rigid roof are in the same range of values defined by Magliulo et al. [108].

Respect to the preliminary case study, in the main case study there are huge differences in the first period between deformable and rigid roofs models.

Isostatic pendulum solution shows a lowering of the first period respect the period of the bare frame, a correct behaviour but totally different respect a preliminary case study where, probably, similar dimensions of height and length brought an increase of period regard bare frame.

The main conclusions concerned comparison with different height are listed above:

- In all cases of the deformable roof, all periods of the structure are higher than those obtained by the formulas in the scientific literature (except in the case of pendulum solution all the other periods are more or less aligned on a value);
- In the case of the rigid roof, integrated, pendulum and rocking solutions are the cases that values of first periods with panels represented by beam elements are near the formulas deriving from Magliulo et al.;
- Cantilever and existing solutions for beam and wall elements have similar periods between them because both static schemes are based on the upper or lower sliding of the panels. Using shell elements to represent panels, further sensitivity analyses regarding the friction coefficient used in the existing solution should be made to align this case with the others. (For cantilever solution the evaluation of friction coefficient done with experimental tests reported in Dal Lago et al. [106] is taking into account);
- All cases with shell elements and deformable roof are those with more variability of the period between several solutions;
- First periods obtained from pendulum solution models with rigid roof and cladding panels made with beam, wall and shell (in case of infinitely rigid links between panels and between panels and structure) have values

similar with the formulation obtained from Magliulo to calculate the period. In numerical model utilised to derive the formula, the author uses a pendulum solution with shell elements for cladding panels and rigid connections between panels and between panels and structure.

- The cantilever solution model is the case where the choice of the type of element for the representation of the cladding panels (beam, shell and wall) does not affect the first period;
- The first periods of integrated, pendulum and rocking solutions with rigid roof are the cases that are closer to the periods calculated with formulas provided by scientific literature;
- In case of the rigid roof, cladding panels realised with wall elements provide very low periods; on the contrary, cladding panels modelled with shell elements give high periods of the structure;
- The formula described by NTC 2018 provides high periods compared to those obtained from industrial frame building with cladding panels and rigid roof but low period considering deformable roof.

The main conclusions about different lengths are listed above:

- In case of rigid deck, the increase in the length of the structure does not lead some significant variations of the period; on the contrary, in case of deformable deck, the major length of structure brings an increase of first period independent from the type of element of panel (beam, shell and wall);
- The difference in length of the structure of about 1/3 of the entire structure (passing from 54mt to 72mt) slightly affect the period;
- The formula of Magliulo captures the variability of the period according to the length about the pendulum, rocking and integrated solutions;
- The USGS formula of 1949 reports similar results to those found by Magliulo as it also counts the incidence of a length over the period.

Figures 6.73-6.113 show a comparison between the periods concerning the same type of vertical cladding panels realised with different elements (beam, shell, and wall) and a comparison between the different types of cladding panels represented (existing building, integrated solution, etc.) with the same elements in the numerical model varying the height and the length.

Also, the modal shapes corresponding to the first period for the cases analysed with a rigid roof with a height of a structure equal to 7.76m and with a length of 54mt are reported below.

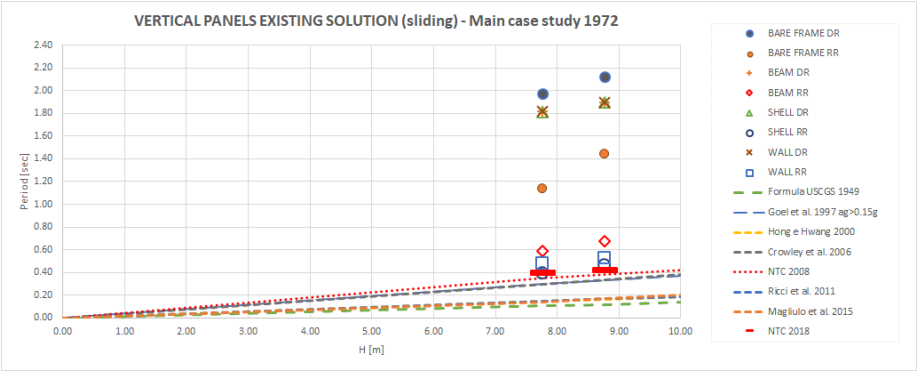

Figure 6.73 First periods of the main case study with vertical panels existing solution – several heights.

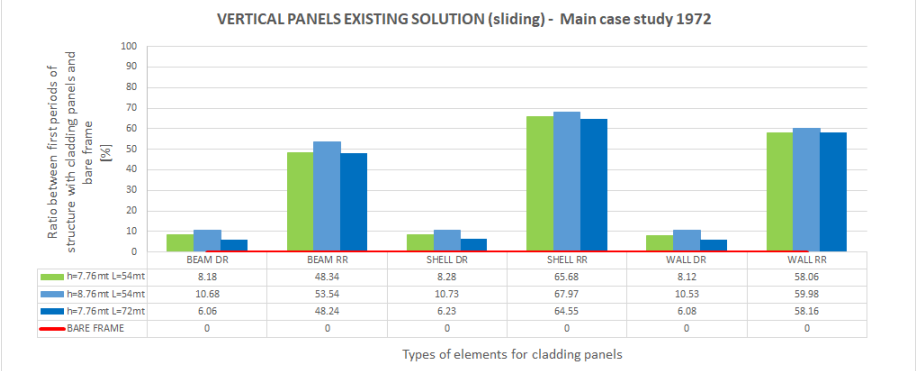

	BEAM DR	BEAM RR	SHELL DR	SHELL RR	WALL DR	WALL RR
h=7.76 mt L=54mt	8.18	48.34	8.28	65.68	8.12	58.06
h=8.76 mt L=54mt	10.68	53.54	10.73	67.97	10.53	59.98
h=7.76 mt L=72mt	6.06	48.24	6.23	64.55	6.08	58.16
BARE FRAME	0	0	0	0	0	0

Figure 6.74 Ratio [%] between first periods of the structure with vertical panels existing solution and bare frame.

Figure 6.75 First periods of the main case study with vertical panels existing solution – several lengths.

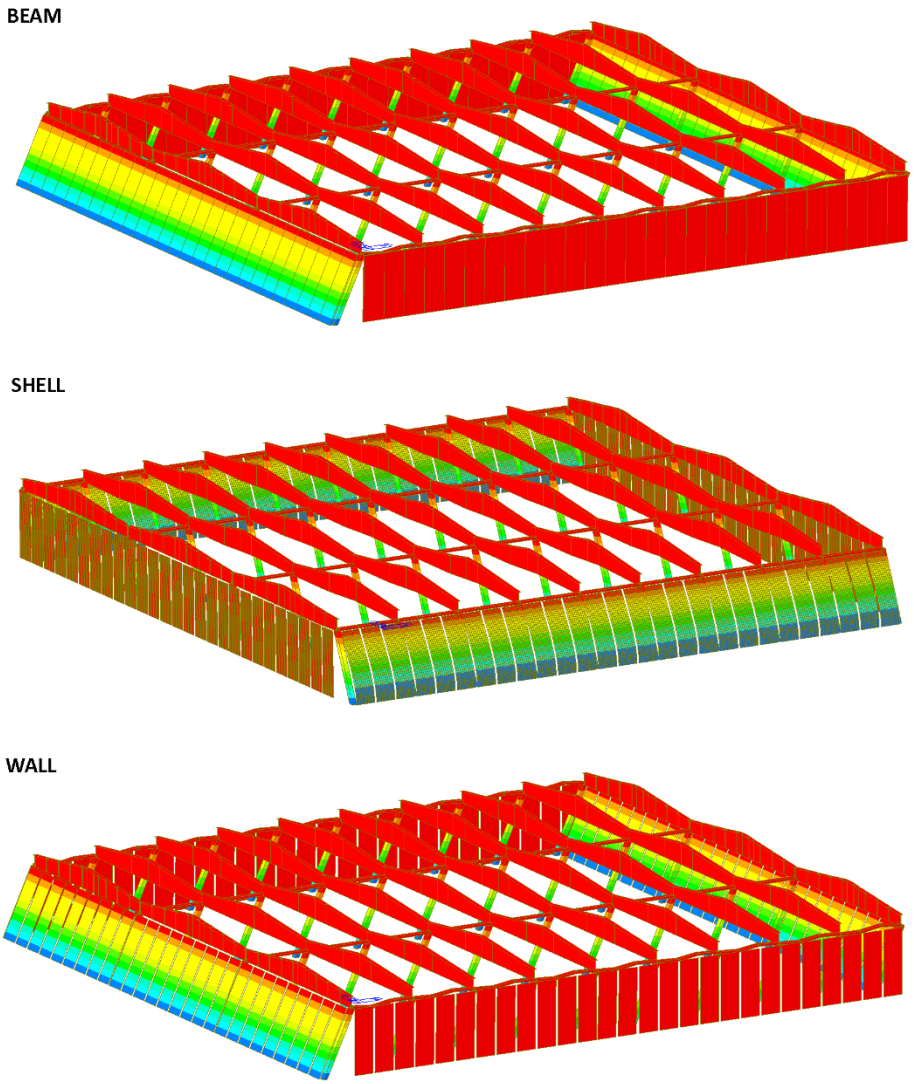

Figure 6.76 First periods mode shapes of vertical panels existing solution with rigid roof.

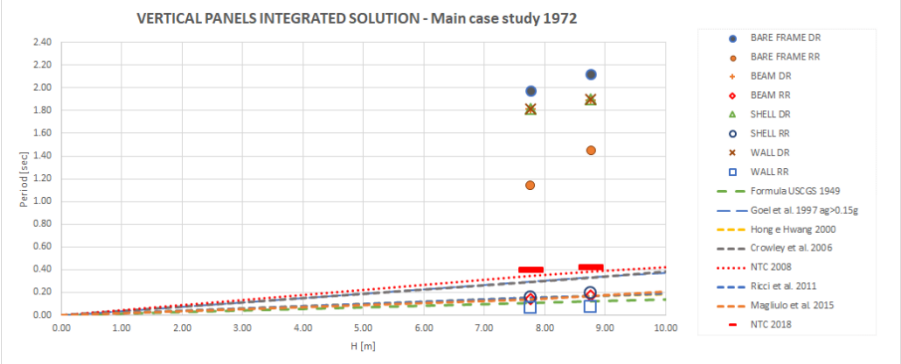

Figure 6.77 First periods of the main case study with vertical panels integrated solution – several heights.

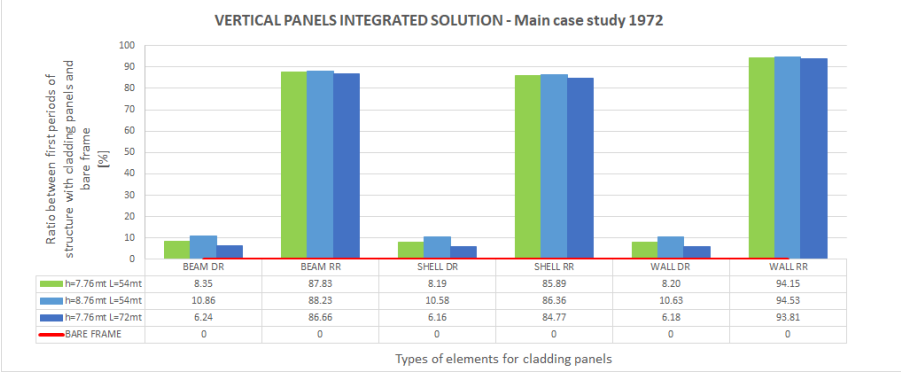

Figure 6.78 Ratio [%] between first periods of the structure with an integrated solution and bare frame.

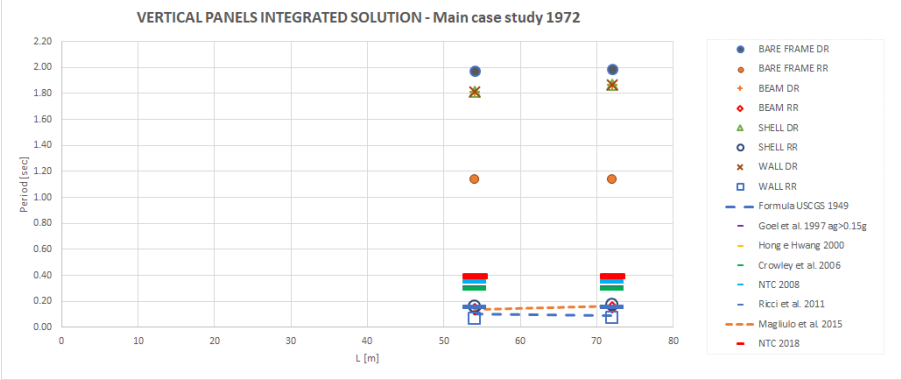

Figure 6.79 First periods of the main case study with vertical panels integrated solution – several lengths.

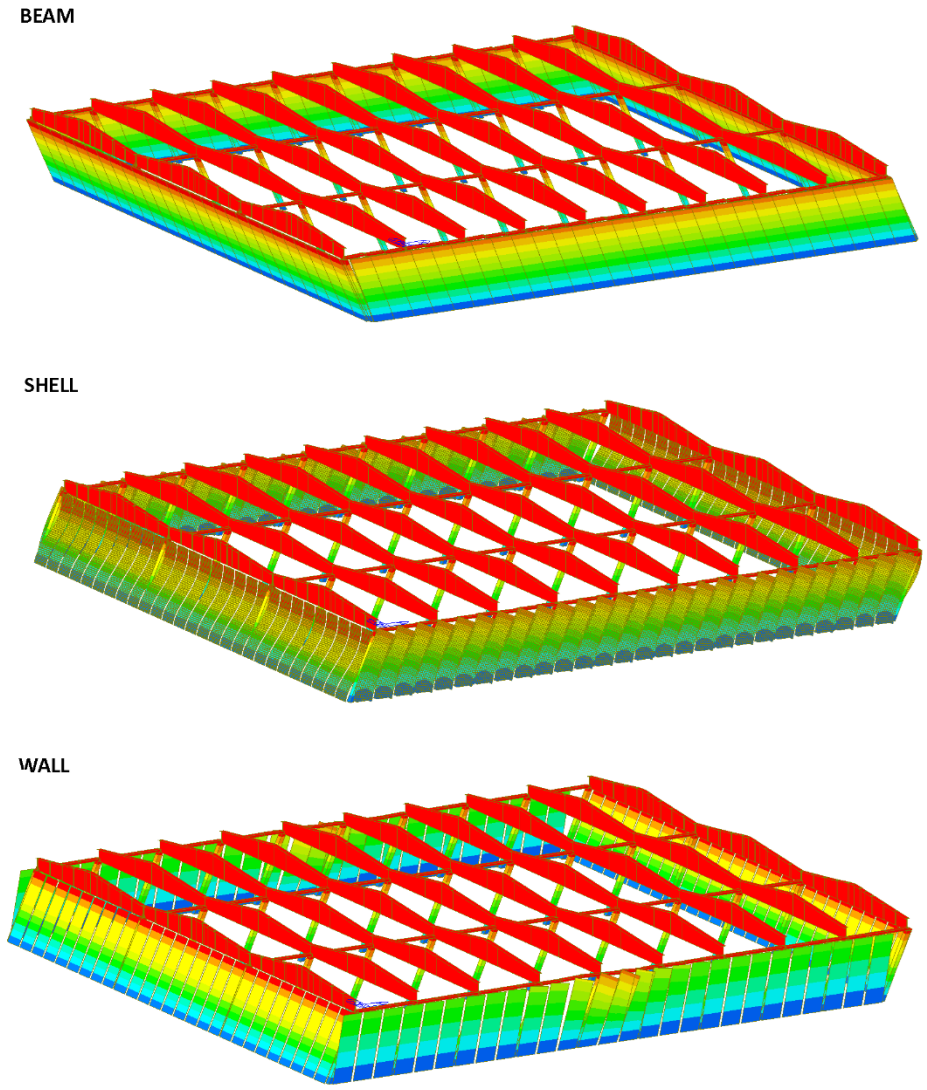

Figure 6.80 First periods mode shapes of vertical panels integrated solution with rigid roof.

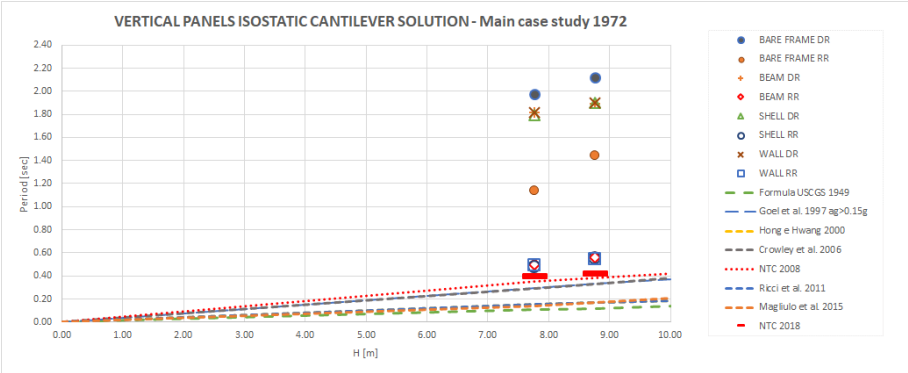

Figure 6.81 First periods of the main case study with isostatic cantilever solution – several heights.

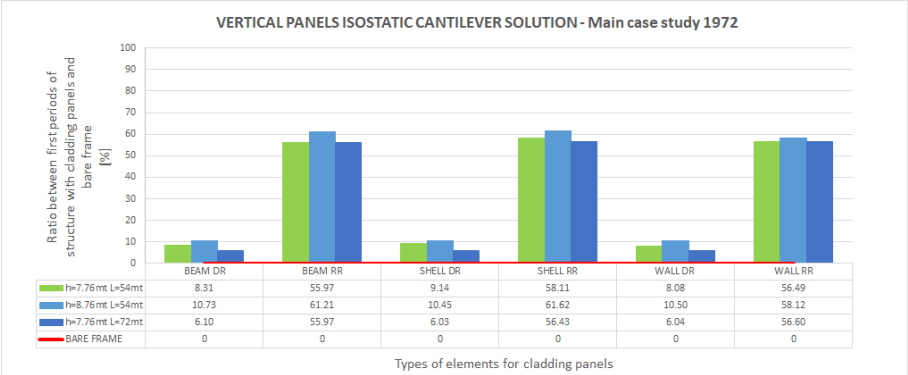

	BEAM DR	BEAM RR	SHELL DR	SHELL RR	WALL DR	WALL RR
h=7.76 mt L=54mt	8.31	55.97	9.14	58.11	8.08	56.49
h=8.76 mt L=54mt	10.73	61.21	10.45	61.62	10.50	58.12
h=7.76 mt L=72mt	6.10	55.97	6.03	56.43	6.04	56.60
BARE FRAME	0	0	0	0	0	0

Figure 6.82 Ratio [%] between first periods of the structure with isostatic cantilever solution and bare frame.

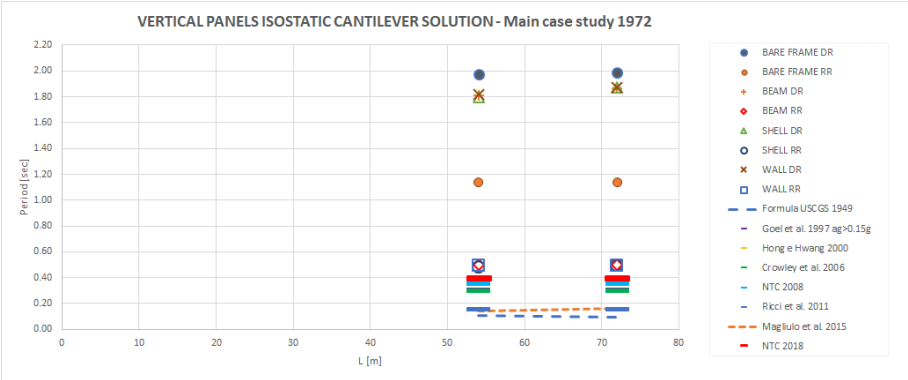

Figure 6.83 First periods of the main case study with isostatic cantilever solution – several lengths.

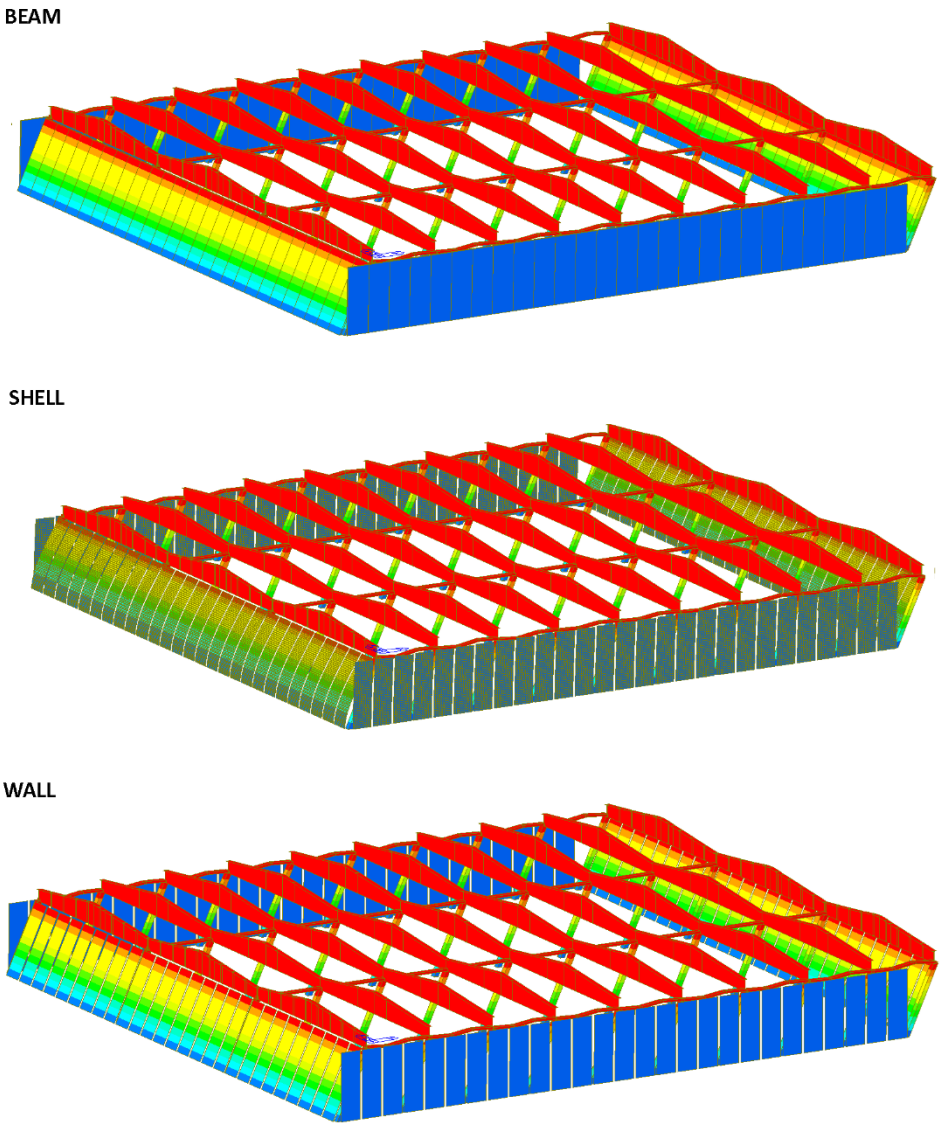

Figure 6.84 First periods mode shapes of vertical panels isostatic cantilever solution with rigid roof.

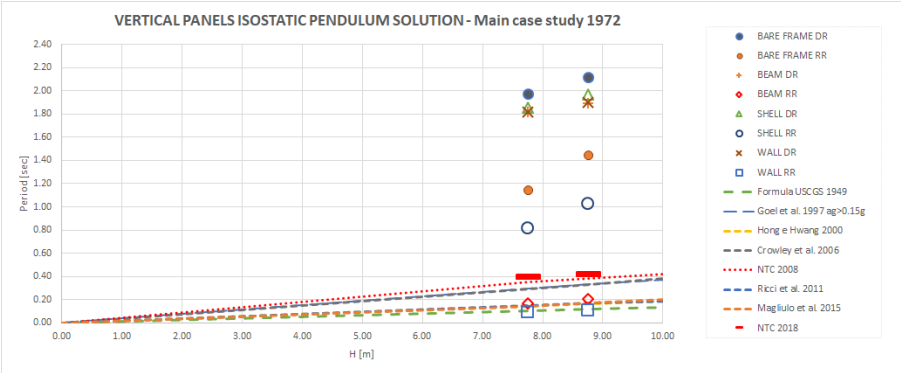

Figure 6.85 First periods of the main case study with isostatic pendulum solution – several heights.

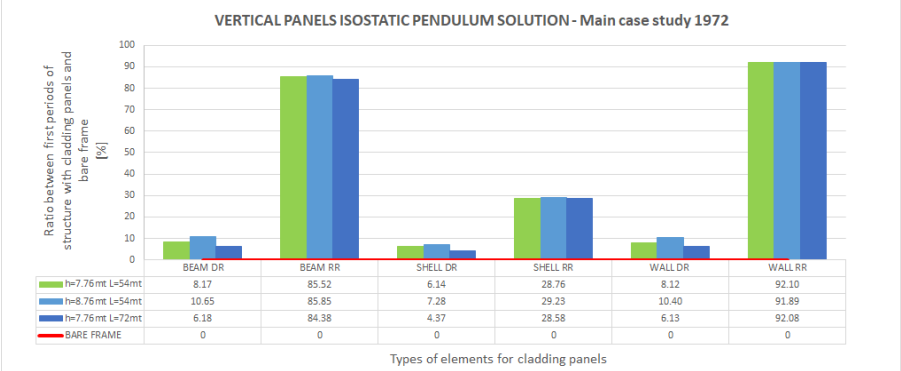

	BEAM DR	BEAM RR	SHELL DR	SHELL RR	WALL DR	WALL RR
h=7.76 mt L=54mt	8.17	85.52	6.14	28.76	8.12	92.10
h=8.76 mt L=54mt	10.65	85.85	7.28	29.23	10.40	91.89
h=7.76 mt L=72mt	6.18	84.38	4.37	28.58	6.13	92.08
BARE FRAME	0	0	0	0	0	0

Figure 6.86 Ratio [%] between first periods of the structure with isostatic pendulum solution and bare frame.

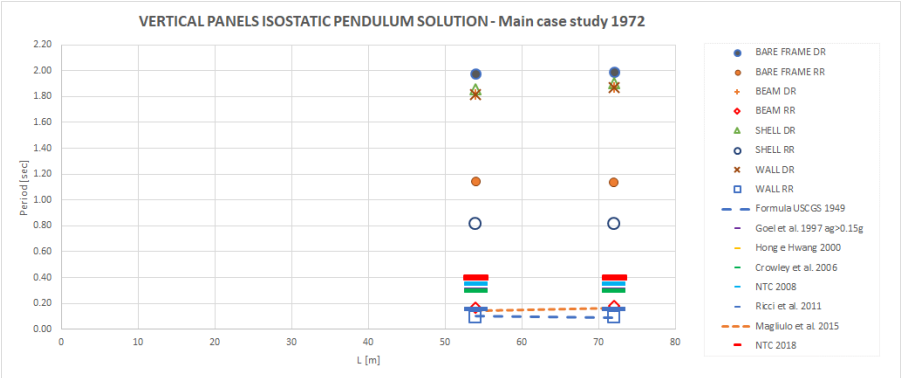

Figure 6.87 First periods of the main case study with isostatic pendulum solution – several lengths.

BEAM

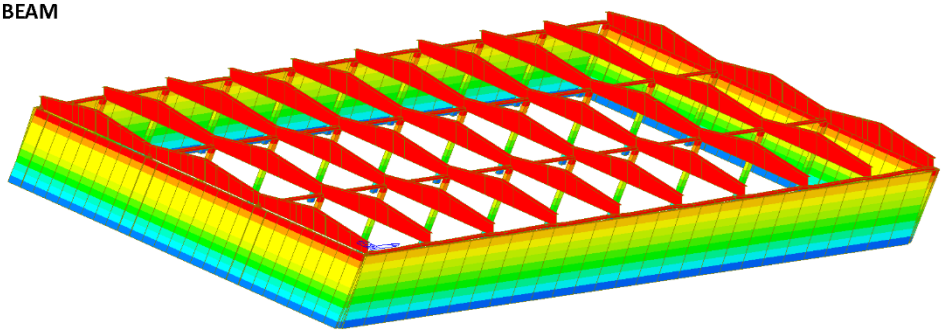

SHELL

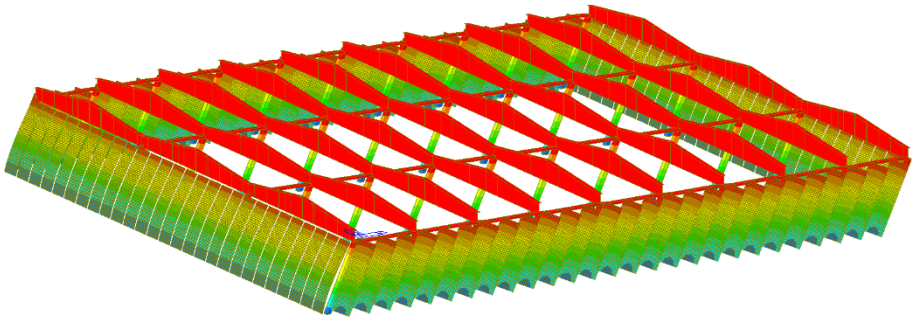

WALL

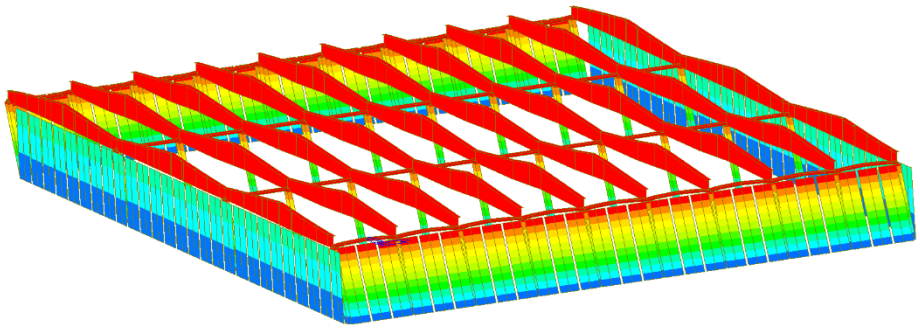

Figure 6.88 First periods mode shapes of vertical panels isostatic pendulum solution with rigid roof.

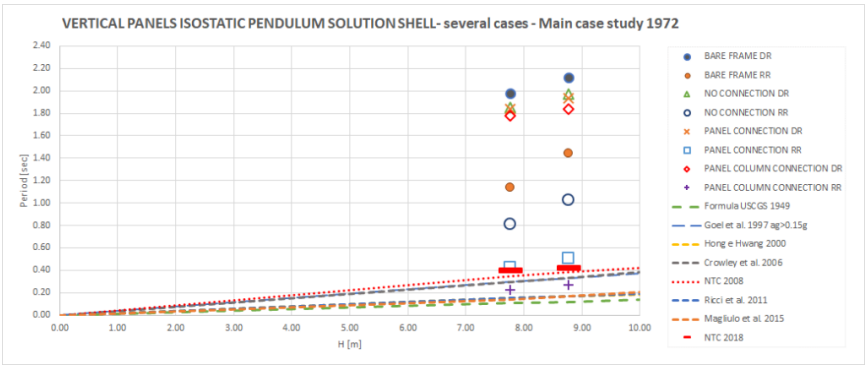

Figure 6.89 First periods of the main case study with isostatic pendulum solution SHELL (several cases) – variable heights.

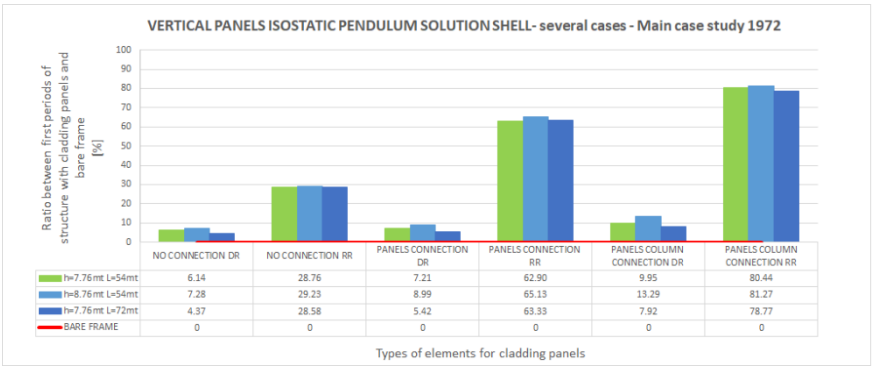

	NO CONNECTION DR	NO CONNECTION RR	PANELS CONNECTION DR	PANELS CONNECTION RR	PANELS COLUMN CONNECTION DR	PANELS COLUMN CONNECTION RR
h=7.76 mt L=54mt	6.14	28.76	7.21	62.90	9.95	80.44
h=8.76 mt L=54mt	7.28	29.23	8.99	65.13	13.29	81.27
h=7.76 mt L=72mt	4.37	28.58	5.42	63.33	7.92	78.77
BARE FRAME	0	0	0	0	0	0

Figure 6.90 Ratio [%] between first periods of the structure with isostatic pendulum solution SHELL (several cases) and bare frame.

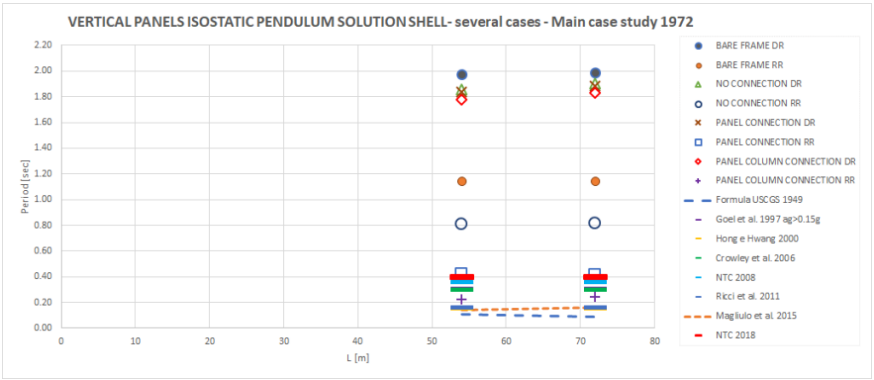

Figure 6.91 First periods of the main case study with isostatic pendulum solution SHELL (several cases) – variable lengths.

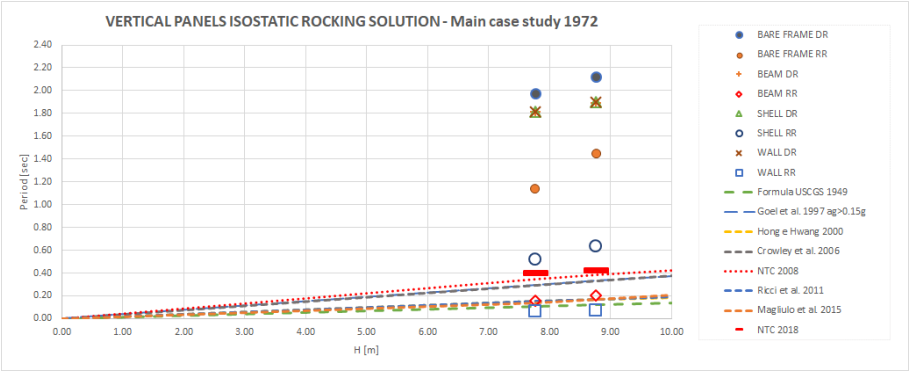

Figure 6.92 First periods of the main case study with an isostatic rocking solution – several heights.

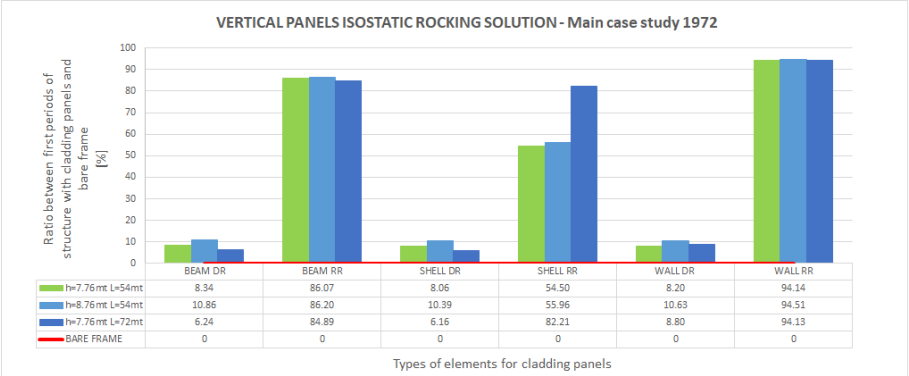

Figure 6.93 Ratio [%] between first periods of the structure with an isostatic rocking solution and bare frame.

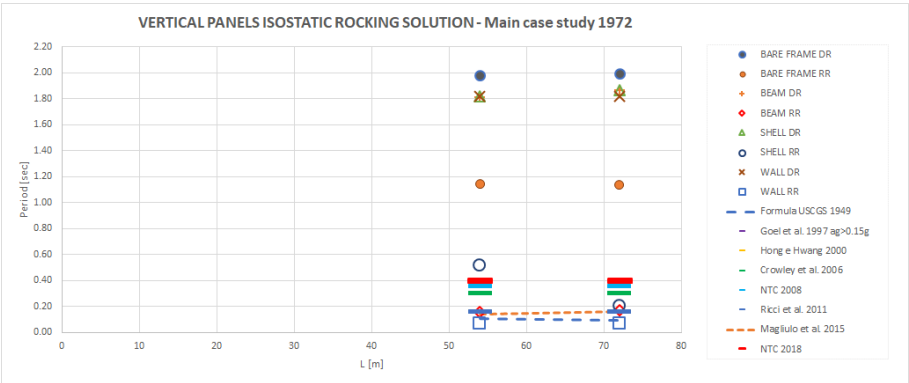

Figure 6.94 First periods of the main case study with an isostatic rocking solution – several lengths.

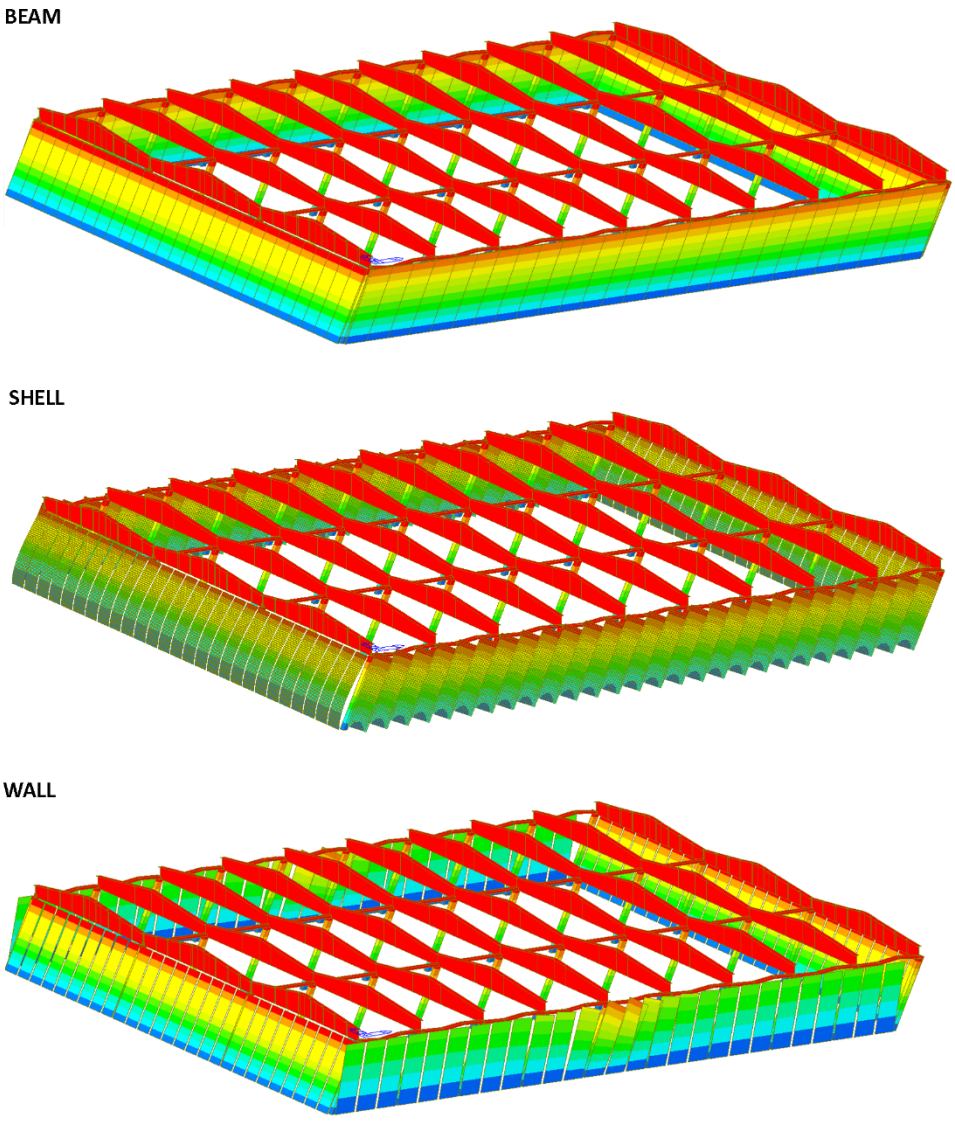

Figure 6.95 First periods mode shapes of vertical panels isostatic rocking solution with rigid roof.

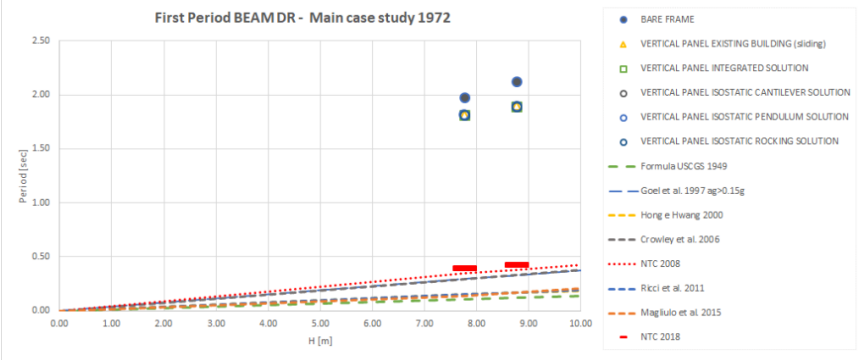

Figure 6.96 First periods of the main case study with panels realised with BEAM Deformable Roof (height).

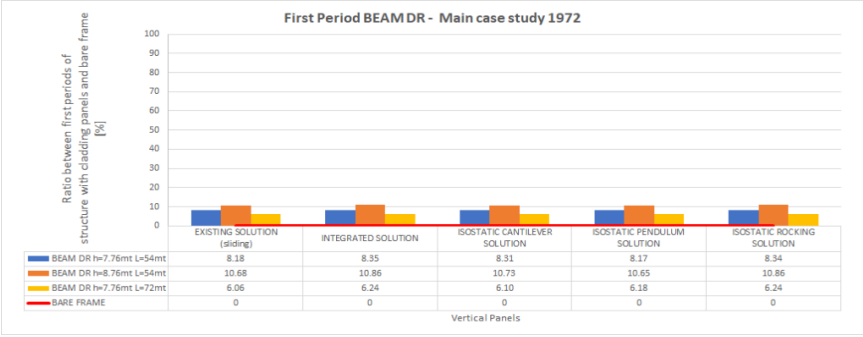

Figure 6.97 Ratio [%] between first periods of the structure with cladding panels realised with BEAM and bare frame – Deformable Roof.

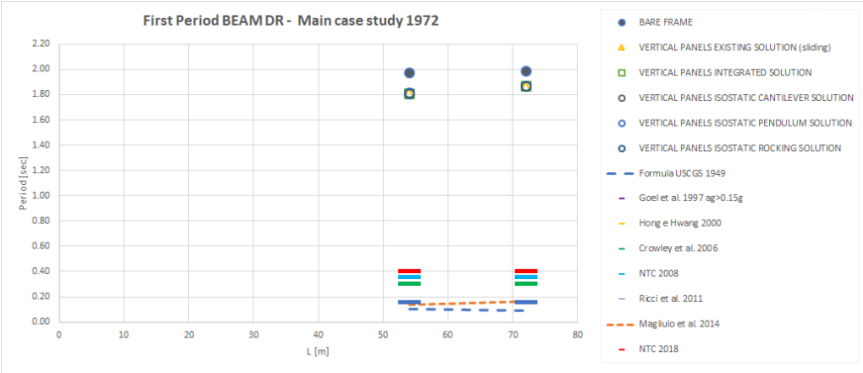

Figure 6.98 First periods of the main case study with panels realised with BEAM Deformable Roof (length).

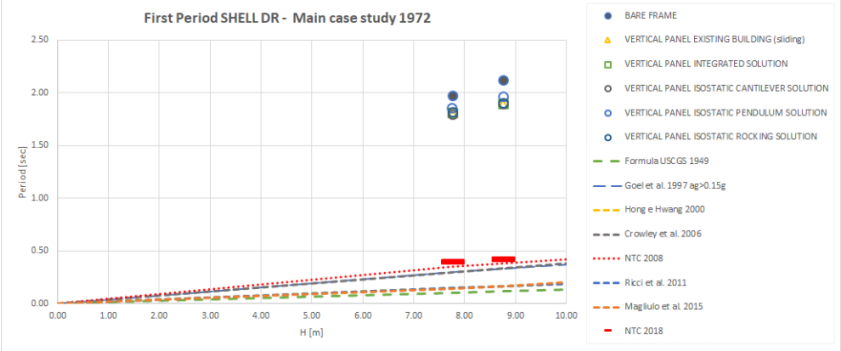

Figure 6.99 First periods of the main case study with panels realised with SHELL Deformable Roof (height).

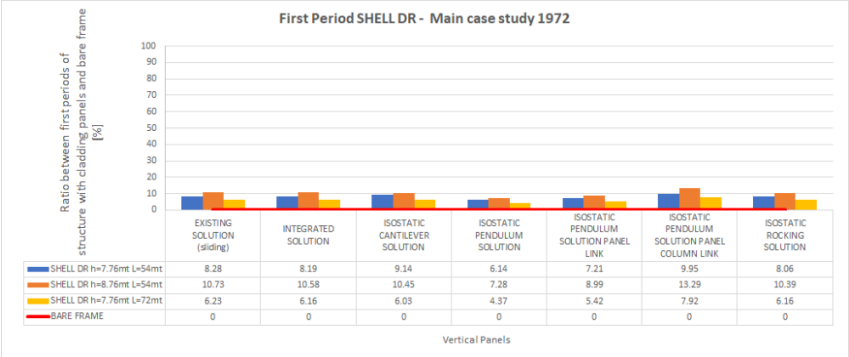

	EXISTING SOLUTION (sliding)	INTEGRATED SOLUTION	ISOSTATIC CANTILEVER SOLUTION	ISOSTATIC PENDULUM SOLUTION	ISOSTATIC PENDULUM SOLUTION PANEL LINK	ISOSTATIC PENDULUM SOLUTION PANEL COLUMN LINK	ISOSTATIC ROCKING SOLUTION
SHELL DR h=7.76mt L=54mt	8.28	8.19	9.14	6.14	7.21	9.95	8.06
SHELL DR h=8.76mt L=54mt	10.73	10.58	10.45	7.28	8.99	13.29	10.39
SHELL DR h=7.76mt L=72mt	6.23	6.16	6.03	4.37	5.42	7.92	6.16
BARE FRAME	0	0	0	0	0	0	0

Figure 6.100 Ratio [%] between first periods of the structure with cladding panels realised with SHELL and bare frame – Deformable Roof.

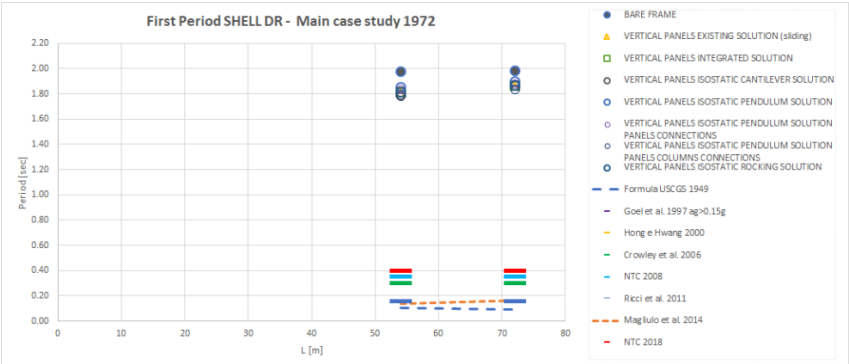

Figure 6.101 First periods of the main case study with panels realised with SHELL Deformable Roof (length).

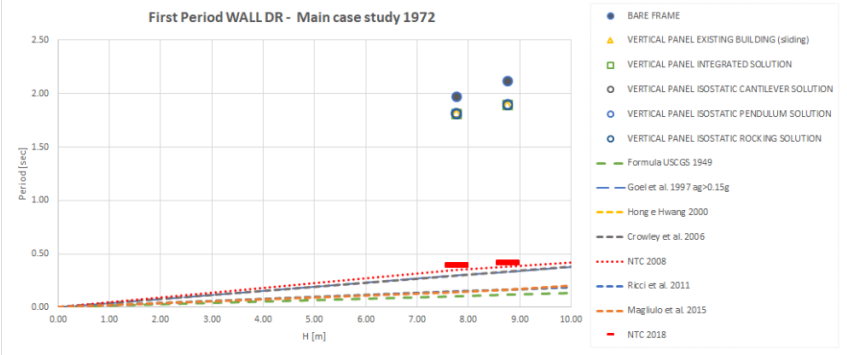

Figure 6.102 First periods of the main case study with panels realised with WALL Deformable Roof (height).

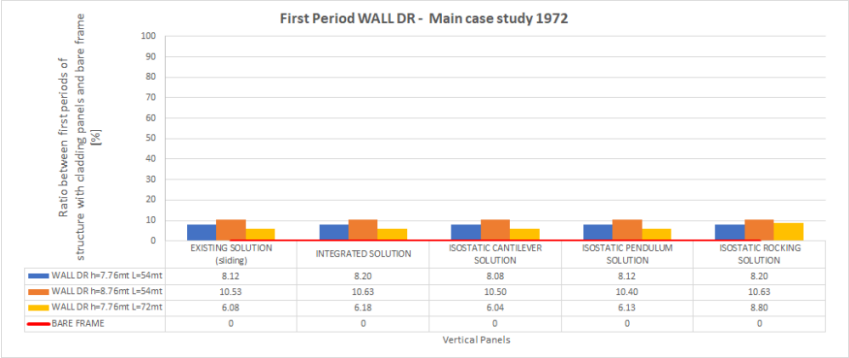

Figure 6.103 Ratio [%] between first periods of the structure with cladding panels realised with WALL and bare frame – Deformable Roof.

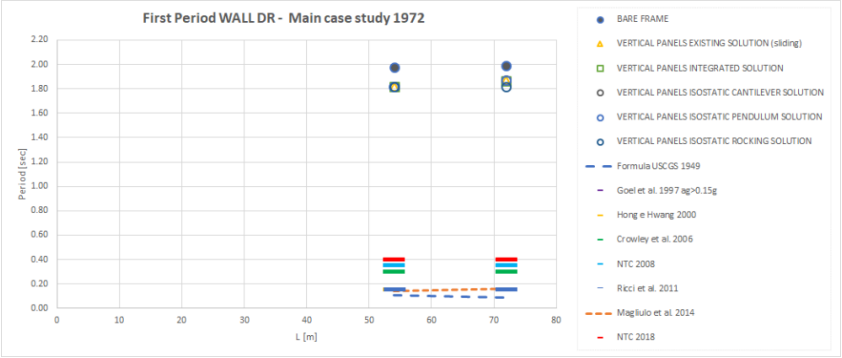

Figure 6.104 First periods of the main case study with panels realised with WALL Deformable Roof (length).

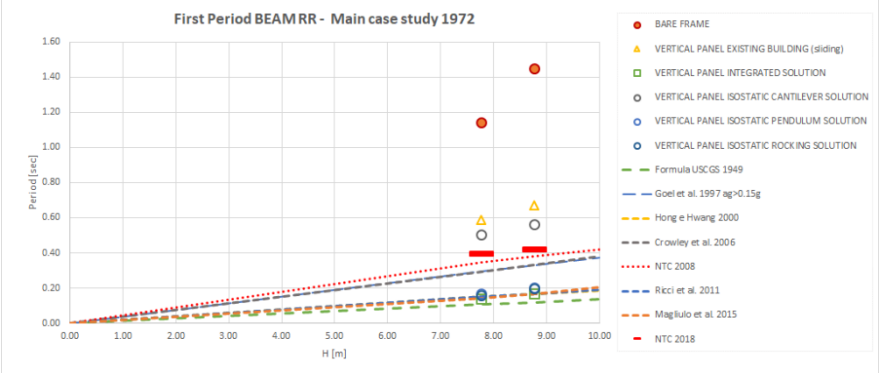

Figure 6.105 First periods of the main case study with panels realised with BEAM Rigid Roof (height).

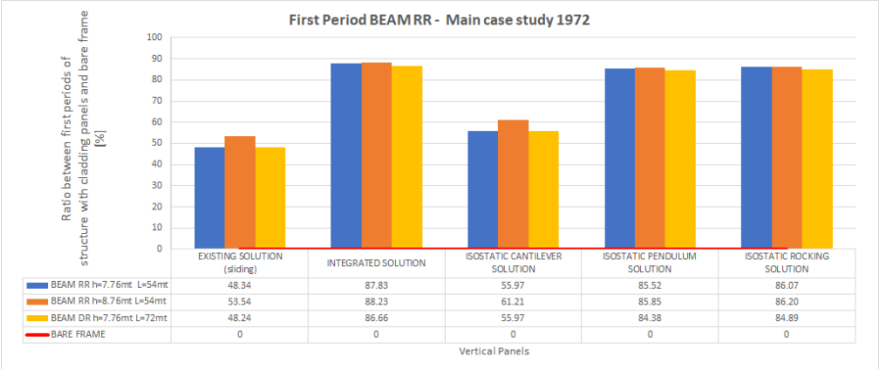

	EXISTING SOLUTION (sliding)	INTEGRATED SOLUTION	ISOSTATIC CANTILEVER SOLUTION	ISOSTATIC PENDULUM SOLUTION	ISOSTATIC ROCKING SOLUTION
BEAM RR h=7.76mt L=54mt	48.34	87.83	55.97	85.52	86.07
BEAM RR h=8.76mt L=54mt	53.54	88.23	61.21	85.85	86.20
BEAM DR h=7.76mt L=72mt	48.24	86.66	55.97	84.38	84.89
BARE FRAME	0	0	0	0	0

Figure 6.106 Ratio [%] between first periods of the structure with cladding panels realised with BEAM and bare frame – Rigid Roof.

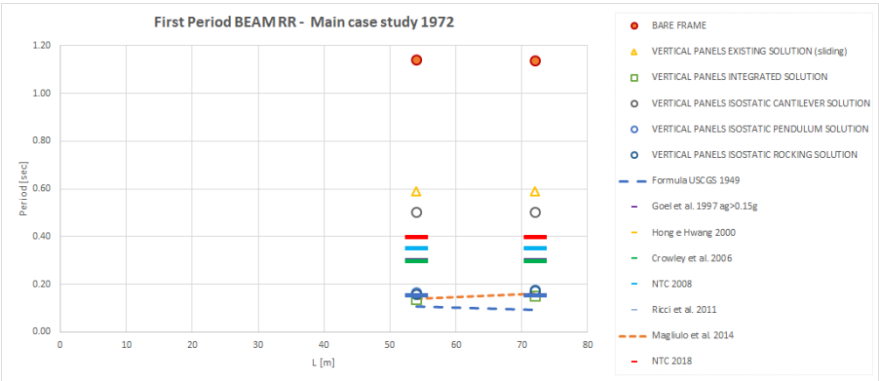

Figure 6.107 First periods of the main case study with panels realised with BEAM Rigid Roof (length).

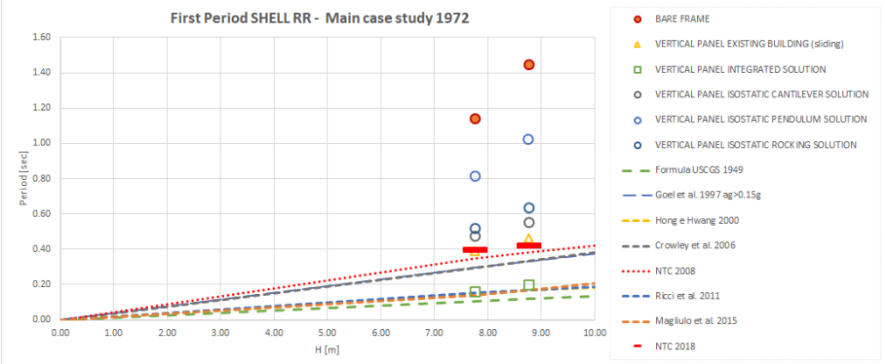

Figure 6.108 First periods of the main case study with panels realised with SHELL Rigid Roof (height).

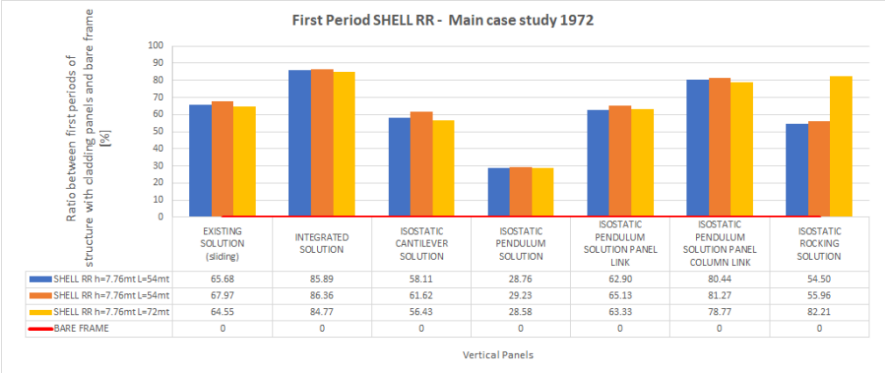

Figure 6.109 Ratio [%] between first periods of the structure with cladding panels realised with SHELL and bare frame – Rigid Roof.

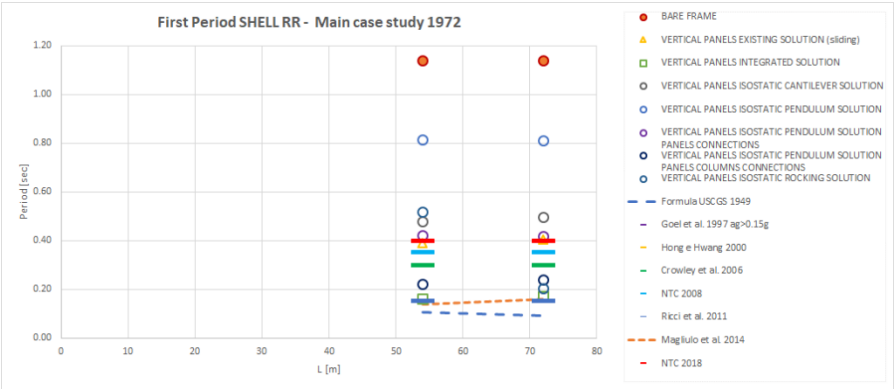

Figure 6.110 First periods of main case study with panels realised with SHELL Rigid Roof (length).

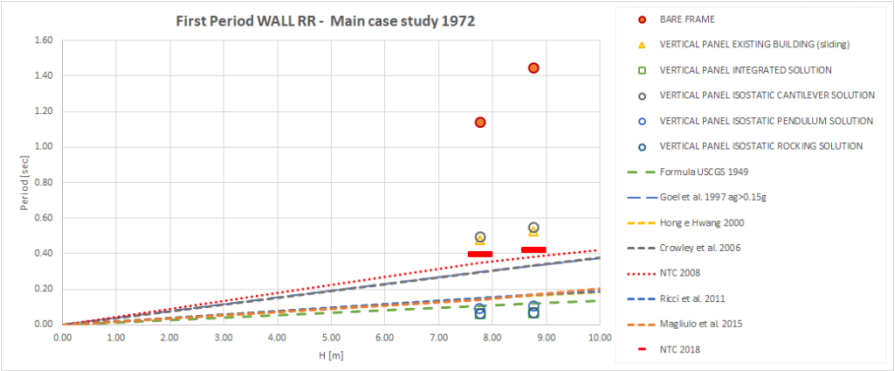

Figure 6.111 First periods of the main case study with panels realised with WALL Rigid Roof (height).

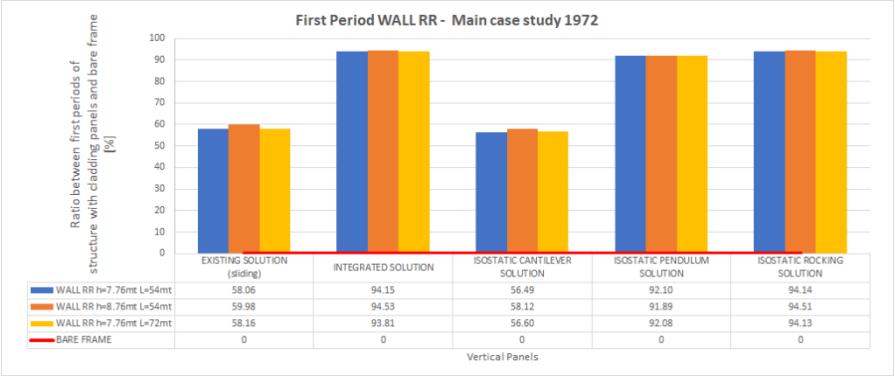

	EXISTING SOLUTION (sliding)	INTEGRATED SOLUTION	ISOSTATIC CANTILEVER SOLUTION	ISOSTATIC PENDULUM SOLUTION	ISOSTATIC ROCKING SOLUTION
WALL RR h=7.76mt L=54mt	58.06	94.15	56.49	92.10	94.14
WALL RR h=8.76mt L=54mt	59.98	94.53	58.12	91.89	94.51
WALL RR h=7.76mt L=72mt	58.16	93.81	56.60	92.08	94.13
BARE FRAME	0	0	0	0	0

Figure 6.112 Ratio [%] between first periods of the structure with cladding panels realised with WALL and bare frame – Rigid Roof.

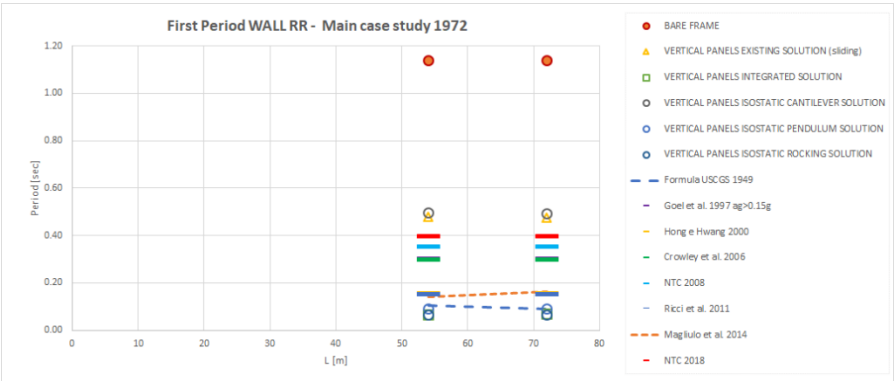

Figure 6.113 First periods of the main case study with panels realised with WALL Rigid Roof (length).

6.4.2.2 Comparison between infinitive and real stiffness of out of plane connections

In Tables 6.10-6.12 first periods of the original model (height of 7.76m and length of 52 m) with an infinitive and real stiffness of out of plane connections according to Belleri et al. [118] are reported.

	BEAM					
	DEFORMABLE ROOF			RIGID ROOF		
	Dir.	INFINITIVE STIFFNESS	REAL STIFFNESS	Dir.	INFINITIVE STIFFNESS	REAL STIFFNESS
		[sec]	[sec]		[sec]	[sec]
BARE FRAME	X	1.9771	1.9771	X	1.1411	1.1411
EXISTING SOLUTION	X	1.8154	1.8155	X	0.5895	0.5903
INTEGRATED SOLUTION	X	1.8121	1.8124	X	0.1389	0.1728
ISOSTATIC CANTILEVER SOLUTION	X	1.8128	1.813	X	0.5024	0.5024
ISOSTATIC PENDULUM SOLUTION	X	1.8155	1.8157	X	0.1652	0.2015
ISOSTATIC ROCKING SOLUTION	X	1.8122	1.8124	X	0.1589	0.1784

Table 6.10 First periods of models with vertical cladding panels realised with beam elements.

	SHELL					
	DEFORMABLE ROOF			RIGID ROOF		
	Dir.	INFINITIVE STIFFNESS	REAL STIFFNESS	Dir.	INFINITIVE STIFFNESS	REAL STIFFNESS
		[sec]	[sec]		[sec]	[sec]
BARE FRAME	X	1.9771	1.9771	X	1.1411	1.1411
EXISTING SOLUTION	X	1.8133	1.8135	X	0.3916	0.3919
INTEGRATED SOLUTION	X	1.8152	1.8154	X	0.161	0.1964
ISOSTATIC CANTILEVER SOLUTION	X	1.7964	1.7965	X	0.478	0.4780
ISOSTATIC PENDULUM SOLUTION	X	1.8557	1.8558	X	0.8129	0.8129
ISOSTATIC PENDULUM SOLUTION + PANEL TO PANEL CONNECTIONS	X	1.8346	1.8347	X	0.4234	0.4316
ISOSTATIC PENDULUM SOLUTION + PANEL TO COLUMN CONNECTIONS	X	1.7803	1.7808	X	0.2232	0.2302
ISOSTATIC ROCKING SOLUTION	X	1.8178	1.818	X	0.5192	0.5208

Table 6.11 First periods of models with vertical cladding panels realised with shell elements.

	WALL					
	DEFORMABLE ROOF			RIGID ROOF		
	Dir.	INFINITIVE STIFFNESS	REAL STIFFNESS	Dir.	INFINITIVE STIFFNESS	REAL STIFFNESS
		[sec]	[sec]		[sec]	[sec]
BARE FRAME	X	1.9771	1.9771	X	1.1411	1.1411
EXISTING SOLUTION	X	1.8166	1.8168	X	0.4786	0.4809
INTEGRATED SOLUTION	X	1.8149	1.8151	X	0.0667	0.1104
ISOSTATIC CANTILEVER SOLUTION	X	1.8174	1.8175	X	0.4965	0.4965
ISOSTATIC PENDULUM SOLUTION	X	1.8165	1.8167	X	0.0902	0.1458
ISOSTATIC ROCKING SOLUTION	X	1.8149	1.8151	X	0.0669	0.1105

Table 6.12 First periods of models with vertical cladding panels realised with wall elements.

Assuming the real stiffness of the connections, there are no differences of first periods with the cases of the infinite stiffness of out of plane connections considering models with deformable roofs.
In integrated, pendulum and rocking solutions with cladding panels realised with beam and wall elements, small differences in the first period are observed with rigid roof.
The behaviour of the two cases analysed are shown in Figures 6.114-6.119.

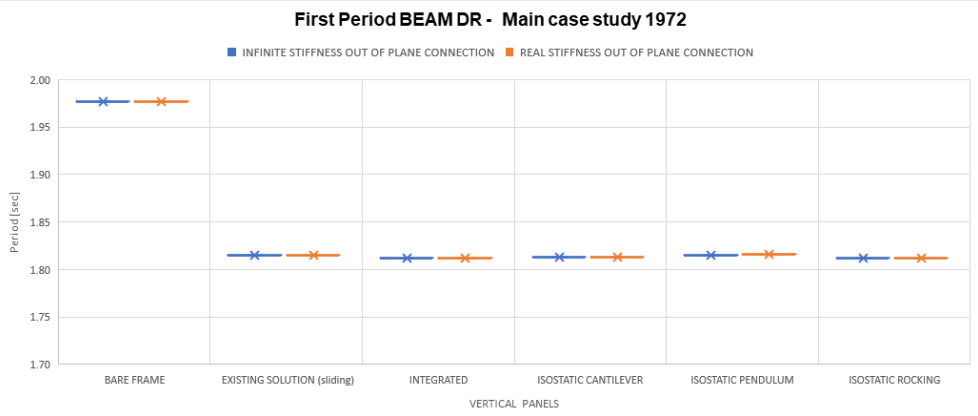

Figure 6.114 First periods of the main case study with panels realised with infinitive/real stiffness out of plane connections BEAM - Deformable Roof.

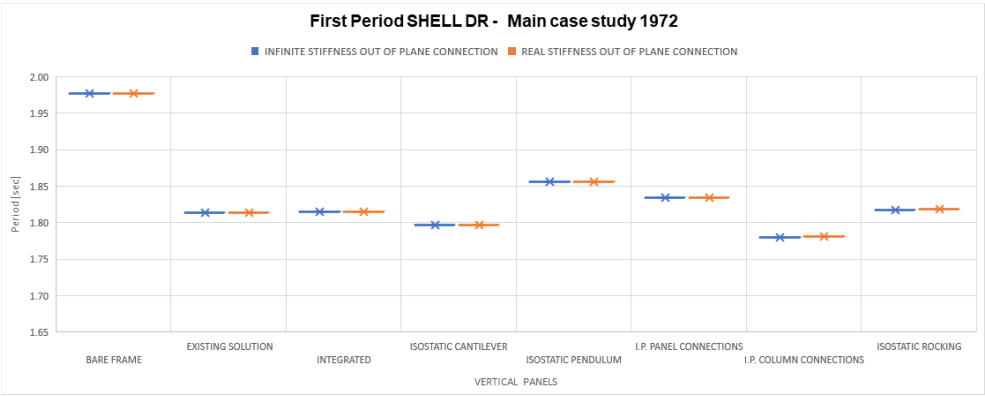

Figure 6.115 First periods of the main case study with panels realised with infinitive/real stiffness out of plane connections SHELL - Deformable Roof.

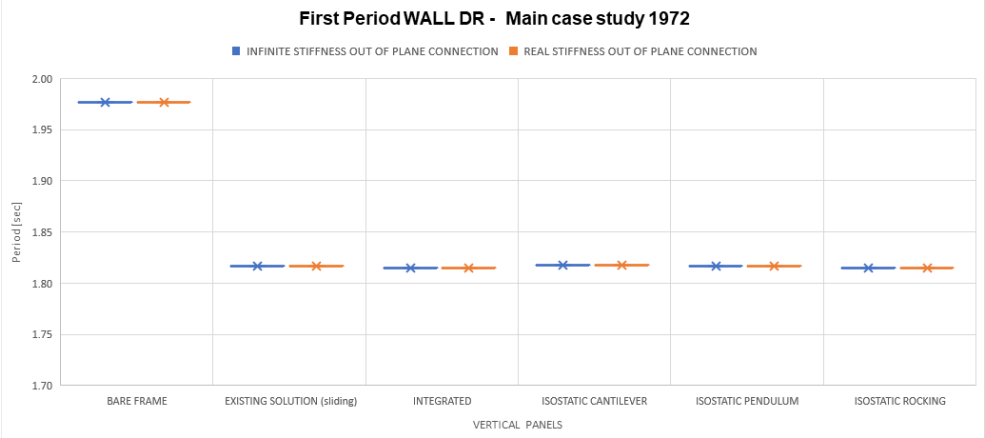

Figure 6.116 First periods of the main case study with panels realised with infinitive/real stiffness out of plane connections WALL - Deformable Roof.

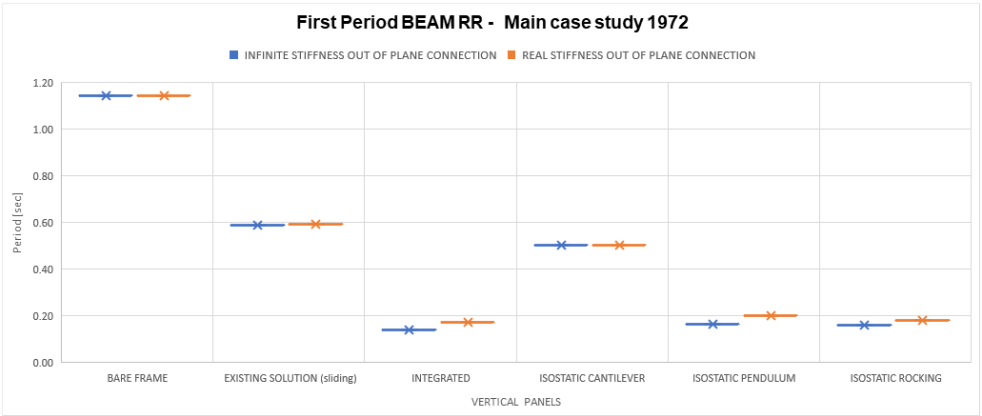

Figure 6.117 First periods of the main case study with panels realised with infinitive/real stiffness out of plane connections BEAM - Rigid Roof.

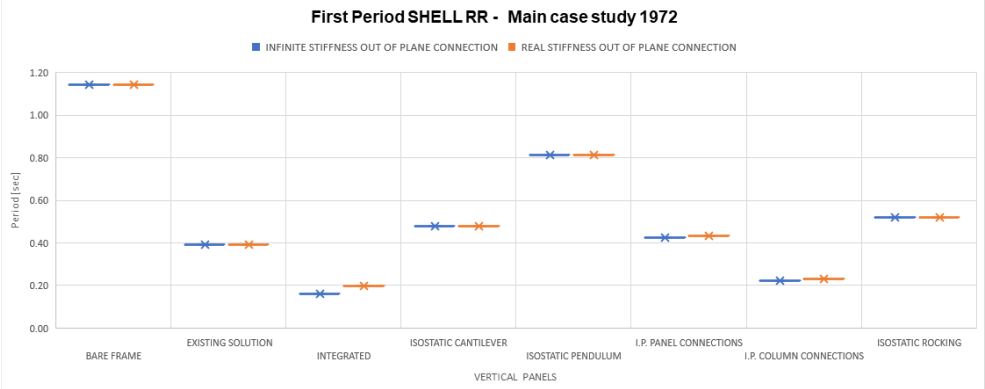

Figure 6.118 First periods of the main case study with panels realised with infinitive/real stiffness out of plane connections SHELL - Rigid Roof.

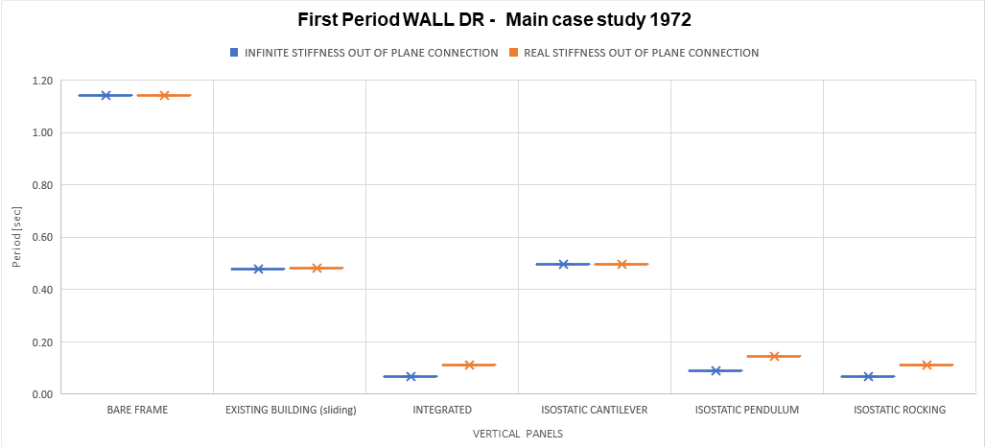

Figure 6.119 First periods of the main case study with panels realised with infinitive/real stiffness out of plane connections WALL - Rigid Roof.

6.4.2.3 Comparison with the asymmetrical model

In Tables 6.13-6.15 first periods of the original symmetrical model (height of 7.76mt and length of 52mt) and asymmetrical model are reported.

	BEAM					
	DEFORMABLE ROOF			RIGID ROOF		
	Dir.	SYMMETRICAL MODEL	ASYMMETRICAL MODEL	Dir.	SYMMETRICAL MODEL	ASYMMETRICAL MODEL
		[sec]	[sec]		[sec]	[sec]
BARE FRAME	X	1.9771	1.9694	X	1.1411	1.0315
EXISTING SOLUTION	X	1.8154	1.8075	X	0.5895	0.5837
INTEGRATED SOLUTION	X	1.8121	1.8029	X	0.1389	0.1435
ISOSTATIC CANTILEVER SOLUTION	X	1.8128	1.8064	X	0.5024	0.5038
ISOSTATIC PENDULUM SOLUTION	X	1.8155	1.7556	X	0.1652	0.1713
ISOSTATIC ROCKING SOLUTION	X	1.8122	1.8030	X	0.1589	0.1642

Table 6.13 First periods of models with vertical cladding panels realised with beam elements.

	SHELL					
	DEFORMABLE ROOF			RIGID ROOF		
	Dir.	SYMMETRICAL MODEL	ASYMMETRICAL MODEL	Dir.	SYMMETRICAL MODEL	ASYMMETRICAL MODEL
		[sec]	[sec]		[sec]	[sec]
BARE FRAME	X	1.9771	1.9694	X	1.1411	1.0315
EXISTING SOLUTION	X	1.8166	1.8042	X	0.4786	0.3979
INTEGRATED SOLUTION	X	1.8149	1.8055	X	0.0667	0.1665
ISOSTATIC CANTILEVER SOLUTION	X	1.8174	1.8091	X	0.4965	0.4972
ISOSTATIC PENDULUM SOLUTION	X	1.8165	1.8520	X	0.0902	0.7772
ISOSTATIC ROCKING SOLUTION	X	1.8149	1.8093	X	0.0669	0.5189

Table 6.14 First periods of models with vertical cladding panels realised with shell elements.

	WALL					
	DEFORMABLE ROOF			RIGID ROOF		
	Dir.	SYMMETRICAL MODEL	ASYMMETRICAL MODEL	Dir.	SYMMETRICAL MODEL	ASYMMETRICAL MODEL
		[sec]	[sec]		[sec]	[sec]
BARE FRAME	X	1.9771	1.9694	X	1.1411	1.0315
EXISTING SOLUTION	X	1.8166	1.8078	X	0.4786	0.4807
INTEGRATED SOLUTION	X	1.8149	1.8052	X	0.0667	0.0692
ISOSTATIC CANTILEVER SOLUTION	X	1.8174	1.8088	X	0.4965	0.4978
ISOSTATIC PENDULUM SOLUTION	X	1.8165	1.8082	X	0.0902	0.0902
ISOSTATIC ROCKING SOLUTION	X	1.8149	1.8052	X	0.0669	0.0695

Table 6.15 First periods of models with vertical cladding panels realised with wall elements.

Main conclusions of this comparison between symmetrical and asymmetrical situations are reported below:

- No great differences are observed between first periods of symmetrical and asymmetric structures (Bare frame with rigid roof is the only case with significative changes in term of periods);
- Small differences are detected with the use of shell and wall elements with the representation of cladding panels (if beam elements are considered, it does not change anything substantially);
- The geometrical and load asymmetries of the structures do not affect the first period if cladding panels are considered.

The behaviour of the two cases analysed is shown in Figures 6.120-6.125.

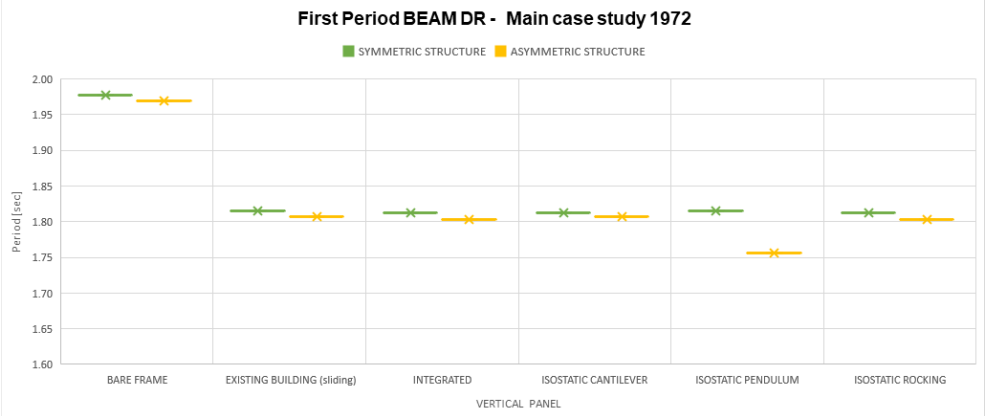

Figure 6.120 First periods of symmetric/asymmetric structures of the main case study with panels realised with BEAM - Deformable Roof.

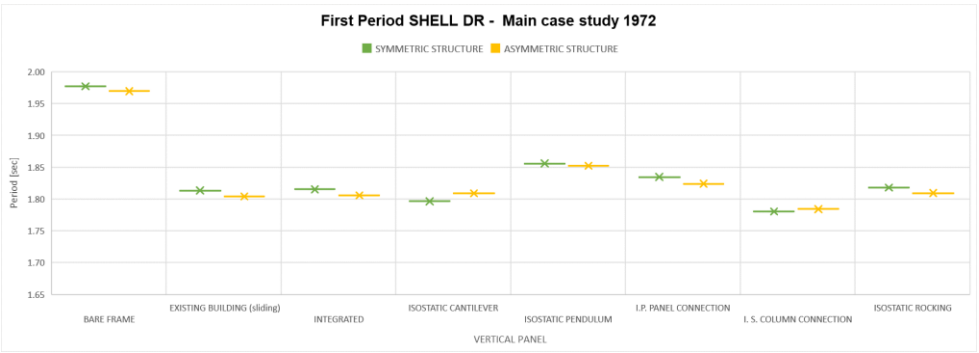

Figure 6.121 First periods of symmetric/asymmetric structures of the main case study with panels realised with SHELL - Deformable Roof.

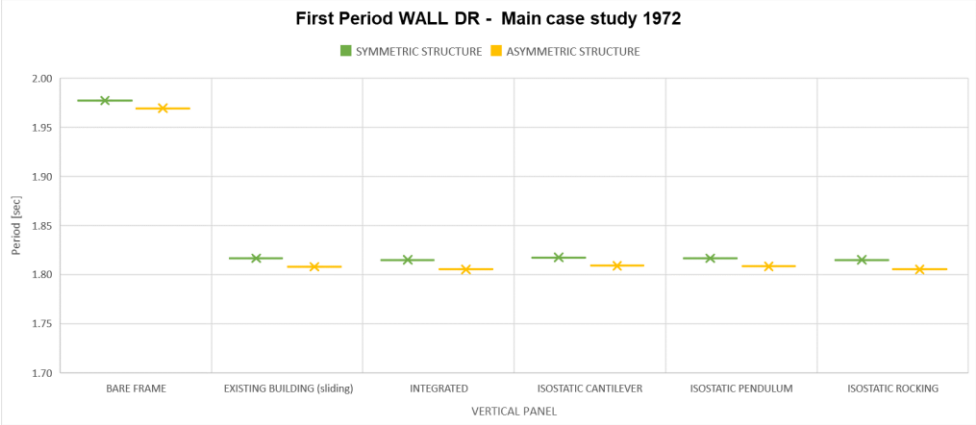

Figure 6.122 First periods of symmetric/asymmetric structures of the main case study with panels realised with WALL - Deformable Roof.

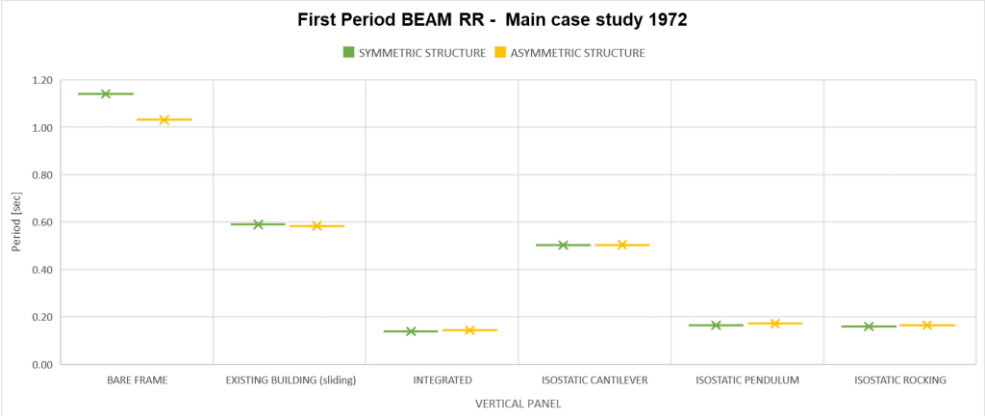

Figure 6.123 First periods of symmetric/asymmetric structures of the main case study with panels realised with BEAM - Rigid Roof.

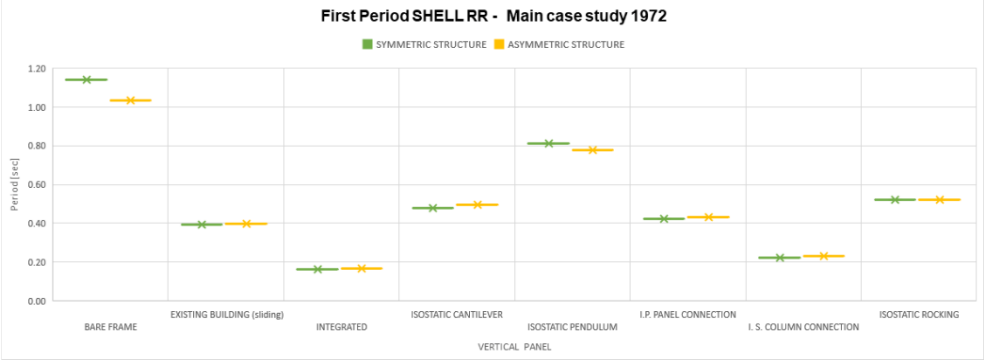

Figure 6.124 First periods of symmetric/asymmetric structures of the main case study with panels realised with SHELL - Rigid Roof.

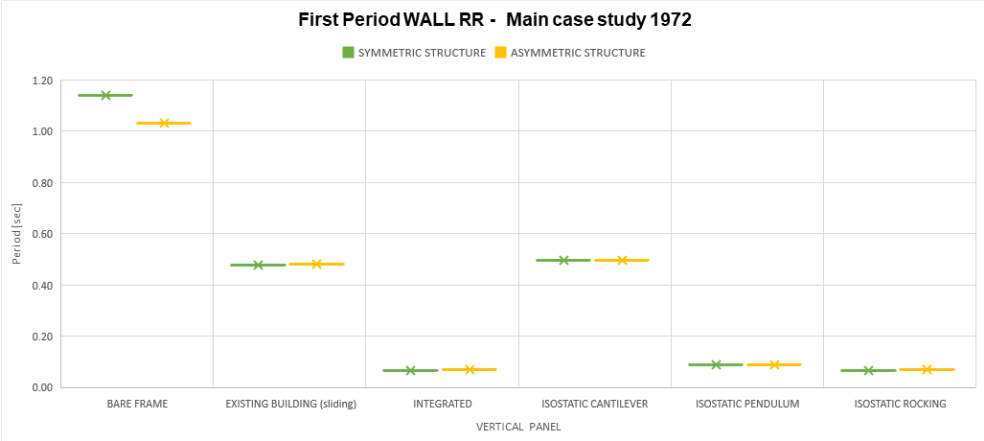

Figure 6.125 First periods of symmetric/asymmetric structures of the main case study with panels realised with WALL - Rigid Roof.

Regarding the participant mass of the first period, significant differences between symmetric and asymmetric structures are observed only in the case of bare frame and pendulum solution for beam and shell elements with deformable roof. Participant mass of first periods of deformable and rigid roof for all type of solutions and elements are reported in Figures 6.126-6.131.

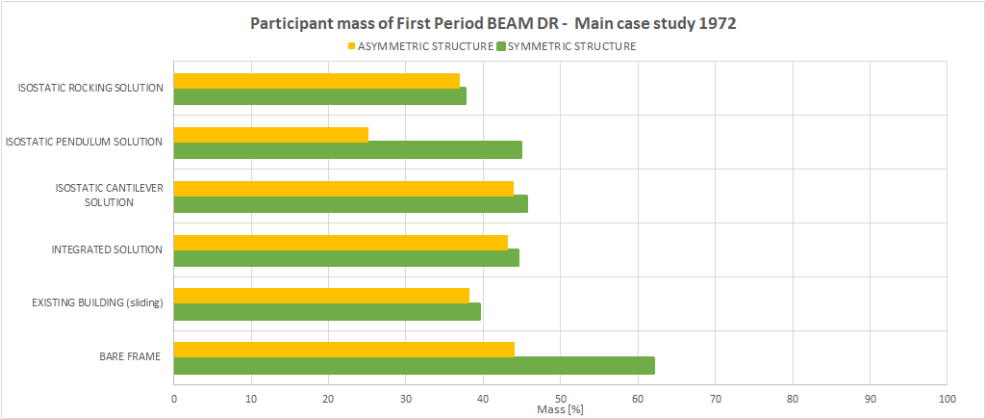

Figure 6.126 Participant mass of first periods of symmetric/asymmetric structures of the main case study with panels realised with BEAM - Deformable Roof.

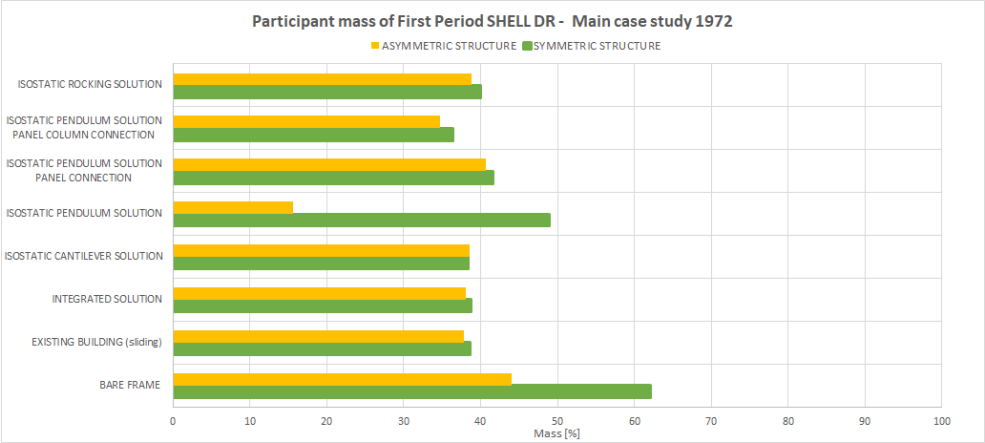

Figure 6.127 Participant mass of first periods of symmetric/asymmetric structures of the main case study with panels realised with SHELL - Deformable Roof.

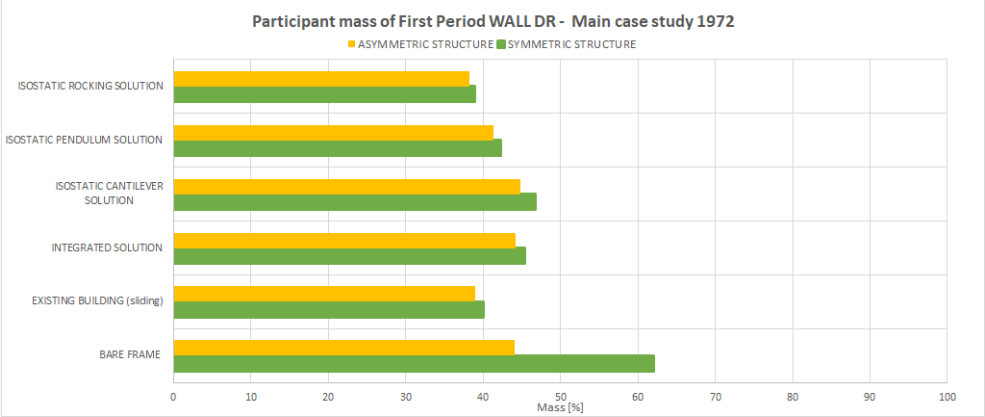

Figure 6.128 Participant mass of first periods of symmetric/asymmetric structures of the main case study with panels realised with WALL - Deformable Roof.

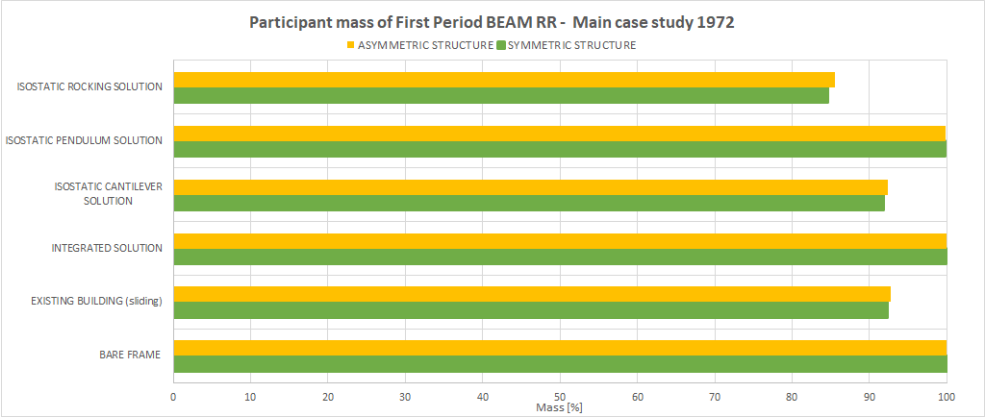

Figure 6.129 Participant mass of first periods of symmetric/asymmetric structures of the main case study with panels realised with BEAM - Rigid Roof.

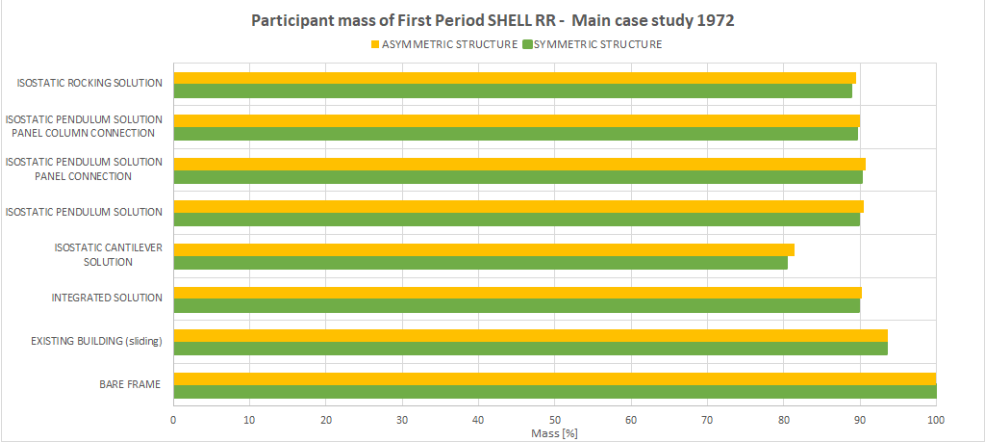

Figure 6.130 Participant mass of first periods of symmetric/asymmetric structures of the main case study with panels realised with SHELL - Rigid Roof.

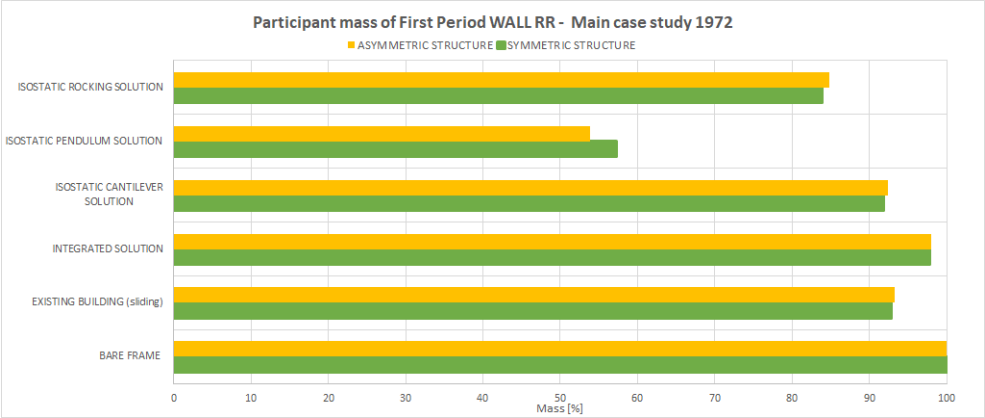

Figure 6.131 Participant mass of first periods of symmetric/asymmetric structures of the main case study with panels realised with WALL - Rigid Roof.

6.5 Future work

From an analytical point of view, a deepening of horizontal cladding panels cases of the precast building will be realised to permit the application of studies of the preliminary case to a building with common plan dimensions of the industrial structure (Experimental tests with horizontal cladding panels realised by Scalbi et al. [119] demonstrate that these elements alter masses and stiffness and the overall dynamic response of the structure in a more complex manner compared to vertical cladding panels).
From an experimental point of view, it will be suitable an Operational Modal Analysis under ambient vibrations test of precast building with cladding panels to validate in numerical analysis the hypothesis done of fastening devices of existing, isostatic and integrated solutions. Finite element model calibration of precast structure using ambient vibrations is done in Osmancikli et al. [120].

References

[1] CEB-FIP. Model Code 2010. 2010. doi:10.1007/s13398-014-0173-7.2.

[2] Asprone D, De Risi R, Manfredi G. Defining structural robustness under seismic and simultaneous actions: an application to precast RC buildings. Bull Earthq Eng 2016;14:485–99. doi:10.1007/s10518-015-9820-4.

[3] Ministero dei Lavori Pubblici. Decreto Ministeriale per aggiornamento delle "Norme Tecniche per le Costruzioni" - NTC 2018 2018:1–198.

[4] Presidente della Repubblica. Legge 25 novembre 1962, n. 1684 "Provvedimenti per l'edilizia, con particolari prescrizioni per le zone sismiche". 1962:1–31.

[5] Presidente della Repubblica. Legge 5 novembre 1971, n. 1086. "Norme per la disciplina delle opere di conglomerato cementizio armato, normale e precompresso ed a struttura metallica". 1971.

[6] Presidente della Repubblica. Legge 2 Febbraio 1974, n. 64. "Provvedimenti per le costruzioni con particolari prescrizioni per le zone sismiche". 1974.

[7] Ministero dei Lavori Pubblici. Decreto ministeriale 3 marzo 1975. "Approvazione delle norme tecniche per le costruzioni in zone sismiche". 1975.

[8] Ministero dei Lavori Pubblici. Decreto Ministeriale 3 Dicembre 1987. "Norme tecniche per la progettazione , esecuzione e collaudo delle costruzioni prefabbricate". 1987:1–16.

[9] Ministero dei Lavori Pubblici. Decreto Ministeriale 16 Gennaio 1996 "Norme tecniche per le costruzioni in zone sismiche". 1996.

[10] Ordinanza Presidente del Consiglio dei Ministri. Ord. P.C.M. 20 marzo 2003 n. 3274 "Primi elementi in materia di criteri generali per la classificazione sismica del territorio nazionale e di normative per le costruzioni in zona sismica". 2003.

[11] Circolare Ministero dei Lavori Pubblici. Circolare LL.PP. 16 Marzo 1989 n. 31104. 1989.

[12] Ministero dei Lavori Pubblici. Decreto Ministeriale 9 Gennaio 1996 "Norme tecniche per il calcolo, l'esecuzione ed il collaudo delle strutture in cemento armato, normale e precompresso e per le strutture metalliche." 1996:1–135.

[13] Circolare Ministero dei Lavori Pubblici. Circolare 10 Aprile 1997 , n. 65 /AA .GG . "Istruzioni per l ' applicazione delle « Norme tecniche per le costruzioni in zone sismiche » di cui al decreto ministeriale" 1997:1–30.

[14] Ministero dei Lavori Pubblici. Decreto Ministeriale 14 Gennaio 2008. “Norme tecniche per le costruzioni” 2008.
[15] Uni En. Eurocode 8: Design of Structures for earthquake resistance - Part 1: General Rules, Seismic Actions and Rules for Buildings. 2005. doi:[Authority: The European Union per Regulation 305/2011, Directive 98/34/EC, Directive 2004/18/EC].
[16] Contegni M, Palermo A, Toniolo G. Strutture prefabbricate: Schedario Dei Collegamenti 2007.
[17] Contegni M, Palermo A, Toniolo G. Strutture prefabbricate: Catalogo delle tipologie esistenti 2008.
[18] Contegni M, Palermo A, Toniolo G. Strutture prefabbricate: Schedario di edifici prefabbricati in C.A. 2008:206.
[19] Bellotti D, Casotto C, Crowley H, Deyanova MG, Germagnoli F, Lucarelli E, et al. Capannoni monopiano prefabbricati : distribuzione probabilistica dei sistemi e sottosistemi strutturali dagli anni sessanta ad oggi. Progett Sismica 2014;5:41–70. doi:10.7414/PS.5.3.41-70.
[20] Consiglio Nazionale delle Ricerche. CNR 10025/84 Istruzioni per il progetto, l’esecuzione e il controllo delle strutture prefabbricate in conglomerato cementizio e per le strutture costruite con sistemi industrializzati 1984.
[21] Consiglio Nazionale delle Ricerche. CNR 10025/98 Istruzioni per il progetto, l’esecuzione e il controllo delle strutture prefabbricate in conglomerato cementizio e per le strutture costruite con sistemi industrializzati 1998.
[22] Assobeton. Linee Guida ASSOBETON per la progettazione sismica di strutture prefabbricate 2009.
[23] Negro P, Toniolo G. Design Guidelines for Connections of Precast Structures under Seismic Actions. 2012. doi:10.2777/37605.
[24] Colombo A, Lamperti M, Negro P, Toniolo G. Design Guidelines for Wall Panel Connections. 2016. doi:10.2788/546845.
[25] Colombo A, Negro P, Toniolo G, Lamperti M. Design Guidelines for Precast Structures with Cladding Panels. 2016. doi:10.2788/956612.
[26] Gruppo di Lavoro Agibilità Sismica dei Capannoni Industriali. Linee di indirizzo per interventi locali e globali su edifici industriali monopiano non progettati con criteri antisismici 2013.
[27] Gruppo di Lavoro Agibilità Sismica dei Capannoni Industriali. Linee guida per riparazione e rafforzamento di elementi strutturali, tamponature e partizioni. Reluis 2013.
[28] Gruppo di Lavoro Agibilità Sismica dei Capannoni Industriali. Manuale per la compilazione della scheda di valutazione di danno e agibilità post-sisma per

edifici a struttura prefabbricata o di grande luce (GL-AeDES) 2014.
[29] Magliulo G. The Emilia Earthquake Seismic Performance of Precast Reinforced Concrete Buildings 2014.
[30] Bournas DA, Negro P, Taucer FF. Performance of industrial buildings during the Emilia earthquakes in Northern Italy and recommendations for their strengthening. Bull Earthq Eng 2014. doi:10.1007/s10518-013-9466-z.
[31] Savoia M, Buratti N, Vincenzi L. Damage and collapses in industrial precast buildings after the 2012 Emilia earthquake. Eng Struct 2017;137:162–80. doi:10.1016/j.engstruct.2017.01.059.
[32] Liberatore L, Sorrentino L, Liberatore D, Decanini LD. Failure of industrial structures induced by the Emilia (Italy) 2012 earthquakes. Eng Fail Anal 2013;34:629–47. doi:10.1016/j.engfailanal.2013.02.009.
[33] Poiani M, Gazzani V, Clementi F, Milani G, Valente M, Lenci S. Iconic crumbling of the clock tower in Amatrice after 2016 central Italy seismic sequence: advanced numerical insight. Procedia Struct Integr 2018;11:314–21. doi:10.1016/j.prostr.2018.11.041.
[34] Gazzani V, Poiani M, Clementi F, Milani G, Lenci S. Modal parameters identification with environmental tests and advanced numerical analyses for masonry bell towers: a meaningful case study. Procedia Struct Integr 2018;11:306–13. doi:10.1016/j.prostr.2018.11.040.
[35] Mollaioli F, AlShawa O, Liberatore L, Liberatore D, Sorrentino L. Seismic demand of the 2016–2017 Central Italy earthquakes. Bull Earthq Eng 2018. doi:10.1007/s10518-018-0449-y.
[36] Capozzi V. Comportamento sismico dei collegamenti nelle strutture prefabbricate 2009:294.
[37] Dal Lago B, Negro P, Dal Lago A. Seismic design and performance of dry-assembled precast structures with adaptable joints. Soil Dyn Earthq Eng 2018;106:182–95. doi:10.1016/j.soildyn.2017.12.016.
[38] Belleri A, Marini A, Riva P, Nascimbene R. Dissipating and re-centring devices for portal-frame precast structures. Eng Struct 2017. doi:10.1016/j.engstruct.2017.07.072.
[39] Magliulo G, Capozzi V, Fabbrocino G, Manfredi G. Neoprene-concrete friction relationships for seismic assessment of existing precast buildings. Eng Struct 2011;33:535–8. doi:10.1016/j.engstruct.2010.11.011.
[40] Ercolino M, Magliulo G, Manfredi G. Failure of a precast RC building due to Emilia-Romagna earthquakes. Eng Struct 2016;118:262–73. doi:10.1016/j.engstruct.2016.03.054.
[41] Clementi F, Scalbi A, Lenci S. Seismic performance of precast reinforced

concrete buildings with dowel pin connections. J Build Eng 2016;7:224–38. doi:10.1016/j.jobe.2016.06.013.
[42] Vintzeleou EN, Tassios TP. Mathematical Models for Dowel Action under Monotonic and Cyclic Conditions. Mag Concr Res 1986. doi:10.1680/macr.1986.38.134.13.
[43] Fédération internationale du béton. Task Group 6.2. Structural connections for precast concrete buildings - Bullettin n. 43. 2008.
[44] Soroushian P, Obaseki K, Rojas MC, Sim J. Analysis of Dowel Bars Acting Against Concrete Core. J Proc 1986. doi:10.14359/10657.
[45] Psycharis IN, Mouzakis HP. Shear resistance of pinned connections of precast members to monotonic and cyclic loading. Eng Struct 2012;41:413–27. doi:10.1016/j.engstruct.2012.03.051.
[46] Kremmyda GD, Fahjan YM, Tsoukantas SG. Nonlinear FE analysis of precast RC pinned beam-to-column connections under monotonic and cyclic shear loading. Bull Earthq Eng 2014;12:1615–38. doi:10.1007/s10518-013-9560-2.
[47] Magliulo G, Ercolino M, Cimmino M, Capozzi V, Manfredi G. FEM analysis of the strength of RC beam-to-column dowel connections under monotonic actions. Constr Build Mater 2014;69:271–84. doi:10.1016/j.conbuildmat.2014.07.036.
[48] Zoubek B, Isakovic T, Fahjan Y, Fischinger M. Cyclic failure analysis of the beam-to-column dowel connections in precast industrial buildings. Eng Struct 2013;57:276. doi:10.1016/j.engstruct.2013.09.036.
[49] Zoubek B, Fischinger M, Isakovic T. Estimation of the cyclic capacity of beam-to-column dowel connections in precast industrial buildings. Bull Earthq Eng 2015;13:2145–68. doi:10.1007/s10518-014-9711-0.
[50] Ferrara L, Toniolo G. Design approach for diaphragm action of roof decks in precast concrete building under earthquake 2008:963–8.
[51] Belleri A, Torquati M, Riva P. Seismic performance of ductile connections between precast beams and roof elements. Mag Concr Res 2014;66:553–62. doi:10.1680/macr.13.00092.
[52] Osanai Y, Watanabe F, Okamoto S. Stress transfer mechanism of socket base connections with precast concrete columns. ACI Struct J 1996. doi:10.14359/9686.
[53] Saisi AE, Toniolo G. Precast R.C. columns under cyclic loading : An experimental programme oriented to EC8. Stud e Ric - Politec Di Milano Sc Di Spec Costr Cem Armato 1998.
[54] Dal Lago B, Toniolo G, Lamperti Tornaghi M. Influence of different mechanical column-foundation connection devices on the seismic

behaviour of precast structures. Bull Earthq Eng 2016;14:3485–508. doi:10.1007/s10518-016-0010-9.
[55] Belleri A, Riva P. Seismic performance and retrofit of precast concrete grouted sleeve connections. PCI J 2012;57:97–109. doi:10.15554/pcij.01012012.97.109.
[56] Cornali F, Belleri A, Marini A, Riva P. Influence of modelling assumptions in the expected loss evaluation of a precast industrial building. Procedia Eng 2017;199:3510–5. doi:10.1016/j.proeng.2017.09.499.
[57] Rodrigues D, Crowley H, Silva V. Earthquake loss assessment of precast RC industrial structures in Tuscany (Italy). Bull Earthq Eng 2018;16:203–28. doi:10.1007/s10518-017-0195-6.
[58] Demartino C, Vanzi I, Monti G. Probabilistic estimation of seismic economic losses of portal-like precast industrial buildings. Earthq Struct 2017;13:323–35. doi:10.12989/eas.2017.13.3.323.
[59] Bolognini D, Borzi B, Pinho R. Simplified pushover-based vulnerability analysis of traditional Italian RC precast structures. 14 Th World Conf Earthq Eng 2008:1–8.
[60] Casotto C, Silva V, Crowley H, Nascimbene R, Pinho R. Seismic fragility of Italian RC precast industrial structures. Eng Struct 2015;94:122–36. doi:10.1016/j.engstruct.2015.02.034.
[61] Palanci M, Senel SM, Kalkan A. Assessment of one story existing precast industrial buildings in Turkey based on fragility curves. Bull Earthq Eng 2017;15:271–89. doi:10.1007/s10518-016-9956-x.
[62] Mezzapelle PA, Scalbi A, Clementi F, Lenci S. The Influence of Dowel-Pin Connections on the Seismic Fragility Assessment of RC Precast Industrial Buildings. Open Civ Eng J 2017. doi:10.2174/1874149501711011138.
[63] Beilic D, Casotto C, Nascimbene R, Cicola D, Rodrigues D. Seismic fragility curves of single storey RC precast structures by comparing different Italian codes. Earthq Struct 2017;12:359–74. doi:10.12989/eas.2017.12.3.359.
[64] Ercolino M, Bellotti D, Magliulo G, Nascimbene R. Vulnerability analysis of industrial RC precast buildings designed according to modern seismic codes. Eng Struct 2018;158:67–78. doi:10.1016/j.engstruct.2017.12.005.
[65] Babič A, Dolšek M. Seismic fragility functions of industrial precast building classes. Eng Struct 2016;118:357–70. doi:10.1016/j.engstruct.2016.03.069.
[66] Brunesi E, Nascimbene R, Parisi F, Augenti N. Progressive collapse fragility of reinforced concrete framed structures through incremental dynamic analysis. Eng Struct 2015;104:65–79. doi:10.1016/j.engstruct.2015.09.024.
[67] Paolini C, Pugnaletto M. Reinforced brick light-weight vaults 2017.

[68] Fabbrocino G, Verderame GM, Manfredi G. Experimental behaviour of anchored smooth rebars in old type reinforced concrete buildings 2005;27:1575–85. doi:10.1016/j.engstruct.2005.05.002.
[69] Vamvatsikos D, Allin Cornell C. Incremental dynamic analysis. Earthq Eng Struct Dyn 2002;31:491–514. doi:10.1002/eqe.141.
[70] Fajfar P, Gašperšič P. THE N2 METHOD FOR THE SEISMIC DAMAGE ANALYSIS OF RC BUILDINGS. Earthq Eng Struct Dyn 1996. doi:10.1002/(SICI)1096-9845(199601)25:1<31::AID-EQE534>3.0.CO;2-V.
[71] Clementi F, Gazzani V, Poiani M, Antonio Mezzapelle P, Lenci S. Seismic Assessment of a Monumental Building through Nonlinear Analyses of a 3D Solid Model. J Earthq Eng 2018. doi:10.1080/13632469.2017.1297268.
[72] Clementi F, Gazzani V, Poiani M, Lenci S. Assessment of seismic behaviour of heritage masonry buildings using numerical modelling. J Build Eng 2016. doi:10.1016/j.jobe.2016.09.005.
[73] Clementi F, Quagliarini E, Monni F, Giordano E, Lenci, S. Cultural Heritage and Earthquake: The Case Study of “Santa Maria della Carità” in Ascoli Piceno. Open Civ Eng J 2017. doi:10.2174/1874149501711011079.
[74] Takeda T, Sozen MA, Nielsen NN. Reinforced Concrete Response to Simulated Earthquakes. J Struct Div ASCE 1970. doi:10.1017/CBO9781107415324.004.
[75] Baker JW. Efficient analytical fragility function fitting using dynamic structural analysis. Earthq Spectra 2015. doi:10.1193/021113EQS025M.
[76] Chandramohan R, Lin T, Baker JW, Deierlein GG. Influence of Ground Motion Spectral Shape and Duration on Seismic Collapse Risk. 10th Int Conf Urban Earthq Eng 2013.
[77] Iervolino I, De Luca F, Cosenza E. Spectral shape-based assessment of SDOF nonlinear response to real, adjusted and artificial accelerograms. Eng Struct 2010;32:2776–92. doi:10.1016/j.engstruct.2010.04.047.
[78] Iervolino I, Galasso C, Cosenza E. REXEL: Computer aided record selection for code-based seismic structural analysis. Bull Earthq Eng 2010;8:339–62. doi:10.1007/s10518-009-9146-1.
[79] Iervolino I, Cornell CA. Record selection for nonlinear seismic analysis of structures. Earthq Spectra 2005;21:685–713. doi:10.1193/1.1990199.
[80] Jalayer F. Direct probabilistic seismic analysis: implementing non-linear dynamic assessments. Dep Civ Environ Eng 2003.
[81] Baker JW. Code supplement to efficient analytical fragility function fitting using dynamic structural analysis. Earthq Eng Res Inst 2015;31:579–99. doi:10.1193/021113EQS025M.

[82] Banerjee AK, Pramanik D, Roy R. Seismic structural fragilities: Proposals for improved methodology per spectral matching of accelerogram. Eng Struct 2016;111:538–51. doi:10.1016/j.engstruct.2016.01.002.
[83] Hatzigeorgiou GD, Liolios AA. Nonlinear behaviour of RC frames under repeated strong ground motions. Soil Dyn Earthq Eng 2010;30:1010–25. doi:10.1016/j.soildyn.2010.04.013.
[84] Di Sarno L. Effects of multiple earthquakes on inelastic structural response. Eng Struct 2013;56:673–81. doi:10.1016/j.engstruct.2013.05.041.
[85] Hatzivassiliou M, Hatzigeorgiou GD. Seismic sequence effects on three-dimensional reinforced concrete buildings. Soil Dyn Earthq Eng 2015;72:77–88. doi:10.1016/j.soildyn.2015.02.005.
[86] Furtado A, Rodrigues H, Arêde A, Varum H. Assessment of the mainshock-aftershock collapse vulnerability of RC structures considering the infills in-plane and out-of-plane behaviour. Procedia Eng., 2017. doi:10.1016/j.proeng.2017.09.107.
[87] Furtado A, Rodrigues H, Varum H, Arêde A. Mainshock-aftershock damage assessment of infilled RC structures. Eng Struct 2018;175:645–60. doi:10.1016/j.engstruct.2018.08.063.
[88] Oyguc R, Toros C, Abdelnaby AE. Seismic behavior of irregular reinforced-concrete structures under multiple earthquake excitations. Soil Dyn Earthq Eng 2018;104:15–32. doi:10.1016/j.soildyn.2017.10.002.
[89] Zhai CH, Bao X, Zheng Z, Wang XY. Impact of aftershocks on a post-mainshock damaged containment structure considering duration. Soil Dyn Earthq Eng 2018;115:129–41. doi:10.1016/j.soildyn.2018.08.013.
[90] Raghunandan M, Liel AB, Luco N. Aftershock collapse vulnerability assessment of reinforced concrete frame structures. Earthq Eng Struct Dyn 2015. doi:10.1007/978-94-007-2288-0.
[91] Hosseinpour F, Abdelnaby AE. Fragility curves for RC frames under multiple earthquakes. Soil Dyn Earthq Eng 2017;98:222–34. doi:10.1016/j.soildyn.2017.04.013.
[92] Hosseinpour F, Abdelnaby AE. Effect of different aspects of multiple earthquakes on the nonlinear behavior of RC structures. Soil Dyn Earthq Eng 2017;92:706–25. doi:10.1016/j.soildyn.2016.11.006.
[93] Di Trapani F, Malavisi M. Seismic fragility assessment of infilled frames subject to mainshock/aftershock sequences using a double incremental dynamic analysis approach. Bull Earthq Eng 2018. doi:10.1007/s10518-018-0445-2.
[94] Mitropoulou CC, Lagaros ND, Papadrakakis M. Numerical calibration of

damage indices. Adv Eng Softw 2014. doi:10.1016/j.advengsoft.2014.01.007.
[95] Y.J.Park, A.H.S.Ang. Mechanistic seismic damage model for reinforced concrete. J Struct Eng ASCE 1985. doi:10.1061/(ASCE)0733-9445(1985)111:4(722).
[96] Kunnath SK, Reinhorn AM, Abel JF. A computational tool for evaluation of seismic performance of reinforced concrete buildings. Comput Struct 1991. doi:10.1016/0045-7949(91)90165-I.
[97] DiPasquale E, Cakmak AS. Detection of seismic structural damage using parameter-based global damage indices. Probabilistic Eng Mech 1990. doi:10.1016/0266-8920(90)90008-8.
[98] Pierdicca A, Clementi F, Maracci D, Isidori D, Lenci S. Damage detection in a precast structure subjected to an earthquake: A numerical approach. Eng Struct 2016;127:447–58. doi:10.1016/j.engstruct.2016.08.058.
[99] Powell GH, Allahabadi R. Seismic damage prediction by deterministic methods: Concepts and procedures. Earthq Eng Struct Dyn 1988. doi:10.1002/eqe.4290160507.
[100] Negro P, Lamperti Tornaghi M. Seismic response of precast structures with vertical cladding panels: The SAFECLADDING experimental campaign. Eng Struct 2017;132:205–28. doi:10.1016/j.engstruct.2016.11.020.
[101] Dal Lago B, Biondini F, Toniolo G. Friction-based dissipative devices for precast concrete panels. Eng Struct 2017;147:356–71. doi:10.1016/j.engstruct.2017.05.050.
[102] Toniolo G, Dal Lago B. Conceptual design and full-scale experimentation of cladding panel connection systems of precast buildings. Earthq Eng Struct Dyn 2017. doi:10.1002/eqe.2918.
[103] Zoubek B, Fischinger M, Isaković T. Cyclic response of hammer-head strap cladding-to-structure connections used in RC precast building. Eng Struct 2016;119:135–48. doi:10.1016/j.engstruct.2016.04.002.
[104] Belleri A, Torquati M, Marini A, Riva P. Horizontal cladding panels: in-plane seismic performance in precast concrete buildings. Bull Earthq Eng 2016;14:1103–29. doi:10.1007/s10518-015-9861-8.
[105] Dal Lago B, Biondini F, Toniolo G, Lamperti Tornaghi M. Experimental investigation on the influence of silicone sealant on the seismic behaviour of precast façades. Bull Earthq Eng 2017;15:1771–87. doi:10.1007/s10518-016-0045-y.
[106] Dal Lago B, Lamperti Tornaghi M. Sliding channel cladding connections for precast structures subjected to earthquake action. Bull Earthq Eng 2018.

doi:10.1007/s10518-018-0410-0.
[107] Psycharis IN, Kalyviotis IM, Mouzakis HP. Experimental investigation of the response of precast concrete cladding panels with integrated connections under monotonic and cyclic loading. Eng Struct 2018;159:75–88. doi:10.1016/j.engstruct.2017.12.036.
[108] Magliulo G, Ercolino M, Manfredi G. Influence of cladding panels on the first period of one-story precast buildings. Bull Earthq Eng 2015;13:1531–55. doi:10.1007/s10518-014-9657-2.
[109] Ercolino M. Seismic Behaviour of One-Story Precast Buildings 2014.
[110] ATC. Tentative Provisions for the Development of Seismic Regulations for Buildings: A Cooperative Effort with the Design Professions, Building Code Interests and the Research Comunity. 1978.
[111] Chopra AK. Dynamics of structures : theory and applications to earthquake engineering. Pearson Educ 2007. doi:10.1002/9781118599792.
[112] Goel RK, Chopra AK. Period Formulas for Moment-Resisting Frame Buildings. J Struct Eng 1997. doi:10.1061/(ASCE)0733-9445(1997)123:11(1454).
[113] Hong LL, Hwang WL. Empirical formula for fundamental vibration periods of reinforced concrete buildings in Taiwan. Earthq Eng Struct Dyn 2000. doi:10.1002/(SICI)1096-9845(200003)29:3<327::AID-EQE907>3.0.CO;2-0.
[114] Crowley H, Pinho R. Simplified Equations for Estimating the Period of Vibration of. First Eur Conf Earthq Eng Seismol 2006. doi:1122.
[115] Ricci P, Verderame GM, Manfredi G. Analytical investigation of elastic period of infilled RC MRF buildings. Eng Struct 2011. doi:10.1016/j.engstruct.2010.10.009.
[116] Biondini F, Dal Lago B, Toniolo G. Role of wall panel connections on the seismic performance of precast structures. Bull Earthq Eng 2013;11:1061–81. doi:10.1007/s10518-012-9418-z.
[117] Dal Lago B, Bianchi S, Biondini F. Diaphragm effectiveness of precast concrete structures with cladding panels under seismic action. Bull Earthq Eng 2018. doi:10.1007/s10518-018-0452-3.
[118] Belleri A, Cornali F, Passoni C, Marini A, Riva P. Evaluation of out-of-plane seismic performance of column-to-column precast concrete cladding panels in one-storey industrial buildings. Earthq Eng Struct Dyn 2018;47:397–417. doi:10.1002/eqe.2956.
[119] Scalbi A, Tornaghi ML, Negro P. SAFECLADDING PROJECT : PSEUDODYNAMIC TESTING ON PRECAST STRUCTURES WITH HORIZONTAL CLADDING PANELS. 16th Eur. Conf. Earthq. Eng., 2018.
[120] Osmancikli G, Bayraktar A, Türker T, Uçak Ş, Mosallam A. Finite element

model calibration of precast structures using ambient vibrations. Constr Build Mater 2015;93:10–21. doi:10.1016/j.conbuildmat.2015.05.096.